DEVELOPMENT AND CHARACTERISATION OF HOLMIUM AND ERBIUM LASERS FOR THE ABLATION OF BIOLOGICAL TISSUE

by Phillip S. Jones, B.Sc. (Hons.)

Thesis Presented for
The Degree of Doctor of Philosophy (Ph.D.)
of the University of London

Department of Medical Physics and Bioengineering
University College London
April 1993

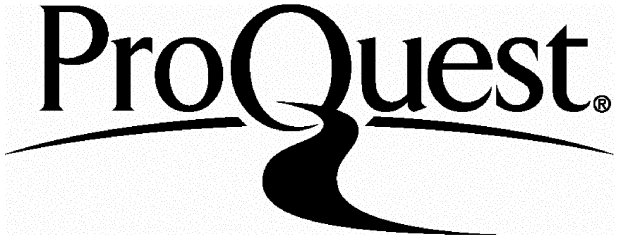

Abstract

The development of pulsed laser systems operating in the infrared at 2.1μm and 2.94μm, based on Cr:Tm:Ho:YAG and Er:YAG laser crystals, and the ability of these lasers to ablate biological tissue is reported. Thermal lensing in the laser crystals has been investigated and found to be the main factor restricting the operating ranges of these lasers. Additionally, increases in the threshold of holmium lasers due to thermal population of the lower laser level increases the amount of heat dissipated in the crystal lattice, leading to increased thermal lensing. Thus, the divergence properties of resonators containing these crystals depends, additionally, on the operating temperature. Modelling of the divergence behaviour of resonators based around Cr:Tm:Ho:YAG and Er:YAG laser crystals in simple resonator geometries is demonstrated using computer based ray tracing algorithms. The temporal behaviour of these lasers has been experimentally assessed and compared to a 'rectangular pump pulse' theory. Using this theory it is possible to predict the delay between the start of the excitation pulse and the start of the laser pulse but not the duration of the output pulse. The reasons for this are discussed.

Pulses of 2.94μm radiation ablate soft tissue more efficiently than similar pulses of 2.1μm. Mass loss due to laser radiation is shown to be linear with dose for the 2.1μm radiation. However, at 2.94μm mass removal is impeded at high doses by the extension of a charred zone into the ablation crater. Operation at high fluences is required to overcome this problem. However, there is an increase in mechanical damage to surrounding tissue and a change in crater shape at fluences greater than 0.085 J mm^{-2} coinciding with a significant impulse being imparted to the tissue. The maximum mass loss per unit of delivered energy at 2.1μm and 2.94μm are approximately 48% and 60% of that expected for ablation of a pure water target. Routes for the energy loss are discussed. The energy lost in the form of kinetic energy is determined experimentally to be less than 1% of the total energy delivered. A linear model was found to best described the ablation performance at both wavelengths. The implications of these findings are discussed.

Acknowledgements

I am indebted to the following for their contributions to this work.
It might be taken for granted that I would thank my academic supervisor, Tim Mills, for his contribution. His patience has surely been beyond the call of duty and, at times, beyond reasonable expectations. Most notable towards the end of this project has been his attention to detail. The quality of grammar in this thesis is a testament to his vigilance. I am grateful that our friendship has flourished during my association with the University, rather than suffered as a result of it. I am also grateful for the understanding of Tim's wife Maggie who has allowed me to disturb so many of their family weekends with my visits.

I should thank the other members of the Department of Medical Physics at UCL, particularly John Clifton, for their constant interest in the progress of my work which, almost in its entirity, has been conducted out of sight and could easily have been out of mind. Amongst these individuals the greatest source of inspiration has been Matthias Essenpreis who, by being so annoyingly good at everything, has inspired me to seek out my own strengths. I am grateful for his help and support, not to mention his Germanic planning during our visit to ASLMS in Florida.

The work for this thesis has been carried out at my employers, Lumonics Ltd in Rugby, Warwickshire. I am particularly grateful to all of the Lumonics employees who have quietly encouraged and supported me during the past four years. I am also grateful to the 'Company' for their support during this project, particularly in allowing the project to continue when the business direction was forced to change. Special thanks amongst my close colleagues go to Mark Richmond for his useful discussions and, in the latter part of the project, to Graham Burrows for making the right decisions and taking the right actions when they were needed.

My thanks also go to all of the researchers whom I have contacted and who have been more than willing to share with me their latest findings. Particularly useful has been the assistance of the crystal suppliers, particularly at Litton, who have furnished me with literature and free $LiNbO_3$ crystals.

Thanks also go to Mike Walsh, Mike Keightley and Norman Heggarty for their help in the preparation of this thesis.

Finally, I wish to thank my parents for their faith in my ability, even though they didn't have a clue what I was doing, and to Sonya Paterson for her strength and devotion.

CONTENTS

APPENDICES

FIGURES

CHAPTER 1

CHAPTER 2

CHAPTER 3

3.8 Oscilloscope trace of the first few laser pulses obtained from a 580mm long laser resonator when operated from 'cold'. The effect of changes in the thermal lensing causes the output to increase and then decrease as the resonator moves towards an instability region.

3.9 Laser output performance over a range of operating temperatures for a 370mm long resonator containing a 3"x4mm diameter Er:YAG rod pumped at 3Hz.

3.10 Change in laser output energy with temperature for a 370mm long resonator fixed pump pulse energies of 102J, 83J and 65J.

3.11 Change in laser slope efficiency and laser threshold with temperature.

3.12 Photomicrograph of damage to the end faces of the Er:YAG rod. Damage typically appeared either as a) small point damage sites or b) larger regions which appeared to be either an accumulation of many small damage sites or the enlargement of single damage sites, due to prolonged use of the crystal once damaged. Larger damage areas were visible to the naked eye.

3.13 Change in output beam divergence from a 370mm long, plane symmetric resonator with average lamp power.

3.14 Change in output beam quality from a 370mm long, plane symmetric resonator with average lamp power.

3.15 Variation in focal length induced in a 3"x4mm diameter Er:YAG rod with average pump power.

3.16 Variation in focal length induced in a 3"x4mm diameter Er:YAG rod with average pump power. A comparison between this work and the work of Frauchiger et al[50].

3.17 Comparison of the change in measured beam divergence with average pump power from a 470mm long resonator with the divergence predicted by the model.

3.18 Fraction of average lamp power absorbed by an Er:YAG laser crystal, calculated using the results for the variation in induced focal length with average pump power.

3.19 Variation in thermal lens focal power of a 3"x4mm diameter Er:YAG rod with average pump power.

3.20 Typical oscilloscope trace obtained during measurement of the delay between the start of the excitation pulse (left hand trace) and the laser pulse (right hand pulse).

3.21 Change in the measured delay between the start of the flashlamp excitation pulse and the start of laser action with lamp discharge energy. The repetition rate and resonator length being varied in order to change the laser threshold.

3.22 Change in the measured delay between the start of the flashlamp excitation pulse and the start of laser action with normalised discharge parameter, r. The repetition rate and resonator length being varied in order to change the laser threshold.

3.23 Comparison between the measured output pulse duration and that predicted from the rectangular pulse delay-to-lasing theory.

3.24 Change in output pulse duration with output pulse energy for a number of different operating conditions, each producing different laser threshold energies.

CHAPTER 4

CHAPTER 5

5.8 Experimental configuration for monitoring the laser light reflected from the ablation plume into different angles.

5.9 Experimental configuration for monitoring the laser light reflected from the ablation plume into angles greater than 90° and therefore originating above the tissue surface.

5.10 Typical temporal profile of the output laser pulse at 2.94μm.

5.11 Temporal profile of laser light reflected and scattered from or near the tissue surface into an angle of about 10° to the normal during pulsed laser ablation of tissue at 2.94μm. The pulse fluence was about 0.11 J mm^{-2}
a) After about 3 seconds exposure
b) After about 20-30 seconds exposure

5.12 Temporal profile of laser light reflected and scattered from or near the tissue surface into an angle of about 50° to the normal during pulsed laser ablation of tissue at 2.94μm. The pulse fluence was about 0.11 J mm^{-2}.
a) After about 3 seconds exposure
b) After about 20-30 seconds exposure.

5.13 Temporal profile of laser light reflected and scattered from or near the tissue surface into an angle of about 50° to the normal during pulsed laser ablation of tissue at 2.94μm. The pulse fluence was about 0.046 J mm^{-2}.
a) After about 3 seconds exposure.
b) After about 20-30 seconds exposure.

5.14 Temporal profile of laser light reflected and/or scattered from above the tissue into an angle of at $>90°$ during pulsed laser ablation of tissue at 2.94μm. The pulse fluence was 0.11 J mm^{-2}.

APPENDIX FIGURES

TABLES

APPENDIX TABLES

CHAPTER 1

Introduction

Laser ablation of soft biological tissue, with minimal thermal damage to adjacent tissue, remains an objective of designers of surgical lasers. Transmission of such laser wavelengths using flexible optical fibres is also highly desirable. A system incorporating these two features would allow flexible endoscopic tissue ablation, thus greatly enlarging the range and quality of surgical procedures that could be performed endoscopically. An ideal system would be based on a solid state laser operating in the near infrared. This is because solid state lasers are inherently simpler, do not require gases to operate and can be made more compact. Thus, solid state systems can, theoretically, be made more reliable, allowing greater lengths of time between routine maintenance. The choice of infrared wavelengths is based on the fact that, beyond about 1.5μm, absorption of light in tissue is dominated by water which constitutes between 60% and 80% of the tissue mass. Therefore, tissue processing using wavelengths in the infrared, will not be affected by the degree of vascularisation or the presence of tissue chromophores other than water.

Currently, the two main solid state laser wavelengths of interest for laser ablation of soft tissue are 2.1μm and 2.94μm, which are available from YAG crystals doped with holmium and erbium ions, respectively. Recently, as a result of improved crystal compositions, there has been an increasing number of publications aimed at furthering the development of these lasers into practical devices. These improvements have largely arisen as a result of the commercial interest in laser systems for ablating tissue. However, the depth of knowledge on these systems still remains deficient, particularly in the field of high efficiency, repetitively pulsed systems, such as those required for commercial devices. Also, there have been a number of recent publications based on trials with prototype versions of these lasers. However, there has been only a limited number of reports into the basic physics of the interaction with tissue using these wavelengths. Such work is essential if commercial systems are to provide the very best solution that can be offered.

Work in this thesis extends the understanding of the operation of laser systems based on holmium or erbium doped crystals. The interaction of the high pulse energies obtained from these lasers with biological tissue is investigated to further develop the understanding of the physics of this interaction.

1.1 Tissue Effects in Laser Therapy

Laser light delivered to tissue can produce a number of different biological effects. These effects can be grouped under four headings: photochemical, photoablative, photothermal and photomechanical. In the first of these the laser provides a way of initiating a reaction within the tissue to change the tissue in a predetermined way. An example of this is photodynamic therapy, PDT, whereby a photoactive drug administered to a cancer undergoes a photochemical reaction releasing a cytotoxic agent (probably singlet oxygen) when irradiated with light of a specific wavelength. Because the cancer is targeted by the treatment light as well as, perhaps, the drug, due to its possible, preferential retention by tumour tissues, the cancer is destroyed efficiently and with minimal damage to surrounding healthy tissues.

The second group of effects describes the way in which tissue is removed by a direct molecular bond breaking process. The energy of a photon absorbed by the tissue can exceed the energy of molecular bonds in the tissue causing molecular fragments to be released without heating the tissue. As a high photon energy is required to perform this task, this process is usually only observed for short laser wavelengths in the U.V. region of the optical spectrum, such as those obtained from excimer lasers. However, it has been suggested that a similar process may occur at longer wavelengths by a multi-photon process[2]. As a result of the nature of the interaction, there is little or no thermal damage to the remaining tissue. Use of this interaction is currently being made in eye surgery where part of the corneal surface is precisely ablated by UV laser light without causing thermal damage to correct refractive errors of the eye[3].

At longer wavelengths, in the visible through to the infrared portion of the optical spectrum, the interactions observed in tissue are typically photothermal. Light absorbed by tissue raises the local temperature possibly leading to changes in the tissue. Before the advent of lasers, Henriques established that the degree of heating, and the time over which the heating takes place, determines the biological effect observed[4]. The changes in tissue due to heating can be divided into three regions: coagulation, vaporisation and carbonisation. When tissue is heated, the cells are

disrupted and proteins are denatured. The tissue contracts, which in vascularised tissue can cause the blood supply to be halted. The net effect of these processes is the condition called coagulation. When coagulated, the tissue optical properties are modified[5] and the tissue whitens. The coagulated tissue is eventually replaced by scar tissue.

Continued heating of coagulated tissue leads initially to further water loss through evaporation from the tissue surface, and then to carbonisation of the remaining material. The carbonised layer absorbs most of the laser light falling on it and, without water present to act as a heat sink, is raised to above 100°C. Heat generated in the carbon layer is then carried away by convection from the tissue surface and by conduction into the tissue, extending the zone of coagulation as well as the zone of carbonisation.

Coagulation is cell death, which may be a desired result. However, it may also extend the healing period. Extension of the healing period is also caused by carbonisation although, due to the nature of the residue, the time taken for the healing process to remove carbonised tissue is greater than for coagulated tissue. The extended time taken for a lesion to heal also means that the risk of infection is higher. Therefore, it is seldom desirable to take tissue beyond a state of coagulation to the point of charring.

Where laser energy is absorbed in a small volume of tissue, or where the intensity with which it is delivered is high, the local temperature can be raised sufficiently high that any further input of energy provides the latent heat required to cause vaporisation. In addition to mass removal by vaporisation the process can be enhanced by the explosive vaporisation of intracellular water. The type of effect which occurs depends on the properties of the laser beam, such as its wavelength, duration and energy and the way in which it is absorbed or scattered within the tissue. As a general rule, weakly absorbed and weakly scattered wavelengths result in a larger zone of heating and lead to coagulation and ultimately carbonisation. Strongly absorbed or highly scattered wavelengths can provide the necessary energy densities to produce vaporisation with varying amounts of ablation and coagulation depending on the rate at which it is delivered.

The fourth type of effect observed in laser irradiated tissue is photomechanical. Although arising as a result of photothermal or photoablative processes, the effect is distinctly non-thermal. Laser energy deposited at high enough intensities can interact with the tissue surface via various thermal and non-linear

optical paths to produce a plasma. Light energy delivered during the lifetime of the plasma is absorbed via the inverse Bremsstrahlung effect[6] causing the plasma temperature to increase and the plasma to expand. The rapid expansion of the plasma is sufficient to produce a shock wave above the tissue surface which, in a liquid environment, is coupled into the tissue producing tearing or fracture[7]. An example of this is laser lithotripsy in which dye or Q-Switched Nd:YAG laser pulses are used to fragment urinary and biliary calculi *in situ*[8].

1.2 Propagation of Light in Tissue

The nature of the interaction observed depends on the total energy delivered and the way in which it is deposited in the tissue. Of fundamental importance is the wavelength which determines the depth to which the light propagates into the tissue. In soft tissue the penetration depth is determined by the attenuation properties of the main tissue constituents, these being blood, melanin and water, Figure 1.1. In the visible portion of the spectrum, water is transparent and blood and melanin determine the optical characteristics of the tissue. In a simple analysis the distribution of light in this spectral region can be described by a series of scattering and absorption events. The probability of a single photon being scattered or absorbed is quantified by the cross-sections, σ_s and σ_a respectively. For wavelengths between 590nm and 1.35μm, where scattering dominates[10], the light distribution incident on the surface of the tissue is rapidly modified as the light propagates through the tissue. In contrast, for wavelengths below 590nm the attenuation of light in tissue is dominated by absorption, and the intensity profile is preserved in the tissue. The amount of scattering and absorption which occurs determines the overall depth to which the light penetrates in the tissue as well as the distribution of the light within the tissue.

For the neodymium:YAG laser which has an output wavelength of 1.06μm the strong scattering results in a rapidly modified intensity profile and a depth of penetration in soft tissue of about 2.5mm[9]. The strong absorption by haemoglobin at the 514.5nm output wavelength of the argon ion laser results in a typical penetration depth, in contrast to the Nd:YAG beam, of only 700μm[9] with a negligible amount of beam spread due to scattering. Consequently, the argon ion laser is much better at depositing the high energy dosages required to achieve tissue vaporisation while the Nd:YAG laser is excellent for heating large volumes to temperatures at which coagulation occurs.

Beyond 1.35μm the tissue absorption curve is similar to the attenuation curve

for water, Figure 1.1, indicating that in this spectral region, attenuation is dominated by the tissue water content[10].

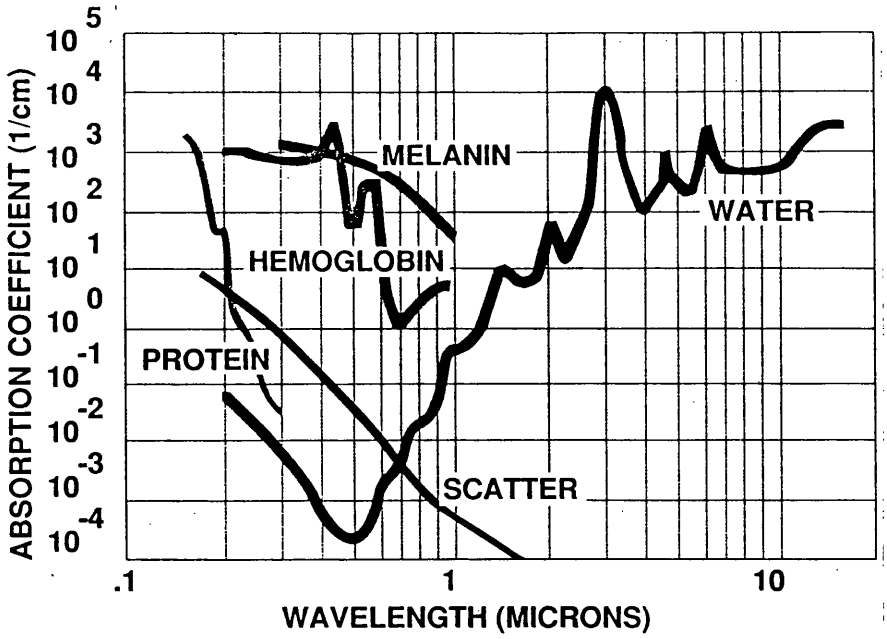

Figure 1.1 Absorption characteristics of the key constituents of soft tissue. (By kind permission of Coherent Hull Ltd).

Due to the strong absorption at these wavelengths, the effects of scattering can be neglected in models of light propagation, and the Lambert-Bouguer Law can therefore be applied to describe the reduction in light intensity with propagation distance into the tissue. The rapid attenuation and the absence of scattering means that these wavelengths are suited to heating small volumes of tissue in a precise zone so as to produce ablation with a minimal amount of coagulation.

1.3 Medical Infrared Lasers

Currently the most important lasers used in therapeutic laser surgery are the Nd:YAG and CO_2 systems which emit at 1.06μm and 10.6μm respectively. In a continuous wave (CW) mode both these lasers are capable of producing beams of up to 100W from compact systems, which is sufficient to affect large tissue volumes such as tumours[11]. The CO_2 laser is well suited to tissue ablation because of its strong absorption in tissue which, being due to the water content in tissue, is independent of tissue pigment. The strong absorption also results in a depth of thermal damage of about 100μm which is deep enough to cause haemostasis of small blood vessels while being shallow enough not to extend the healing period.

Besides the wavelength of the incident laser light, the depth of thermal damage can be controlled by the rate of energy delivery. If the energy is delivered in pulses, which are short compared to the time taken for the heat to be conducted away from the exposure zone, then all of the delivered energy will contribute to heating the exposed zone and not the periphery. If, additionally, enough time is left between the pulses for any residual heat left in the tissue by the preceding pulse, to be conducted away so that it represents only a background level of heating, then there will be no accumulation of delivered heat which would otherwise cause additional coagulation. The characteristic time for heat conduction to be significant may be given, for a one dimensional geometry, by[12]

$$\tau_{th} = x_a^2/4K \quad (1)$$

where τ_{th} is the thermal time constant and is defined as the time taken for the local temperature to fall to 1/e of its original value, x_a is the attenuation depth of the light in tissue and K is the thermal diffusivity of tissue. Thermal diffusivity is a measure of how quickly heat diffuses through a substance and equal to the thermal conductivity divided by the specific heat capacity and the density. To avoid heat diffusing into tissues outside the irradiated volumes the pulse duration, t_p, should be much less than τ_{th} and the interpulse (cooling) period much greater than τ_{th}.

Several authors have proposed suitable parameters for obtaining reduced thermal damage with the CO_2 laser beam[13,14] and currently several manufacturers offer a 'super pulse' capability on their systems in which trains of pulses, each approximately 10μs in duration are delivered at repetition rates set to minimise thermal damage and tissue charring. Other authors have described the clinical effects of pulsing the CO_2 laser claiming reductions in the depth of thermal damage from 50μm to 10μm[15]. However the 10.6μm wavelength cannot yet be transmitted through either solid or hollow optical fibres without unacceptable losses, risk of fibre fracture or the use of toxic substances. Therefore CO_2 lasers are presently restricted to beam delivery via articulated arms and direct line of sight applications and are most often found in specialities such as gynaecology and ear, nose and throat surgery.

Unlike the CO_2 laser, which uses a mixture of gases as the active medium and an electric discharge as the excitation method, the Nd:YAG laser is based on a solid state crystal in which neodymium ions are substituted for yttrium ions in crystals of yttrium aluminium garnet (YAG). The excitation source for these lasers is typically one or more krypton or xenon arc lamps. This combination provides for better long term reliability of the system. The Nd:YAG laser light output can be conveniently

coupled into small diameter optical fibres allowing delivery of the beam to areas under endoscopic guidance. The Nd:YAG laser is therefore ideally suited to endoscopic procedures which can be carried out through small incisions or natural orifices in the body thereby reducing the time taken for both the procedure and the post-operative recovery. However, due to the relatively low absorption at this wavelength, the Nd:YAG laser is not well suited to precise excision of tissues.

The low absorption and strong scattering of the Nd:YAG wavelength is an essential feature in the endoscopic control of bleeding gastric ulcers. The relatively large volume heated by the beam leads to contraction of the tissue around the bleeding vessel which rapidly constricts the blood flow and causes haemostasis, stemming the blood loss. The disadvantage of the Nd:YAG laser is that the reduction of the precision, due to strong scattering and weak absorption, can increase the depth of thermal damage during ablation procedures which can lengthen the healing time[16]. Despite these restrictions the 1.06μm beam is still often used for debulking tumours endoscopically where some of the tissue is coagulated by the laser beam and then left to slough away naturally. In some cases the degree of heating is enough to achieve vaporisation of the tumour during the procedure although sloughing is still the predominant mechanism of mass removal.

1.4 New Solid State Medical Lasers

1.4.1 Holmium lasers at 2.1μm

Due to an increased amount of interest by the military, who consider it potentially suitable for eyesafe rangefinding, much effort has recently[17] been expended in developing the multiply doped crystal Chromium:Thulium:Holmium (CTH) crystals which operate at 2.1μm. However, as a spin-off to this research, surgeons and medical laser physicists are beginning to get access to solid state laser sources which emit sufficiently far into the infrared to be strongly absorbed by the water in tissue but which can still be delivered through low OH silica fibres. Comparing the water attenuation characteristics of this laser wavelength with the 10.6μm emission from the CO_2 laser[18] it is seen that the CO_2 light is absorbed an order of magnitude more strongly, suggesting a less precise interaction with tissue for the CTH laser output. However, in early trials Lane et al[19] compared the *in vitro* response of soft tissue to a 2W CW CO_2 laser to the response to the 2.06μm emission from a cryogenically cooled CTH:YLF crystal at the same powers. Under identical operating conditions the authors observed identical ablation craters and thicknesses of thermal damage

indicating that identical lesions to those observed with the CO_2 laser can be created with a beam of 2.06μm light. This has led to the suggestion that CTH lasers may supersede the CO_2 laser due to the favourable fibre optic beam delivery possibilities.

Laser action at 2.1μm from the holmium ion was first reported by Johnson et al in 1962[20] although the crystal had to be cooled to cryogenic temperatures to avoid thermal population of the lower laser level. The addition of sensitisers such as erbium, which absorb over a larger portion of the flashlamp emission spectrum than the holmium ion, produced notable improvements in the efficiency[21,22] though cryogenic cooling was still required. Under cryogenic conditions, Beck and Gürs[23] achieved 50W continuous output at an overall laser efficiency of 5% and a slope efficiency of 6.5% which are amongst the highest efficiencies ever reported for CW solid state lasers. In 1985 the Russian, Antipenko, first indicated that practical room temperature operation could be achieved by the addition of chromium ions to enhance the absorption spectrum with thulium ions providing a means of transferring the absorbed energy from the chromium to the holmium via a cross-relaxation process[24].

The first reports by western researchers of room temperature pulsed laser operation with the scheme described by Antipenko occurred in 1987 when Storm reported on the room temperature performance obtained from a 3" x 4mm diameter crystal[25], achieving a reduction in the threshold of almost 50% compared to the erbium sensitised crystals and a slope efficiency of 0.7%. Subsequently, much effort has been expended in identifying the correct proportions of the constituents to use in doping the host[26] as well as investigating the different host crystals[27] to determine which combination offers an advantage in terms of improving the lasing efficiency even further. The result of these efforts is a large amount of data based on spectroscopic observations which has revealed many interesting features of the pump scheme. These include the process by which excited energy from the chromium levels is transferred to the holmium $^5I_7$ level via a two stage process in the thulium ion during which a single excited state Tm $^3F_4$ splits to produce two excited ions at the $^3H_4$ level[28]. Precise excitation using an Alexandrite laser[29] has revealed that the quantum efficiency of this process approaches 1.76 providing a considerable boost to the excitation process. However, although the pump scheme is well understood, successful theoretical modelling of the processes has not yet been demonstrated[30].

Practical demonstrations of the improvements in room temperature laser performance achieved by investigating the spectroscopy of the CTH mixture have been reported from a number of research groups. Of these the Naval Research Laboratories in Washington D.C. have reported[31] on the performance of a single

flashlamp pumped rod doped with 0.8% chromium, 5.76% thulium and 0.36% holmium from which they achieved a pulsed slope efficiency of 5.1% and laser threshold as low as 28J, leading to an overall efficiency of 2.8%. Teichmann et al[32] have also reported high room temperature efficiencies although their work was orientated to higher individual pulse energies achieving up to 17J pulse^{-1} from a crystal pumped with twin flashlamps. Both the high efficiency work by the N.R.L. and the high pulse energy work of Teichmann et al were carried out at a repetition rate of 1Hz and there has only been limited data on the operation of these systems at higher repetition rates. In their paper on the 17J laser Teichmann et al report on the performance of a system, with an output energy of 1.28J at 1Hz, as the repetition rate is increased to 4Hz, observing a reduction in the output with increasing frequency. This phenomenon is attributed, by them, to thermal population of the lower laser level, a fact supported by the work of Charlton[33]. However, Bowman et al report[34] on measurements of the thermal lensing of the YAG rod, used by Quarles et al at N.R.L., revealing lensing considerably stronger than that experienced with the Nd:YAG crystal. When Marion measured the thermal properties of CTH:YAG he found a factor of three reduction in the thermal conductivity of the multiply doped crystal[35] strongly suggesting that this was the reason for the extra lensing observed and possibly the real reason for the reduction in the laser energy reported earlier.

For this reason it was anticipated that high repetition rates and continuous wave operation would be difficult to obtain practically from simple 'rod and two mirror' resonators. However, Hamlin et al have recently reported[36] the results of experiments with CTH:YAG crystals mounted in special pumping chambers designed to place the rod and lamp within 8.5mm of one another. For 1Hz operation with a 5mmϕx6" long rod the slope efficiency was 5.5%, exceeding even that seen previously by Quarles et al, and resulting in an overall efficiency of an impressive 3.1%. For a smaller 3mm diameter rod similar pumping chambers (based on $BaSO_4$ as the reflector material) could be operated at repetition rates up to 25Hz with only a 20% reduction in the laser output energy compared to the 1Hz results. Smaller diameter rods may be expected to be more sensitive to thermal lensing because of the greater thermal gradient expected across the rod per unit of absorbed energy. However, Hamlin's work suggests that the lower capture angle between the flashlamp emission and the rod, combined with possibly improved cooling conditions, may allow the detrimental effects of thermal lensing to be contained at least under certain operating conditions.

The future of solid state lasers undoubtedly belongs to the diode laser which is capable of pumping laser crystals directly into the excitation bands of the crystal. For

the CTH:YAG laser this will bring a double benefit. First, direct pumping into the $^3F_4$ level will allow reduction in the amount of wasted energy deposited into the crystal lattice which ends up as heat causing thermal lensing while still allowing benefit to be gained from the two-for-one cross-relaxation process in the thulium. Secondly, direct pumping at 785nm into the thulium ion will remove the need for the chromium sensitiser. This will reduce the strain in the crystal caused by the chromium ion which distorts the lattice due to its larger size than the aluminium ion which it replaces. An improvement in the thermal transport characteristics such as the thermal conductivity, which depends on the integrity of the lattice to be efficient, should then be observed. Although slope efficiencies of between 19 and 52% have been reported for diode pumped CTH:YAG lasers, the powers are still in the milliwatt level and are insufficient for medical applications involving tissue ablation. It is believed that flashlamp pumping will remain dominant for at least the next five years until diodes become affordable enough to incorporate into commercial systems.

Recently, there have been reports of laser action from crystals doped with thulium and chromium only in which the active laser ion is the thulium. Pinto et al[37] have reported laser action in the wavelength range 1.945μm to 2.014μm, much closer to the local peak in the water absorption curve. However, laser efficiencies at the more strongly absorbed 1.945μm wavelength remain low, although Quarles et al[38] have reported pulsed efficiencies of the longer wavelength comparable to those reported for the Cr:Tm:Ho:YAG laser system[31].

1.4.2 Erbium lasers at 2.94μm

The longest laser wavelength currently available from a practical solid state laser is the 2.94μm emission obtained from erbium doped crystals. The absorption depth at this wavelength in water has been measured by Esterowitz at less than 1μm[39], several orders of magnitude less than either the CO_2 laser or the CTH:YAG laser thus implying an even more precise interaction with soft tissue than provided by either the 10.6μm or 2.1μm beams. However, the strong absorption by OH bonds in silica and glass fibres, means that this wavelength must either rely on fragile or non bio-compatible fibres[40] or, alternatively, articulated arm delivery. Despite this disadvantage the precision afforded by this laser has led to much interest in recent years and it has been optimistically described as the 'ideal medical scalpel'[18].

At infrared wavelengths, beyond 2.5μm, modelling of the interaction with tissue has a higher chance of success, due to the very rapid absorption and insignificance of any scattering effects. This is demonstrated by the elegant, but

simple, analysis, performed by McKenzie[41], who correctly predicted the typical depth of thermal damage in soft tissue, due to the CO_2 laser beam, to be 10μm. Such small zones of coagulation are typical of the lesions observed when tissue is ablated by short optical wavelengths such as those obtained from excimer lasers which are said to ablate tissue by producing single photons with enough energy to break the molecular bonds which hold the tissue together[42]. The first suggestions that processing tissue with the erbium laser would be similar to the results with excimer lasers were made by Esterowitz in 1985[43] and subsequently more detailed comparisons have been performed[44] which have confirmed this early hypothesis.

Due to the strong absorption of the erbium laser light by soft tissue it has been easier to carry out detailed experiments to evaluate the mass removal ability of the erbium laser. The experiments may be carried out using a variety of techniques which provide quantifiable data on the performance allowing more reliable comparisons to be drawn across the range of experimental set ups and tissue types. Amongst these have been techniques developed by Walsh and Deutsch of mass loss[45] and time to drill[46] both of which, at the energy levels available, have revealed an efficient process of ablation at 2.94μm, which in soft tissue is linear with increasing pulse energy density[46]. However for hard tissues, such as bone, the rate of ablation becomes sublinear beyond a threshold where plasmas occur and is believed to be due to the plasma blocking the incoming light leading to a reduction in the ablation[47]. Walsh et al have also speculated that dessication of the hard tissue may also reduce the ablation efficiency although plasma blocking appears the primary cause[46].

The erbium ion emits at a number of key wavelengths although it is its emission at 2.94μm at one of the peaks of the water absorption curve which has resulted in the interest from the medical physics community. As a dopant into laser crystals, erbium is ideal because of its size which is comparable to the yttrium it replaces in the YAG crystal. This allows it to be doped into the host at relatively high concentrations (about 50%) by comparison with neodymium which can only be doped up to approximately 1.4% before significant distortion of the lattice occurs. The broad absorption bands of the crystal, which overlap well with the emission from the output from xenon flashlamps, add to this crystal's beneficial features. However under normal conditions the laser process would be considered as a self-terminating four level scheme due to the lower laser level which is longer lived than the upper laser level by an order of magnitude[48]. True four level laser action is obtained without termination of the scheme as a result of a cross transfer process which depletes the lower $^4I_{13/2}$ level creating an excited state in the $^4I_{9/2}$ level. This is equivalent to a photon of approximately 800nm being absorbed and can contribute

again to populating the upper laser level[49].

The quality of the crystals available has delayed the development of erbium lasers. Although the first reports of stimulated emission at 2.94μm are recorded in 1975 by Zharikov[48] it was not until 1987 that powers of practical significance were reported by Frauchiger et al who achieved energy levels in the region of 300mJ for a Fixed-Q mode[50]. In the intervening years several researchers speculate on the beneficial[51,52] and detrimental[48] effects of impurity ions although currently none are purposely included to enhance the pump process. The practical observations made by Frauchiger and subsequent work by researchers at the Schuster Laboratory at the University of Manchester indicate that higher average powers and high repetition rates from the erbium based lasers may be limited by thermal effects, such as lensing which is twice as strong as identical crystals doped with the neodymium ion[50]. However, Charlton et al have recently demonstrated thresholds as low as 32J and laser slope efficiencies as high as 2.8% which leads to the speculation that repetition rates up to 40Hz may be practical[53].

For both the holmium and erbium crystals there exist only limited data on the performance of practical systems, particularly of a form which provides answers to the key questions in the design stages of the system, namely the effects of external influences such as temperature, and more importantly details of thermal effects within the crystal which contribute to the thermal lensing of the crystals. The last mentioned has so far prevented successful modelling of laser resonators using these crystals.

1.4.3 Other solid state lasers

Besides lasers based on holmium and erbium ions, there are other laser sources for which there will be an increasing level of interest in the future. Amongst these, the most noteworthy are the Ti:Sapphire, Alexandrite and Cr:Tm:YAG lasers. Both the Ti:Sapphire and the Alexandrite lasers are tunable sources and, as such, are likely to have most impact in the clinical areas now dominated by dye lasers. Both lasers also tune in the visible to near-infrared region of the optical spectrum and, consequently, are useful mainly to selectively excite pigmented tissues. Currently, the main medical application of the Ti:Sapphire laser is for tissue excitation in fluorescence spectroscopy, while for the Alexandrite laser the main applications, currently, are treatment of skin lesions, such as tattoos, and lithotripsy.

Development of the Cr:Tm:YAG laser is still very much in its infancy and crystals of this material are more difficult to obtain than either Cr:Tm:Ho:YAG or

Er:YAG crystals. However, the laser output, which, at about 2μm, is closer to the local peak in the water absorption curve, will surely be of use in future therapeutic laser systems, particularly as the output may be delivered to the treatment site via conventional all-silica optical fibres. This laser is also tunable over a small wavelength range close to the water absorption peak, although with much reduced efficiency. Therefore, it may be anticipated that this laser may eventually find a use where low powers are required and a greater degree of control over penetration depth is seen as an advantage. In therapeutic medicine, this may be in coronary angioplasty or similar procedures.

Despite the promising futures for these laser sources, they are not included in this work due either to their lack of availability or the unsuitability of their output power or wavelength to the subject of the work in this thesis, namely the ablation of soft tissue.

1.5 The Research and its Objectives

The purpose of the work in this thesis is two-fold. Firstly it aims to improve our understanding of the holmium and erbium lasers to allow the design and construction of practical devices for medical applications. Implicit in this work is establishing the predictability of the performance of the lasers using general laser theories verified by experimental work. Of key interest is the beam divergence of laser resonators containing these laser crystals as this determines the spotsize which can be obtained for a given focusing lens, and the modelling of conceptual systems. Consequently, the lensing which occurs in the crystals due to pump pulse energy lost to the lattice is determined experimentally and subsequently used to predict the performance of a conceptual resonator. The conceptual resonator is then constructed and the divergence measured over a range of parameters. A comparison is made between the real and modelled case to verify the predictions.

The holmium laser is often referred to in the literature as being a three level[33] or quasi-three level[54] system. To clarify the discussion which arises from this description theories for the delay time taken from the start of the excitation pulse to the start of the laser pulse for three and four level systems are developed and used to assess whether a three or four level scheme offers a more appropriate description of the laser. Additionally, these theories are used to show whether it is possible to predict the delay between the start of the excitation pulse and the laser output pulse. The reason for describing the holmium laser scheme as three level is the dependence

of the laser threshold on the temperature of the coolant water. The magnitude of this effect is investigated and the rate of change compared to a theory based on changes to the Boltzmann population of the lower laser level. Because the predictability of the laser in key areas such as temporal performance and its dependence on variations in the coolant temperature is equally important to any laser system, the analyses carried out for the holmium laser are repeated for the case of the erbium laser.

The characterisation of lasers for tissue ablation must consider practical aspects of beam delivery. For the erbium laser this work has been carried out previously by Whitehurst et al[55] who reported on the different transmission losses obtained for a range of fibres designed to operate at the 2.94μm erbium laser wavelength. To fill the gap for the 2.1μm beam, the transmission losses measured for small diameter low OH silica fibres are reported.

Due to the deeper penetration of the 2.1μm holmium laser light compared to the 2.94μm erbium laser light, consideration is given to ways of reducing the extent of the resulting thermal damage. Cross[56] established that a reduction in the depth of thermal damage could be obtained by delivering the output of a 1.06μm Nd:YAG laser in Q-Switched rather than Fixed-Q pulses, and this fact provided the impetus to consider Q-Switching the holmium laser. Although no tissue experiments were carried out at the holmium wavelength due to crystal damage which occurred at useful Q-Switch output levels, experience was gained as a result of Q-switching using an intra-cavity electro-optic crystal. The results of this work are presented briefly to identify the difficulties in operating such systems.

The second aspect of the work in this thesis is to assess the ability of each of the laser wavelengths to ablate soft tissue, and to consider further the efficiency with which this process is achieved. The laser wavelengths obtained from the holmium and the erbium lasers are strongly absorbed in soft tissue due to the high water content. The transfer of light energy to heat energy in such small volumes results in rapid heating which is sufficient to cause explosive vaporisation of the tissue. Previously the pulse energy levels available from these lasers have meant that to achieve ablation from a single pulse, it was necessary to focus the laser light to small spots of less than 1mm diameter. The high pulse energies available from lasers developed during this work have allowed laser ablation of soft tissue to be investigated at fluences comparable to those used by previous workers but with larger beam diameters. These conditions reveal new information about the accuracy and efficiency of the ablation of tissue with light from holmium and erbium based lasers.

Because the propagation of both wavelengths in tissue is dominated by absorption, the mass-loss technique is applied to assess qualitatively the capability of each to remove tissue mass. The efficiency is assessed in absolute terms for a number of different parameters at both laser wavelengths and then compared in relative terms to the mass loss expected from a pure water target. This allows the ablation performance of 2.1μm and 2.94μm light to be compared and contrasted. Also, by comparing the mass of tissue removed with that expected for a pure water target, the efficiency of the mass removal process can be assessed. The energy deficit identified in this manner leads on to an investigation of possible, non-ablative routes for energy consumption. The maximum velocities of the particles leaving the ablation site are measured and used, in conjunction with the mass loss data, to calculate the amount of laser energy converted to kinetic energy. The results of this are followed by further investigations into the possible routes of energy 'loss'.

The characterisation of high pulse energy erbium and holmium lasers at repetition rates above 1Hz is reported. These new areas of operation allow access to new regimes of tissue ablation with lasers. The work of others is extended to quantify the efficacy of these lasers in ablating tissue in these new operating regimes. The routes by which energy not consumed in raising the tissue to the vaporisation temperature is dissipated are investigated.

CHAPTER 2

Development of the Holmium Laser

2.1. Introduction

2.1.1 Historical review

Laser action at 2.1μm from the $^5I_7$ level of holmium was first reported by Johnson et al in 1962[20]. The narrow absorption bands of the holmium ion, though, were unsuitable for efficient flashlamp pumping. In 1966, Johnson et al reported[21] on improved laser performance from the holmium ion in which flashlamp light was absorbed and transferred to the holmium ion via erbium, ytterbium and thulium ions. The main reason for the improvement was the broad absorption in the visible region of the optical spectrum of the erbium ion and a cross-relaxation process which transferred excitation to thulium and then to the upper laser state of holmium. However, efficient laser operation was limited to cryogenic temperatures due to thermal population of the terminal laser level, the highest sublevel of which lies at only $\approx 530 cm^{-1}$ above ground.

In the 19 years following Johnson's early observations, there were no further reports of a multiply doped crystal in which erbium, ytterbium and thulium are used to transfer flashlamp energy to holmium, only those in which erbium and thulium are used. There is no documented evidence for the exclusion of the ytterbium ion although a likely reason would be the absorption bands of the ytterbium ion which, being centred around 0.9μm, may have been considered to be beyond the output spectrum of the pump sources therefore making its presence unnecessary.

The sensitivity of the Er:Tm:Ho:YAG crystal, also known as alpha-beta ($\alpha\beta$) and alphabet holmium:YAG, to temperature was demonstrated by Remski and Smith[57] by measuring the changes in the laser threshold energy between 90K and

300K. A slow rate of change below 200K produced thresholds for a 50mm x 3mm diameter αßHo:YAG crystal, pumped with a xenon flashlamp, of about 8J. However, above 250K the rate of change increased rapidly resulting in thresholds in the region of 70J at 300K indicating the very strong dependence on temperature. Additionally, Johnson et al identified[21] that, as a result of the changes in thermal population of the lower laser level, different transitions were observed depending on the operating temperature.

Despite the laser thresholds which increase with temperature, Chicklis et al reported respectable room temperature operation of αßHo:YLF in both Fixed-Q and Q-Switched modes[58]. Using a rotating mirror to modulate the resonator losses, Q-Switch energies in excess of 500mJ were obtained for flashlamp discharge energies of only 100J. The authors attribute this performance to the insensitivity of the fluorescent lifetime of the upper laser level to temperature in YLF allowing a greater amount of energy to be stored. When Chicklis et al compared the Fixed-Q mode performance of the alphabet mixture in YLF and YAG hosts[59], they observed slope efficiencies in YLF over twice those observed in YAG. Additionally the YAG was found to suffer from internal damage far sooner than the YLF crystal prompting them to encourage further work on the αßHo:YLF based lasers.

Continuing work at cryogenic temperatures continued to show the promise of the sensitiser scheme. Moving from Fixed-Q operation of HoF_3[60] to continuous-wave operation of αßHo:YAG at 77K, Devor et al[22] achieved 20W average output power at an overall efficiency of 4%. Using a rotating mirror Q-Switch, over 70% of the CW power was obtained in a series of spikes 100-300ns in duration, further emphasising the excellent energy storage capabilities of the system. Further increases in the CW operating efficiency were subsequently reported by Beck and Gürs[23] who recorded an output of 50W and a 6.5% slope efficiency from an αßHo:YAG crystal, cooled to 77K with liquid nitrogen. To date this remains one of the most efficient, lamp-pumped, CW laser ever reported.

Despite the recommendations of Chicklis et al, investigative work continued on the sensitised Ho:YAG crystal, alongside that with the YLF crystal, due to the favourable reports by Beck and Gürs and the better high power handling characteristics compared to YLF, although cryogenic cooling was still required[61,62].

The most significant breakthrough in the development of a room temperature system operating around 2μm occurred in 1985 when Antipenko[24] published the first results of room temperature operation of a YAG crystal doped with chromium in

place of erbium. For the first time, room temperature operation comparable to that obtained previously only for the YLF crystal was combined with the better thermo-mechanical characteristics of the YAG crystal. Since 1985 further improvements in the laser efficiency have continued to be reported, most, though not all, relying on the chromium:thulium:holmium:YAG (CTH:YAG) crystal.

Following the early reports by Russian researchers[24,63] the first reports by western groups using flashlamp pumped CTH:YAG occurred in 1987 when Storm et al[25] reported a 0.75% slope efficiency and a 45J threshold energy for a 3"x4mm ϕ crystal. To maximise the flashlamp light absorption and the energy transfer, but to minimise the reabsorption by the holmium ion, the concentrations of the dopants were selected to be 2.5% chromium, 5.6% thulium and 0.36% holmium.

Rosenbaum et al[64] followed up the work of Storm et al by investigating the role of chromium in the sensitisation process and the effect of the host material. Compared to YSAG and YSGG host materials, the YAG host was found to provide superior cross transfer of the excitation energy to the thulium levels thereby leading to improved laser performance. By reducing the chromium concentration to only 0.8%, slope efficiencies up to 3.8% were observed for free-running mode operation with a similar threshold to that reported previously by Storm et al. The authors cite the reduction in thermal effects with a reduction in the chromium concentration. From the considerations of Duczynski et al[28], though, the effects were probably also due to better cross-relaxation between the chromium and thulium ions due to a reduction in the lattice strain which is caused by the substitution of chromium ions into the aluminium sites, the former having a significantly larger ionic radius than the aluminium which it replaces. The pursuit of hosts in which large amounts of chromium can be incorporated without suffering lattice distortion effects has been reported[28] although YAG remains the most common host due to its better thermo-mechanical properties.

Further improvements in the laser performance were reported soon after the work of Rosenbaum et al by the same team of researchers (and the same labs' in which Storm's work was carried out). Slope efficiencies of 5.1% and laser threshold energies as low as 28J were reported by Quarles et al[31,65]. The dopant concentrations in this system were identical to those used by Rosenbaum et al with the improvements arising from the choice of a focusing geometry pumping chamber in contrast to the diffuse nature of the pumping used by Rosenbaum et al.

Despite increasing efficiencies and pulse energies which, under exceptional

circumstances, approached 17J[32], operation at repetition rates above 1Hz was limited. Moulton et al commented on the reason for this in their posted paper at CLEO in 1989, measuring induced thermal lensing significantly stronger than that observed in the Nd:YAG crystal. However the dependence of the population of the terminal laser level has led some researchers[32,33] to suggest that heat accumulation is principally responsible for reductions in output energy observed at higher power loadings. Recently, the lensing parameter has been measured for a CTH:YAG rod[66] at between 4 Dioptres kW^{-1} and 7.2 Dioptres kW^{-1} which supports the observations made by Moulton et al of thermally induced lensing much greater than that reported for neodymium doped YAG. In the first, and long overdue, measurements of the thermo-mechanical properties of the CTH:YAG crystal, Marion[35] measured the thermal conductivity of the CTH:YAG crystal at 0.0664 W cm^{-1} K^{-1}, approximately half of the thermal conductivity of Nd:YAG. This explains, in part at least, why a higher degree of thermal lensing is observed for the CTH:YAG crystal compared to the Nd:YAG crystal.

The restrictions which strong thermal lensing place on laser resonator design can be overcome to allow high repetition rate operation of Fixed-Q CTH:YAG lasers. Becker et al[67] have demonstrated operation at repetition rates up to 21Hz without significant reductions in either the laser threshold energy or the slope efficiency using small diameter rods. This is in apparent contradiction to the theory of thermal lensing which predicts shorter induced focal lengths in smaller diameter rods. Thus, resonators containing smaller diameter rods would be expected to be more sensitive to thermal lensing than resonators containing larger diameter rods. However, Becker's results show that high repetition rate operation in small diameter rods can be achieved, due probably to a combination of improved cooling conditions around the smaller rods and the lower fraction of total flashlamp light being absorbed by the laser crystal. The significant results of Becker et al are only marred by their suggestion that it is necessary to obtain a critical, elevated temperature within the laser rod before efficient operation can be achieved. The effect on which this claim is based, namely the maximum output energy being obtained at 9Hz rather than repetition rates at either lower or higher rates, is almost certainly due to optimisation of the resonator performance as thermal lensing allows an increasing number of transverse modes to oscillate in the resonator, thereby extracting the energy stored in the rod more efficiently. Beyond the 9Hz operating level, the resonator is simply beginning to exhibit 'rollover', a familiar phenomenon in continuous wave Nd:YAG laser designs[68] where strong lensing takes the resonator out of a stable condition and the number of transverse modes drops again, thereby reducing the efficiency of the energy extraction.

Recently, Hamlin et al have presented results[36] which improve on both the efficiency and repetition rate performance previously reported by Quarles et al and Becker et al respectively. Returning to a diffuse pumping chamber, but of a different design to that used by Rosenbaum, slope efficiencies of 5.5% are reported for a 6"x5mmϕ rod doped to the now standard dopant concentrations described earlier[31,64,65]. Using filter glasses in the pumping chamber to filter flashlamp light that would otherwise only contribute to heating the laser crystal, repetition rates up to 25Hz are reported, again with a small diameter rod, with only a 12% reduction in the output energy compared to the 1Hz laser performance.

Despite reports of laser action at 2.1μm from the holmium ion as long ago as 1962, it is only since 1985 that progress has been made towards efficient room temperature operation. Several research groups have reported on the performance of laser crystals based around the holmium ion in YAG, sensitised with chromium and thulium. However, the data gained from these systems is, in some cases, incomplete and in others needs corroboration.

2.1.2 Spectroscopy and Pump Scheme

The addition of chromium and thulium to crystals containing holmium enhances the absorption bands in the visible region of the optical spectrum. Figure 2.1 shows the key levels in the chromium, thulium and holmium which play a part in the laser process.

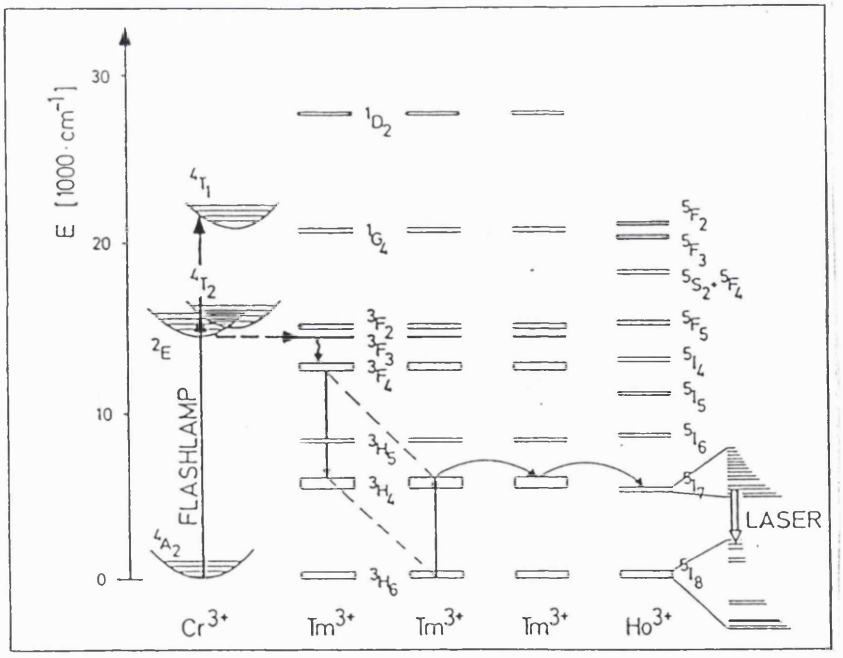

Figure 2.1 Pump scheme of the Cr:Tm:Ho:YAG laser (after Teichmann et al[32])

Most of the flashlamp light is absorbed by the broad $^4A_2 \rightarrow {}^4T_1$ and $^4A_2 \rightarrow {}^4T_2$ transitions in chromium which overlap well with the discharge spectrum obtained from pulsed xenon flashlamps, Figure 2.2. Non-radiative relaxation from these levels[27] to the ^2E chromium level is followed by a mixture of radiative and non-radiative energy transfer[69] to thulium, via the $^3F_3$ level, to excite the $^3F_4$ level. Although a mixture of transfer processes, Armagan et al have shown that the radiative parts of the processes account for only 3% of the total transfer and consequently the sequence is often described as being non-radiative[34]. Accurate data on the transition time between donor and acceptor levels in Cr and Tm is not available for a YAG host. However, Alpat'ev et al[70] have reported that, for a GSAG host, 90% of the chromium excitation is transferred in approximately 10μs. It might be assumed that the transfer time in a YAG crystal would be either similar or less due to its stronger crystal field. However, Bowman et al[71] are only able, from observation of the gain recovery following Q-Switching, to predict a transfer time less than 100μs.

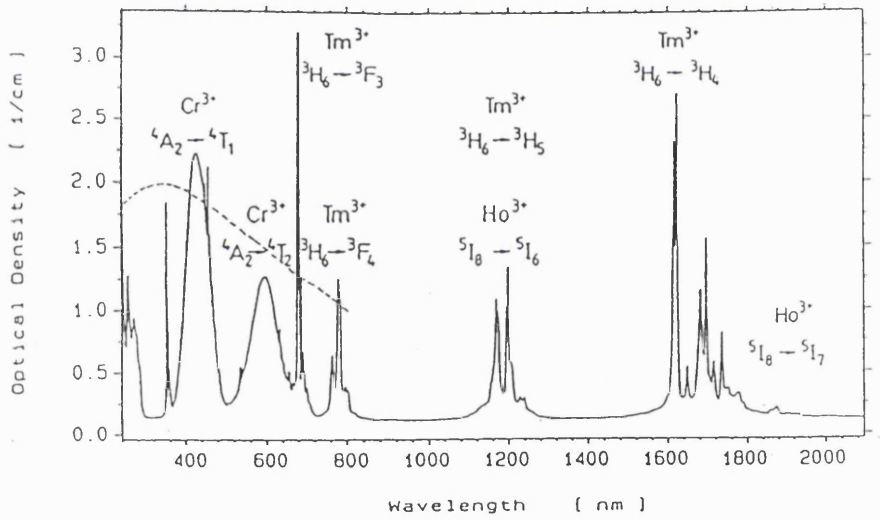

Figure 2.2 Cr:Tm:Ho:YAG absorption spectrum and emission envelope of xenon flashlamps (after Teichmann et al[32])

The $^3F_4$ level then cross-relaxes with the $^3H_6$ level to produce two excited $^3H_4$ states. Again there is no data on the characteristic time for this splitting to take place in YAG and it is necessary to assume a similar value to the 20μs reported for a YSAG host by Alpat'ev[70]. A final cross-relaxation process then takes place between the Tm $^3H_4$ level and the $^5I_7$ level in holmium which is the upper laser level for the 2.1μm laser transition. Using an Alexandrite laser, operating at 0.785μm, to selectively excite the $^3F_4$ thulium level, Kintz et al have shown[29] that the quantum yield in the upper laser level of holmium, as a result of the two-for-one process in thulium, is as high as 1.76. Thus, thulium plays a vital role, not only in transferring

the energy absorbed by the chromium to the holmium ions, but also in enhancing the efficiency. In so doing, this process also reduces the amount of heat generation in the crystal.

There has been much discussion on the degree of coupling between the Tm $^3H_4$ and the Ho $^5I_7$ levels[72,73]. Fan et al[74] have shown that the Tm $^3H_4$ and Ho $^5I_7$ states are thermally coupled, i.e. a Boltzmann statistical analysis is adequate to describe the relative populations. Fan et al[74] and Bowman et al[71] are in general agreement that the thermalisation time is approximately 20μs although Noginov claims characteristic times of 200μs and 667μs for Tm($^3H_4$)→Ho($^5I_7$) and Ho($^5I_7$)→Tm($^3H_4$) respectively[75]. A practical result of this is that the recovery time of the $^5I_7$ level will limit the number of Q-Switch pulses which can be extracted, at reasonable power levels, from a 300μs long Fixed-Q pulse, to approximately three (assuming 100μs are required to fully recover the gain from reference[71]).

The $^5I_7$ is split into 15 Stark components although only a few of the lower sub-levels contribute to the laser process[71]. Bowman et al have observed laser action at nine distinct wavelengths between 2.080μm and 2.128μm and have additionally identified the energy of the sublevels of the manifolds between which the laser action occurs. Their data is reproduced in Table 2.1.

Wavelength (μm)	Upper State (cm^{-1})	Terminal State (cm^{-1})
2.1275	5221	522
2.1207	5221	503
2.1107	5242	503
2.1051	5242	492
2.0963	5224	458
2.0899	5242	458
2.0883	5242	452
2.0839	5296	501
2.0803	5224	418

Table 2.1 Laser transitions in Cr:Tm:Ho:YAG identified by Bowman et al[34].

Laser action from the $^5I_7$ level in holmium terminates in the $^5I_8$ manifold, which is also the ground state of the holmium ion, consequently the terminal laser levels are

all strongly influenced by temperature with the level of occupancy determined by Boltzmann statistics. Ashurov et al[76] predict the existence of 17 Stark sublevels of the terminal laser level although only 11 of these have been identified. The high thermal population of the $^5I_8$ manifold means that laser inversion is mainly obtained between the upper levels. Consequently, laser transitions emanating from the $^5I_7$ levels tend to terminate in the higher levels of this manifold.

Under diode laser pump conditions Fan et al have observed[74] that the intensity of the fluorescence from the Ho $^5I_7$ manifold reduces with increasing pump intensities. This has been attributed to an upconversion process which depletes the $^5I_7$ level and populates the $^5I_5$ level using energy released as a result of the decay of the Tm $^3H_4$ level to ground, Figure 2.3 Excitation lost to the $^5I_5$ level is then transferred to the Ho $^5I_6$ level, before cross-relaxing to the Tm $^3H_5$ level and then to the Tm $^3H_4$ level which may either decay or contribute to the pump process. Under flashlamp pumping conditions, Bowman et al have also observed evidence of a loss mechanism[34]. This was evident in a sublinear dependence of the excited fraction of the holmium ions with the flashlamp pump density, calculated from gain measurements. The action of a loss scheme is also evident by the reduction in the fluorescence lifetime of the Ho $^5I_7$ level which falls, almost exponentially, from 9.0ms at an interpolated zero pump intensity level, to about 2ms beyond pump densities of 200 J cm^{-3}.

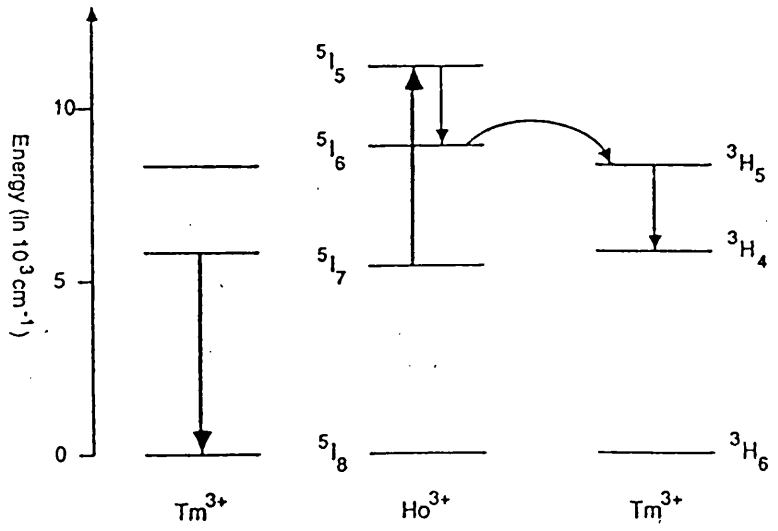

Figure 2.3 Schematic of upconversion loss process proposed by Fan et al in Ref. [74]

Bowman et al[34] have also observed that the emission wavelength is a function of the output mirror reflectivity. In their experiments, the laser wavelength became progressively shorter as the reflectivity (which is assumed to have a flat response

with wavelength over the operating range) was reduced. According to the authors, this is due to the difference in the emission cross-sections and the thermal populations. Additionally, at pump energies above threshold, operation at a single laser wavelength persisted due, allegedly, to clamping of the upper laser level population which depletes the upper levels of the competing transitions.

2.1.3 Effect of rod dopant concentration

The concentration of each of the three dopants in CTH based laser crystals plays a key role in the efficiency of the system. With such a complicated sensitisation and cross-relaxation process leading to population of the upper laser level it is not surprising that much research, both theoretical[26,69,73] and practical[65,74], has been required to optimise the laser performance. Indeed, it is thought that different concentrations may be needed according to the use of the laser[77], eg. between Fixed-Q and Q-Switched laser performance[77]. The improvements which can be gained from the judicious choice of dopant concentration can best be exemplified by the improvement in performance gained by the group at the Naval Research Laboratories (NRL) in Washington DC. By the reduction in the amount of chromium present in a YAG host from 2.5% to 0.8%, Rosenbaum et al[64] achieved a fourfold increase in the slope efficiency compared to that reported previously by Storm[25].

The general rules for the relative concentrations of the three dopants have been discussed by several researchers[27,32]. In summary:

i) A moderate concentration of chromium ions is required to absorb all of the flashlamp light incident on the crystal. However, the concentration must not be so high as to prevent pump light from reaching the centre of the rod and creating a non-uniformly distributed population inversion. Nor should the concentration of chromium ions be so high as to distort the lattice which increases the probability of energy loss by phonon emission, thereby reducing the cross-relaxation efficiency and impairing the thermal properties of the crystal.

ii) A high concentration of thulium ions is required to maximise the cross-transfer of energy from the chromium to holmium ions. Additionally the two-for-one process of thulium excitation relies on diffusion between adjacent thulium ions thereby inferring the need for high concentrations. Conversely, the thulium level, being thermally linked to the $^5I_7$ holmium level, may adversely affect the laser threshold by providing a de-excitation route for laser light reabsorbed by the holmium ions.

iii) Because the terminal laser level is thermally populated at room temperature, the

holmium population must be kept low to avoid reabsorption of the laser wavelength.

Currently, the two main suppliers of CTH:YAG crystals supply crystals to the dopant concentrations used successfully by Quarles et al[31] and Fan et al[74]. The crystals used in the work for this thesis were obtained from both suppliers having the dimensions and standard dopant concentrations as given in Table 2.2. The host crystal was Yttrium Aluminium Garnet (YAG) chosen because of its superior thermo-mechanical characteristics and its general availability.

Rod 1	3" x 5mmϕ Supplied by Litton Airtron [Charlotte, NC, USA]	
Rod 2	4" x 4mmϕ " " " " "	
Rod 3	4" x 4mmϕ " " " " "	
Rod 4	3" x 5mmϕ Supplied by Union Carbide [Roditi Corp. Ltd, UK]	
	Litton	Union Carbide
Chromium	0.85at% ($8.18 \times 10^{19} cm^{-3}$)	1.00at% ($9.62 \times 10^{19} cm^{3}$)
Thulium	5.90at% ($8.20 \times 10^{20} cm^{-3}$)	5.76at% ($8.01 \times 10^{20} cm^{-3}$)
Holmium	0.36at% ($5.00 \times 10^{19} cm^{-3}$)	0.36at% ($5.00 \times 10^{19} cm^{-3}$)

Table 2.2 Dimensions and dopant concentrations of rods used in experiments

The laser performance of rods having identical dimensions but differing in the dopant concentrations (a result of having been sourced from different suppliers) was compared under identical operating conditions. The 3"x5mmϕ rods (Rod No.1 and No. 4) were operated consecutively at 1Hz in a resonator 455mm long. The rods were pumped by the discharge from a xenon flashlamp, having an arc length 67mm and an arc diameter of 4mm. The pumping chamber was made from Spectralon and was inspected both before and after use to ensure degradation of the reflector surface did not influence the results (see Appendix 1).

Figure 2.4 shows that, at a constant temperature of 20°C, for a given input energy, more laser output was obtained from rod No. 1, being the one containing lower concentrations of both the chromium and thulium ions. The difference in the slope efficiencies of the two rods is 2.2% and the difference in the laser thresholds 5%, neither of which is large compared to the error in the measurement.

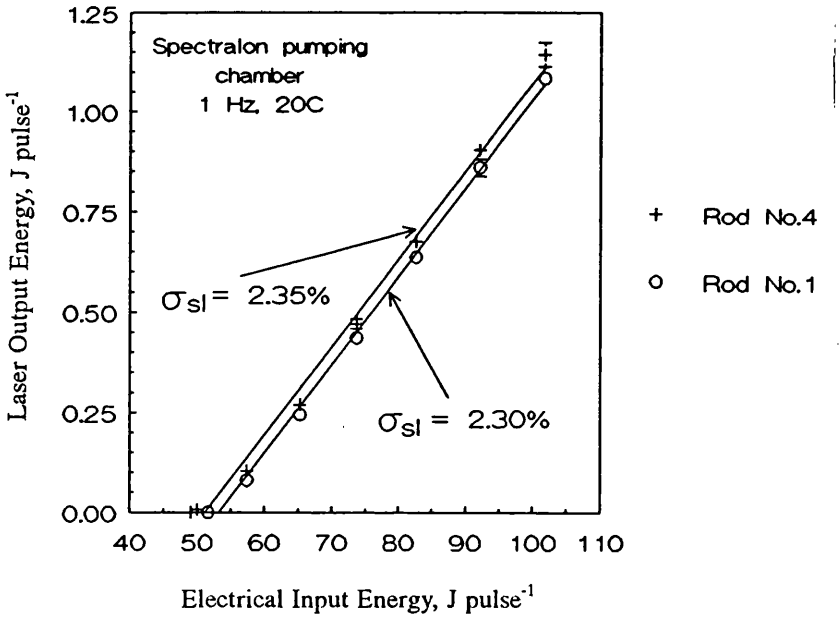

Figure 2.4 Laser output energy obtained from rods from different suppliers, the rod dimensions and excitation conditions remaining constant.

It can be concluded that there is no noticeable difference in the laser efficiency of the rods from the two suppliers. Although Rosenbaum et al[64] observed a large increase in the laser efficiency over the results of Storm et al[25] for a decrease in the chromium concentration, the differences in chromium between the two rods examined here are small compared to those changes. Thus, the similar results obtained for these rods does not contradict the findings of those earlier workers.

This result is also in keeping with the experimental data of Armagan et al[26] who found that chromium to thulium transfer rates were not greatly affected by increasing the chromium concentration. In this case, the percentage difference in concentrations is greatest for the chromium ion rather than the thulium ion which changes by only 2.5%, compared to the 17.5% change in the chromium concentration, and can therefore be considered as a constant.

2.2 Performance Optimisation

To optimise the performance of a laser, it is first necessary to identify the variables within the system. Next, it is necessary to determine which of the variables are truly variable throughout the characterisation process, that is, which aspects of the design can be varied throughout the study and which need to be fixed early on because of the

difficulty and expense involved in altering them later on. Finally, it is essential to specify what parameter is being optimised. Preceding work has concentrated on increasing the room temperature laser efficiency and it is the aim of this work to extend the understanding of each of the key variables on this aspect of the laser performance. It is also the object of this work to investigate the reasons why, under some conditions, this performance cannot always be obtained. Outside the scope of the variables considered here are the dopant concentrations which, being the subject of much work by other groups, has lead to a standard set of dopant concentrations being offered by the main suppliers of CTH:YAG crystals. Additionally the investigations of the effect of pump pulse duration beyond the limits of standard capacitor discharge circuitry was not considered because of the necessary development of the power supply which would be beyond the practical scope of this work. The following subsections detail the optimisation and characterisation of the CTH:YAG laser with the 'once only' variables.

2.2.1 Pumping chamber and flashlamps

The object of the pumping chamber is to transfer the flashlamp pump light to the crystal in order to create a population inversion within the crystal. Ideally, light which does not contribute to the pumping process should not be transferred. However, attempts to selectively filter out unwanted pump light, without loss of overall laser efficiency, have, so far, proven unsuccessful[36]. Quarles et al have used a silvered ellipse as a pumping chamber with the rod and flashlamp lying at each of the foci to ensure the maximum light transfer. However such chambers do not stay highly efficient due to tarnishing of the reflector surfaces which occurs with continued use. An alternative is to use a closely coupled chamber made from, for example, alumina ceramic which, despite being less efficient than the silvered ellipse, does not degrade with use and can be expected to operate without signs of deterioration for in excess of thirty years[78]. Other proprietary materials are becoming available, one of which is Spectralon (SRM-99LG, Labsphere Inc., North Sutton, NH, USA). However, there exists only sales literature on the performance of this material and no long term testing to establish its durability.

Recently, pumping chambers in which the 'reflector' is tightly packed $BaSO_4$ have become more widely available. The $BaSO_4$ is protected from the cooling water, which flows around the rod, by an oval section Pyrex tube which allows the powder, behind the tube, to be as close as possible to both the rod and the flashlamp. With the exception of the silvered ellipse the chambers detailed above represent a typical cross-section of chambers known as 'close-coupled diffuse' and which generally

provide a more homogeneous distribution of pump light in the rod due to the scattering which takes place in the material.

Despite the excellent results obtained by Quarles et al[31] using the silvered pumping chamber only chambers of a the close-coupled type were considered for use in the laser system. This was because of the lifetime problems associated with the metallic surface of the ellipse. Appendix 1 details the experimental work to determine the most efficient pumping chamber for use with the CTH:YAG crystal. The results of this work showed that the Spectralon chamber gave approximately 10% more laser output than the $BaSO_4$ chamber, under identical pump configurations, and that both Spectralon and $BaSO_4$ chambers produced over twice the output that could be obtained from the ceramic chamber. However, rapid degradation of the Spectralon material under the test pump conditions resulted in the $BaSO_4$ chamber being preferred for use with the subsequent tests.

For optimum energy transfer between the discharge circuit and the flashlamp, it is necessary to calculate the appropriate lamp matching parameters using the equations derived by Emmett and Markiewicz[79]. Appendix 2 shows the results of these calculations and the design of the flashlamp circuit used with the laser.

The choice of gas used in the flashlamps is determined, for a given laser crystal, by the excitation bands of the laser ion. Chromium is added to thulium and holmium to provide strong absorption in the visible portion of the optical spectrum which overlaps well with the emission from xenon filled flashlamps, Figure 2.2. Consequently, publications in which CTH:YAG is operated in pulsed mode report only the use of xenon filled flashlamps. The 5.1% slope efficiency performance reported by Quarles et al[31] was obtained with a xenon filled lamp having an arc length of 63.5mm and an internal bore (arc diameter) of 4mm. The gas fill pressure used was 630 Torr. Most lamp manufacturers supply a standard fill pressure of 450 Torr which represents a practical level to ensure reliable lamp triggering[80]. Consequently, it was appropriate to investigate whether the lamp gas pressure had an effect on the overall laser efficiency. This was done by comparing the output energy obtained over a range of pump energies with lamps identical but for the gas pressure.

A simple resonator was formed between a plane output coupler and a 5m radius of curvature rear mirror. The mirror reflectivities were 80% and 100% respectively. The rod (No. 2) was placed in a $BaSO_4$ pumping chamber (IR Sources, NH, USA) located in the centre of the resonator. Water flowed over the crystal at an input temperature of 20°C. Energy was discharged from the capacitor bank, at a

frequency of 1Hz, into a xenon filled flashlamp. The arc length of the lamp was 92mm and the internal bore 4mm diameter. Fill pressures of 630 Torr and 450 Torr were used for comparison. The resonator was aligned by adjusting the rear mirror to maximise the output, measured using a PbS photodiode (Graseby Infrared Ltd., Newmarket, Suffolk) and integrating circuit. The output energy was determined by measuring the power with a calibrated calorimeter (Model 20, Laser Instrumentation, Chertsey, England) and the repetition rate using a Philips PM6665 frequency monitor. Figure 2.5 shows that, at 5Hz operation, the lamp filled to 450 Torr produced marginally better efficiency than the 630 Torr version although the difference was not larger than the error in the measurement. Due to the availability of the flashlamps filled to 450 Torr as a standard item, and the marginally superior laser performance obtained, all further work was conducted with lamps filled with xenon to a gas pressure of 450 Torr.

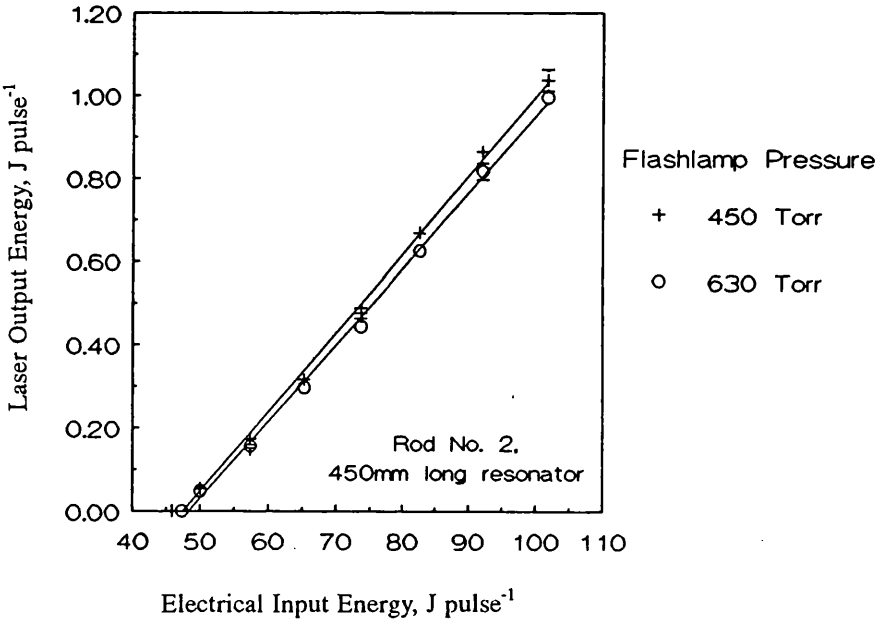

Figure 2.5 Laser output energy obtained from a 4"x4mm diameter rod excited with the pulsed emission from xenon flashlamps filled to 450 Torr and 630 Torr, the pump geometry remaining otherwise constant.

2.2.2 The optimum laser output coupling reflectivity

The resonator formed around a laser crystal includes a highly reflecting optic ($R \approx 100\%$) at one end and a partially transmitting optic at the other end, through which the laser output is obtained. The reflectivity of the output coupling optic affects the power which can be extracted from the resonator. Using the Rigrod analysis, Siegman[81] shows that the output power, at a high pump energy, is a function of both

the front and rear mirror reflectivities. To maximise the output, the rear mirror reflectivity should always be as high as possible while the single pass gain of the crystal determines the optimum output mirror reflectivity. In general, for low gain systems, high reflectivity optics are required to maximise the output, Figure 2.6 (a), while, for high gain systems, the output is not so sensitive to the reflectivity of the output coupler, Figure 2.6 (b).

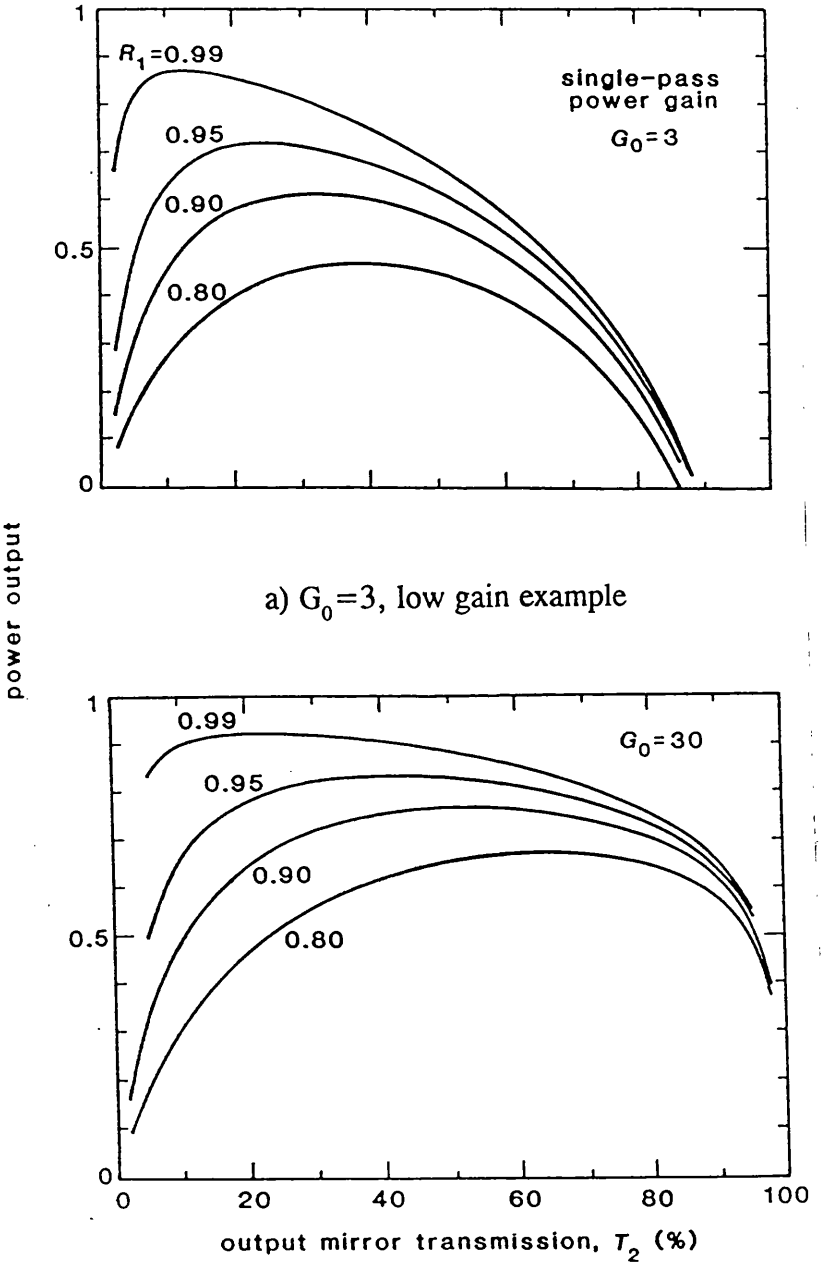

Figure 2.6 Effect of output coupler reflectivity on laser output - from the Rigrod Analy sis (After Siegman[81])

For example, for CW Nd:YAG lasers, which operate near threshold conditions and are consequently low gain, typical output coupler reflectivities range between 80% and 98%[82]. In contrast, pulse-pumped Nd:YAG lasers operate with relatively high gain and, typically, there is little difference in the output energy obtained for output mirror reflectivities between 30% and 50%[82].

Determination of the optimum output coupler reflectivity for a given laser can proceed via a number of routes. One is to apply the analysis derived by Koechner[82] using the data collected from measuring the threshold energies for a number of known output couplings. There exists a practical restriction on many researchers that the large number of optics required to complete this task leads to prohibitive expense. Consequently, alternative techniques are required. An alternative would be to apply the Rigrod analysis. However, according to Siegman, this would require obtaining solutions to a transcendental equation and would be beyond the practical scope of this work. A more common approach, used by others[31,32], is to use a selection of available optics to determine empirically the most suitable output coupler. By comparing the output energy from a laser under identical operating conditions other than the output coupler reflectivity, it is often possible to 'best guess' the most suitable reflectivity.

An experimental resonator was constructed to determine the optimum output coupler reflectivity. A 3"x5mmϕ rod (No.4) was housed in a $BaSO_4$ pumping chamber and pumped by a single xenon flashlamp at a repetition rate of 1Hz. The resonator was formed between a rear mirror, having a 5m concave radius of curvature, and a plane output coupler. Three output coupler reflectivities were available for analysis: 60%, 80% and 90% reflecting. The resonator was 455mm long with the rod lying approximately at the geometrical centre. Water flowed over the rod at 22°C to cool it.

The output energies obtained for each output coupler reflectivity, over a range input energies to the flashlamps, are shown in Figure 2.7.

The highest output energies obtained for any given input energy were obtained for the 90% reflecting optic followed by the 80% optic and lastly the 60% optic. Figure 2.8 shows the data from Figure 2.7, recast to show the changes in output energy for fixed pump energies over the range of reflectivities. Included in the figure are data points for 0 and 100% reflectivities where, although not experimentally measured, the output would be zero[81].

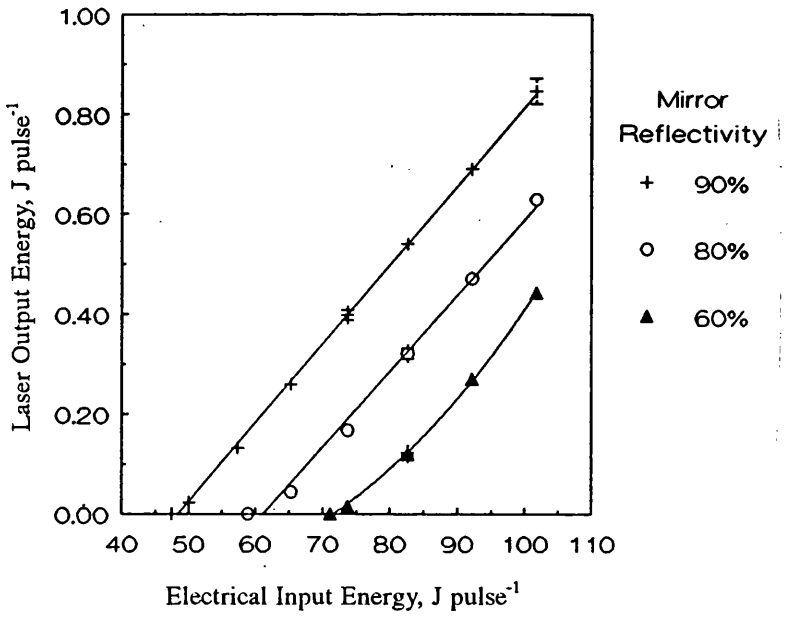

Figure 2.7 Laser output energy obtained over a range of pump pulse energies for different output coupler reflectivities. The pump configuration remaining constant.

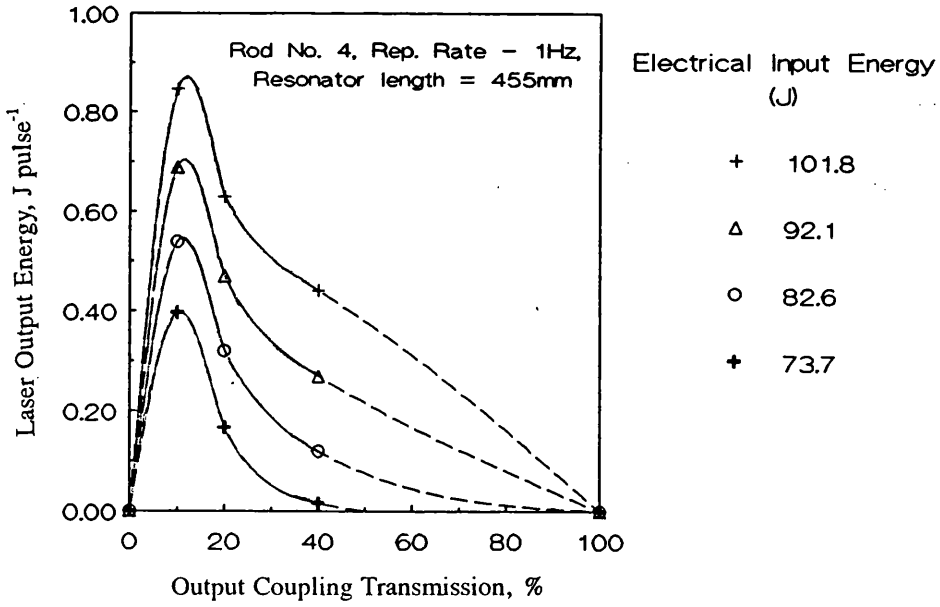

Figure 2.8 Effect of output coupling mirror reflectivity on laser output energy for a number of fixed pump pulse energies.

From the general shape of the curve linking the data points, it is easy to conclude that the system is most similar to the low gain examples given by Siegman, being very sensitive to the output coupler reflectivity. This result, although qualitative, is also in agreement with the results obtained by Bowman et al[34] who measured a small signal gain of $0.18cm^{-1}$ ($G_0 \approx 1.2$ and 1.7 for 3" and 4" long rods respectively) at

comparable pump energy densities.

From the experimental results, it can be concluded that the maximum output energy for a given pump energy would be obtained for output coupling optics having reflectivities of 90±5%. However, an increasing amount of power circulating within the resonator as a result of higher reflectivity mirrors can, in some cases, lead to the peak power damage threshold of the optical coatings being exceeded, leading to catastrophic damage. Koechner shows that[83] the intensity of circulating power, I, incident on the resonator mirrors is given by

$$P_{out} = AI(1-R_1)R_1^{-½} \quad (2)$$

where A is the cross-sectional area of the rod, R_1 is the reflectivity of the output coupling mirror and P_{out} is the output power of the laser. Thus, from the output energy and pulse duration, it is possible to determine the power densities within the cavity for each of the mirror reflectivities. Figure 2.9 shows the calculated intracavity power density, derived from the measured output energy at the maximum pump level, for each mirror reflectivity.

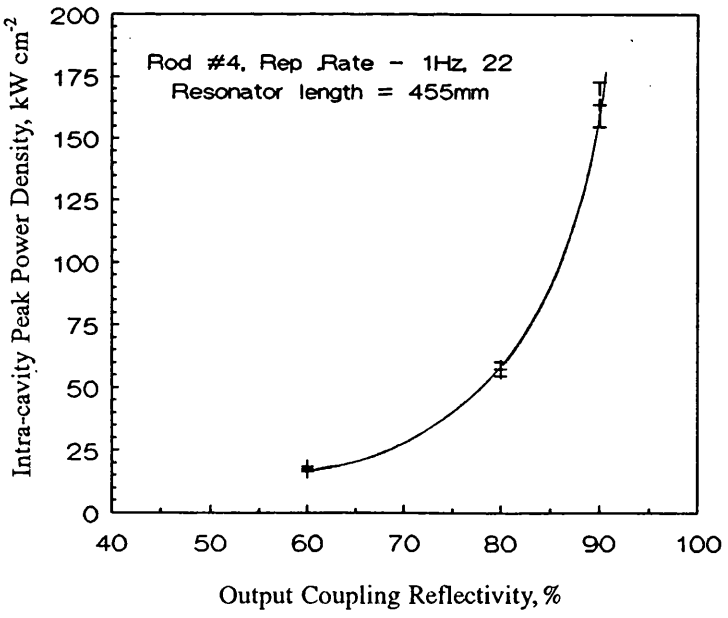

Figure 2.9 Effect of output coupling mirror reflectivity on intracavity power density.

The intra-cavity power density is shown to increase with reflectivity, increasing rapidly at higher reflectivities, such that, for an increment of only 10%, between 80% and 90% the power density is increased by almost a factor three. Although no reliable data exists on the damage threshold of optics operated over

prolonged periods of time at 2.1μm, the 80% reflecting optic was selected for all future work so as to reduce the risk of optical damage, while maintaining reasonable output energies.

2.2.3 The effect of rod dimensions

The dimensions of the rod influence a great many factors but an in-depth discussion on the relative merits of different sized rods is not warranted here. General observations can be made as follows:

i) Light from the flashlamp, which travels to the walls of the pumping chamber before being reflected towards, and absorbed by, the laser crystal, is reduced in intensity due to the imperfect reflection properties of the pumping chamber. Consequently more efficient energy transfer can be obtained if the rod receives more of the pump radiation directly from the flashlamp. Larger rods present larger capture angles, and, therefore, are generally pumped by a greater proportion of the flashlamp light, leading to greater efficiency.

ii) The energy deposited in a large diameter laser crystal as a result of flashlamp light absorption is distributed over a greater cross-sectional area than in a small diameter rod of the same length, pumped with the same amount of energy. Because the gain depends on the energy deposited per unit volume, the gain developed is reduced[84]. Considering the Rigrod analysis described earlier, higher reflectivity output coupling optics would, therefore, be anticipated for the larger rods.

iii) The thermal lensing characteristics of a rod are outlined in Appendix 4, The focal length of a rod lens, formed as a result of heating the crystal with unused flashlamp light, varies linearly with the rod cross-sectional area. Therefore, thermal lensing has a squared relationship with the radius of the laser rod. Large diameter rods can therefore be used to greater average input powers before thermal lensing causes roll-over of the laser resonator. However, this fact has to be reconciled with the fact that larger diameter rods present a larger capture angle to the flashlamp and the fraction of flashlamp light absorbed is therefore also increased. Thus, the practical relationship between rod diameter and lensing, for a given set of pumping conditions, must also consider the effect the increase in total absorption by larger rods. The need for this is highlighted by the work of Hamlin et al[36] in which smaller diameter rods were shown to allow operation at higher repetition rates than larger diameter rods

before thermal roll-over occurred. The output energies in that work were noticeably reduced for the smaller diameter rod, indicating that the smaller diameter rod had absorbed a smaller fraction of the available pump light, thus explaining the higher repetition rate performance of the smaller diameter rods.

iv) Considering the geometry of the resonator, the diameter of the rod is often the limiting aperture which defines the order of the highest transverse mode which can exist in the resonator. Thus, by simple arguments, smaller diameter rods will place a greater restriction on these modes, leading to a better output beam quality (divergence). However, the improvement in beam quality outside the resonator is mirrored inside the resonator and can lead to intra-cavity optical damage, particularly where highly reflective output couplers are used, as indicated by equation (2).

v) From the theory of thermal lensing developed in Appendix 4, it can be seen that the length of the laser rod plays no role in determining the thermally induced rod lens. However, for rods with the same diameter, longer lengths will reduce the heat loading per unit length, therefore reducing the risk of thermal fracture.

Comments i) and ii) appear to be contradictory, suggesting that larger rods could be more efficient (i) and at the same time exhibit lower gain (ii). The reconciliation of these two observations arises from the fact that each can play a part in reducing or increasing the laser output, but that the net result depends on the relative sizes, as well as the pump levels. For example, close to laser threshold smaller diameter rods would exhibit higher gain due to a better concentration of the laser gain and, therefore, would have a lower energy threshold. However, above threshold, the ability to collect the flashlamp light more efficiently increases the output energy from the larger rod compared to that which could be achieved with the smaller rod. Additionally, when the laser is operated in a Q-Switched mode, again well above threshold, gain saturation would occur sooner in the smaller diameter rod. The lower gain, combined with the larger storage capacity of a larger diameter rod, assuming equal lengths, would therefore result in higher maximum laser energies being obtained from the larger rod before saturation occurs.

For most laser crystals the decision on rod size is made from considering the above effects and determining where compromises can be made. However, in the case of CTH:YAG, the thermal properties restrict the average pump power which can be applied to approximately 200 W $inch^{-1}$ of pumped length[85], thereby adding an

additional consideration. To reduce the risk of thermal fracture crystals having dimensions of 3"x5mmϕ and 4"x4mmϕ were chosen for study. The choice of the 5mmϕ rod was based on the earlier work by Quarles et al[31,65]. The choice of the 4mmϕ rod was made because of the anticipated improvements to beam quality. The length of the 4mm diameter rod was chosen to reduce the thermal loading per unit volume and to maintain a high gain length.

Rods from the same supplier (Litton Airtron, Charlotte, NC, USA) with the same dopant concentrations, and having the dimensions given above, were operated at 1Hz in a close coupled Spectralon pumping chamber. The pumping chamber was used prior to any signs of deterioration of the reflector surface. A single xenon flashlamp was used to excite the crystal with a maximum electrical discharge of 102 J pulse^{-1} (see Appendix 2). The lamps were chosen to pump effectively the maximum possible length of the crystals. These had arc lengths of 67mm and 92mm for the 3" and 4" long rods, respectively. The resonator geometry used was the same as that described in Section 2.2.2. The output energy at a given pump level was determined using the calibrated calorimeter. Figure 2.10 shows that the 4"x4mmϕ rod outperformed the 3"x5mmϕ rod over the complete test range producing up to 1.13 times the energy output of the larger diameter rod.

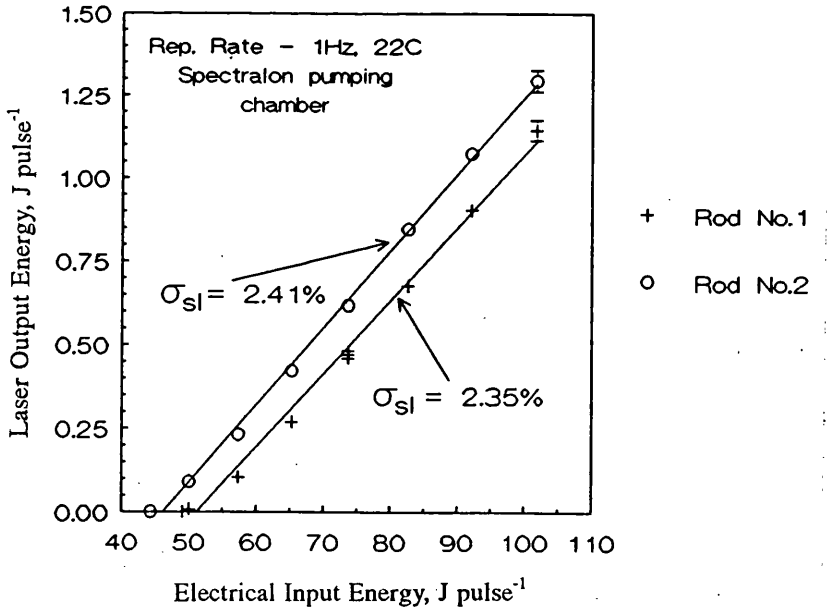

Figure 2.10 Comparison of output energies obtained from CTH:YAG rods having differing dimensions, operated under otherwise identical pump configuration.

Although further work may reveal the relative importance of the factors[82] described in (i) - (v) above, it was acceptable, for the aims of this study, to conclude that

further attention should be directed towards the longer, thinner crystals due to a higher laser efficiency and an expected improvement to beam quality.

2.2.4 Resonator optimisation

The geometry of the resonator determines the transverse mode structure of the beam. The effects can be observed as changes to the transverse spatial profile of the beam in the near field (within the Rayleigh Range), measured with scanning apertures or CCD camera systems. In the far field the profile is changed too, indicating a change in the divergence properties of the beam emerging from the resonator. The geometry of a laser resonator is characterised by the g-parameters which, for a resonator containing a thin lens of focal length f, is given by[86] $g_n = 1\text{-}L/R_m\text{-}d_n/f$, where the subscripts can be 1 or 2 but $n \neq m$ and identify the components. Here, L is the total physical length of the resonator and d_n is the distance between the rod centre and the mirror having a radius of curvature R_n.

It is reasonable to assume that this equation holds when the focal length of the rod is long compared to the resonator length and then the critical dimensions are referenced to the centre of the rod, as shown in Figure 2.11.

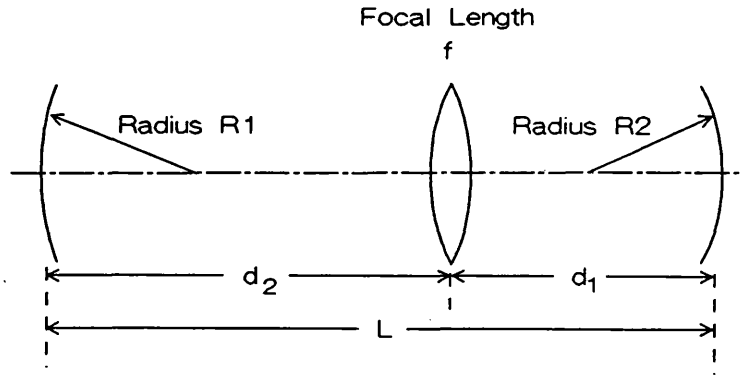

Figure 2.11 Geometry of a stable laser resonator containing an intra-cavity lens.

The resonator is critically stable when the product $g_1g_2 = 1$, representing the set of conditions when only the lowest order transverse mode is supported in the resonator. For $g_1g_2 > 1$, the resonator is unstable; for $g_1g_2 < 1$, the resonator is stable and the laser will support a number of transverse modes. The stability regions are displayed graphically in Figure 2.12.

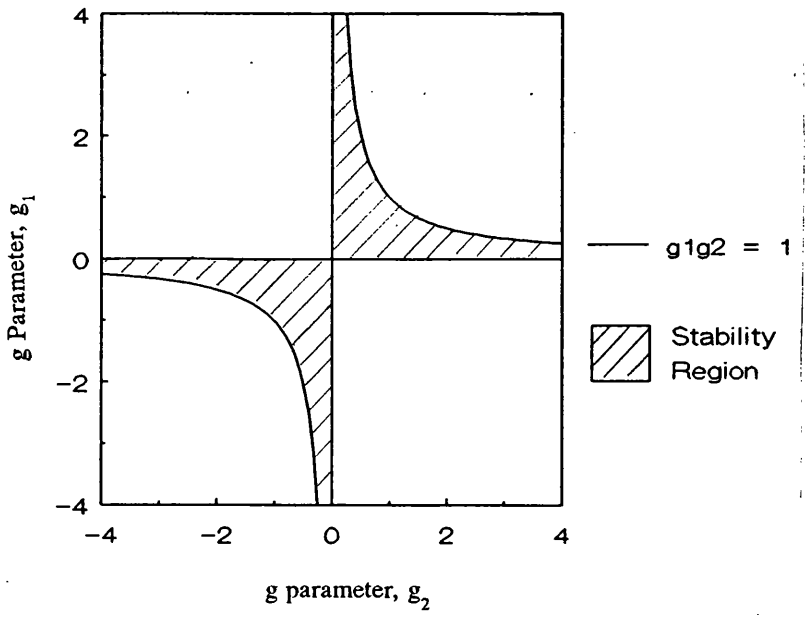

Figure 2.12 Stability diagram for laser resonators.

Changes in the lensing within the resonator cause changes in the value of g_1g_2 which cause its locus to progress around the diagram. The resonator may become more or less stable as a result of changes in the thermal lensing. This effect is apparent from changes in the position of g_1g_2 on the Figure. The efficiency with which stored energy is extracted from a laser rod depends on the number of transverse modes oscillating in the resonator. Geometries well within the boundaries of stability, where a greater number of transverse modes are able to oscillate, will, therefore, extract more energy than less stable versions.

The effect of changes in the resonator geometry, and consequently the stability conditions, were investigated for resonators containing 3"x5mmϕ and 4"x4mmϕ rods (Nos. 1 and 4). Both rods were pumped by a single xenon flashlamp although, due to availability of components the 3"x5mmϕ rod was operated in a ceramic pumping chamber while a $BaSO_4$ chamber was used with the 4"x4mmϕ rod. A resonator was formed between an 80% reflecting plane output coupler and a 5m radius of curvature rear mirror. The pumping chamber was situated so that the centre of the rod lay about 200mm and 255mm from the output and rear optics, respectively. The stability conditions were varied by changing the amount of heat input to the crystal so as to change the amount of rod lensing which occurred. To achieve this, the pulse energy was kept constant while the pump pulse repetition rate was varied between 1Hz and 6Hz. The output energy was monitored, using the

calibrated calorimeter to determine the effect of the changing resonator geometry on the efficiency with which the transverse modes extracted energy stored in the rod.

Figure 2.13 shows that there is a noticeable change in the laser output energies for both crystals, over the range of pulse repetition rates. At an electrical input of 102 J pulse^{-1}, the resonator containing the 4mm diameter rod is observed to reach a maximum output energy at 4Hz, being 18% greater than the energy output obtained at 1Hz, Figure 2.13 (a).

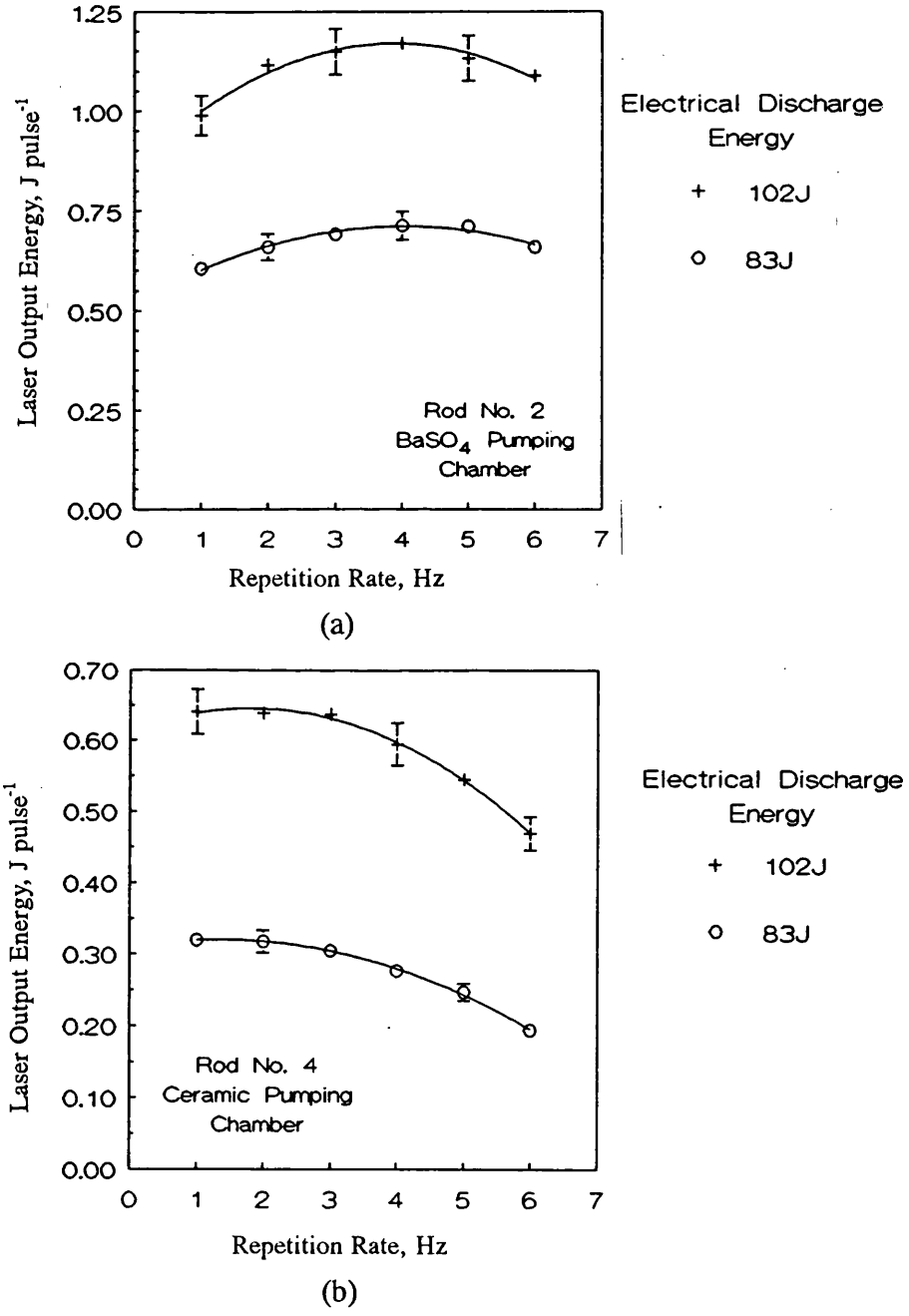

Figure 2.13 Effect of repetition rate on laser output energy at two different pump pulse levels in a 455mm long laser resonator containing a) 4"x4mm diameter CTH:YAG rod and b) a 3"x5mm diameter CTH:YAG rod.

In contrast, the resonator containing the 5mm diameter rod starts at a maximum at 1Hz., thereafter reducing its output until, at 6Hz and at maximum pumping, the energy is only about 75% of its level at 1Hz, Figure 2.13 (b).

These facts imply a greater change in the lensing of the 5mm diameter crystal over an equivalent pumping range, in keeping with the practical observations of Hamlin et al[36] and Becker et al[67], but, again, in contradiction with the theoretical linear relationship between the focal length and the rod radius. However, this discrepancy with theory can be explained by the fact that the theoretical approach (Appendix 4) does not consider the way in which the absorbed fraction of energy changes with rod radius, nor can the theory take account of the different transfer efficiency of each pumping chamber type. Unfortunately it was not possible to compare the performance of the two rods in identical pumping chambers which would have eliminated the second of these factors. However, the work of both Hamlin et al and Becker et al shows that, under circumstances where identical pumping chamber materials are used, larger rods are still found to lens more strongly than smaller diameter rods, in keeping with the indications from this work.

The strong dependence of the laser output energy on the pulse repetition rate has been reported elsewhere by others[32,33,36,67]. However, increasing thermal population of the lower laser level rather than thermally induced lensing has been cited as the cause of the reduction by some[67]. To determine the magnitude of the effect thermal lensing had on the reduction in the laser performance, the experiment described above was repeated at fixed input energies of 83 J $pulse^{-1}$ and 102 J $pulse^{-1}$ and at a fixed repetition rate of 5Hz. The rear leg of the resonator was then increased and the output energy recorded for each position of the rear mirror. The experiment was carried out for both 3" and 4" long laser rods. However, in the case of the latter, focusing within the resonator resulted in damage to the rear mirror, and the experiment was abandoned. The results for the 3"x5mmmϕ rod, shown in Figure 2.14, indicate that the roll-off in output energy with increasing length of the rear resonator leg is rapid. It can also be seen in the figure that, at increasing resonator lengths, the output energy obtained for the highest pump pulse energy is less than the energy at lower drive levels. This too indicates strong thermal lensing which is sufficient, at the maximum average drive level of 509W, to produce lensing in the rod strong enough to cause the resonator to become unstable, but which, at the lower average drive level of 413W, is still weak enough not to have a major effect on the efficiency of energy extraction.

Although thermal population may account for some of the reduction in output

in this experiment, the average input power is a constant, and, therefore, the additional heat causing this thermal population can only come from the energy deficit resulting from changes in the stability conditions. Without the changes in stability there would be no energy deficit and therefore it can be concluded that changes in the resonator geometry are the main cases of the reduction in output energy, and not thermal population changes.

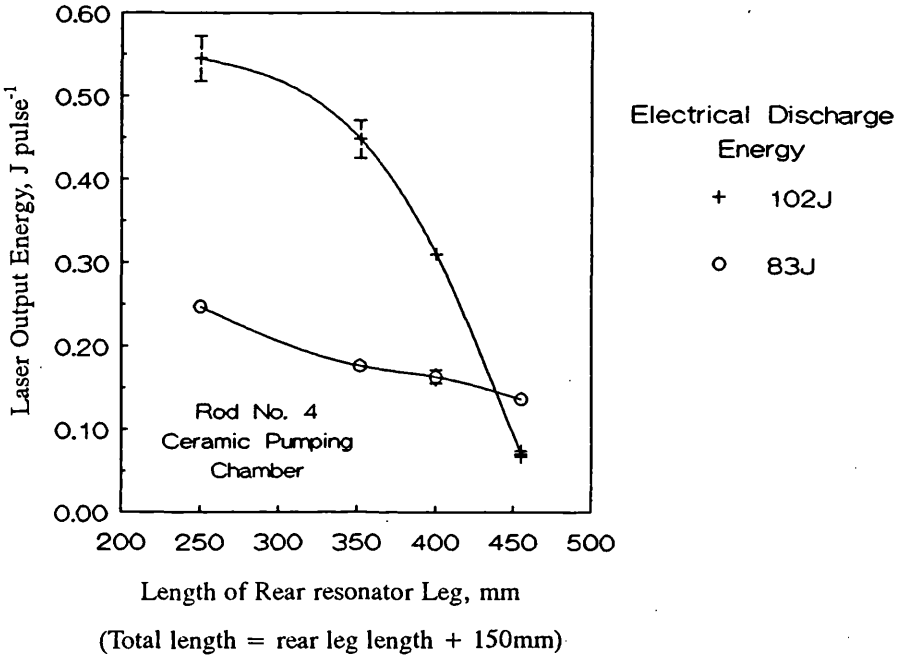

Figure 2.14 Variation in laser output energy with extension of the resonator length for a resonator containing a 3"x5mm diameter rod, the pump pulse energy remaining constant.

2.2.5 Conclusions

Aspects affecting the performance of a laser based around the CTH:YAG crystal have been investigated. Particular attention has been paid to the components of the system which are usually specified before the system is operated. Firstly, the relative performance of different pumping chamber materials has shown that, to achieve high output efficiencies, while maintaining long periods between servicing, chambers made from $BaSO_4$ are superior to either Spectralon or ceramic. The former was found to degrade rapidly with use, resulting in reduced efficiency. The latter was less efficient over all operating conditions, a feature attributed to the relatively large grain size which is formed during the firing process and which results in less efficient scattering of shorter wavelengths.

Previous work has suggested that silvered pump chambers may be more effective in transfering pump light to the CTH:YAG crystal than diffuse chambers using $BaSO_4$[31]. Recently, though, Hamlin et al[36] have demonstrated slope efficiencies up to 5.5% with a new design of $BaSO_4$ chamber, compared to the 5.1% reported in reference [31], indicating the sensitivity of performance to chamber design, even when the 'reflector' material remains unchanged.

Similarly, it has been shown here that the output energy at a given pump level, is strongly dependent on the reflectivity of the output coupler optic. This implies that a system has low gain and, consequently, that the differences between the slope efficiencies reported in references [31] and [36] may also be attributable to this factor. Comparisons performed between 60%, 80% and 90% reflecting output mirrors have shown here that a 90% optic produces the greatest laser efficiency, although the associated increase in intra-cavity power density increases the potential for optical damage to an unacceptable limit.

Further justification for selecting the 80% reflecting optic for further work is based on considering the rod dimensions. Smaller diameter rods are known to produce higher gain due to the greater density of energy deposition thus suggesting, from considering the behaviour of systems with the Rigrod analysis, that a lower reflectivity optic would be nearer the optimum than for the larger diameter rods.

The laser performances of two rods, one 3"x5mmϕ, the other 4"x4mmϕ, were compared under near identical operating conditions to determine which was the most efficient. At 1Hz, the 4" long rod was found to produce about 13% more energy than the 3" version despite having a total rod volume smaller by approximately 17% than the 3" rod. Additionally, at increasing repetition rates the output energy from the resonator containing the 4"x4mmϕ rod was found to increase, peaking at 4Hz. In contrast, the output from the 3"x5mmϕ rod in an identical resonator geometry was found to reduce with increasing repetition rate. The dominant cause of this effect was demonstrated to be thermally induced lensing, which, for the experimental configuration used, appeared to be greater at a given average input power for the 5mmϕ rod than the 4mmϕ rod. This result was in contradiction with theoretical considerations but in keeping with the results of others and easily explained by the variations in absorbed energy between the two systems. The lensing of both crystals was shown to affect the geometry of the resonators leading to changes in the g-parameters for each resonator in such a way as to change the energy extraction efficiency.

2.3 Effect of Thermal Populations in the Holmium Laser Crystal

The addition of sensitisers chromium and thulium to holmium has allowed the development of efficient room temperature holmium lasers. However, the low lying terminal laser level still influences the laser performance. Bowman et al report[66] that, with changes in the output coupler reflectivity, different laser transitions operate in the 2μm region, due to the different thermal populations of the terminal laser levels. Previously, Johnson et al[21] had observed output at three different wavelengths which depended only on the operating temperature. Thermal population of the sublevels of the terminal laser level also affects the laser threshold.

In the early years of holmium lasers Remski and Smith[57] demonstrated the effect of temperature by measuring the threshold pulse energy required to produce lasing in a 50mm long, 3mmϕ αßHo:YAG rod. Below 200K the threshold was found to increase almost linearly with temperature at a rate of about 0.1 J K^{-1} whereas, above 200K, the rate increased rapidly approaching 1.3 J K^{-1} at room temperature. Lotem et al[87] repeated the work of Remski and Smith but additionally measured the changes in slope efficiency with temperature comparing αßHo:YLF to αßHo:YAG. Due to a peak in the slope efficiency curve of the YLF crystal, they found the maximum overall laser efficiency was at 130K, rather than at the lowest operating temperature. However, the YAG sample did not show such a peak and the maximum output was, therefore, obtained for the lowest temperatures. The reason for this is unexplained but may be, in part, due to any of the temperature dependent effects identified by Armagan et al. These include temperature induced changes in the fluorescent lifetime of the $^3H_4$ thulium level[88], which in YAG has a different form to YLF. Additionally, in YAG, temperature dependencies have been identified in the intensity of the chromium emission (to transfer excitation energy to thulium) and the lifetime of the chromium emission[69]. Successful modelling of the combined thermal effects is still awaited.

Several authors have reported attempts to predict the changes in threshold energy of the CTH:YAG crystal at room temperatures. The most ambitious, to date, has been the attempt of Teichmann et al[32] who considered the gain conditions at threshold and related these to the thermal populations of both the Tm $^3H_4$ and Ho $^5I_7$ levels using a single experimental point to deduce the 'excitation' factor, the only unknown in their analysis. The resulting prediction was observed to rapidly diverge from the set of experimental data points although both theory and data points showed a linear dependence with temperature over the temperature range. It is the aim of this work to determine whether a simpler approach, considering only the thermal

population of the Ho $^5I_7$ level, provides an adequate description of the variation in threshold energy.

2.3.1 Theoretical considerations

Laser action in the holmium ion takes place between $^5I_7$ and $^5I_8$ levels. Nine laser transitions have been identified so far[34], the strongest transition being at 2.121μm. Changes in thermal population of the terminal laser level[21], as well as mirror reflectivity[34] can determine the wavelength at which laser operation is observed. From the work of Bowman et al[34] the four strongest transitions have terminal laser levels lying between 492cm^{-1} and 522cm^{-1} above ground level.

The thermal populations of two energy levels are related by the Boltzmann equation

$$N_2 = N_1 \exp-((E_2-E_1)/kT) \quad (3)$$

where N_1 and N_2 are the populations at energy levels E_1 and E_2, where $E_2 > E_1$. Here, k is Boltzmann's constant and T is the absolute temperature. In normal, thermal equilibrium conditions, the population difference between two levels E_2 and E_1 is

$$\delta N_{(1\rightarrow 2)} = N_2[1-\exp(-(E_2-E_1)/kT)] \quad (4)$$

Siegman[89] develops the theory for population inversion in a four level laser relating the difference between upper and lower laser levels, N_3-N_2 to the atomic pump rate, w_p, as

$$N_3-N_2 = \frac{N_0(1-ß)w_p\tau_{rad}}{1+(1+ß)\alpha w_p\tau_{rad}} \quad (5)$$

where ß is the ratio of populations N_2/N_3, α is a quantum efficiency depending on the decay rates of the pump level and the upper laser levels and τ_{rad} is the radiative lifetime between the upper and lower laser levels. N_0 is simply the sum of all the populations involved in the laser process. Near threshold ß$\approx$1 and, if $w_p\alpha\tau_{rad} \ll 0.5$, then equation (5) reduces to

$$N_3-N_2 = N_0(1-ß)w_{p,thr}\tau_{rad} \quad (6)$$

where $w_{p,thr}$ is the atomic pump rate at threshold and is assumed to be proportional to the energy discharged by the flashlamp. Assuming that the population of N_2 at laser threshold is fixed by the thermal conditions and that population of level N_3 does not reduce N_2, then equation (6) becomes

$$N_3 - N_1 \exp[-E_2/kT] = N_0(1-\beta) w_{p,thr} \tau_{rad} \quad (7)$$

where N_1 is the ground level population. If N_1 is constant, again either population of level N_3 does not deplete it, or the level of depletion is an insignificant amount, and the fluorescent lifetime is constant over the temperature range[26] then the pump rate required to populate state N_3, then w_p becomes temperature sensitive. Assuming w_p is proportional to the flashlamp pump pulse intensity, I_{in}, via

$$w_p = GI_{in} \quad (8)$$

where G is simply a proportionality factor which includes the laser pump pulse duration, then equation (7) can be rewritten

$$E_{in,thr} = \frac{N_3 - N_1 \exp[-((E_2)/kT)]}{N_0(1-\beta)\tau_{rad} G} \quad (9)$$

where $E_{in,thr}$ is the energy required to be delivered during the pump pulse in order to reach threshold. The threshold energy is therefore expected to vary with temperature according to the thermal population of the lower laser level.

Siegman also describes the factors contributing to the output intensity of a laser as

$$I_{out} = \left[\frac{w_p}{w_{p,thr}} - 1 \right] \frac{\delta_e I_{sat}}{2} \quad (10)$$

where the ratio $w_p/w_{p,thr}$ replaces Siegman's R_p due to the relationship described in equation (8). Here δ_e and I_{sat} are the external loss coefficient and the saturation intensity, both of which are essentially fixed. Thus the slope efficiency of the laser output depends on the pump rate *relative* to the threshold pump rate. Although the threshold pump rate is temperature sensitive the relative pump rates are not. Consequently, the slope efficiency is not expected to be temperature sensitive.

2.3.2 Measurement of the effect of temperature on laser performance

The effect of temperature on the laser performance was assessed using the 4"x4mmϕ rod, No. 2, pumped by the emission from a single xenon flashlamp in a $BaSO_4$ pumping chamber. Water flowed over the rod and lamp simultaneously, at a temperature determined by the setting on a circulator/chiller unit (RTE-110B, Neslab, Netherlands), at a rate of approximately 4.5$l$min^{-1}. The temperature was monitored at both the input and output manifolds and was found to be consistently different by approximately 2°C, due to heat transfer from the lamp and rod. To allow comparison with the work of others, the temperature of the input manifold is used as the reference. The laser was operated at 5Hz at all times with a plane, 80% reflecting output coupler. Output energies over a range of discharge pulse energies, and for three different resonator geometries, were measured using the calibrated calorimeter to first measure the power before deriving the individual pulse energies.

Figures 2.15 (a), (b) and (c) show the results obtained over the available range of input energies and over the temperature range from 20°C to 35°C. Figure 2.15 (a) shows the data obtained for a resonator where both the distance from the output coupler mirror to the middle of the laser rod and the distance between the same point in the rod and the 5m radius of curvature rear mirror, was 150mm.

It is clear that increasing the crystal temperature increases the laser threshold energy, although the overall slope efficiency appears to be constant. Figures 2.15 (b) and (c) differ only in that the rear dimension of the resonator was increased to 250mm and 305mm respectively. However, the effect of this increase has a dramatic effect on the laser performance, with energy roll-over, similar to that observed when the cavity length is increased, occurring at increased temperatures. Figure 2.16 (a) shows the changes in output energy with increasing temperature for a constant input energy of 74J.

Data for the 300mm and 400mm long resonator are presented at a pump pulse energy which is well above the laser threshold and for which the pulse energy does not appear to have been affected by roll-over. It is clear that the energy decreases with increasing temperature, but that the length of the cavity, for the set of conditions selected, makes no impact on the performance. Data from the 455mm long resonator is not included as roll-over occurs much sooner, due to the sensitivity of longer resonators to thermal lensing, and 'normal' output at the selected pump pulse energy could therefore not be obtained.

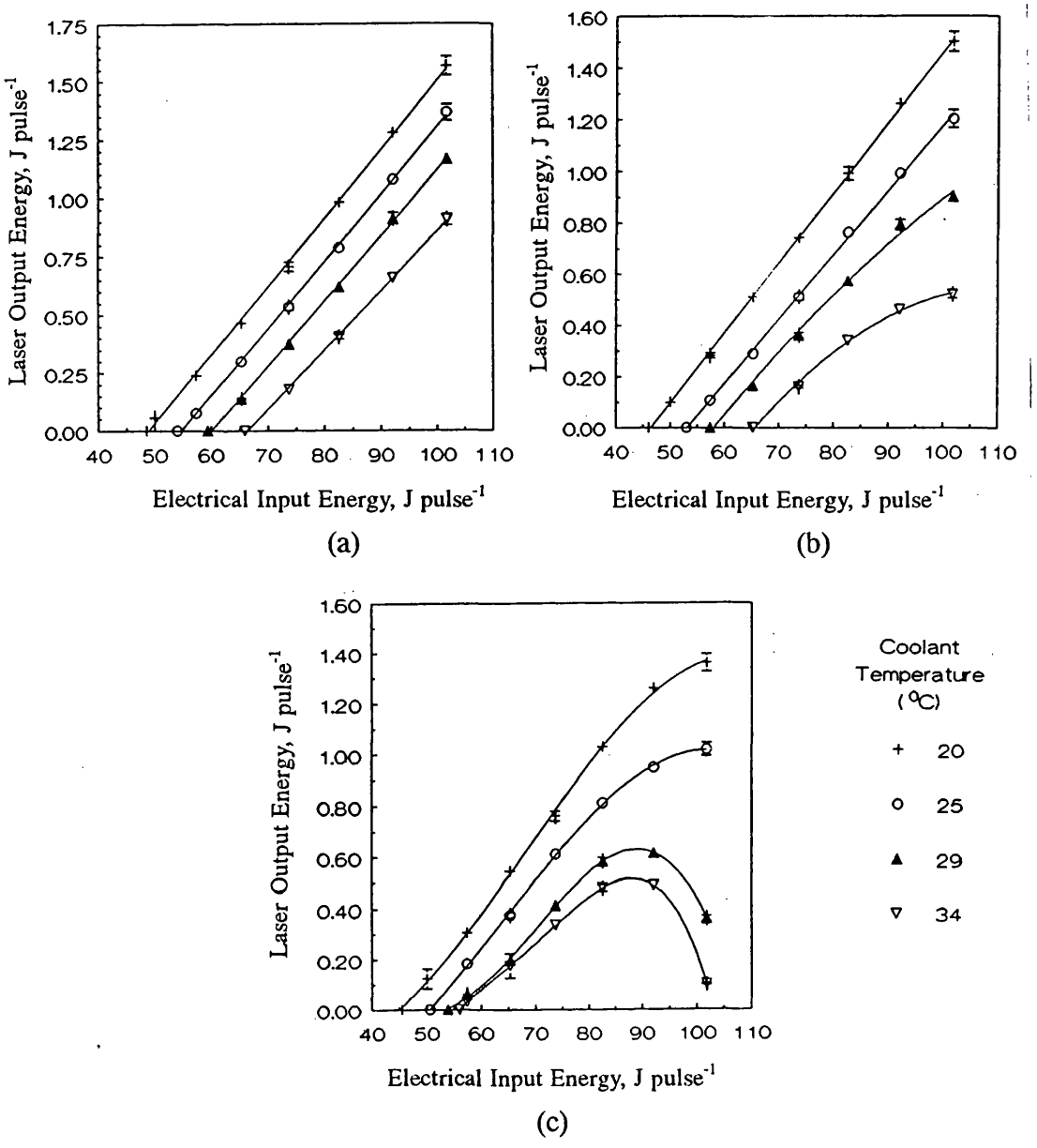

Figure 2.15 Laser output performance obtained over a range of operating temperatures for (a) a 300mm long resonator, (b) a 400mm long resonator and (c) a 455mm long resonator.

Figure 2.16 (b) shows the equivalent results at a higher pump pulse energy of 102J. Results for all three resonators are included here as it is the object of the figure to highlight the effect of thermal roll-over on the laser output. The reduction in the output energy from the laser, over the measurement range, reduces linearly in all cases. However, the rate of reduction is much greater for the longer resonator, falling by over 90% for a 10°C rise in the coolant temperature. By comparison, the 300mm long resonator falls by only 25% over the same temperature range. Figures 2.16 (a) and (b) imply that thermal population of the lower laser level is not the only factor having a direct effect on the laser efficiency.

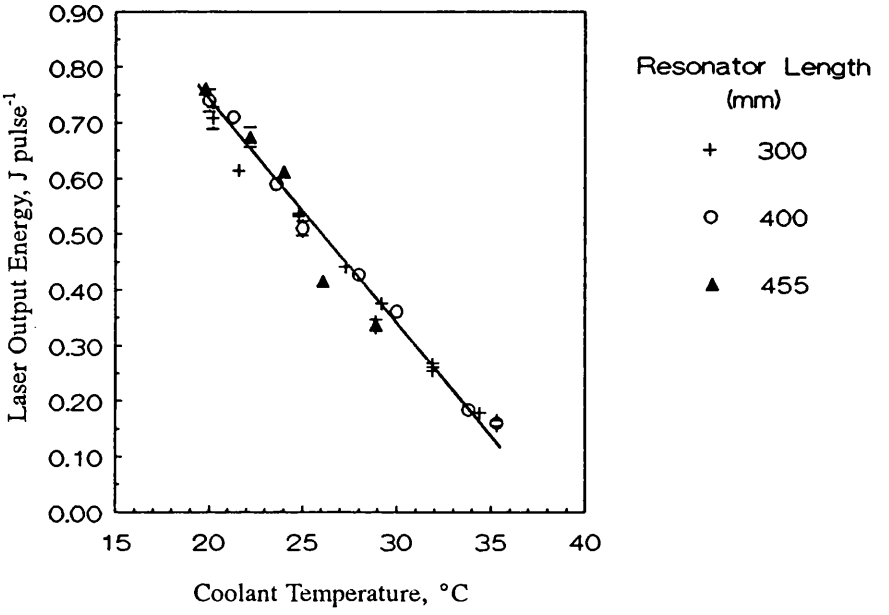

(a)

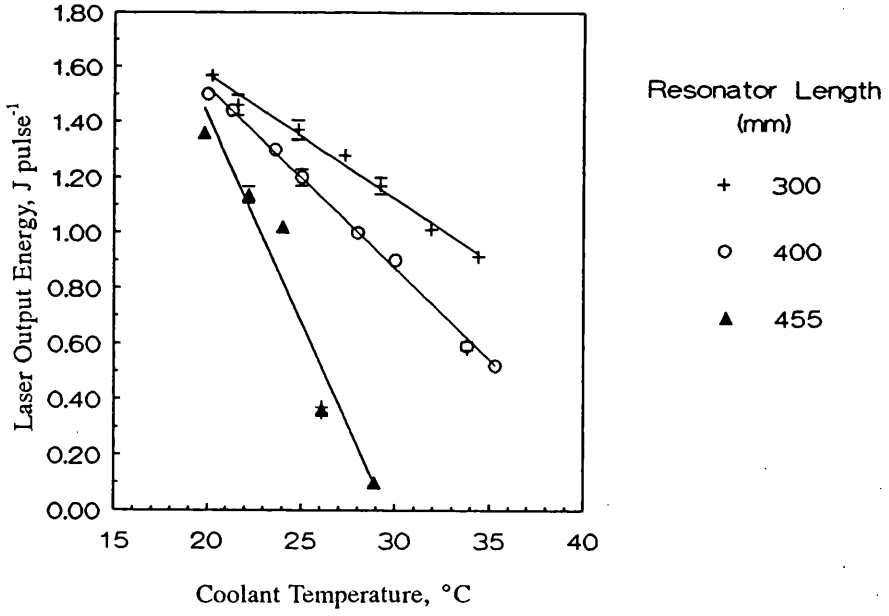

(b)

Figure 2.16 Change in laser output energy with temperature for resonators having lengths 300, 400 and 455mm at fixed pump pulse energies of (a) 74J and (b) 102J.

Figure 2.17 shows the change in laser slope efficiency obtained by linear regression techniques for the different resonators as a function of operating temperature. Again, the data for the longest resonator is absent due to the difficulty in obtaining a straight line fit to the set of data.

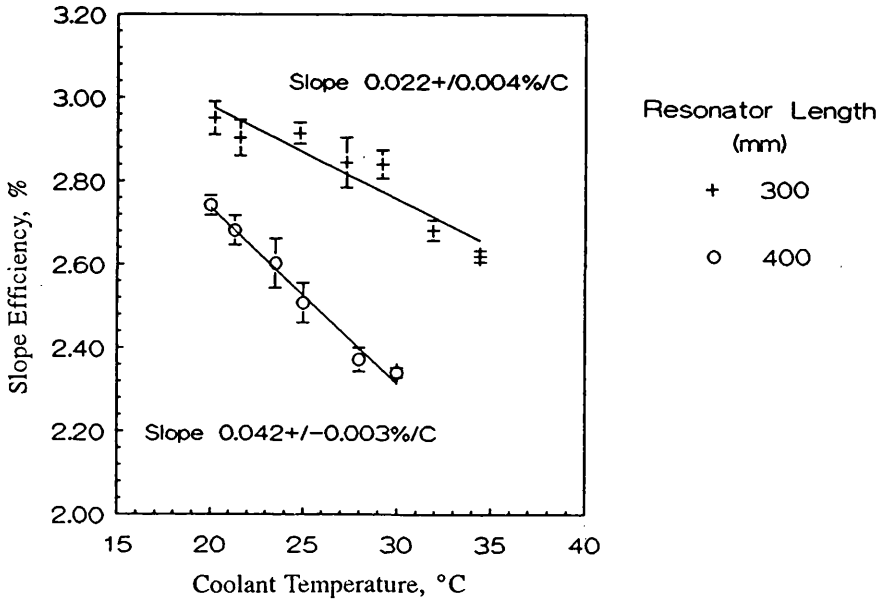

Figure 2.17 Change in laser slope efficiency with temperature for a 300mm and a 400mm long resonator.

The laser slope efficiency appears to be temperature dependent, reducing by an amount which appears to depend on the resonator configuration. However, the rate of reduction is small, approximating to a 1% reduction in the slope efficiency for the 300mm long resonator and about 1.6% for the 400mm long resonator for every degree rise above 20°C.

Changes in the threshold energy, determined from the intercept with the x-axis for the 'above threshold, below roll-over' set of data points, are shown in Figure 2.18 against temperature. Despite differences in the resonator geometries, the threshold is shown to vary linearly with temperature, irrespective of the resonator geometry. From linear regression the rate of change of laser threshold energy for the 300mm and 400mm resonators is 1.159 ± 0.06 J $°C^{-1}$. Insufficient data points were available to calculate threshold values for the 455mm long resonator due to the effect of roll-over.

Figure 2.19 shows the same experimental data plotted against the relative population of the $522cm^{-1}$ terminal laser level calculated using equation (3). It can be seen that there is a linear relationship between the thermal population in the terminal laser level and the threshold, as predicted by equation (9). However, Figure 2.18 also shows a linear relationship against temperature, suggesting that the experimental range (20-35°C) is too small to establish the relationship proposed in the equation.

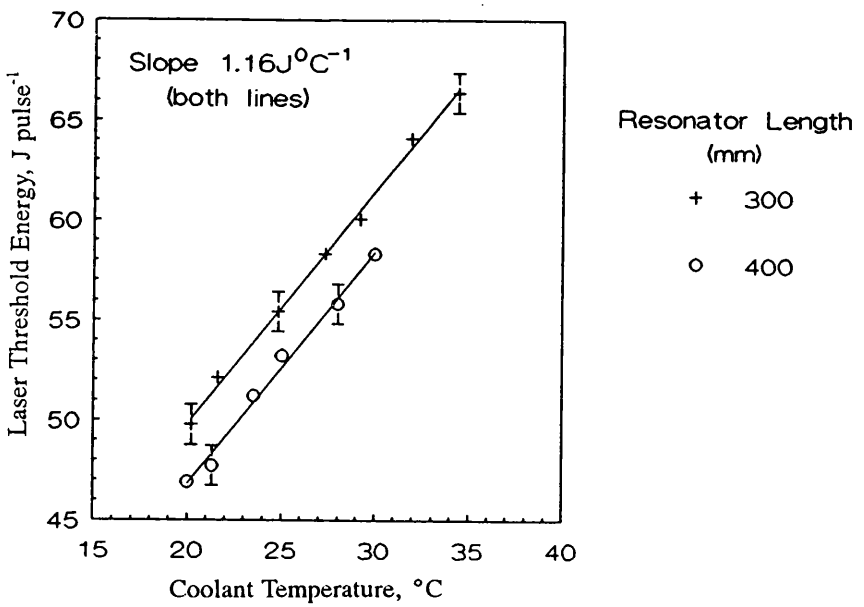

Figure 2.18 Change in laser threshold energy with temperature for a 300mm and a 400mm long resonator.

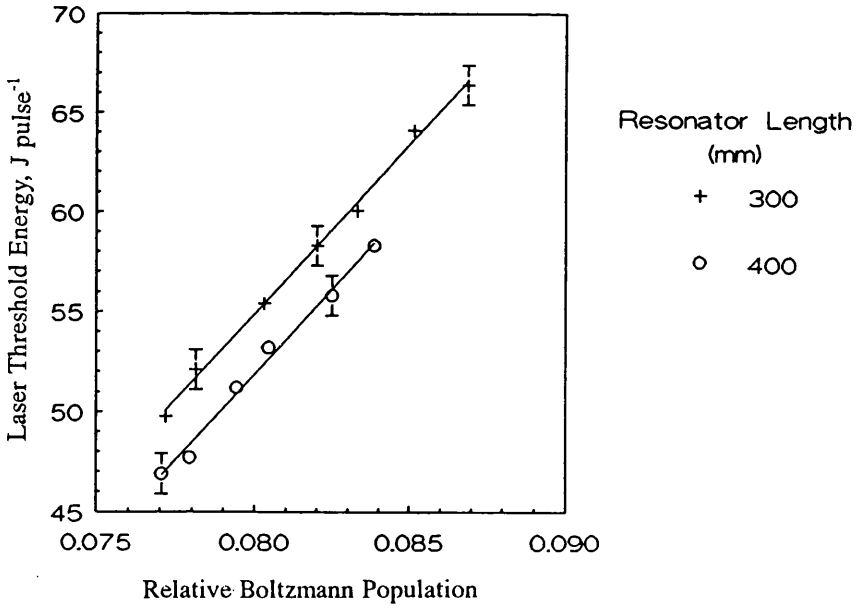

Figure 2.19 Change in laser threshold energy of a 300mm and a 400mm long resonator with thermal population of the terminal laser level.

Figure 2.20 graphically shows the reason for this. Calculated, using the $522cm^{-1}$ energy level as an example, the exponential relationship is essentially linear over a large range of temperatures from -100°C to +150°C. Thus, to truly test the validity of equation (9) would require measurements taken over a 250°C temperature range,

including cryogenic temperatures, which is beyond the practical limits of this work.

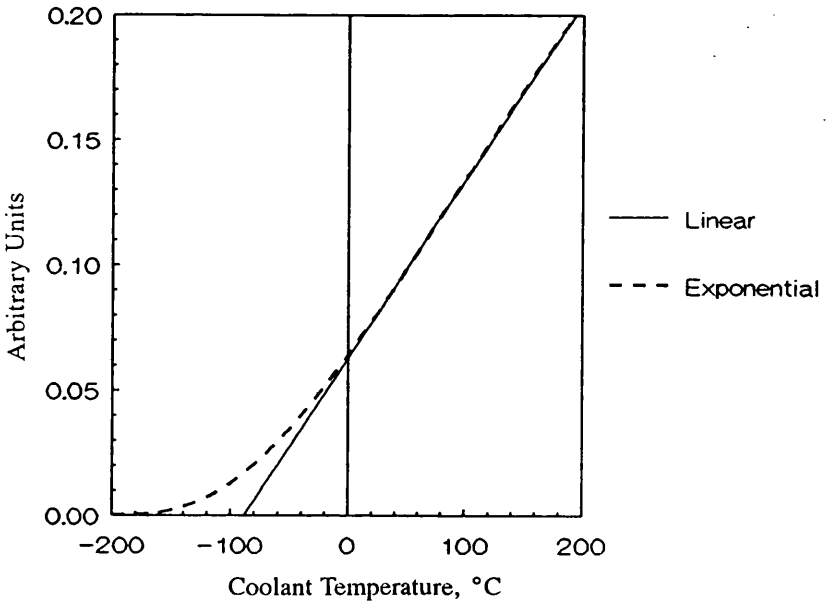

Figure 2.20 Comparison of the exponential variation of the laser threshold with thermal population of the 522cm^{-1} terminal laser level with a linear relationship.

2.3.3 Discussion

The simple theory developed to predict the change in laser threshold caused by changes in the operating temperature predicts a linear relationship with the occupancy of the terminal laser level. This has been demonstrated experimentally although the changes in threshold are linear with temperature also. This is due to the fact that,over the experimental range of temperatures, the population of the terminal laser level, as determined from Boltzmann calculations, is also linear with temperature. When Barnes et al[90] recently carried out a similar analysis, over the temperature range 120K to 200K, they too found a linear relationship with the occupancy of the terminal laser level supporting the results presented here. Barnes et al also observed a reduction in the slope efficiency of their laser which was linear with the thermal population of the upper laser level (including a contribution made by the Tm $^3F_4$ level). Although, again, the data presented here is over too small a temperature range to confirm their observation, the linear relationship with temperature, reported here, translates equally well into a linear relationship with occupancy if the thermal population is, as expected, varying linearly over the test range of temperatures.

Although the changes in laser slope efficiency with temperature, observed for the different laser resonator geometries, are consistent with one another there is a

noticeable offset between the two sets of data which is not predicted in equation (9). The data shows that thresholds for the longer resonator are consistently higher than for the shorter resonator. This can easily be explained if one considers that the resonator becomes geometrically less stable as the length increases. Burrows implies, in reference [91], that changing the resonator geometry can increase or decrease the laser threshold, depending on the design chosen. It is believed that extension of resonator length is here creating higher thresholds.

Despite operating at a constant average input power, which results in a constant amount of thermal lensing[92], rollover of the output energy, similar to that observed earlier when the dimensions of the resonator were increased, was observed here for increasing temperatures. The effect is again attributed to changes in the geometry of the resonator, although in this case it is proposed that stored energy which is not extracted as useful laser light causes the effect. Hodgson[93] has shown that the focal length of a thermally induced lens in a Nd:YAG crystal depends not only on the average operating power, but also on the reflectivity of the output coupler. The effect of the output coupling reflectivity on the laser output power was demonstrated earlier both theoretically and by practical example. It is proposed that some of the energy deficit results in additional crystal heating, thereby increasing the amount of thermal lensing. The nature of Hodgson's results would seem to support this hypothesis. It is proposed here that the output energy deficit, resulting from operating at increased temperatures, causes increased amounts of thermal lensing, which, in the CTH:YAG crystal operated in resonators with geometries like those used here, is sufficient to cause changes to the stability of the laser resonator. As the resonator length is increased, the effect of lensing becomes more noticeable, eventually leading to premature rollover of the resonator. The effect could be exaggerated by the fact that a reduction in laser output, due to higher laser thresholds at higher temperatures, causes increased lensing, which itself can reduce the energy extracted, thereby increasing the amount of heat generated in the crystal raising the threshold, reducing the extracted energy increasing the lensing and so on until either an equilibrium level is reached or laser action ceases.

2.3.4 Conclusions

Thermal effects have been shown to affect both the threshold and slope efficiency of the laser operation. A simple theory, proposed to describe the nature of the relationship between the threshold and temperature appears to hold although a limited operating range prevents this being demonstrated conclusively. Dependence of the laser slope efficiency on the operating temperature has also been demonstrated. This

is contrary to the simple theory proposed earlier but in keeping with the relationship proposed and demonstrated by Barnes et al[90]. Thermal effects have, for the first time, been shown to affect the stability of the laser resonator. This is attributed to residual flashlamp energy, which is not extracted as useful laser energy due to the higher laser thresholds at higher temperature. The extra energy left in the crystal causes increased thermal lensing which, in the CTH:YAG crystal, is sufficient to cause rollover of some resonators.

To avoid temperature effects in CTH:YAG lasers it is necessary to control the temperature of the crystal. From the results presented here it is suggested that coolant control to better than $\pm 0.5°C$ is required. Greater variations in the temperature may cause not only reduced output due to elevated thresholds but also lead to thermally induced rollover of the resonator.

2.4 Thermomechanical Effects

It has been shown how changes in the stability conditions of the resonator can affect the efficiency with which energy stored in the rod can be extracted. In the experiment described in section 2.3.2, changes in the output energy were caused by a change in the transverse mode structure within the crystal caused by the thermally induced lensing of the laser rod. Changes in the stability conditions of the resonator also affect the divergence angle of the rays emerging from the resonator. Control of these angles is essential if small focused spotsizes are to be obtained as the spotsize at the focal plane of a lens varies linearly with the divergence. Consequently, it is often the object of laser resonator design to achieve minimum divergence angles in order to obtain either the highest light intensities to achieve a process, such as the cutting of metals, or to couple the light into small diameter optical fibres.

The output divergence angles from an empty resonator i.e. one which does not contain any intra cavity optics, can be predicted using the matrix methods[94]. More complicated resonators can be modelled using the same techniques although computers are frequently required to deal with the more demanding designs. Resonators containing heated laser rods can also be modelled although with an increasing degree of approximation due to the fact that several factors contribute, each to an unknown extent, in determining the degree of lensing. Computer based models vary in their approach to thermally induced lensing, some approximate the rod lens to a single thin lens, while others treat the rod as a duct with a refractive index varying quadratically across its diameter. The latter provides the closest

approximation to the real case where a quadratically varying refractive index accounts for about 75% of the total lensing power[92]. However, reliable data is seldom available to use in such models as the data obtained from experiments is usually given as the lensing parameter, K, in the form of a dioptric power per kilowatt of average input power, which is most suited for use in the thin lens approximation models. The following sections describe the measurement of the thermally induced lensing of a CTH:YAG rod to produce a simple equation relating the rod lens focal length to the average pump power. Additionally, the method of measurement and assessment results in data which describes the rod lens in the form of a duct.

2.4.1 Thermal lensing in CTH:YAG crystals

Significant lensing in the CTH:YAG crystal compared to Nd:YAG was first alluded to in 1989 by Moulton[95] who reported induced focal lengths, in a 75mmx5mmϕ crystal, of about 30cm for an average pump power of 400W. Antipenko et al[96] confirmed Moulton's observation of strong thermal lensing indicating that a linear relationship existed between the average pump power and the dioptric power of the thermally induced lens. Additionally they observed that the rate of change of lensing with average pump power (a constant for a given crystal and pump configuration) varies linearly with concentration of the thulium ion at an approximate rate of 1.3 kW m (Tm conc.%)$^{-1}$. The authors do not speculate on the reason for this change although it is unlikely that thulium concentration is solely responsible for thermally induced lensing, nor, as they imply, would the rate of induced lensing fall to zero at a zero thulium concentration.

Bowman et al[34] have measured the rate of change of the dioptric power for 4mm and 5mm diameter rods and have confirmed a linear relationship between dioptric power and average pump power of 4.0 Dioptres kW^{-1} and 7.2 Dioptres kW^{-1} respectively. Again the differences in the figures is contrary to that expected from theory, the smaller diameter rod exhibiting weaker lensing than the larger diameter rod. The reason for this is again due to changes in the amount of pump light absorbed by the rods which increases with rod radius and possible changes to the cooling conditions. Additionally, Bowman's results include measurements from both single and double lamp pumping chambers, further complicating any attempts to resolve the main reasons for the departure from lensing theory. Recently, Bowman has indicated[97] that these figures represent an average figure, the true variation in rod lensing, for a 4mm diameter rod, being best described as being between the limits of 3 Dioptres kW^{-1} and 5 Dioptres kW^{-1}.

Although software to model laser resonators is currently available, there has been no published data indicating successful modelling of the divergence characteristics of resonators containing CTH:YAG crystals.

2.4.2 Experimental measurement of the rod lens

Thermal lensing, its causes and the experimental measurement of thermally induced rod lenses are discussed in Appendix 4. Measurement of the thermal lens in a 4"x4mmϕ CTH:YAG rod (No. 3) was performed using the indirect method described in the appendix. In summary, the output beam from a resonator with a known geometry was focused using a lens of focal length 300mm. The diameter of the spot in the focal plane was determined and from this the beam divergence was calculated, as described in Appendix 3. The diameter of the output beam from the resonator, at a position 10mm from the output coupler, was also measured. The resonator was formed between a plane, 80% reflecting, output mirror and a 5m radius of curvature rear mirror separated by 470mm. The rod and single xenon flashlamp were housed in a $BaSO_4$ pumping chamber, located midway between the two mirrors, with water flowing over both simultaneously at a temperature, measured at the input manifold, of 25°C. The average input power was varied using the voltage applied to charge the capacitors and the laser firing rate.

The data obtained for the divergence was plotted and a third order polynomial fit applied to the complete set of data points. From the resulting equation the divergence at any defined pump power could be determined. The resonator was then modelled on a personal computer using LaserTrace[98]. The rod was described in the model in terms of its length and diameter while the induced lensing was calculated by the program using equation (A4.6). The variables in the software were the average pump power and the percentage absorbed by the rod. The former was determined by the operating point while the latter provided the variable used to influence the result. Typically, the divergence predicted by the model was the same as that expected from the polynomial fit to the experimental data for absorbed percentages between 10 and 20%. Also, it was necessary to define the percentage absorption to two decimal places in order to achieve predicted divergences to within 2.5% of the experimental values. However, it was found that the output diameter predicted by the model was consistently larger than the experimental value. This was presumed to be due to the interpretation of the beam diameter by the software which considered the beam diameter to be the maximum extent of the ray bundle, whereas the experimental spotsize was the diameter containing 86.5% of the total beam energy (see Appendix 3). Consequently, the rod radius, defined in the software, was reduced until the

predicted beam diameter was within 2.5% of the measured value.

A set of input parameters was, therefore, iteratively modified to produce the same theoretical output divergence and beam diameter as that measured experimentally. The effective back focal length of the rod lens, created by the set of input parameters, was then 'measured' with the software by passing a parallel beam through the rod lens and determining the distance from the end of the rod to the focal plane. The effective focal length was then obtained from the sum of the back focal length and half the rod length divided by the crystal refractive index (BFL+l/2n).

2.4.3 About LaserTrace

LaserTrace is a PC based ray tracing program developed by Walther Goethals, Senior Optical Engineer at Lumonics Ltd, Rugby, England. The ray tracing algorithms are based on the equations derived by O'Shea in his standard text on optics[99]. The input form to the program allows the user to define light sources including laser beams and point sources. Optical paths can then be defined, including transmission between dielectric media having spherical surfaces, free space propagation, fibre transmission (limited to fibres of zero length with beam quality degradation factors taken from those determined experimentally by Schildbach[100]) and transmission through ducts. The former is used to form lenses although ideal lenses, without any thickness, can be defined with zero aberrations. The latter is used to describe graded index optics and is used also to describe thermally induced rod lensing. In combination these elements can be used to describe optical arrangements, such as beam delivery systems, which can be modelled prior to construction.

For the modelling of laser resonators, it is necessary to 'unfold' the resonator replacing the mirrors with ideal lenses (ie without any aberrations), as is done for matrix analyses of resonators. A point source of highly divergent light at the laser wavelength then provides the input which is periodically focused by the resonator components until, after a number of 'traverses', the ray bundle distribution is reproduced at the same point in the resonator for each pass. The output screen of the software reveals the extent to which the beam reproduces itself as it propagates. Subsequent screens detail, numerically, the dimensions and maximum angles of the ray bundle at the interfaces between each of the optical surfaces. Figure 2.21 (a) shows an example of the input field describing a 400mm long symmetric resonator, containing a 4"x4mm diameter rod, pumped at an average input power of 500W where 15% of the pump power is being absorbed by the crystal. Figure 2.21 (b) are samples of the resulting input and output screens annotated to indicate key features.

```
Modelling of a 400mm Long Symmetric Resonator
HoYAG                                          Defines wavelength
5                                              Defines accuracy (0..10)
|-----------------|-|
SOURCE      - 2 7
DRIFT       - 149.2
YAGROD      - 4 101.4 0 500 15
DRIFT       - 149.2
DRIFT       - 149.2
YAGROD      - 4 101.4 0 500 15
DRIFT       - 149.2
   :        :   :
   :        :   :
   :        :   :
DRIFT       - 149.2
YAGROD      - 4 101.4 0 500 15
DRIFT       - 149.2
*****************************
Definitions
YAGROD - Diameter(mm) Length(mm) End face curvatures(m) Pump power(W) Crystal absorption
(%)
DRIFT    - Distance(mm)
```

Figure 2.21 (a) - Input form to LaserTrace raytracing software

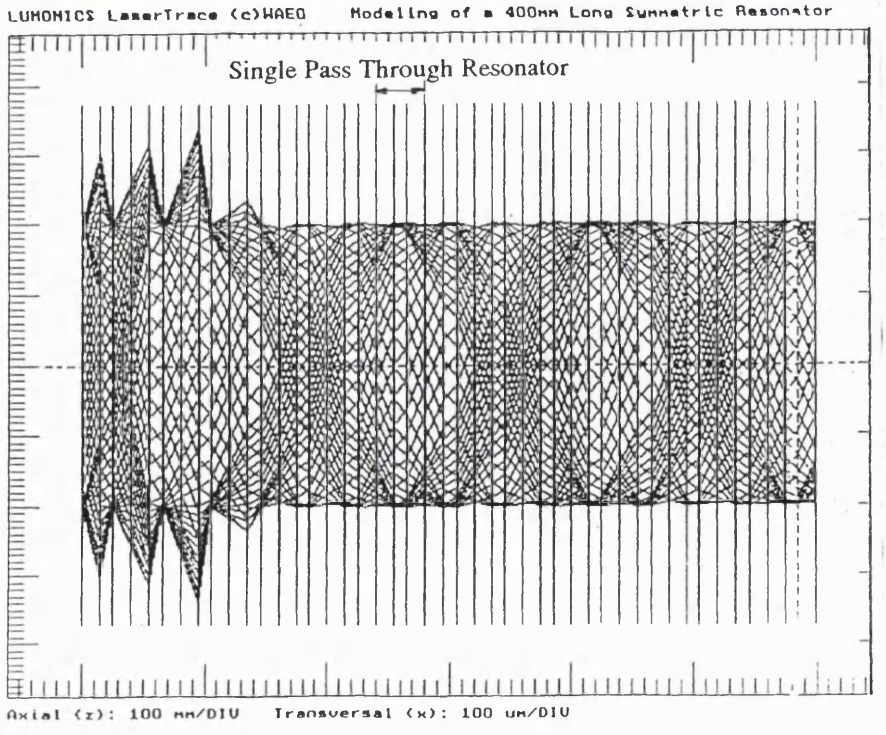

Figure 2.21 (b) i - Raytrace screen showing simulation of 'unfolded' resonator

LUMONICS LaserTrace (c)WAEG Modelling of a 400mm Long Symmetric Resonator

#	Z-Co-ord (mm)	Diam (mm)	Offset (mm)	½Div (mrad)	Point (mrad)	M^2	RaRa (mm)	T	Magn	Image @(mm)	EFL (mm)
0	0.000	4.000	-	7.000	-	27	363.8	☼	1.000	0.000	∞
1	149.2	6.089	-	7.000	-	27	363.8	<	1.000	-149.2	606.1
2	250.6	4.000	-	8.252	-	22	219.8	<	0.954	-278.6	606.1
3	399.8	5.150	-	8.252	-	22	219.8	<	0.708	-427.8	606.1
4	549.0	6.299	-	8.252	-	27	219.8	<	0.461	-577.0	606.1
5	650.4	4.000	-	4.676	-	17	515.1	<	0.350	-∞	428.4
:	:	:	:	:	:	:	:	:	:	:	:
:	:	:	:	:	:	:	:	:	:	:	:
:	:	:	:	:	:	:	:	:	:	:	:
41	5448.0	3.996	-	4.513	-	13	420.2	>	-0.357	-50184	-428.4
42	5597.2	3.987	-	4.513	-	13	420.2	=	-0.009	-50333	-428.4
43	5746.4	4.002	-	4.513	-	13	420.2	<	0.340	-50483	-428.4
44	5847.8	3.999	-	4.606	-	13	403.4	>	0.452	585.4	-600.3
45	5997.0	3.959	-	4.606	-	13	403.4	=	0.701	436.2	-600.3

****

Definitions

½Div	-	Half angle beam divergence
RaRa	-	Rayleigh Range
EFL	-	Effective Focal Length
☼	-	Source type; incoherent light source, used to simulate spontaneous emission
>,<	-	Coverging and diverging beams
=	-	Beam waist

Figure 2.21 (b) ii - Results Screen from LaserTrace raytracing software

2.4.4 Results

The variation, with average pump power, of measured output beam divergence and beam diameter at the output from the resonator is shown in Figures 2.22 and 2.23. As expected, the beam divergence increases with average pump power while the output diameter remains approximately constant, at approximately 2.25mm , over the full operating range. The distribution of the divergence data, where the average pump power is constant but the repetition rate used to obtain the average power is varied, suggests that lower divergence angles may be obtained for lower repetition rates. This can be explained by the differential heating which occurs due to higher pulse energies being extracted at the lower repetition rates (and therefore higher single

pulse energies) compared to higher repetition rates.

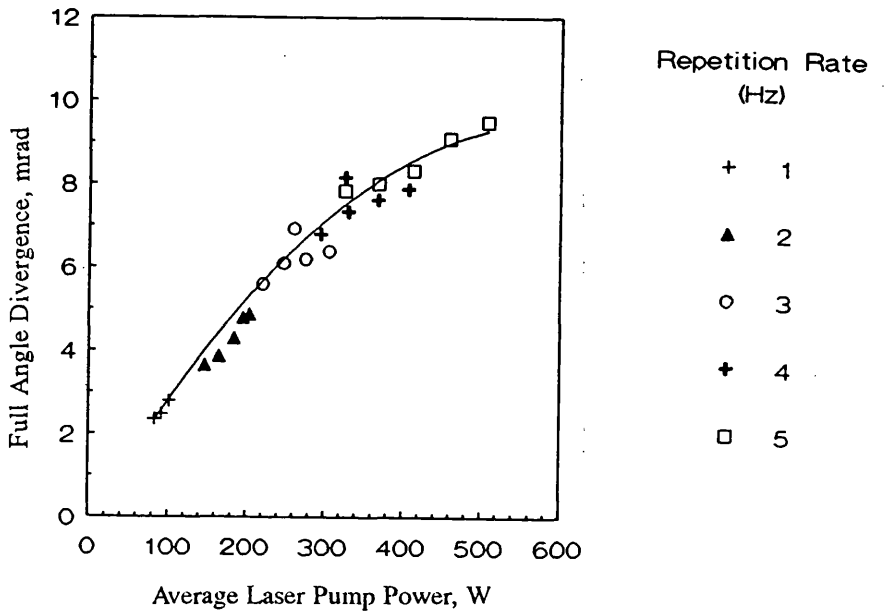

Figure 2.22 Change in output beam divergence from a 470mm long resonator with average lamp power.

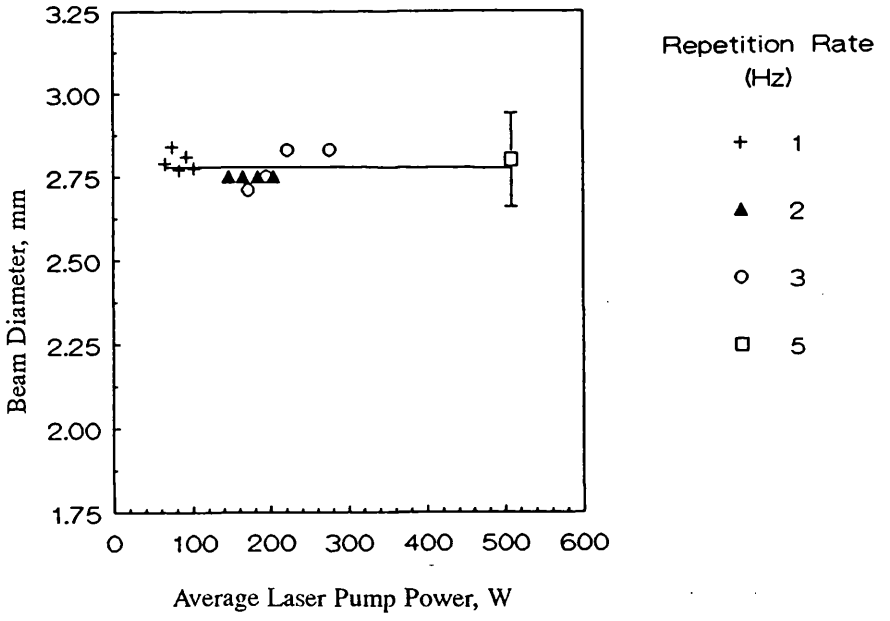

Figure 2.23 Change in output beam diameter from a 470mm long resonator with average lamp power.

From the divergence data the rod focal length was determined using the LaserTrace software. Figure 2.24 shows the variation in the focal length of the thermally induced rod lens with increasing pump power.

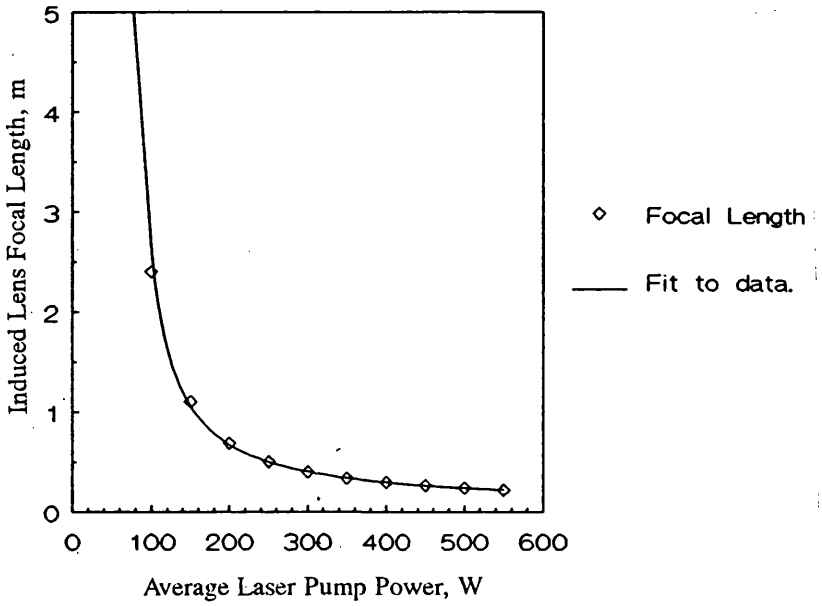

Figure 2.24 Variation in focal length induced in a 4"x4mm diameter CTH:YAG rod with average pump power.

Applying a power fit to the data yields the relationship between effective focal length and pump power of

$$\text{focal length, m} = \frac{3024}{(\text{Power Input, W})^{1.527}} \qquad (11)$$

which is of the form used by others[92] and where the power is in keeping with the range of values described in Appendix 4.

Comparing this experimental result to the data supplied by Bowman, Figure 2.25, it can be seen that, at average pump powers in excess of about 200W, a shorter induced focal length is reported here. This is undoubtedly due to the method used to determine the rod lens, which in Bowman's case was a direct method, but which could not yield information of the sort which could be used in our computer model. Generally, though, the results presented here are in reasonably good agreement with the data of Bowman as well as those of Moulton et al.

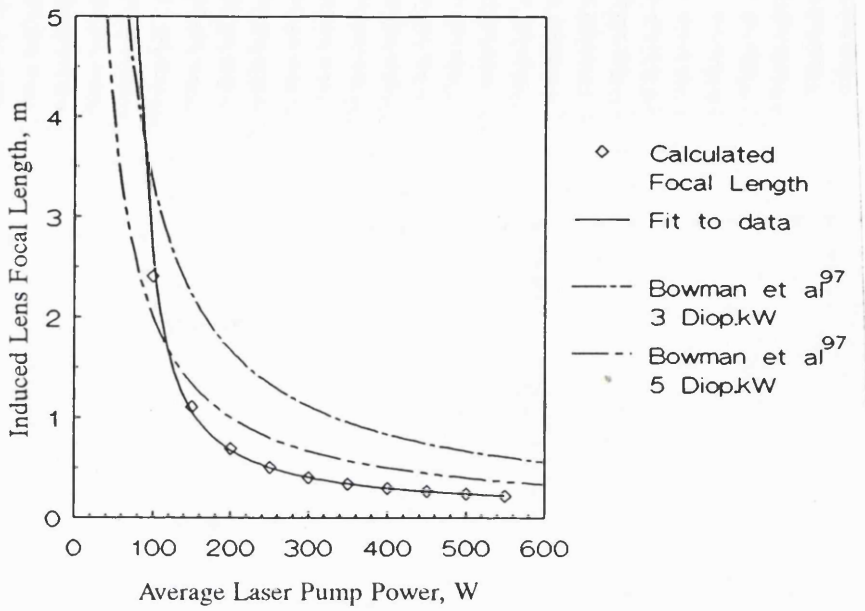

Figure 2.25 Variation in focal length induced in a 4"x4mm diameter CTH:YAG rod with average pump power. A comparison between this work and the work of Bowman et al[97].

2.4.5 Modelling of beam divergence from a second resonator

The performance of a 300mm long, symmetric resonator was then predicted using the thermal lensing data obtained from the initial experiments. The rod diameter in the model was again set to approximately 2.3mm to take account of the differences between theoretical and experimental interpretation of beam diameter. The output beam diameter and divergence from a real version of the resonator were then measured and compared to the results of the computer simulations. Figure 2.26 confirms again that the measured output beam diameter remained constant through the range of operating powers, although, for the shorter resonator, the typical diameter measured was approximately 2.5mm, roughly 10% larger than for the 470mm long resonator.

Figure 2.27 shows the change in full angle beam divergence from the 300mm resonator compared to the predictions from the model. It may be expected, from general resonator theory, that the shorter resonator will produce a higher beam divergence at a given pump power than the 470mm version and this is clearly seen if Figures 2.22 and 2.27 are compared.

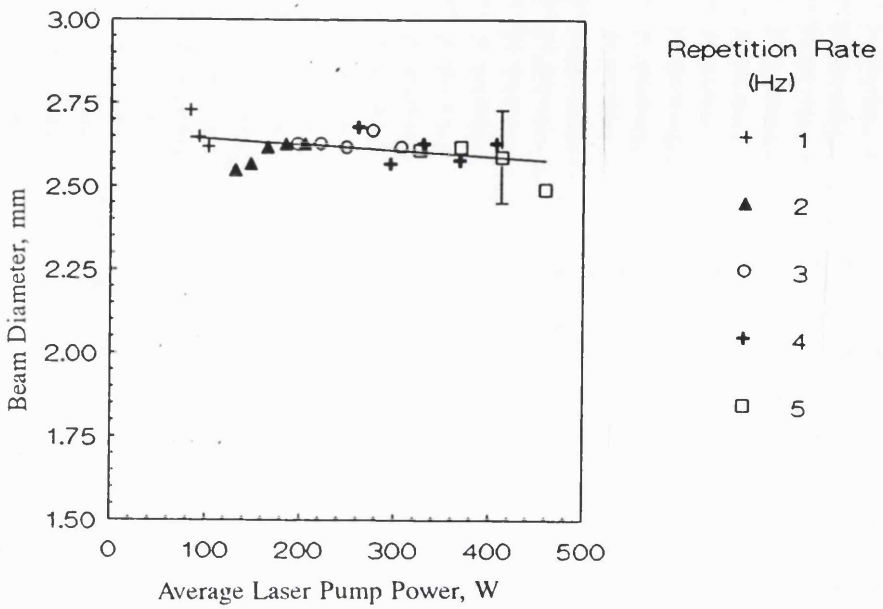

Figure 2.26 Change in output beam diameter from a 300mm long resonator with average lamp power.

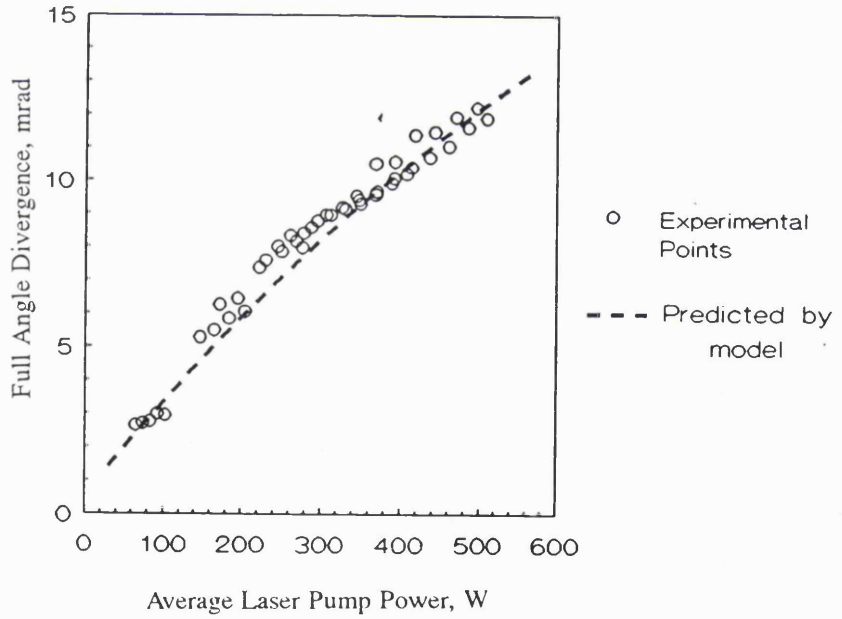

Figure 2.27 Comparison of the change in measured beam divergence with average pump power from a 300mm long resonator with the divergence predicted by the model.

Also, it is well known that shorter resonators are less sensitive to changes in the thermal lensing of the laser crystal. Although this reduces the possible deviations between experiment and theory the agreement between the two, demonstrated in

Figure 2.27 is still excellent. Analysis of a resonator design for which changes in the rod lensing would produce noticeable changes in the output beam divergence were not performed due to a lack of optics suitable for use within the resonator (i.e. anti-reflection coated components). Also, the rapid roll-off in the output energy which occurred, even for small increases in the resonator length, would have restricted the range of measurement points which could be taken.

2.4.6 Analysis of heating efficiency in CTH:YAG crystals

Thermal lensing in laser crystals arises from the accumulation of heat deposited in the crystal, by the flashlamp, and which is not re-emitted as light nor carried away by the cooling water. In equation (A4.7) the absorbed power is shown to be linearly related to the average power, delivered by the capacitors, to the lamp. Combining equation (11) and equation (A4.7) it is possible to estimate the proportion, δ_p, of the average pump power absorbed by the laser crystal. Assumed in the analysis is that the lensing in the rod is caused only by the thermal variations in the refractive index, photo-elastic effects and the effect of expansion at the rod ends being sufficiently small as to be ignored.

The results of this calculation are shown in Figure 2.28 and reveal that the fraction of flashlamp power (and consequently energy) absorbed by the rod increases with average pump power.

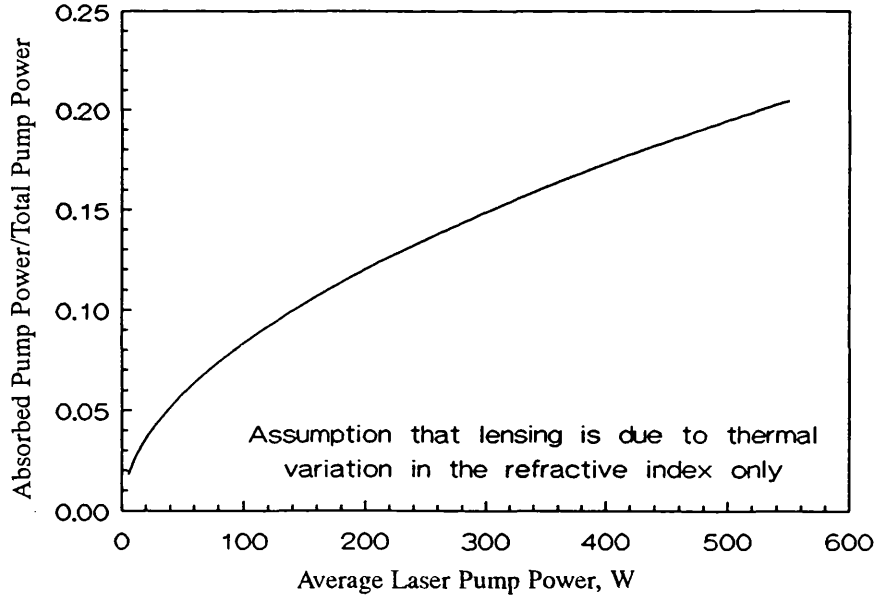

Figure 2.28 Fraction of average lamp power absorbed by the laser crystal, calculated using the results for the variation in induced focal length with average pump power.

Although the result is derived from experimental data in the range of average powers below 550W, the form of the resulting equation suggests that the fraction of light absorbed increases sublinearly approaching 30% absorption at an average pump power of 3kW.

There exists no published data for the CTH:YAG crystal against which to compare this result, however, data presented by Koechner, based on his work with CW lasers, suggests that up to three times as much heat is absorbed by the CTH:YAG laser crystal compared to Nd:YAG[101]. The reasons for this are mainly due to the absorption characteristics of the dopants especially those of the chromium ion which exhibits broad absorption bands in the blue/green region of the spectrum. Bowman et al also report significant heating in the CTH:YAG crystal indicating that 12-15 times the amount of energy delivered as laser output is converted to thermal energy. The authors of that work conclude only that a significant proportion of the absorbed pump radiation does not lead to the formation of excited holmium ions. It may also be possible that the de-excitation scheme, proposed by Fan et al[74] also serves to increase the amount of pump radiation converted to thermal energy. This does not explain the increase in the fraction of pump radiation converted to heat in the results presented here as the average power was varied using repetition rate as well as pump pulse energy. Consequently, identical pump pulse energies contribute data at several points on the x axis.

2.4.7 Discussion

The increase in the amount of flashlamp light converted to heat, reported here, most likely arises from the approximate nature of the analysis, where all the lensing is attributed to thermal variations in the refractive index with stress and end effects being ignored. Additionally, some of the variation with average power may arise from the fact that the focal length of the induced rod lens does not vary with the inverse of the average pump power, as predicted by theory. The reason for this can be explained using the thermal time constant theory developed in Appendix 4. At repetition rates where the rod is allowed to cool significantly between pulses the heating distribution developed is not parabolic. Most of the flashlamp light is absorbed near the outside of the rod creating a thermal profile, and subsequently a variation in the refractive index, which makes the rod act like a negative, rather than a positive lens. From Appendix 4, the critical repetition rate for a 4mm diameter CTH:YAG rod is about 2.5Hz. If the lensing data for the rod is then recast, with a straight line fit applied to the data points obtained at repetition rates greater than 2.5Hz (>200W), the resulting graph confirms the linear relationship between

average pump power and induced focal power, Figure 2.29. The straight line also looks intuitively correct, having an intercept at the origin where the lensing is zero. Also in keeping with the arguments presented is the fact that the data points near to the origin imply, for a near zero average pump power, that the rod will act as a negative lens, rather than a positive one, a result of the rod heating being concentrated around the edges of the rod rather than accumulating at the rod centre.

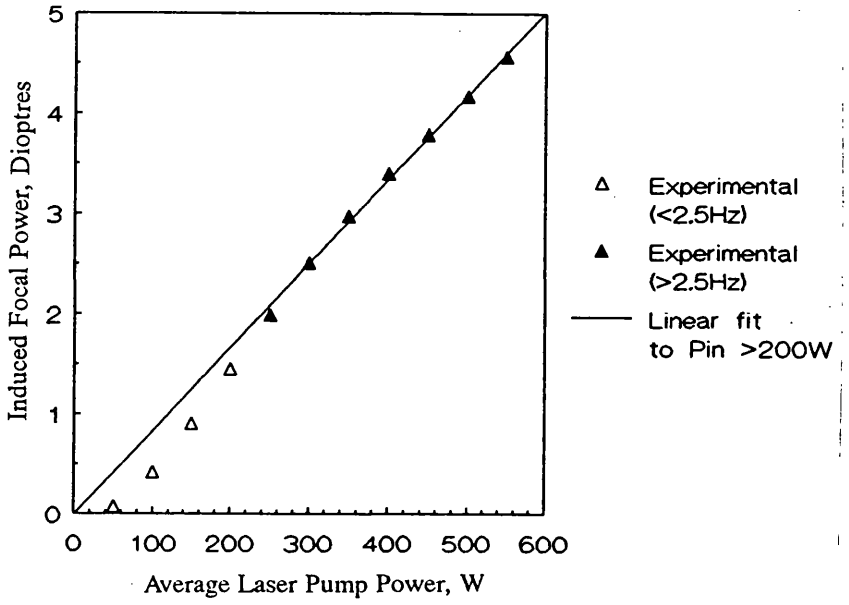

Figure 2.29 Variation in thermal lens focal power with average pump power.

The linear relationship between focal power and average pump power indicates thermal lensing which increases at a rate of 8 Dioptres kW^{-1}, twice that reported by Bowman for a rod of the same diameter. The reason for the differences between the results reported here and Bowman's may be due to the method of measurement, which, in Bowman's case was a direct method, and additionally the fact that Bowman's crystal was part of 'a uniformly pumped amplifier' suggesting two or more flashlamps. Although multiple flashlamps allow increased energies to be delivered to the crystal they also reduce the transfer efficiency, observed as an overall reduction in the laser efficiency. This is due to the walls of the pumping chamber being further away from the rod to accommodate the extra lamps, thereby reducing the focusing efficiency. Typically reductions in laser efficiency between 30 and 50% are reported[102,32] in keeping with the discrepancy in induced lensing reported here.

Thermal lensing is the cause of changes in the output beam divergence from resonators. Between 5% and 20% of the available pump power is converted to heat

while up to 2% appears as useful laser output. This is consistent with the heat generation reported by Bowman et al[34] for the single flashlamp chamber. An empirical power fit to the experimental lensing data takes account of the fact that, at low repetition rates, the thermal profile is not parabolic, being influenced by the relatively large fraction of energy deposited around the edges of the crystal. The form of this equation is consistent with that reported elsewhere although the lensing increases at a rate almost an order of magnitude greater than Nd:YAG[103].

Using ray tracing software, it was possible to accurately predict the divergence performance of a 300mm long symmetric resonator over the pump range 60-500W although it was necessary to modify the diameter of the rod used in the model to take account of differences in the definition of spotsize between the ray tracing program and experiment.

2.5 Transient Laser Performance

The output pulse duration of Fixed-Q lasers depends only weakly on the lifetime of the upper state. Excitation energy emitted from the flashlamp is stored in the upper laser level until sufficient ions are excited to create a population inversion. If the spontaneous decay rate from the excited state is fast, compared to the excitation rate, then population inversion may never be obtained. This is exemplified by the observations of Huber[104] who observed higher threshold energies with increasing lamp pulse durations. Because his data has not been published elsewhere, it is produced here, for information, as Figure 2.30. Once laser action has been initiated, the upper state lifetime plays a lesser role as excited states are depopulated by stimulated emission before spontaneous emission can occur.

The delay-to-lasing is the time taken from the start of the pump pulse to the start of laser action and is simply the period of time during which the population inversion is built up until the gain in the resonator exceeds the loss. The theory describing the characteristic delay-to-lasing is different for three and four level lasers due to the number of ions required to be elevated to excited states in each. Delay-to-lasing theory is developed in Appendix 5, using the work of Siegman[105] and Zverev[106] for three and four level lasers respectively.

The CTH:YAG laser is often described as a three level, or quasi three level, laser due to the effect of thermal population on the laser threshold energy. By evaluating the performance of flashlamp pumped systems operating in a Fixed-Q

mode, and comparing against the separate theories for the delay-to-lasing, it will be seen whether the scheme is most appropriately described by three or four level theory with a temperature sensitive lower laser level.

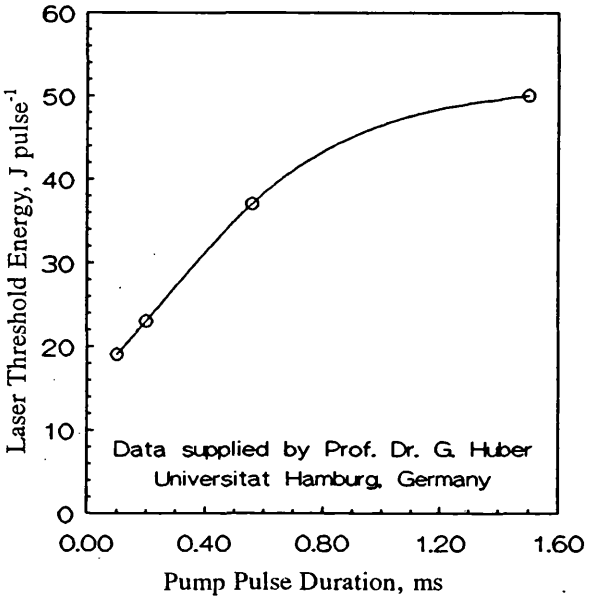

Figure 2.30 Change in laser threshold with excitation pulse duration, after Huber[104]

2.5.1 Differences between theory and practise

The temporal profile of the pump pulse from the flashlamp in pulse laser systems depends on the configuration of the discharge circuit. Most Fixed-Q lasers rely on a capacitative discharge, consequently the light output from the lamp, which follows the current waveform, has a quasi-Gaussian shape. Unfortunately, the theories of Siegman and Zverev are based on rectangular pump pulses. Despite efforts to 'square up' the discharge, the emission from the lamp seldom resembles a rectangular pulse more often being bell shaped in appearance. Exceptions to this are pulse pumped high power lasers where rectangular pump pulses can be obtained although only for discharges in excess of about 2.0ms. Attempts to formulate the theory for Gaussian shaped pulses or simpler polynomial functions results in equations which can only be solved numerically and present a considerable level of complexity beyond the scope of this thesis. Previously reported work does not, in general, discuss in detail the nature of either the pump pulse, or the output temporal profile. However, it is clear that, to obtain the maximum efficiency, short pump pulse durations are required, thereby necessitating capacitative discharge circuitries and the inconveniences associated with them when comparing against rectangular wave theory. Fortunately, it is possible to calculate an equivalent rectangular pulse duration based on the fact

that, for the rectangular pulse case, the maximum delay-to-lasing will occur at a pump level just above the laser threshold energy. In this instance all of the flashlamp discharge is being used to achieve population inversion and the delay-to-lasing, t_d, will be the same as the rectangular pump pulse duration, T_p. At higher pump energies some of the delivered energy will end up as useful laser output and t_d will be less than T_p. The equivalent rectangular pulse duration is the maximum delay-to-lasing observed for the actual pulse duration. To compare the theory, describing the delay-to-lasing for three and four level, it is therefore necessary to use the equivalent pump pulse duration, T_p, rather than the actual temporal profile, T_f.

2.5.2 Measurement of the delay-to-lasing

The delay between the start of the flashlamp pump pulse and the onset of laser action was measured over a range of operating conditions. A 4"x4mmϕ rod, housed in a $BaSO_4$ pumping chamber and pumped with a single flashlamp was located approximately at the centre of a symmetric resonator where the distance between the mirrors was 470mm. The output was monitored using a PbS photodetector (Graseby Infrared Ltd., Newmarket, Suffolk) connected directly to the 50Ω input of a Tektronix 2445B, 200MHz oscilloscope. The sweep was triggered using the sync. from the laser power supply which was derived from the flashlamp trigger circuitry. The temporal profile of the flashlamp emission was displayed simultaneously with the laser temporal profile. The flashlamp emission had a quasi-Gaussian appearance with a duration (FWHM) of 350μs, Figure 2.31, while the duration of the laser emission varied according to the pump level.

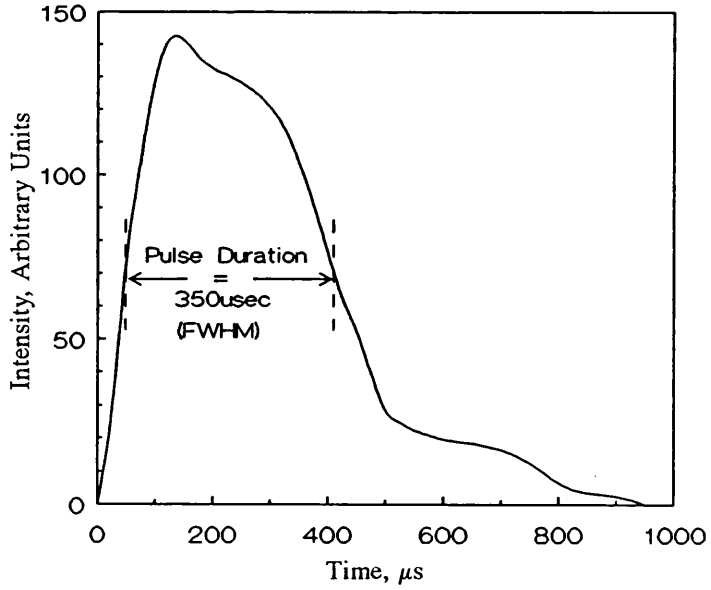

Figure 2.31 Typical temporal profile obtained from a xenon flashlamp pumped by the discharge from the two stage circuit shown in Figure A2.6.

The time between the start of the excitation pulse and the laser emission was measured using the 'time elapse' feature on the oscilloscope. Figures 2.32 (a), (b) and (c) show the oscilloscope traces obtained for operation at 5Hz and input energies of 83 J pulse^{-1}, 92 J pulse^{-1} and 102 J pulse^{-1}, respectively. The results show clearly the reduction in delay-to-lasing as the input energy is increased.

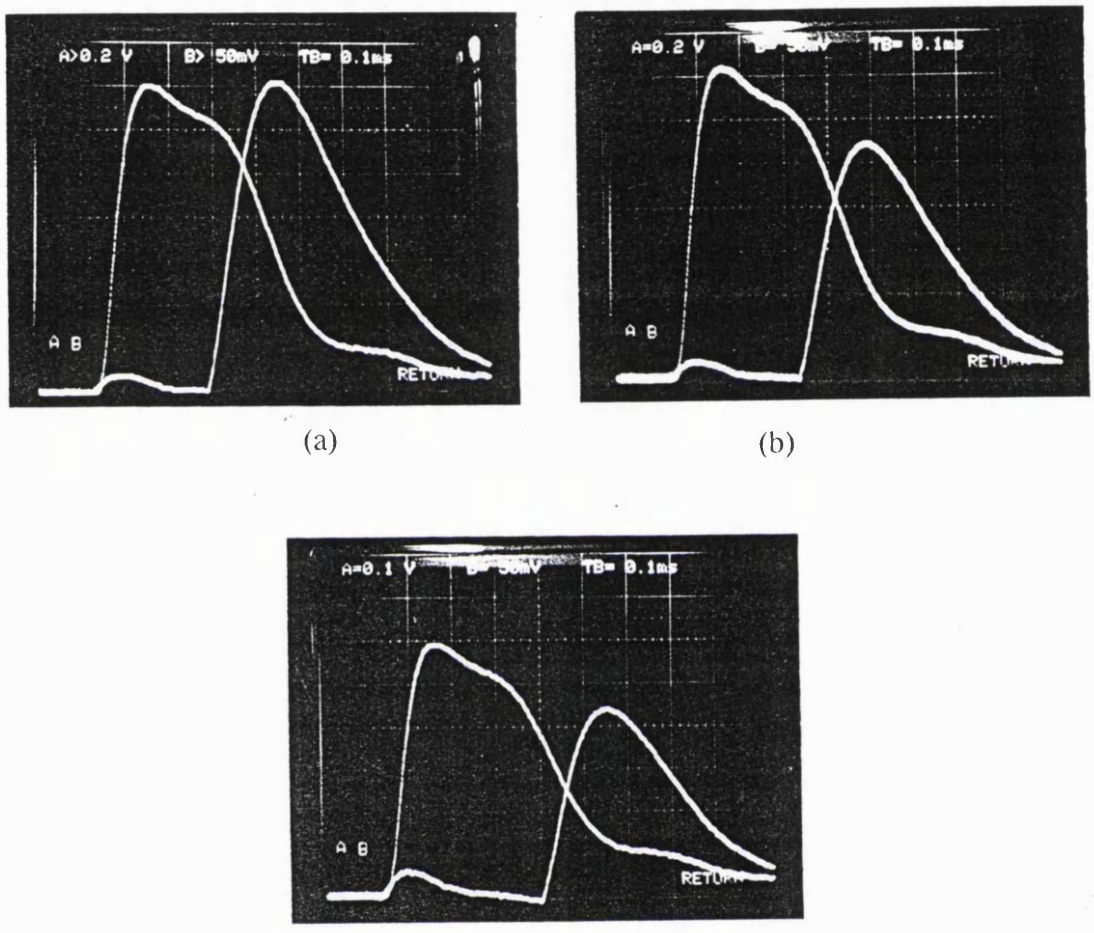

(a) (b)

(c)

Figure 2.32 Measurement of the delay-to-lasing between the flashlamp pulse (left hand pulse) and the laser pulse (right hand pulse) at three typical lamp discharge energies a) 102J, b) 92J and c) 83J. Note the increasing delay between the start of the flashlamp and laser pulse with decreasing pump energy. The timebase is 100μs/division.

To allow data to be obtained for different operating conditions the temperature of the coolant flowing over the laser crystal was varied, so as to raise the laser threshold. The results, shown in Figure 2.33, indicate that the reduction in the delay may have some temperature dependence. However, from the theory (Appendix 5) it is known that the delay to lasing depends not on the pump energy, but on the ratio of

the discharge energy to the threshold energy, r.

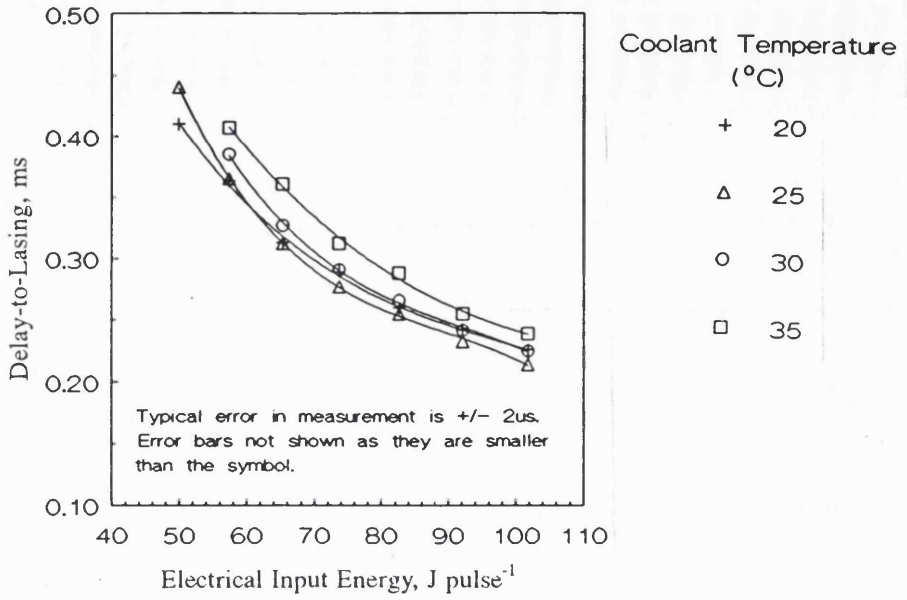

Figure 2.33 Change in the measured delay between the start of the flashlamp excitation pulse and the start of laser action with lamp discharge energy. The operating temperature being varied in order to change the laser threshold.

Figure 2.34 shows the same set of data where,this time, the x data is r, the ratio of the discharge energy to the threshold energy[105]. Shown also are the theoretical curves for three and four level systems using equations (12a) and (12b) from Appendix 5.

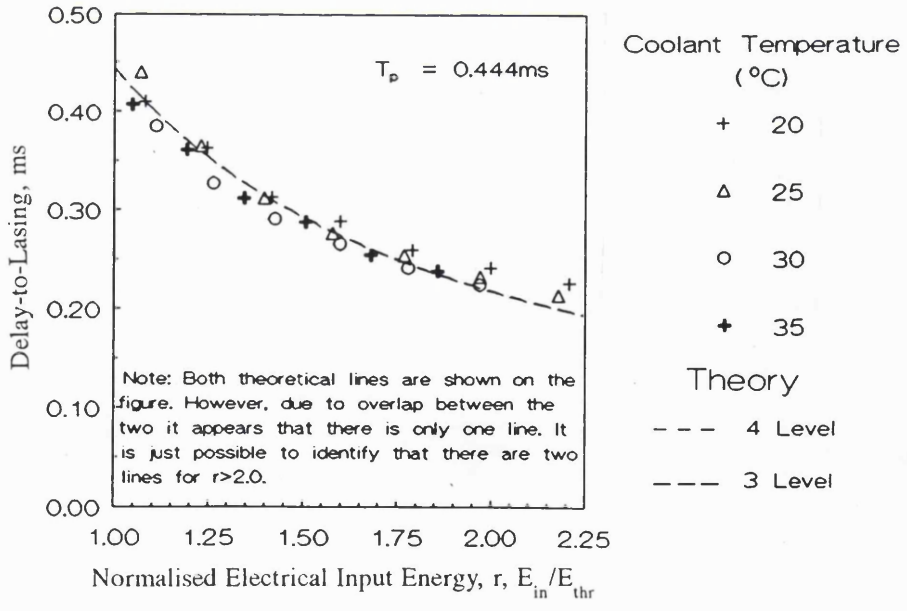

Figure 2.34 Change in the measured delay between the start of the flashlamp excitation pulse and the start of laser action with normaised discharge parameter, r. The operating temperature being varied in order to change the laser threshold.

Here the relationship between the pump rate, W_p, and the discharge energy is assumed to be linear (from equation A5.8). The fluorescent lifetime used in the calculation is 9.0ms, which is the lifetime predicted by Bowman et al as being the intrinsic lifetime in the absence of pump energy[34]. The pulse duration, T_p, is 0.444ms which was obtained from the intercept with the Y axis for a 3rd order polynomial fit to all the experimental points where r, the excitation energy ratio, was less than 1.25. To allow calculation of the predicted delay for a three level system it was necessary to calculate the atomic pump rate at threshold, $W_{p,thr}$. This was done by numerically solving equation (5.12a) for the threshold condition (i.e. T_d = 0.444ms) using a computer based mathematic package (MathCad, Version 2.5, MathSoft Inc., Cambridge, Mass.). The result of this process was a value of $W_{p,thr}$ of 1610sec^{-1}. Calculation of the drive level, relative to the threshold pump rate was then possible via equation (A5.8). Thus, although the x axis in Figure 2.34 is in terms of the energy ratio, r, the three level theory is plotted against the pump rate ratio, α, as given in Appendix 5. The results of the experiment show an interesting feature. Namely that, although three and four level theories differ, identical curves are obtained for each. Both theories appear to fit the data well, indicating that future systems may be modelled from just the threshold data using either three or four level theories. Additionally, it is clear that the rectangular pulse duration, T_p, derived from the experimental results, provides a useful approximation for the purpose of the theory despite the true pulse shape being more Gaussian in appearance.

2.5.3 Laser pulse duration

In the rectangular pulse theory the laser output pulse is assumed to rise instantaneously and thereafter follow the shape of the flashlamp light envelope, Figure 2.35. The laser pulse ends when the pump light ceases. Therefore, the duration of the laser pulse, T_d, can be predicted by subtracting the delay-to-lasing time, t_d, from the flashlamp duration

$$T_d = T_p - t_d \qquad (12)$$

Clearly this is independent of whether the laser scheme is three or four level, depending only on the pump pulse duration and the experimental delay.

This theory was investigated briefly, the experimental data providing useful information of a general nature for later work. The temporal profile of the laser pulse was monitored using an InAs photovoltaic detector (Laser Monitoring Systems, Newland Business Park, Hull) linked to the 50Ω input of an oscilloscope (Gould 465,

100MHz, 200 Megasample(second)$^{-1}$). A typical trace is shown in Figure 2.36.

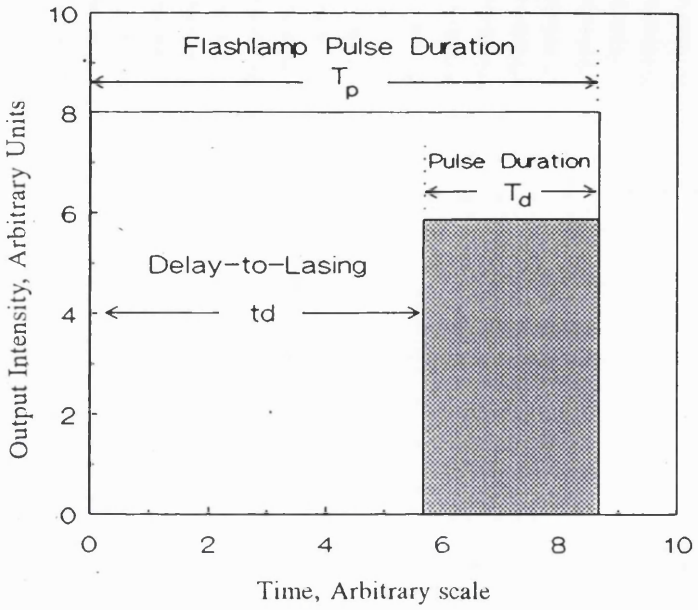

Figure 2.35 Critical times in the rectangular pulse theoretical approach to delay-to-lasing.

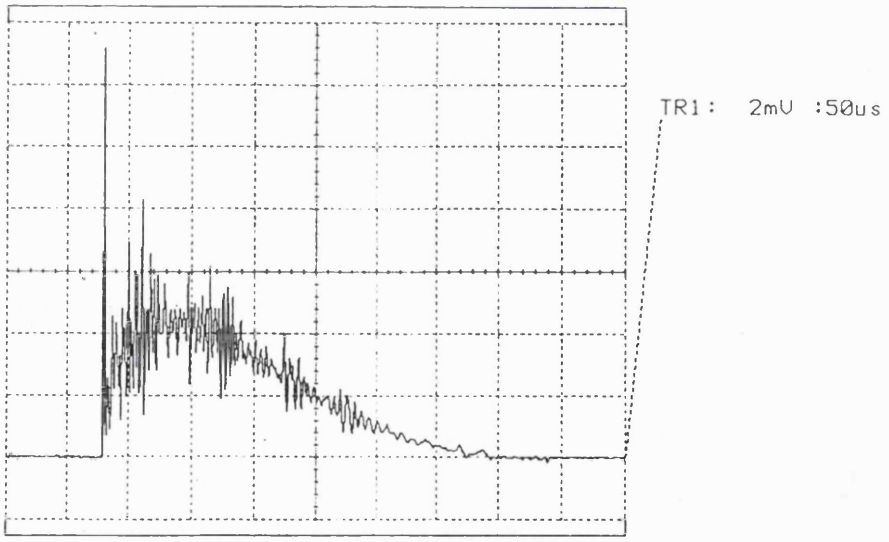

Figure 2.36 Typical temporal profile of the pulse output from the CTH:YAG laser.

The output commenced with a large pulse with a peak approximately three times that of the rest of the pulse. The remainder of the pulse consisted of a train of spikes which were not separate, therefore the profile resembled that of a continuum. This is very much the normal, characteristic profile of a low to moderate gain, Fixed-Q laser pulse. The pulse duration at the full width half maximum (FWHM) was determined using the functions on the 'scope. For consistency, the maximum was taken as the

peak point in the imaginary smooth curve describing the output emission envelope, not including the first spike. This is the standard way to make the measurement allowing the measurement to be made with apparatus not capable of resolving the spiky nature of the pulse.

Figure 2.37 shows that, according to the rectangular pulse theory, the pulse duration obtained should increase with the normalised discharge ratio, r, at a sublinear rate. However, in practise, the pulse duration rises rapidly between r=1 and r=1.25 thereafter remaining constant. Additionally, despite having demonstrated that the delay to lasing is a function of the parameter r, it is observed that a different constant pulse duration is obtained for different operating temperatures. The difference between the 20°C and 30°C data points is about 50μs being greater than the difference of 20μs, calculated from the errors of each measurement.

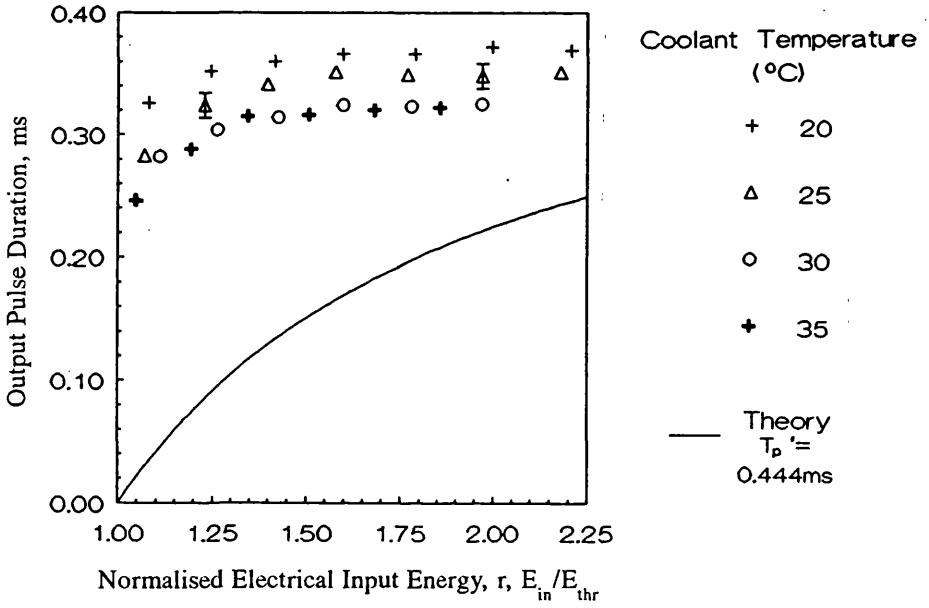

Figure 2.37 Comparison between the measured output pulse duration and that predicted from the rectangular pulse delay-to-lasing theory.

2.5.4 Discussion

The reason for the deviation between theoretical predictions of the pulse duration and the experimentally determined value can be attributed largely to the inaccuracy of the model. In the previous section, where the delay to lasing was predicted with some accuracy, the start of the laser pulse was marked by a rapid increase in laser intensity. Such is the rate of rise that, at the instant that the pulse emerges, the

temporal profile looks exactly like that of a rectangular pulse. The same is also true of the pump pulse which, while not rising as rapidly as the output pulse, increases rapidly, compared to the total duration of the pulse. For the pulse duration, though, several features work against, rather than towards, making the theory fit the practise. For example the FWHM duration of the output pulse is quite different from the duration defined for a rectangular pulse and, whereas with the delay-to-lasing theory it was valid to describe an equivalent pump pulse duration, it would be of no use to define an equivalent output pulse duration here. The ease of measurement of the rapid leading edges of the pump and emission pulses are countered in the measurements of pulse duration by a slowly varying trailing edge. Using the experimental data it is interesting to apply the simple approaches embodied in equations (A5.12a) and (A5.12b) and equation (12) of this thesis. Simply stated, the maximum output pulse duration should be the pump pulse duration. The experimental data shows that the maximum achieved pulse duration is 320-370μs approximately the same as the measured pump pulse duration of 350μs. As some of the delivered pump energy is required simply to reach laser threshold, and, from the earlier laser measurements this has been shown to be about 30% of the maximum available pump energy, it was expected that the delay-to-lasing, t_d, would not approach zero and, therefore, the output pulse duration would not approach that of the pump pulse. The experimental observations show that, even at the maximum drive level, the delay-to-lasing does not approach zero. The conclusion from this fact and measurement of the laser pulse duration is that lasing continues for a period after the end of the excitaion pulse. For the CTH:YAG laser this period appears to be of the order of microseconds, in keeping with the transfer times between sensitising ions reported by others [70,71]. Thus, it is suggested that excitation of the upper laser level continues after the end of the flashlamp excitation pulse due to the delays in transferring energy between the sensitisation dopants chromium and thulium.

Besides the theoretical analysis of pulse duration it is useful to know the pulse duration for specification purposes. Additionally, when modelling the interaction of laser light with other media it is often essential to know the duration of the pulse in order to know the peak power during the delivery. For this reason Figure 2.38 is included to show the variation in pulse duration with the output energies obtained. This shows that, for output pulse energies above 0.5J, the FWHM pulse durations range between 0.35ms and 0.32ms for 20°C to 35°C operation, respectively.

2.5.5 Conclusions

Certain aspects of the transient performance of the CTH:YAG laser can be successfully predicted using laser theory. Specifically, agreement between theory and practise has been demonstrated for the delay between the start of the excitation pulse and the laser emission. However, in order to make the prediction it is necessary to calculate either an equivalent rectangular pump pulse duration when using four level laser theory, or alternatively, the atomic excitation rate at threshold, $W_{p,thr}$, when three level theory is applied. It has been demonstrated that the end result from each theory is the same, therefore, the four level theory approach is recommended as the equivalent pulse duration can easily be derived from a limited number of experimental points. In contrast the three level theory requires the more complicated step of numerically calculating the pump rate. Contrary to expectations it is not possible to clarify the three or four level laser description from these experiments.

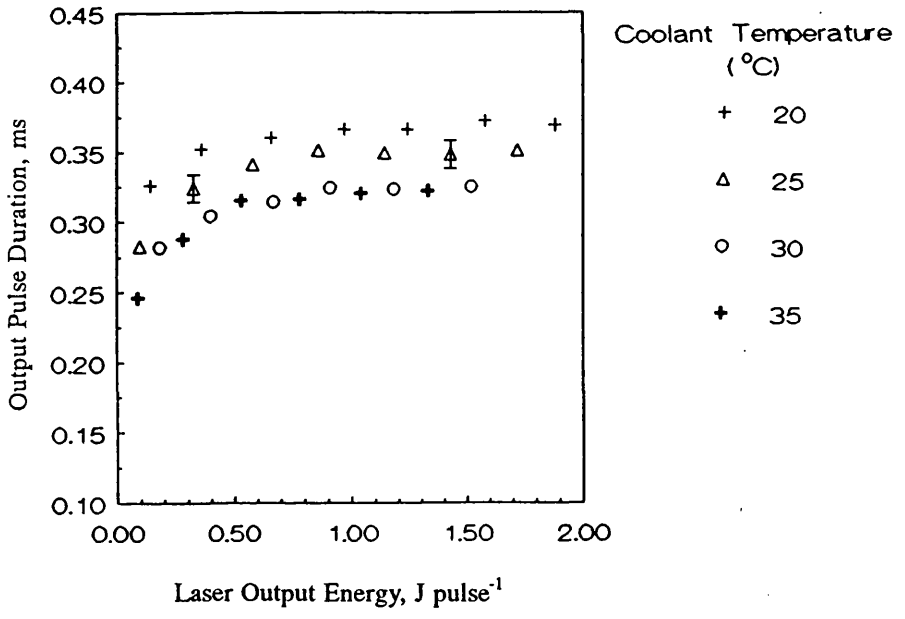

Figure 2.38 Change in output pulse duration with output pulse energy at a number of different operating temperatures.

The simple theory, which predicts the delay-to-lasing performance cannot be used to predict the pulse duration obtained. This is largely due to the shape of the pump and laser output pulses. Attempts to rework the theory to take account of the pump pulse shape result in transcendental equations which could not be solved. The observed laser pulse duration was observed to rise rapidly between r=1 and r=1.25, at which point the output energy was approximately 0.5 J pulse^{-1}. Thereafter the pulse duration was constant at around 345μs (FWHM), in keeping with the pump

pulse duration. Some variation in the final level was observed for different operating temperatures. No explanation of this can currently be offered.

2.6 Fibre Optic Beam Delivery

It is essential, when considering the development of laser systems, to consider the available forms of beam delivery. For lasers operating below 2.5μm and above 400nm, flexible optical fibres are available for delivery of the light to otherwise inaccessible locations. These fibres are made using a silica core and with either a doped silica cladding or other materials having suitable refractive indices. For laser power delivery (rather than data communications), all silica fibres are typically used due their greater power handling capabilities. Beyond 2.5μm, several other materials are available. Amongst these are zirconium fluoride and chalcogenide fibres, although neither of these is bio-compatible. Most promising of the new IR transmitting fibres are the sapphire fibres developed at Stanford[107] although these are not currently commercially available.

The fibre optic transmission characteristics of commercially available all-silica fibres were assessed to establish whether reliable transmission at reasonable power levels could be obtained at the pulse energies available from the lasers. Typically, small diameter fibres with core diameters of 200-400μm are preferred for endoscopic beam delivery due to the increased degree of flexibility offered. Additionally, where high light intensities are required at the distal tip of the fibre to produce the desired effect, such as in laser angioplasty or lithotripsy, then smaller diameters will produce higher local intensities, thereby reducing the need for refocusing optics on the end of the fibre. However, if the peak power density exceeds the damage threshold of the fibre, then the input face of the fibre may be destroyed. Thus, it was necessary to confirm that reliable transmission could be maintained without reductions in the transmission efficiency.

The conditions for coupling laser beams into fibre optics is well known. In summary, the spot diameter on the face of the fibre must not exceed the boundary of the core-cladding interface. To achieve spotsizes comparable to the fibre core size, it is necessary to focus the laser beam using a lens. Typically, the fibre is positioned at the focus of the beam where the spotsize is smallest. Because the focused spot is defined in terms of its 86.5% contained energy diameter and the spatial profile is continuous, the focused spot diameter required for efficient coupling is usually required to be between 80% and 95% of the fibre core diameter. Furthermore, the

input cone angle must not exceed the acceptance angle of the fibre, denoted in radians by the numerical aperture (N.A.) of the fibre. For fibres located at the focus of the lens, this means that the beam quality of the laser beam must comply with the inequality

$$2(\text{N.A.})\phi_f \quad \geq \quad \text{Divergence x Diameter} \qquad (13)$$

where the divergence is the full angle and ϕ_f is the fibre diameter.

Recently, Moslem et al[108] have reported their experience in transmitting light from CTH:YAG lasers into fibres with core diameters as small as 200μm. They found that, in general, lower N.A. fibres transmitted light less efficiently than did fibres having N.A.s around 0.4. For a 200μm diameter, 4m length of fibre, prepared at each end by cleaving, the maximum transmission percentage measured by Moslem et al was 69.5%. Of this, 12% was attributed to losses through scattering or absorption while the amount of light lost through reflections from the end faces amounted to 21% of the incident energy. These transmission percentages are low compared to the losses observed in the transmission of 1.06μm Nd:YAG light in commercial laser systems. In such systems, combined reflection and attenuation losses seldom produce more than a 10% reduction in the available energy after several tens of metres of fibre.

2.6.1 Experimental arrangement

The experimental laser configuration used in these experiments is the same as that reported earlier in this chapter. A 4"x4mmϕ crystal (rod No. 3) was housed in a $BaSO_4$ pumping chamber and pumped with the emission from a single xenon flashlamp. Resonators were formed around the crystal and consisted of plane reflecting optics placed an equal distance either side of the crystal. The length of the resonators used were 300mm and 470mm. From the measurements of beam divergence and output beam diameter made for section 2.4 it was possible to calculate the beam quality for each resonator in terms of the divergence x diameter product, Figure 2.39.

It can be seen that, as might be expected, the beam quality deteriorates with average pump power and is noticeably greater for the shorter resonator. The core diameters of available fibre were 320μm and 200μm with both core and cladding made of silica (FibreGuide Industries, Stirling, NJ, USA). This results in an N.A. of 0.22. This placed restraints on the beam quality required to achieve the conditions,

set out in equation (13), of 140.8mm.mrad and 88mm.mrad, respectively. It can be deduced, therefore, that successful fibre coupling into both fibre diameters should be achievable for either resonator configuration.

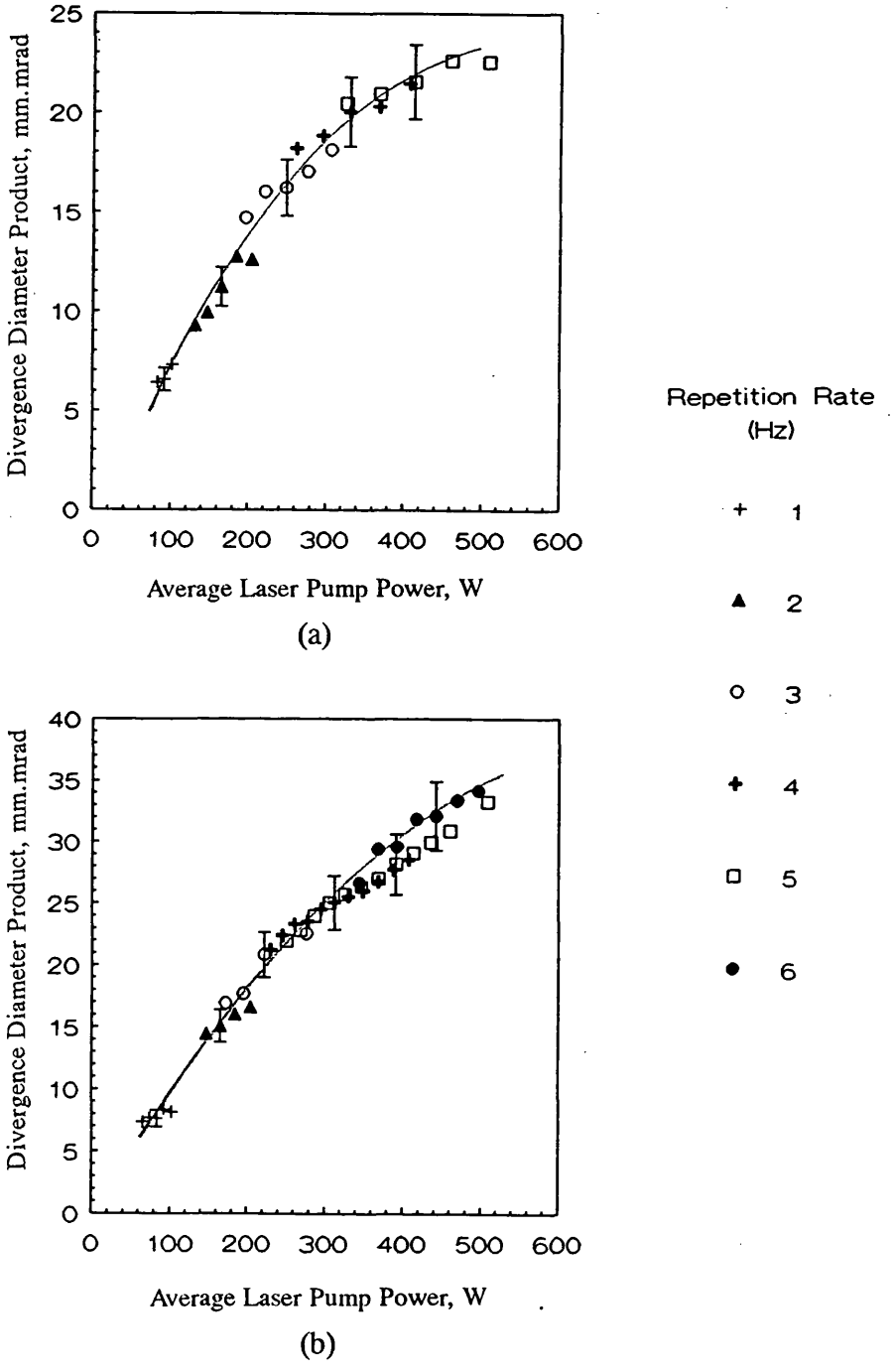

Figure 2.39 Change in output beam quality with average pump power for laser resonators (a) 470mm long and b) 300mm long, each resonator containing a 4"x4mm diameter CTH:YAG rod in a $BaSO_4$ pumping chamber and pumped by a single xenon flashlamp.

The fibres were of a low OH content to minimise the absorption losses at the laser wavelength, Figure 2.40. Their lengths varied between one and two metres. No attempt to straighten the fibres was made, although at no point was the bend radius of the fibres less than the minimum diameters recommended by the manufacturers. Nor were the fibres bent to radii less than those at which Moslem et al measured increased losses. Fibre end faces were wet polished using 3μm followed by 0.3μm paper to achieve a defect-free optical surface.

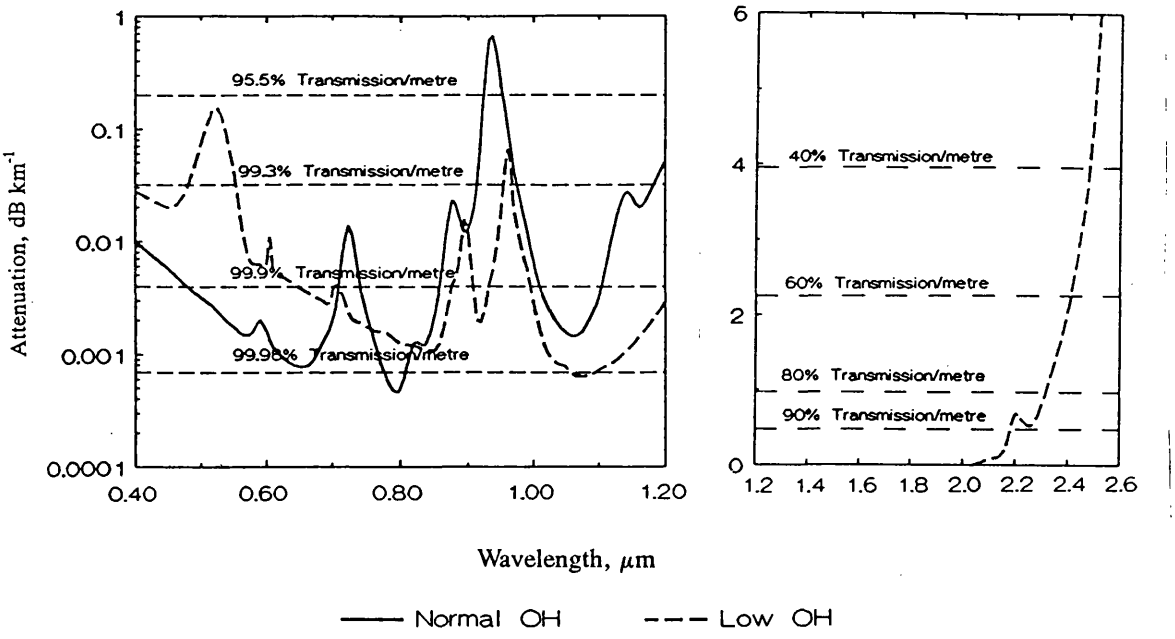

Figure 2.40 Attenuation characteristics of 'normal' and low OH content optical fibre from visible wavelengths through to 2.5μm. (Data courtesy of FibreGuide Industries Inc, Stirling, NJ, USA).

The relationship between the spotsize produced by the action of a positive lens of focal length F (mm), focusing a beam of full angle divergence α (mrad), is given by

$$d_s = F\alpha \qquad (14)$$

Considering the experimental data for the beam divergence from these resonators, and the required spotsizes to achieve a 90% fill of the fibre core diameter, the focal lengths of the lenses required was calculated. Practical considerations based on the resolution of the apparatus available, as well as consideration of the possible effects of lens aberrations which would have increased

the focal diameter, restricted the choice of lenses to >F5 for singlet lenses and >F2.5 for achromat doublets (F*nn* represents the ratio of the lens focal length to the diameter of the beam at the lens). Table 2.3 shows that the result of calculating the focal lengths for direct coupling required lenses of focal lengths as short as 14.5mm. Although within the F-number limits, the practical aspects of working with such short focal length lenses, such as the small depth of focus and limited physical size, make focal lengths of about 15mm impractical.

Resonator length	Percentage fill of fibre diameter	Desired spotsize, μm	Required focal length, mm	Operating F-number
300mm	90% of 200μm	180	14.5	5.7
300mm	90% of 320μm	288	23	9
470mm	90% of 200μm	180	18.9	8.2
470mm	90% of 320μm	288	30.3	13.2

Table 2.3 Calculated required focal lengths for fibre coupling

To increase the focal length of the lens, while maintaining suitability for use with all resonator configurations, it was decided to expand the beam prior to focusing using a modified Galilean telescope. The optical configuration is shown in Figure 2.41.

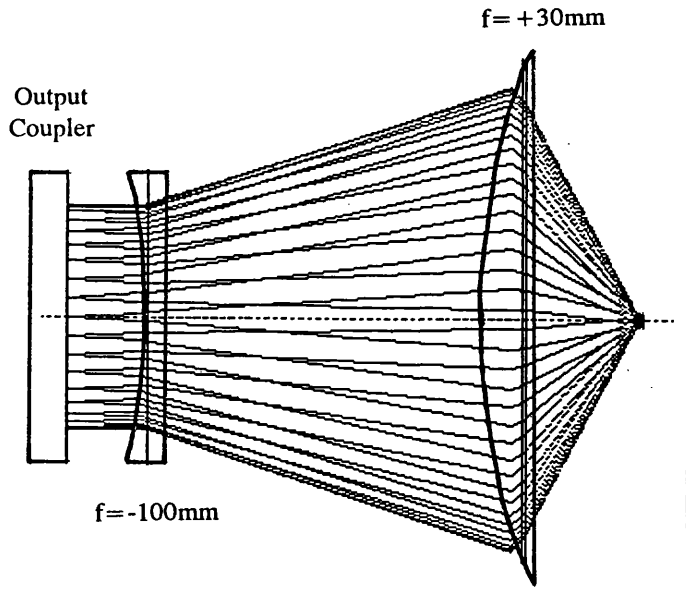

Figure 2.41 Optical configuration used to couple laser output into optical fibres. Figure also shows results of a raytrace through the system for a typical set of input parameters.

A -100mm plano-concave lens, placed at the output of the 470mm long resonator, was used to expand the beam prior to focusing with a +30mm plano-convex element. Both elements were made from fused silica and were selected due to their superior transmission at 2.1μm compared to other, more common materials such as BK7. The separation of the two lenses was determined experimentally to achieve a spotsize of $\leq 180\mu$m (to couple into the 200μm fibre) with a depth of field of greater than ± 0.1mm. In this instance, depth of field was defined as the distance on either side of the minimum spot diameter for which $>99\%$ of the laser beam could still be transmitted through a 200μm aperture, Figure 2.42. The configuration was found to comply with both spotsize and depth of field criteria when the separation of the two lenses was 125mm. At larger separations, the spotsize was reduced, but at the expense of a more restricted depth of field.

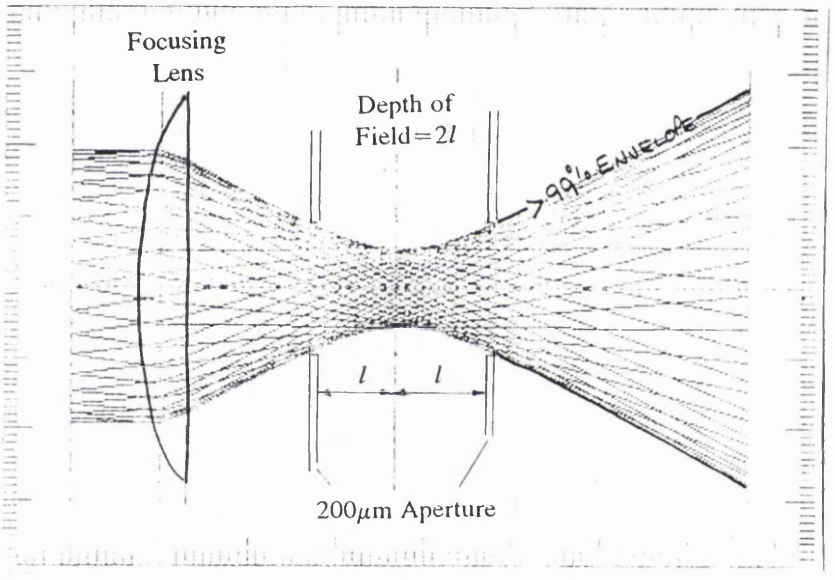

Figure 2.42 Diagrammatic representation of the definition of 'Depth of Field' of a laser beam.

The waist of the beam was located using a 200μm aperture translated along the axis of propagation and centred to achieve the maximum transmission, as monitored by an PbSe diode and an integrating amplifier. The aperture was then back-illuminated with white light and viewed, via the focusing lens, with an adjustable telescope, until the aperture was in sharp focus. The aperture was then removed and replaced with a 200μm fibre, also illuminated at the distal end with white light. The fibre was terminated with a biconic connector, used in many communication fibre optic systems where high tolerances ($\pm 1\mu$m) are demanded. The fibre was screwed into a bulkhead connector and moved along the propagation

axis of the laser light until the core of the fibre came into sharp focus. The position of the fibre was then fixed. Finally, to obtain accurate alignment of the fibre face to the incoming light in the x and y axes, perpendicular to the propagation axis, a small amount of laser light was allowed to fall onto the fibre at below damage threshold levels. The amount of light transmitted was detected using the photodiode sensor. The x-y position of the lens was then adjusted to maximise the signal. It was found that, to maintain laser stability, operating levels well above threshold were required. However, such levels increased the incidence of damage. As a compromise, an 80% reflecting output coupler angled at 45° was used to reflect most of the laser energy. To minimise the beam offset introduced by this optic which would otherwise have resulted in vignetting of the beam at the focusing optic, a second mirror substrate was angled orthoganally to the first and also at 45° degrees to the incoming beam, Figure 2.43.

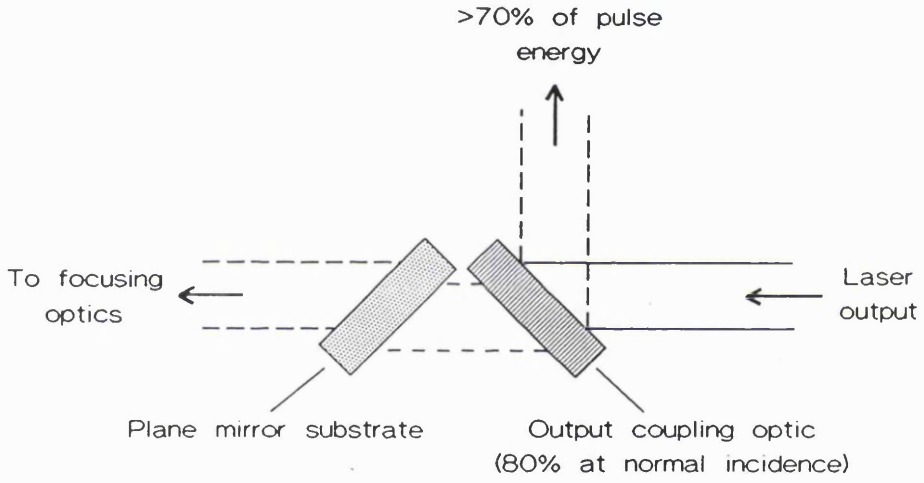

Figure 2.43 Method of reducing the laser beam intensity during fibre optic alignment such that the beam pointing and focusing are not affected.

The transmitted energy after each lens and after the fibre, was monitored using the calibrated calorimeter and compared to the output from the laser to determine the losses at each stage.

2.6.2 Results

The transmission through the negative and positive elements was measured at 90.8% and 91.0% respectively, with the error in each value being $\pm 1\%$. As singlet optics were used, the expected loss per surface, calculated for a normally incident beam[109], was 3.2%, a total expected loss of 6.3%. Although the measured loss at each optic was greater than this, the deviation between theory and practise was not significant to

the results of the fibre transmission measurements. The most likely sources of error were reflection losses from the non-planar surfaces of the optics, as well as absorption loss in the lens material. Up to $89 \pm 1\%$ of the available output was successfully transmitted through the $320\mu m$ fibre giving up to 1.15J of useful laser energy at the output end of the fibre, Figure 2.44. Replacement of this fibre with other, nominally identical fibres, resulted in an average transmission of 87% with none of the fibres transmitting less than 85%.

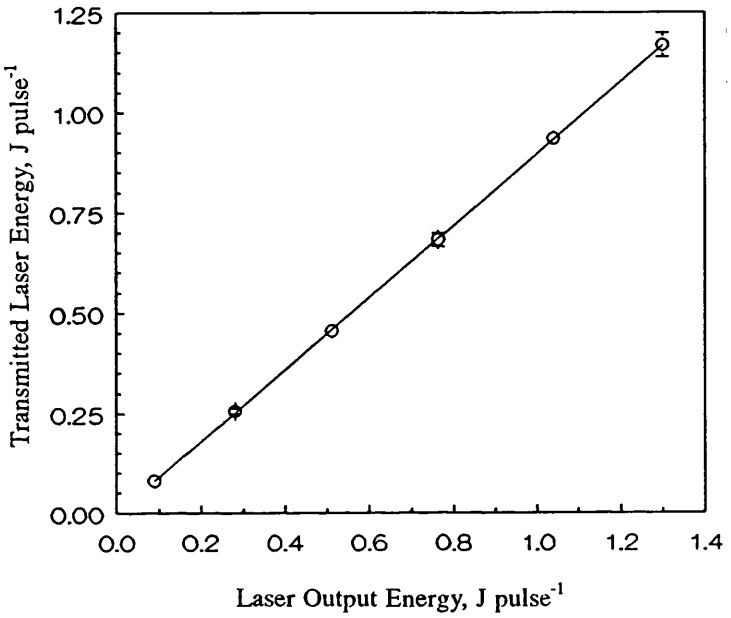

Figure 2.44 Measured energy transmission performance through a $320\mu m$, low OH content fibre.

However, replacement with $200\mu m$ core diameter fibres only once gave the same transmission results and at other times resulted in damage to the input face of the fibre. Inspection of the fibre face did not reveal the cause of the damage. However, it was deduced that, as successful operation had been observed previously, the damage must have been caused by either misalignment of the fibre relative to the beam waist or contamination to the surface of the fibre. Figure 2.45 shows a sample set of laser burns, taken at varying distances from the output end of the fibre and recorded using exposed, matt, photographic paper. The burns were circular in appearance indicating that the fibre tip is free from optical damage or contamination.

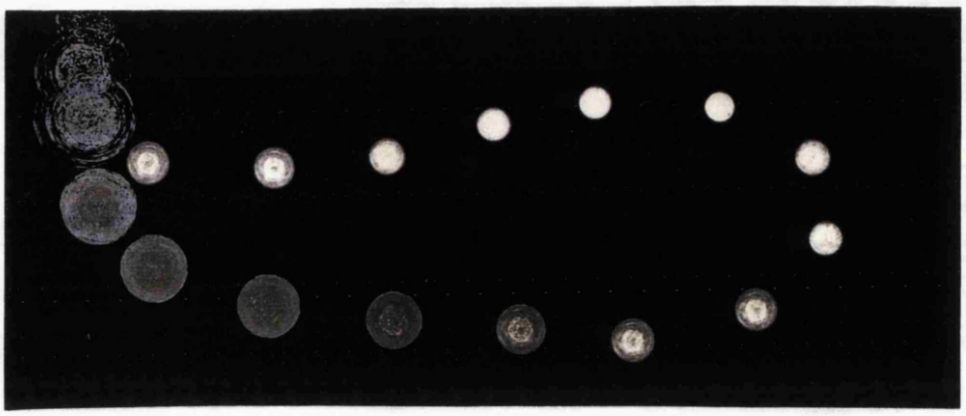

Figure 2.45 Typical laser burns obtained at varying distance from the output end of a 320μm optical fibre recorded using exposed photographic paper. The pulse energy was constant at 1.15J.

2.6.3 Conclusion

Coupling of the 2.1μm laser light through low OH content, all silica fibres has been demonstrated with transmission percentages of up to 89%. This figure is much better than that reported by Moslem et al. It was not possible to establish the loss per metre caused by absorption and scattering. If the loss due to reflection is assumed to be the same as that calculated for the silica optics, then the attenuation loss is 0.11-0.21 dB m^{-1}, in agreement with the 0.14 dB m^{-1} reported by Moslem. The main difference between the configuration described here and the one described by Moslem is in the preparation of the end face of the fibre. Thus, it may be concluded that the improvement in overall transmission is due to the improved end face preparation. Transmission through smaller diameter fibres was demonstrated but with limited success. The main restriction on reliable repeatable performance appears to be the degree of alignment which can be obtained between the fibre face and the incoming beam. Modification of the optical design, either of the laser resonator or the beam coupling optics may result in a better allowance for tolerances but, in the case of the latter, may result in a reduced depth of field.

2.7 Q-Switched Laser Performance

The interest in short pulses at 2.1μm arises from the possibility of using Q-Switched pulses in coherent ranging systems[17]. Additionally, the results of Cross[56] at 1.06μm suggest that such pulses may also lead to a reduction in the depth of damage in tissue during mass removal as a result of delivering the energy in a time less than the characteristic thermal relaxation time. It is this latter suggestion that provides the basis for this preliminary investigation into Q-Switching the 2.1μm CTH:YAG laser. Q-Switching of holmium based lasers has been reported previously by a number of authors. The earliest of these was Chicklis et al[58] who reported room temperature operation producing 500 mJ pulse^{-1} of laser output using a rotating mirror as the optical switch. However, such methods are relatively slow compared to electro-optic switches and the pulses recorded by Chicklis were each greater than 1μs in duration. Devor et al[22] also reported Q-Switched operation with a rotating mirror although, due to a higher rotation rate, they were able to obtain pulses of 150mJ in pulses as short as 100ns. Barnes et al[62] were the first to report Q-Switching using an electro-optic switch. Using a $LiNbO_3$ crystal due to its superior transmission properties at the laser wavelength compared to the more widely used KDP crystal, pulses 30-70ns were obtained from a pulsed system containing as much as 66% of the Fixed-Q energy output indicating the promising storage capabilities of the holmium laser ion. In a continuous-wave version of the laser up to 80% of the CW power could be obtained in a train of pulses if the repetition rate was 200Hz or greater. However, the lasers used by Barnes et al required cryogenic cooling in order to obtain reasonable laser efficiencies and consequently were not representative of practical systems. The first reports of room temperature Q-Switching, at reasonable energy levels, was reported by Alpat'ev[110], again using a $LiNbO_3$ crystal, although the laser crystal was CTH:YSGG. For a flashlamp pump energy of 110J, pulse energies of 80mJ were obtained although the pulse duration was not specified. Subsequently, the same group of researchers report the performance of the same laser, this time apertured to produce a TEM_{00} beam having a pulse duration of 50ns for a 50mJ pulse pumped with a flashlamp energy of 80J[111]. To date there have been no reports, by western researchers, of room temperature, Q-Switched operation at 2.1μm of a flashlamp pumped laser using a $LiNbO_3$ electro-optic Q-Switch.

Recently, Bowman et al[34] have reported on their extensive research into the laser properties of CTH:YAG. Their work includes reports of Q-Switched operation in which the Q-Switch was an acousto-optic cell. The pulse duration was found to depend strongly on the level of pumping, varying between 300ns near threshold to 44ns at the highest pump energies. At the maximum drive level approximately 30%

of the Fixed-Q energy available from the resonator was extracted in a pulse 44ns long. When multiple switching was attempted, 65% of the Fixed-Q energy was extracted in 3 short pulses. The time required to recover the stored energy after the first pulse, was shown to be 70-100ns, after which the second pulse could extract almost as much energy again as the first pulse, indicating the rapid transfer of energy stored in the Tm levels. Bowman calculated the gain recovery time using this data to be 23μs.

2.7.1 Experiment

To evaluate Q-Switching of a flashlamp pumped CTH:YAG laser using a $LiNbO_3$ Q-Switch crystal, a resonator was set up as shown in Figure 2.46. The distance from the middle of the rod to the output coupling mirror was 200mm. To accommodate the Q-Switching apparatus the rear leg of the resonator was extended compared to resonators reported earlier and the total length was 550mm. The front mirror was plane and 80% reflecting while the rear mirror was also plane to compensate for the offset introduced by the addition of the polarising optics. The rod was 4"x4mmϕ (Rod No. 3) and was housed in the $BaSO_4$ chamber pumped by the emission from a single xenon flashlamp. Initially the resonator was operated at 2Hz. This was to allow the laser to achieve some thermal stability while being at such a level to ensure rollover would not occur.

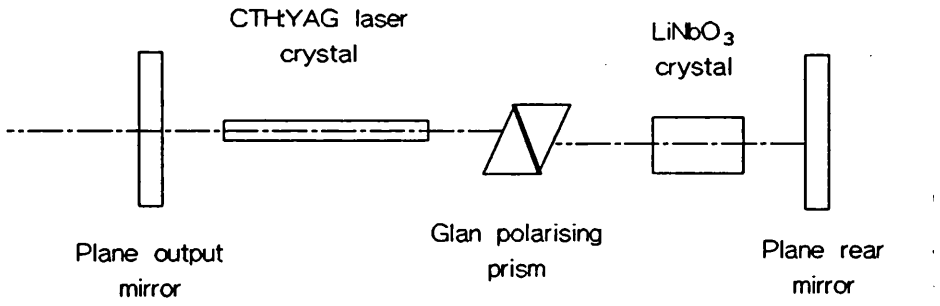

Figure 2.46 Optical layout of resonator used in Q-Switch laser experiments.

Polarisation was achieved using a Glan polariser with Brewster angled faces (Halbo Optics, Essex). For the Q-Switch two crystals were supplied by Litton. Both were supplied uncoated, with plane parallel ends and with opposing side faces coated with gold to act as electrodes. An experimental anti-reflection coating was applied to the first crystal by Lumonics Ltd. The coating consisted of a single MgF_2 layer and was of a thickness based on the requirement for minimum reflectivity based on 1.06μm light and a substrate refractive index of 1.86. Additionally, although the coating was

put down in a vacuum and at an elevated temperature this was somewhat below that recommended by the suppliers due to the lack of suitable mounting apparatus. Consequently, both the thickness of the anti-reflection coating and the quality of the coating were expected to be less than ideal. However, it was hoped that the coating would reduce the intra-cavity loss due to the insertion of the crystal and that the coating would be able to withstand the local power densities within the resonator. As a precaution the second crystal was left uncoated.

The output energy was measured over a range of pump energies using the calibrated calorimeter. Starting with a resonator consisting of a rod and two mirrors, components were added and the reduction in the output energy recorded. Addition of the polariser resulted in a reduction by 70% of the output energy. Subsequent addition of the coated $LiNbO_3$ crystal and operation in a Fixed-Q mode resulted in immediate damage to the crystal surface rendering it unusable. The repetition rate of the laser was then reduced to 1Hz to limit the possibility of intra-cavity focusing onto the surface of the Q-Switch crystal. The crystal was then aligned to ensure that the laser beam would travel along the c-axis of the crystal[112]. A DC voltage was then applied between the electrodes and the optimum voltage identified to achieve the maximum hold off. It was found that 3.5kV was optimum and hold-off could be maintained up to a pump energy of 92J. A pump energy of about 89J was therefore set as the upper limit for Q-Switched operation to reduce the risk from pre-lase damage. The output energy in Fixed-Q and Q-Switched modes was then compared. In addition, an InAs photovoltaic detector (Laser Monitoring Systems, Newland Business Park, Hull), linked directly to the 50Ω input of a 450MHz oscilloscope, was used to monitor the temporal profile of the pulse.

2.7.2 Results and discussion

Figure 2.47 shows the comparative performance of the resonator in both Fixed-Q and Q-Switched modes. At a discharge energy of 81 J $pulse^{-1}$, a Q-Switched pulse energy of 27.7mJ was obtained, 23% of the Fixed-Q energy at the same level.

At pump energies around 82 J $pulse^{-1}$, the temporal profile consisted of a Gaussian shaped pulse with a FWHM pulse duration of 236ns, Figure 2.48 (a). However, at higher pump pulse energies (>88 J $pulse^{-1}$), the output intermittently appeared to consist of a double peaked pulse, with the first pulse having a pulse duration of 198ns and with the second pulse reaching only 28% of the intensity of the first, Figure 2.48 (b).

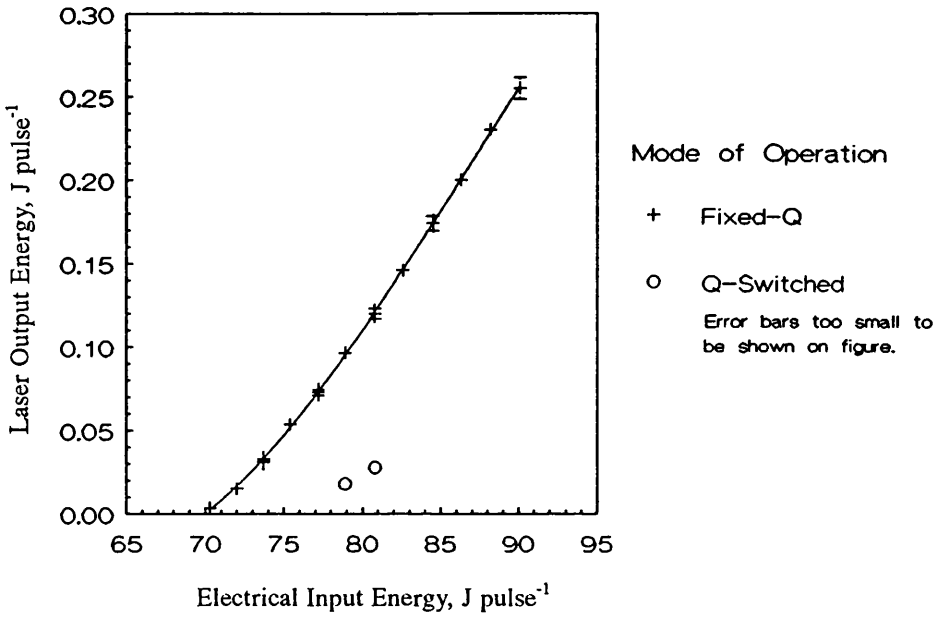

Figure 2.47 Change in Fixed-Q and Q-Switched laser output energy with electrical discharge energy, the pulse repetition being 1Hz, and the optical configuration remaining the same for both modes of operation.

The reduction in the duration of the first main pulse undoubtedly arose from the increase in gain at the higher pump level. However, the reason for the second pulse could not be confirmed before damage to the faces of the $LiNbO_3$ crystal occurred and the experiments were halted.

A likely cause of the effect may be ringing of the high voltage across the circuit due to inadequate impedance matching. The damage to the crystal appeared as a ring of spots on a diameter approximately the same as that of the laser rod. Additionally, a single line of spots bisected the ring, Figure 2.49. Each spot was approximately 250μm in diameter. Calculating the average peak power density incident on the internal optical surfaces, using equation (2), yields a value of 4.5 MW cm^{-2}.

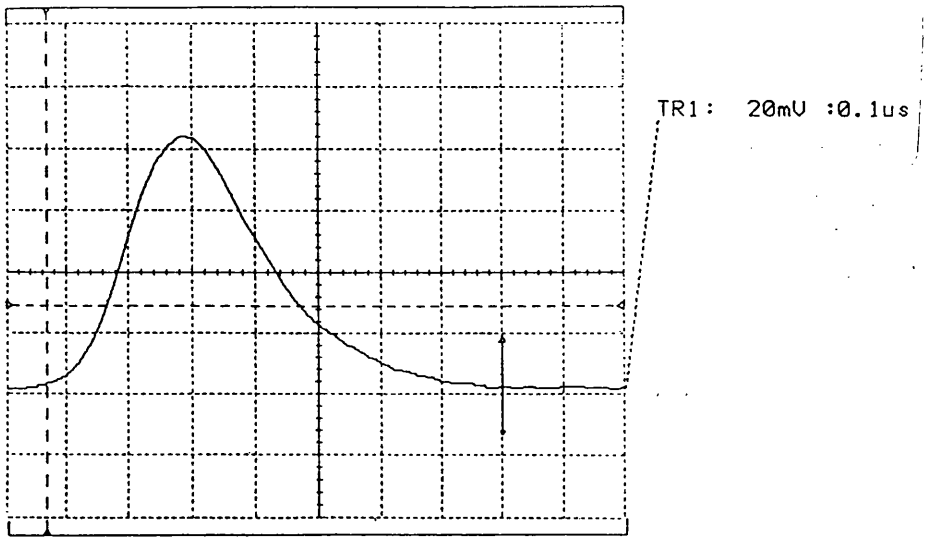

(a)

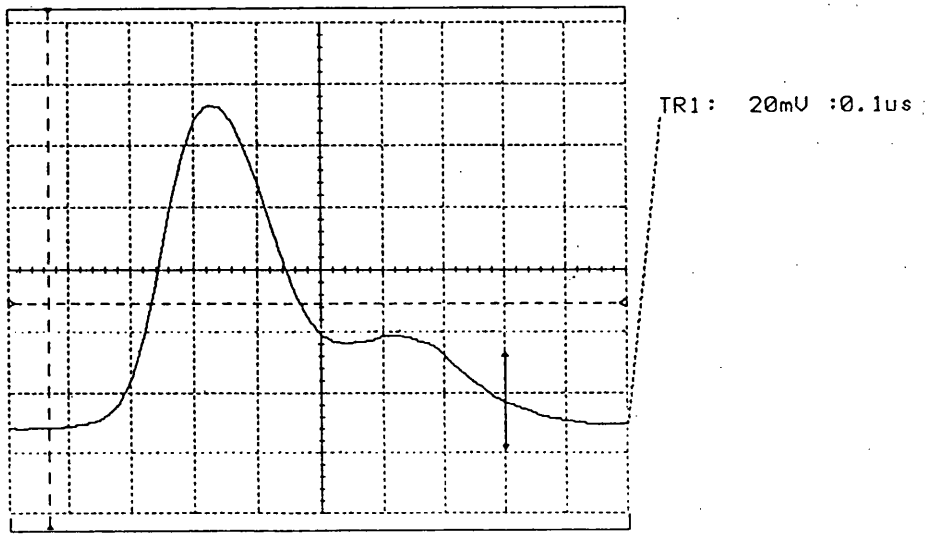

(b)

Figure 2.48 Temporal profile of Q-Switched laser output for electrical discharge energies of a) 82 J pulse^{-1} and b) 88 J pulse^{-1}.

Due to the transverse mode structure of the beam it is likely that the actual power density is considerably greater than this. Also, it is not possible to confirm that the damage is not due to prelasing, especially as the damage was found to occur close to the hold-off limit. In 1976, Koechner[1.13] reported the damage threshold of $LiNbO_3$ crystals to be in the range 6-40 MW cm^{-2} for wavelengths of 0.53μm. In recent years manufacturers of $LiNbO_3$ have claimed great improvements to these figures. However, a lower damage threshold compared to the KDP crystal is still expected due to the higher refractive index in the $LiNbO_3$ crystal which, while enhancing the non-linear effect, simultaneously reduces the damage threshold. The results suggest that damage thresholds still do not exceed 100 MW cm^{-2} compared to damage

thresholds above 400 MW cm^{-2} for KDP.

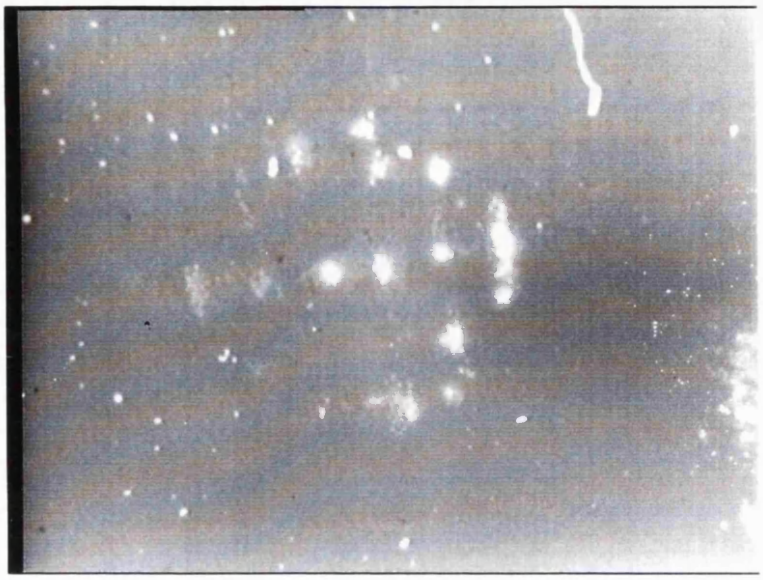

Figure 2.49 Photomicrograph of unpolished face of the $LiNbO_3$ crystal showing pattern of damage.

Despite the limitation due to the peak power damage there remains no current alternative electro-optic material for Q-Switching at relatively long laser wavelengths, such as 2.1μm. To reduce the likelihood of damage, though, it would be appropriate to add an aperture to the laser resonator in order to restrict the transverse mode operation to TEM_{00}, thereby limiting the number of high, localised 'hot spots' occurring within the resonator.

2.8 Summary and Conclusions.

The operation of lasers based on the holmium ion have been examined. The earliest reports of laser emission at 2.1μm between the $^5I_7$ and $^5I_8$ levels occurred in 1962[20] and in 1966[21]. Both publications were the work of a group, led by Johnson, working at the Bell Laboratories. The latter publication considered sensitisation of the laser ion with other elements to enhance the relatively poor absorption characteristics in the holmium ion. Initially, holmium was codoped with erbium which exhibits broad absorption bands in the visible part of the spectrum, and thulium which efficiently channels the pump energy towards the upper laser level. However, operation was still largely restricted to cryogenic temperatures due to thermal population of the lower

laser level. Efficient room temperature operation of a flashlamp pumped holmium laser was first reported in 1985 by Antipenko[24] who substituted chromium for the erbium ions due to their improved overlap with the emission from pulsed xenon flashlamps.

Excitation of the $^5I_7$ level proceeds via broad band absorption of the pump radiation by the Cr ions and cross-relaxation in the Tm ion in which one excited level at $^3F_4$ splits to create two excited states at the $^3H_4$ level. The terminal laser levels lie in the $^5I_8$ manifold, the highest of which is only 522cm^{-1} above ground at room temperature. Thus, operation of the laser is sensitive to temperature variations leading it to be described as a three level system. A total of nine transitions have been identified by Bowman et al[34], lying between 2.084μm and 2.128μm. The line which oscillates depends on the reflectivity of the resonator optics[34] as well as the operating temperature[21].

In the years following Antipenko's publication, western researchers have continued to improve and refine the relative mixture of dopants and the operating conditions. Particularly, workers at the Naval Research Labs. (Washington D.C., USA) have reported significant improvements[31,64] including slope efficiencies of 5.1% and thresholds as low as 28J[65]. However, until recently, operation at repetition rates above 1Hz have not been examined. In a study of the laser properties of CTH:YAG Bowman et al[34] report that thermally induced lensing in the crystal occurs at rates of between 4 Dioptres kW^{-1} and 7 Dioptres kW^{-1} of average pump power, significantly greater than that reported for the Nd:YAG crystal. The consequences of this have been observed by Becker et al[67] who observed rapid roll-off of the available output energy, at a constant pump pulse energy, when the repetition rate was increased. Although some desensitisation to the effect was obtained by using smaller diameter rods, this inevitably resulted in a reduced output energy.

Several CTH:YAG rods having differing dimensions and dopant concentrations have been assessed and the results reported in this Chapter. The aim of this was to increase the understanding of the operation of CTH:YAG as a laser and to provide data useful in the future development of efficient systems capable of operating at repetition rates greater than 1Hz.

Initial tests set the background for the choice of materials used in the later work. In the available measurement range, there was no difference in the laser output energy due to dopant concentrations. Comparing rods of differing dimensions, it was found that improved laser efficiency was obtained for a 4"x4mmϕ rod compared to a

3"x5mmϕ version, despite the former having a smaller total volume. The reason for this was the increased gain length which more than compensated for the better light capturing characteristics of the larger rod. The construction of the laser assembly was then varied to establish the configuration which produced the highest laser efficiency. This was obtained for a 4"x4mmϕ rod, pumped with a xenon flashlamp having cerium doped quartz walls and filled to a pressure of 450 Torr. A fill pressure of 630 Torr produced no significant deterioration of performance. For the 3"x5mmϕ, the optimum laser output coupling reflectivity was assessed using the data for three known reflectivities. The maximum efficiency was predicted to be obtained for reflectivities close to 90%. High intracavity power densities, however, may cause damage to intra-cavity optical surfaces, and, for this reason, an 80% reflecting optic was used in this work. The strong dependence of the output energy on the output coupling reflectivity indicates that the system was of low gain.

A resonator, 455mm long, was constructed around 3"x5mmϕ and 4"x4mmϕ rods. Both systems showed evidence of resonator optimisation which depended on the level of pumping. For the 4"x4mmϕ rod the maximum laser output for a given input energy occurred at 3Hz while for the 3"x5mmϕ rod the maximum occurred at 1Hz. Above 1Hz, the output reduced with increasing repetition rate suggesting a stronger amount of lensing in the larger diameter rod, in keeping with the recent results of Becker et al[67] but in contradiction with the theory developed by Koechner[92]. The reason for this was not investigated but was believed to be due to a combination of the increased amount of flashlamp light captured by the larger rod and changes in the flow of coolant around each of the rods.

The effect of temperature on the laser performance was demonstrated for three resonators of differing dimensions. At low pump energies, the reduction in output due to thermal population of the lower laser level was found to be independent of the resonator configuration. However, at higher pump energies the reduction in energy appeared to depend on both temperature and resonator design, with a faster reduction in the output observed for the longer resonators. This phenomenon is attributed to the increased heat in the crystal as a result of the lower laser efficiency at elevated temperatures. The extra heat causes increased lensing which, in turn, causes the energy to roll off. This is more noticeable in longer resonators than in shorter ones.

The effect of temperature on the threshold energy for laser operation was assessed and compared to the thermal population of the lower laser level, as determined by Boltzmann statistics. It was found that, in keeping with the work of

others over different temperature ranges, the energy required to obtain laser action varied linearly with the Boltzmann population of the terminal laser level. However, analysis of the shape of the curve describing the changes in Boltzmann population revealed that this change was also linear with temperature over the experimental range. While the work is in agreement with that of others, the experimental range is too small to fully confirm the simple relationship proposed.

The magnitude of thermal lensing induced in the crystal by the non-radiative relaxation of absorbed pump radiation has been assessed by a non-direct method which allowed for subsequent resonator modelling. A linear relationship between induced focal power and average pump power, predicted by theory[92], was verified for repetition rates greater than 2-3Hz. Below 2Hz, the experimental results implied that, at a zero pump power, the rod would act as a negative lens. This effect is attributed to the fact that, below 2Hz, thermal relaxation of the rod occurred. Thus, a steady state thermal distribution was never established in the rod, and, consequently, the majority of the heating effect occurred around the periphery of the crystal rather than on axis. Under such conditions, the thermal dependence of the refractive index caused the rod to appear like a negative lens. In the linear portion of the graph of focal power versus average pump power, the focal power of the 4"x4mmϕ rod varied at a rate of 8.0 Dioptres kW^{-1}. To adequately fit a single curve to the experimental data for rod lens *focal length* and average pump power, it was necessary to adopt the same form of empirical equation used by others[92], (equation (A4.8)). In this form, the focal length of the induced rod lens can be described over the average pump power range 50-550W by equation (11). Using the information on the rod lensing in a ray tracing program, the performance of a second resonator configuration was successfully modelled. For both the initial analysis, which resulted in the thermal lensing data, and the later model, it was found necessary to aperture the 4mmϕ rod to a diameter similar to that obtained in preliminary laser experiments. The reason for this lay in the difference between the transverse extent of the beam in the computer model and that defined in the description of multimode laser spotsizes as being 86.5% of the contained energy.

The temporal characteristics of the system were then assessed. The delay between the start of the pump pulse and the onset of laser emission, known as the 'delay-to-lasing', was investigated in an attempt to see whether three or four level laser theory was most applicable to the case of the CTH:YAG laser. It was not within the scope of this thesis to attempt to solve the equations describing the delay-to-lasing for the pump pulse profiles available. Consequently, a simple, rectangular pulse model was applied[105,106]. Although the real pump pulse duration was 350μs

(FWHM), it was found that, in the rectangular pulse theory, a pulse duration of 440μs accurately predicted the real delay-to-lasing. However, when rectangular pulse theory was applied to predict the output pulse duration, theory and practise were found to be irreconcilable over the complete measurement range. The reason for the success in the delay-to-lasing predictions, yet the failure in the pulse duration predictions, lies in the shape of the pump and output pulses where the fast rising edge and slow trailing edges assist in the first theory and detracts in the latter. In keeping with the general theory, though , it was found that the maximum laser output duration was approximately the same as that of the pump pulse duration, indicating that, for a better developed theory, a closer agreement between theory and practise can be expected. In the case of the delay-to-lasing experiments, the predicted delays for both three and four level lasers were identical over the test range, despite different variables and different equations. Thus, while not providing a conclusive answer to the question of three or four level laser behaviour, either theory may be applied depending on convenience.

To demonstrate flexible fibre optic beam delivery, the output from the laser at 5Hz was coupled into 200μm and 320μm core diameter, low OH content, all silica, step index fibres. Transmission, in which 89% of the input light was emitted at the end of 1-2m long fibres, was obtained for the 320μm fibres although alignment problems limited the success of coupling into the 200μm fibre to one occasion. These transmission percentages represent a significant improvement on the figures reported by Moslem et al[108], probably due to the polishing method used in end face preparation. Energies in excess of 1 J pulse^{-1} were available at the end of the fibre indicating that strong thermal lensing need not be a restriction to the delivery of modest but useful average powers through small diameter fibres.

Finally, room temperature operation of a flashlamp pumped, Q-Switched laser, in which the Q-Switch crystal was $LiNbO_3$, is reported for the first time outside the CIS, formerly the USSR. Up to 30mJ of multimode energy were obtained at 1Hz in a pulse approximately 220ns in duration. A more compact Q-Switch assembly would allow for shorter resonator geometries and consequently allow for operation at higher repetition rates. Further work is required to adequately match the high voltage switching circuit used with the $LiNbO_3$ crystal in order to eliminate possible ringing. Despite these improvements the $LiNbO_3$ will still be limited to low peak powers due to its comparatively low damage threshold. Until this latter restriction is overcome, short pulses comparable to Q-Switched Nd:YAG lasers ($<$ 10ns) and at significant pulse energies ($>$ 100mJ) may remain unachievable.

CHAPTER 3

Development of the Erbium Laser

3.1 Introduction

3.1.1 Historical Review

In the last five years there has been an increasing amount of interest in the 2.94μm laser transition which is obtained from erbium doped YAG crystals. This is due to the fortuitous proximity of the laser line to a peak in the absorption profile of soft tissue, which in this region of the optical spectrum is dominated by the water content. However, prior to the first reports of laser action at 2.94μm in erbium doped YAG in 1975[48], operation at several shorter wavelengths had been reported. The first of these occurred in 1962 when Kiss et al[114] reported stimulated emission at 1.612μm from erbium doped $CaWO_4$. Subsequently a number of wavelengths, mainly between 1.6μm and 1.7μm, have been reported[115,116]. For example, Voron'ko et al[117] obtained stimulated emission at three lines around 1.7μm as well as on a single line at 1.26μm.

Despite appearing in a similar wavelength range, transitions at $\approx$1.6μm are the result of a three level pump scheme where the terminal laser level is the ground state of the ion. Conversely, laser transitions at $\approx$1.7μm are the result of a four level pump process terminating at a level $\approx$12400cm^{-1}, well above the ground level. In 1975 Chicklis et al[118] reported room temperature laser operation at 0.85μm from a YLF rod doped with 2% erbium. Here the upper laser level is the same as that of the four level laser scheme at 1.7μm while the lower laser level is the same as the upper laser level of the three level laser scheme. Figure 3.1 summarises these transitions.

In 1965 Johnson et al[119] published the first reports of erbium doped into a YAG host. However, Johnson did not pursue laser action from the erbium ions but

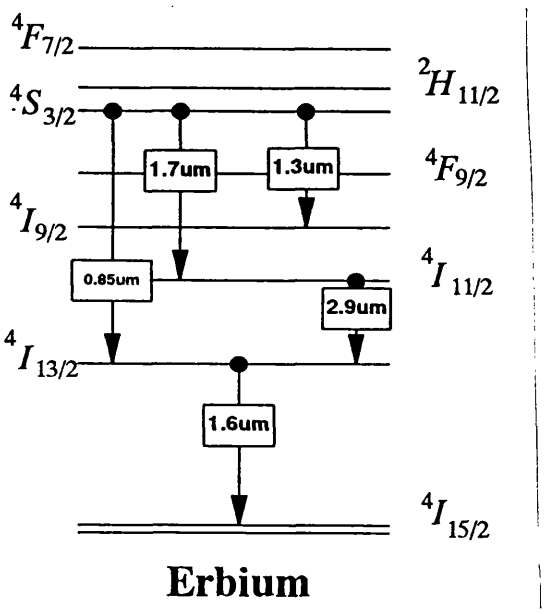

Figure 3.1 Some of the laser transitions in erbium doped crystals, reported in references [48,114..118].

made use of the broad absorption properties of erbium in the visible portion of the optical spectrum to sensitise thulium and holmium ions. At 78K a fortyfold increase in the infrared emission around 2μm from Tm ions was recorded when half the yttrium was replaced with erbium. This results from an efficient transfer between the $^4I_{13/2}$ level in erbium and the $^3H_4$ level in thulium and, as a result, emission from the erbium ion at 1.6μm is no longer observed. Prior to the introduction of holmium lasers sensitised with chromium[24], erbium was used, along with thulium, to achieve room temperature laser operation at 2.1μm[59].

Spectroscopic analysis of erbium doped YAG was performed by Koningstein et al[120]. Although the analysis was carried out at temperatures of 4.2K and 300K the authors present the data for the cryogenic temperatures in greatest detail due to the improved resolution obtained. The results show that the absorption profile is formed by a number of transitions which originate mainly in the ground, $^4I_{15/2}$, level of the erbium ion. Of these the strongest are identified around 785nm and in two bands ranging from 449nm to 484nm and 487nm to 646nm, indicating that efficient pumping by the emission from pulsed xenon flashlamps may be possible. Although limited, spectral data at room temperature confirms strong absorption in bands between 449nm and 462nm and 542nm and 561nm as a result of transitions from the ground level to the $^4F_{5/2}$ and $^4S_{3/2}$ manifolds, respectively.

Laser action at room temperature in the three micron spectral region, in a

YAG host crystal, was first reported by Zharikov et al[48] in 1975. Using crystals in which 10%, 20% and 30% of the mass of yttrium ions was replaced with erbium ions laser emission at 2.936μm was observed as a result of transitions between the $^4I_{11/2}$ and the $^4I_{13/2}$ levels. It was found that as the dopant concentration increased, the laser threshold fell. Despite this, for the maximum available doping level, a rod, having dimensions 60mm x 3mmϕ, still required a pump energy of 90 J pulse^{-1} in order to achieve threshold. Unfortunately, details of the pump configuration were not given. When Zharikov measured the upper and lower state lifetimes it was found that the upper level relaxed in a characteristic time of 320μs, independent of dopant concentration. The lower state decayed with a much longer time constant which depended on the dopant concentration, but was in the region of 1-6ms. Thus, the transition, although four level due to the high lying terminal laser level, was self-terminating. Citing the results of Johnson[119] the authors of this work suggest that codoping with holmium ions may assist depopulation of the lower laser level to prevent this bottlenecking which would otherwise reduce the laser efficiency.

Clearly, from the results of Zharikov et al[48], increasing the concentration leads to improved laser performance. However, despite a similar ionic radius to yttrium, which suggests that up to 100% substitution with erbium may be possible, it was anticipated that concentration quenching would limit the optimum doping level to a much lower proportion. Researchers from the same institution, lead this time by Basiev[49], investigated the effects of concentration on the loss processes in order to optimise the deactivation of the lower laser level without adversely affecting the upper level. Although an optimum dopant level is not specified, the authors show that for an erbium:YAG crystal grown from a pure charge the lower state lifetime is always longer than the upper state lifetime. Basiev suggests that the unintentional inclusion of impurities in the charges from which Zharikov's crystals were grown were responsible for the reduced lower state lifetimes previously reported. By considering the distribution of energy levels in other available dopants Basiev suggests that both thulium and holmium may be suitable ions to include with erbium, in order to encourage preferential deactivation of the lower laser level involved in the laser emission at 2.94μm.

The case for de-activation of the long lived lower laser level with 'impurity' ions was taken up again by Kaminskii et al in their publications[51,52]. By the addition of holmium and thulium ions reductions in the laser thresholds were obtained in crystals of Er:$Lu_2Al_5O_{12}$. At the same time the laser wavelength was found to shift from 2.94μm to 2.699μm. This effect is a result of the depopulation of the lower lying Stark levels of the terminal laser state allowing stimulated emission to take

place involving these sub-levels. The 'red shift' which occurs for the pure erbium laser crystal is here due to the long lived lower laser level and, to a lesser extent, the thermal distribution within the manifold. A similar effect has been reported by Johnson et al[21] for the holmium laser, although in that instance thermal distributions are solely responsible for changes to the emission wavelength. Close inspection of the stimulated emission spectrum resulting from transitions between the $^4I_{11/2}$ and the $^4I_{13/2}$ levels was performed by Zhekov et al[121]. Their work revealed three potential laser wavelengths at 2.6979μm, 2.831μm and 2.9364μm, Figure 3.2. Zhekov managed to obtain laser action on different lines by selectively pumping the crystal in specific wavelength ranges. From this he concluded that wavelength selection could be achieved by selective pumping, making additional use of cross-relaxation process to create population inversion between the desired levels.

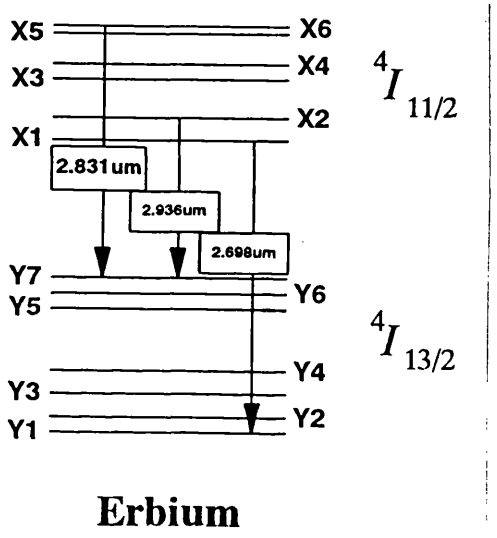

Figure 3.2 Energy levels involved in laser emission at $\approx 3\mu$m (after Zhekov et al[121]).

In a separate publication Zhekov et al[122] describe how deactivation of the lower laser level, by a pump intensity dependent energy transfer process, allowed true four level laser action. Figure 3.3 summarises the 'loss' routes described by Zhekov and reveals that excitation energy lost from the $^4I_{13/2}$ level may contribute to increasing the laser efficiency by promoting an excited state to the $^4I_{9/2}$ level from where it can decay into the, $^4I_{11/2}$, upper laser level. Zhekov suggests that, at sufficiently high pump rates, de-excitation of the $^4I_{13/2}$ may be so efficient that CW lasing may be possible.

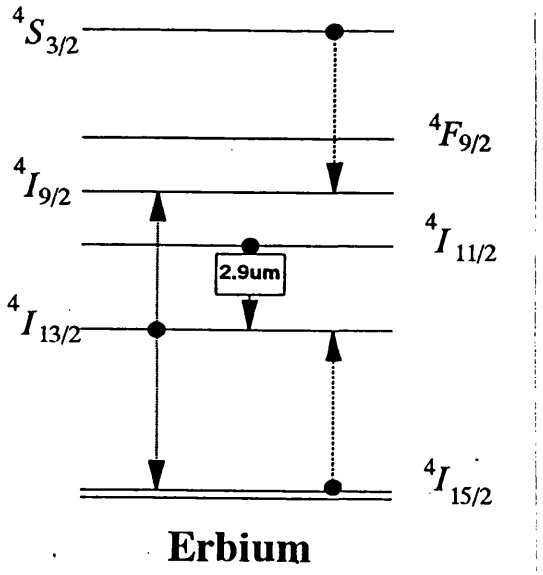

Figure 3.3 Key laser transitions involved in excitation of the 2.94μm laser level in Er:YAG. Dotted lines are the de-excitation routes described by Zhekov in reference [122].

Pollack et al[123] ingeniously demonstrate room temperature CW lasing from the $^4I_{11/2}$ level in an erbium doped CaF_2 crystal. Using six camera flashbulbs, fired sequentially with individual pulse energies below the laser threshold level, a quasi CW pump pulse was generated. Although the individual pump pulse durations were only 15-20ms long, lasing occurred at 2.8μm (the $^4I_{11/2}$ to $^4I_{13/2}$ laser wavelength in CaF_2) for 80ms. The authors conclude that, as the lower state lifetime in this crystal is 20ms, lasing is CW (being significantly longer than the lower state lifetime) and must be due to the upconversion which depletes the lower laser level and enhances the population of the upper level.

In 1987 several more papers were published which further developed the operation of CW erbium lasers. Chou et al[124] reported to the Tunable Solid State Lasers Conference that a laser based on a YLF, crystal cooled to 77K, produced several watts of CW power when pumped with a 1000W tungsten lamp. Cooling the crystal was claimed to reduce the probability of cross-relaxation into the terminal laser level as well as reducing the overall population in the lower laser level manifold. Huber et al[125] reported CW lasing at the same conference, although at room temperature and with the excitation radiation provided by the output from a CW krypton laser at 647nm. In the subsequent general publication of this work[126] the authors describe their work with a variety of hosts and differing compositions including co-doping with both chromium and holmium ions. For Cr:Er:YAG and Cr:Er:YSAG CW laser thresholds of 800mW are reported while for a similarly doped YSGG crystal a reduction in the threshold, to about 250mW, was measured.

The reason given by the authors for this was the effect of the multiphonon quenching which shortened the lifetime of the $^4I_{11/2}$ level. Thus, one would expect Cr:Er:YSGG Q-Switched lasers to be superior to other crystals due to the improved energy storage.

The first reports by western researchers on flashlamp pumped pulsed operation of erbium doped YAG at 2.94μm occurred in 1986, over 10 years after the first reports by Russian workers[48]. Although only a brief paper, the publication by Bass et al[127] represented the first real report relating to practical aspects of operating an erbium laser. The laser output from two rods with erbium concentrations of 33% and 50% were compared to determine the output characteristics. The crystals were operated at room temperature in a silvered cavity pumped by the output from a single xenon flashlamp, the maximum discharge energy of which was 500J. Although higher dopant concentrations are expected to provide better depopulation of the long lived lower laser level and, therefore, higher laser efficiency, the highest outputs were recorded for the lower doped material. The maximum slope efficiency was $\approx$0.625% and the laser threshold typically 80 J pulse^{-1}. The authors stressed the need for more work to confirm this unexpected result. However, to date there have been no published studies on the effect of dopant concentration on laser performance.

In 1987 Frauchiger et al[50] published a useful practical study of an erbium doped YAG laser. Using a 75mm long, 6.35mmϕ crystal, doped to 40at.% and housed in a ceramic pumping chamber laser output was obtained for twin xenon lamp excitation (although only 67mm of the crystal was pumped by the lamps). The resonator was formed between plane dielectric mirrors with reflectivities of 90% and 100%. Despite the high lying terminal laser level, which lies more than 6000cm^{-1} above ground, significant reductions in the laser output were observed for increases in the operating temperature. For an increase in the cooling water from 17°C to 70°C the laser output energy fell, for a 100J pump pulse, from 0.31 J pulse^{-1} to 0.105 J pulse^{-1}. Extrapolating the results presented by Frauchiger et al, it may expected that laser operation would not be obtained above 100°C for any amount of pump energy, although this remains to be proven. The maximum output energy obtained by Frauchiger for a maximum pump pulse of 100J was 0.31J, which occurred when the laser was operated at its lowest temperature of 17°C. The slope efficiency under these conditions was 0.875% and the laser threshold 33J.

Frauchiger et al also investigated some of the thermomechanical properties of the Er:YAG crystal by measuring the thermally induced lensing. Using a HeNe laser the dependence of the induced focal length on the pump power was found to follow

the relation

$$F = \frac{0.5}{P^{1.4}} \qquad (15).$$

where F is the focal length in metres and P is the average pump power delivered by the discharge circuit in watts. Equation (15) indicates that thermal lensing was about four times stronger than in the same sized Nd:YAG crystal. The reasons for this are not discussed in detail but can largely be attributed to an increase in the absorption of the pump light due to the broader absorption bands of the erbium ion and a lower heat conductivity of 5.5 W $m^{-1}K^{-1}$ [128] compared to 14 W $m^{-1}K^{-1}$ for Nd:YAG[129].

Charlton et al describe their practical experience with an Er:YAG laser in reference [53]. For their experimental arrangement, the highest slope efficiencies and the lowest thresholds were obtained when a close coupled $BaSO_4$ chamber was used in preference to the ceramic close coupled or focusing silver ellipse chambers. For a 50% erbium doped crystal 100mm long and with a diameter of 6mm, thresholds as low as 16 J $pulse^{-1}$ and slope efficiencies of 2.5% were measured. Comparisons of the data obtained over a range of pump pulse energies with different reflectivity output couplers revealed that the threshold reduced as the reflectivity increased. At the same time the slope efficiency fluctuated, although not with the same predictability, and consequently, the authors recommend different mirrors at different pump energies in order to obtain the maximum overall efficiency. A reduction in the laser output energy when the coolant temperature is raised is also reported, in keeping with the earlier observations of Frauchiger et al[50]. The authors in this case attribute the effect not only to a change in the Boltzmann distribution and a change to the cross-relaxation efficiency but also to a decrease in the stimulated emission cross-section, line broadening and thermal lensing. The latter is demonstrated by the roll-off of laser energy which occurs with increasing repetition rate with a 40cm long resonator compared to the relative insensitivity over the same range of a 20cm long resonator. The authors also demonstrate that filtering out unwanted pump radiation will reduce the thermal loading, thereby extending the useful range of repetition rates. Unlike Greve et al[130] and Frauchiger et al[50] who chose to use filter glasses between the flashlamp and the laser crystal, the authors of this paper add Rhodamine 640 dye to the coolant water to absorb the unwanted pump radiation which occurs below 600nm. Although a 14% increase in the pump energy is required to maintain the output energy, roll-off of the laser energy does not occur until 35Hz at 41 J $pulse^{-1}$ input for the filtered light case, compared to 25Hz at 36 J $pulse^{-1}$ input, for the normal unfiltered case. From the experimental results, in which 4W was

produced at 40Hz, the authors predict that 100Hz, 10W operation should be feasible.

Recently Spring et al[131] have attempted to explain some of the temperature dependent properties of the erbium ion by calculating the change in population of each of the laser levels. The authors show that the threshold energy for laser action varies linearly with the coolant temperature over the range 4-55°C. However, a clear theory of the temperature dependent behaviour is not presented and this paper does not contribute significantly to understanding the effects of temperature on erbium laser performance.

Besides the YAG crystal, much interest has been shown in the laser properties of other erbium doped crystals. Following on from the earlier work of Weber et al[115,132] and Kaminskii et al[133,134,135], researchers at the Institute of Applied Physics, University of Bern in Switzerland, have published a number of articles based on observations of the laser and spectral properties of $YAlO_3$ (YAP) crystals doped with up to 50at.% erbium. The interesting feature of this laser is the polarisation dependence of the output. Stalder et al reported[136] that for an unpolarised resonator lasing can be obtained on three lines, 2.92μm, 2.79μm and 2.73μm, simultaneously. However, by the simple addition of a Brewster angled plate wavelength selection can be obtained on the individual lines, depending on the orientation of the plate with respect to the crystal axes. This is a result of the anisotropy of the YAP crystal making it a birefringent crystal. In keeping with the results of others[121] the shorter wavelengths are suppressed at increasing pump levels limiting the tunability of this system to low pulse energies only. The authors later report on the effects of including filters within the resonator to select particular wavelengths when operating above the laser threshold of all the transitions[137]. By this method a total of nine lines, resulting from transitions between different sublevels within the $^4I_{11/2}$ and $^4I_{13/2}$ manifolds, are selectively made to lase with wavelengths between 2.718μm and 2.92μm.

Although most interest is still directed towards lasers using erbium doped YAG as the active laser element, there has been an increasing amount of interest in the laser performance of the multiply doped erbium crystals, including those in which energy is transferred between erbium ions and neodymium codopants[138]. Most relevant to this work though, is the continuing development of chromium sensitised Er:YSGG. Initial observations of an improved energy storage capability were first reported by Huber et al[126] in 1987. Al'bers et al[139] hinted at the improvements to the laser efficiency as a result of the chromium sensitising action in their reports of high repetition rate laser operation although it was Moulton et al[140] who performed the first

comprehensive study of this material. The combination of chromium and erbium ions results in a crystal which is nearly black. However, absorption measurements reveal that chromium is the main absorber in two broad bands centred on 450nm and 640nm. When excitation of the near three micron laser line was carried out via the chromium ion it was found that there was no significant difference in the build-up time of the fluorescence at 2.8μm compared to the case when the erbium ion was excited directly. This indicates that transfer between the ions is rapid (approximately 1μs) and consequently loss from the transfer levels is minimised. The lasing properties were demonstrated using a 63mm long, 4mm diameter crystal housed in a silvered elliptical pumping chamber and pumped by the emission from a single xenon flashlamp. Using a 90% reflecting output coupler, threshold energies of 5.1-8.4 J pulse^{-1} were recorded, compared to thresholds of 30-45 J pulse^{-1} for Er:YAG lasers under similar conditions. Additionally, when the repetition rate was increased the authors observed a reduction in the laser pulse energy due to thermal lensing in the crystal which was less than they had observed for the Er:YAG crystal, indicating the real potential of this system for high repetition rate and CW lasers.

Practical demonstrations of CW lasing from Cr:Er:YSGG crystals were first reported by Noginov et al in 1991[141] under 647nm, krypton laser pumping. Recently though, Dinerman and Moulton[142] have reported CW operation in erbium doped YSGG, GGG and YAG crystals by direct excitation of the upper laser level at 970nm using Ti:Sapphire lasers and InGaAs laser diodes. Previously, Kintz et al had demonstrated CW lasing at room temperature in YLF in 1987[143].

The only practical comparison of the laser performance of Er:YAG and Cr:Er:YSGG lasers was performed by Charlton et al[144] at the University of Manchester, England. Despite uncoated rod faces, a threshold energy of 5 J pulse^{-1} was recorded for a 75mm long, 6.2mm diameter Cr:Er:YSGG crystal, compared to 16 J pulse^{-1} for an Er:YAG rod. However, the maximum pulse energy obtained from the YSGG rod was only 0.4J, due to a low slope efficiency which never exceeded 0.6%. When the operating temperature was varied between 10°C and 30°C the laser output from the YSGG crystal remained constant, unlike that of the YAG crystal[53]. However, contrary to the observations made by Moulton et al[140], the laser was sensitive to the pump power induced thermal lensing, although operation at 30-40Hz was obtained from a 250mm long resonator before roll-off occurred. The authors' preliminary experiments in processing biological tissue revealed no marked difference between the Cr:Er:YSGG and Er:YAG lasers. Further work was prevented by a thermally induced fracture of the crystal at an average input power of only 900W. In view of the practical restrictions on average operating power, the

authors conclude that there is little or no advantage to using Cr:Er:YSGG in preference to Er:YAG in medical lasers.

3.1.2 Spectroscopy, Pump Scheme and Effect of Dopant Concentration

The erbium laser scheme has been the subject of much investigation due to the long lived lower laser level which suggests a self-terminating operation. Because the attention given to crystals containing erbium ions has been directed toward obtaining a better understanding of the laser process, much of the literature published on the pump scheme has been included in the previous section of this Chapter as part of the historical review. Figure 3.4 summarises the pump scheme.

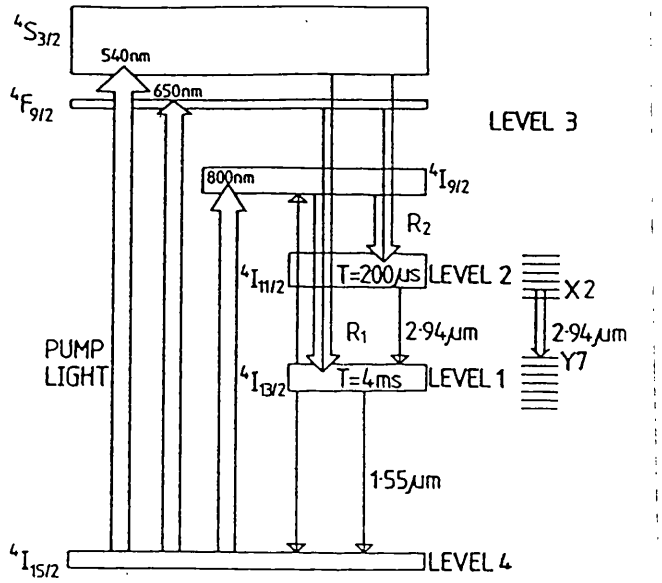

Figure 3.4 Energy level diagram for Er:YAG showing the main pump bands and cross-relaxation paths. (After Charlton et al[53]).

Lasing at 2.936μm takes place between the $^4I_{11/2}$ and $^4I_{13/2}$ levels, respectively. The possibility of a self-terminating laser action was reported in the first publication on 2.94μm laser action from Er:YAG[48]. Using crystals doped with 5, 10, 20 and 30at.% erbium the authors of that work measured an upper state fluorescent lifetime of 320μs independent of concentration. The lower level lifetime, though, was found to be more strongly influenced by the dopant concentration, falling from 6ms to 1ms as the dopant concentration increased. However, when Basiev et al[49] repeated the measurements over the range from 0-100% substitution the results showed that both levels varied with concentration. For the lower level, lifetimes between 6.4ms and 2ms are reported for concentrations between $\approx$0 and 100% respectively. This differs from the results of Zharikov, being much less dependent on concentration.

The authors claim that impurities in the original samples were responsible for depopulation of the lower level. Increasing the intensity of the excitation pulse is also cited as a cause of depopulation via intensity dependent cross-relaxation schemes. The lifetime of the upper state also varies compared to the earlier reports, ranging between 100μs and 70μs as the concentration is increased from $\approx$0 to 100%. Although the authors offer no explanation for this, it is clear from examining the experimental technique of Zharikov et al that their figure of 320μs may have been limited by the duration of their excitation pulse ($\approx$80μs) and the resolution of their detector ($\approx$50μs). In a later publication, the stimulated emission cross-section for the 2.936μm transition is reported by Zharikov[145] to be $\sigma_{se} = 2.6\text{x}10^{-20}\text{cm}^{-1}$, an order of magnitude less than that of 1% doped Nd:YAG[146]. Here the cross-section is reported to be independent of concentration, in keeping with the concentration independent fluorescent lifetime reported by Basiev.

At room temperature, the lowest level of the terminal laser manifold lies 6544cm^{-1} above ground. Therefore, the system is expected to operate independently of temperature. However, this has been proven not to be the case by several authors[53,147]. Spring et al[131] have attempted, unsuccessfully, to explain the temperature dependence of the threshold laser energy in terms of the changes in thermal population while others consider a number of other possible reasons[53]. Amongst the suggested reasons are a change in the cross-relaxation efficiency, a decrease in the stimulated emission cross-section and line broadening. However, it remains unclear as to the relative contributions made by each.

The excitation of erbium doped crystals is complicated by the many cross-relaxation processes which may either enhance or reduce the pumping efficiency. Zhekov et al describe the main processes in reference [122]. To summarise, depopulation of the lower laser level may be obtained at high pump rates and at high concentrations via a process in which the relaxation of the lower laser level to the ground state simultaneously creates an excited state at the $^4I_{9/2}$ level from where it may relax into the upper laser level. In contrast, by the relaxation of an excited state at the $^4S_{3/2}$ level to the $^4I_{9/2}$ level, excitation energy may be transferred to the $^4S_{3/2}$ level, thereby creating an excited state in the lower laser level. Ursu et al[148] have measured the decay time of the $^4S_{3/2}$ level and found that, at concentrations greater than 25at.%, it is less than 0.6μs indicating rapid relaxation from this level. This experiment was done under direct excitation causing transitions between the $^4S_{3/2}$ level and the ground state manifold. It is reasonable to conclude that similar transfer rates would be achieved for broad band excitation, indicating that this cross-relaxation scheme occurs on the timescale of a Fixed-Q laser pulse (150-300μs). No

such data exists for the other schemes.

The absorption spectrum for erbium doped YAG has been measured and analysed by Koningstein et al[120]. At 4.2K the absorption spectrum consists of a large number of transitions in the visible part of the spectrum. The upper laser level lies at the base of the $^4I_{11/2}$ manifold which occupies energy positions between 10252cm^{-1} and 10411cm^{-1}. Thus, direct pumping of the upper laser manifold occurs between wavelengths between 975nm and 961nm. Shorter wavelengths are absorbed by the higher lying levels. The key absorption lines are summarised by Bass et al in reference [127] and are reproduced below in Table 3.1

Wavelength (μm)	Transition
0.80	($^4I_{15/2}\rightarrow{}^4I_{9/2}$)
0.65	($^4I_{15/2}\rightarrow{}^4F_{9/2}$)
0.54	($^4I_{15/2}\rightarrow{}^4S_{3/2}$)
0.52	($^4I_{15/2}\rightarrow{}^2H_{11/2}$)
0.49	($^4I_{15/2}\rightarrow{}^4F_{7/2}$)
0.45	($^4I_{15/2}\rightarrow{}^4F_{5/2}$)
0.44	($^4I_{15/2}\rightarrow{}^4F_{3/2}$)
0.41	($^4I_{15/2}\rightarrow{}^2H_{9/2}$)
0.38	($^4I_{15/2}\rightarrow{}^4G_{11/2}$)

Table 3.1 Summary of absorption wavelengths and responsible transitions in Er:YAG (after Bass et al[127])

The absorption spectrum has been measured for this work using a Perkin-Elmer Spectrometer. The results for a 13mm thick sample of 50at.% doped Er:YAG are shown in Figure 3.5. The measurement was made for absorption against wavelength, where 100% absorption is the normalised maximum absorption. No account has been taken of the reflection losses from the faces of the sample. It can be seen that absorption extends over much of the visible part of the spectrum, thereby justifying the choice of xenon flashlamps, which emit in a broad band throughout this region, as the excitation source.

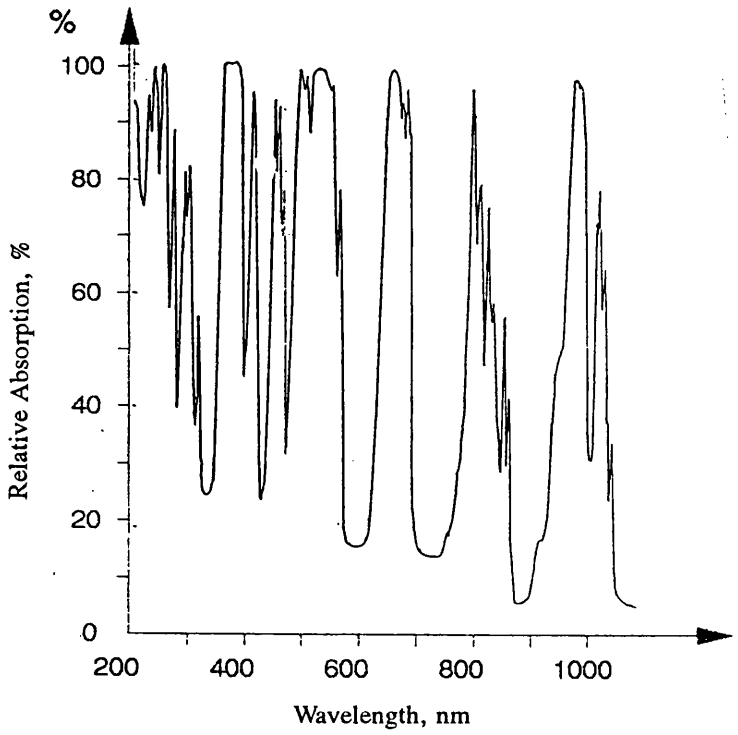

Figure 3.5 Absorption spectrum of 50at.% substituted Er:YAG between 200nm and 1100nm.

Using only the light emitted from the flashlamps in the spectral region between 625nm and 1μm, Zhekov et al[121] observed that, for a YAG crystal doped with 50at.% erbium, lasing occurred preferentially at 2.69μm, but that if the pump level was raised by approximately 40%, lasing could also be obtained at 2.94μm. Increasing the pump level by a further 30% then allowed the transition at 2.83μm to oscillate. However, when the pump range was changed to include light between 300nm and 1μm lasing occurred principally at 2.94μm. In this case operation at 2.69μm could not be obtained, while a 30% increase in the pump level was again required to obtain lasing at 2.83μm.

A similar experiment is reported by Frauchiger et al[149] for the operation of Er:YAP crystals in order to limit the thermal loading on crystals. The authors of that work filter light from the emission of xenon flashlamps and observe similar results to those reported by Zhekov. Specifically, for the full excitation spectrum, down to 400nm, laser operation at 2.92μm is dominant (where 2.92μm in YAP corresponds to the 2.94μm transition in YAG). However, as the pump level is increased, lasing at 2.79μm (2.83μm in YAG) occurs. As the cut-off wavelength of the excitation radiation is increased the 2.79μm line first becomes dominant (ie has the lowest threshold) to be followed by the 2.73μm transition, which is dominant when only

pump wavelengths longer than 715nm are used. This reveals the complicated nature of the build-up of population inversion between the upper and lower laser levels.

3.2 Performance Optimisation

The performance of a laser formed using an erbium doped YAG crystal has been characterised. The object of the work was twofold, firstly to determine whether the erbium laser scheme for the 2.94μm transition obeys the expected laser theory, and secondly to determine the sensitivity of the output to certain key laser parameters. As with the CTH:YAG laser in the preceding Chapter it was necessary to consider certain design aspects at the start of the characterisation and to leave them set for the duration of the remaining work. Like the CTH:YAG laser, this included fixing the pumping chamber and flashlamps and also the rod dimensions, rod dopant concentration and resonator optics, including the output coupling reflectivity. The reason for having to consider the latter group at this stage, rather than allowing some investigative work to be carried out throughout the characterisation experiments, was largely financial. Insufficient funding was available to purchase more than one laser rod and one set of laser optics. Consequently, it was decided to purchase a rod having dimensions 3"x4mmϕ and a set of plane optics consisting of a 100% reflecting rear mirror and an 82.5% reflecting output coupling mirror. Both resonator mirrors were made using germanium substrates, which is transmissive at the 2.94μm laser wavelength and which, therefore, avoids heating of the optics by absorption of the laser light. The choice of reflectivity was not arbitrary but was restricted by availability. Both optics were purchased 'off the shelf' from Laser Power Optics (San Diego, California, USA) with no choice of radii of curvature. The only alternative reflectivity for the output coupler was 50% which, based on the experimental data of Charlton[53], was not expected to provide sufficient feedback to allow lasing to occur.

Unlike the CTH:YAG crystal for which rods of slightly differing dopant concentrations are available from different suppliers, Er:YAG rods are supplied with a standard dopant concentration of 50at.% ($\approx 7x10^{21}cm^{-3}$), irrespective of the manufacturer. The standard concentration arises from efforts made by the crystal manufacturers to provide crystals optimised for efficient laser operation[150]. However, there is no published work, based on comparative laser studies, to support this. Zhekov et al[48] showed that the efficiency of laser action increased with the dopant concentration. A reduction in the lifetime of the $^4S_{3/2}$ with increasing concentration, which can lead to rapid transfer of energy into the upper laser level, has also been reported by Ursu[148]. However, these observations have only been made for crystals up

to concentrations of 25-30% and the results cannot be extrapolated to 50%. From the results of Frauchiger with 30% and 50% doped Er:YAP it is clear that the higher dopant concentration promotes operation of the longer wavelength lines, closer to the water absorption peak. However, in the only relevant publication, Bass et al[127] obtained laser action at 2.94μm for both 33% and 50% erbium doped YAG crystals where superior laser efficiency was obtained for the lower doped sample.

It is shown by the work described in this thesis, and elsewhere[36,67], that, in the case of CTH:YAG, resonators incorporating smaller diameter rods are less sensitive to roll-off of output due to thermal lensing. Frauchiger et al[50] showed that for a 40at.% doped rod the thermally induced lensing is four times stronger than that of the Nd:YAG crystal. Thus, a smaller diameter rod was selected to allow operation at elevated average powers with a reduced risk of thermal rollover compared to a larger diameter rod. The factors affecting the choice of rod dimensions are discussed in more detail in section 2.2.3. Financial restrictions on the choice of rods meant that the only crystal available for characterisation had dimensions 3"x4mmϕ. The crystal used was supplied by Litton Airtron (Charlotte, NC, USA). The end faces were anti-reflection (AR) coated for operation at 2.94μm and were flat, although the crystal was polished with opposing ½° wedges.

3.2.1 Pumping chamber and flashlamps

The choice of pumping chamber is determined by a number of factors. In the first instance it is necessary to consider the dimensions of the rod and the desired transverse mode structure of the beam. Where a low number of transverse modes is required then a focusing pumping chamber may be used to promote gain in the central region of the rod. However, diffuse chambers may be used where large volume energy extraction is more important and beam quality is less important. The absorption spectrum of the laser crystal is also an important factor in determining the material used to reflect the excitation light towards the laser crystal. For the Er:YAG laser, Charlton et al[53] have compared the efficiency of ceramic close coupled, $BaSO_4$ close coupled and silvered elliptical pumping chambers. Their data shows that, under identical circumstances, the $BaSO_4$ chamber resulted in the lowest laser threshold energy when pumped with a xenon flashlamp. The silver ellipse and ceramic each needed more energy to achieve threshold requiring 18% and 46% more discharge energy than for the $BaSO_4$ chamber, respectively. Based on these results the experiments performed in this work were all done using the Er:YAG crystal housed in a $BaSO_4$ pumping chamber (IR Sources, NH, USA). Further details of the pumping chambers used in this work are given in Appendix 1.

To excite the Er:YAG crystal the discharge from a xenon flashlamp was used. This is in keeping with the excitation source used by the authors of the key publications of experimental observations[50,53]. Frauchiger et al[148] have also demonstrated that in the erbium doped YAP crystal excitation below 400nm is necessary in order to promote lasing at 2.92μm rather than the shorter wavelengths available via other transitions within the same manifolds. The broad emission from xenon flashlamps includes a significant amount of excitation energy at wavelengths in this spectral region. The absorption spectrum of a 50at.% doped Er:YAG rod is shown in Figure 3.5 and reveals that the crystal absorbs over much of the visible part of the spectrum, further justifying the choice of a xenon flashlamp. The lamp had an arc length of 67mm and a diameter of 4mm (restricted by the inside diameter of the flashlamp wall material). The maximum electrical discharge was 102 J pulse^{-1} which resulted in a Gaussian shaped discharge pulse as shown in Figure 2.30. Further details about the flashlamps and the charging and discharging circuits are given in Appendix 2.

3.2.2 Resonator optimisation

The effect of resonator optimisation on the measured output energy from a laser and the reasons behind it are discussed in Chapter 2.2.4. To summarise, the energy output from a resonator is influenced by the number of transverse modes oscillating within the resonator. The number of transverse modes is altered by the geometry of the resonator; the curvature of the mirror surfaces, the distance between the mirrors and the strength and distribution of any lensing elements between the mirrors. Changes to any of these may cause changes in the transverse mode structure of the beam and thus to the energy output of the laser. Frauchiger et al[50] use this argument to explain the parabolic nature of their input/output data for an Er:YAG laser system. This is supported by measured thermally induced lensing which is four times greater than that expected for a Nd:YAG rod of similar dimensions. Thus, a greater dependence of the laser output energy on the thermally induced lensing is anticipated.

The influence of thermally induced lensing on the laser output energy was determined experimentally for two resonators. The resonators were each formed between the available optics, described earlier. In both cases the distance between the rod centre and the front mirror was 190mm. The distance between the rod centre and the rear mirror was 180mm in one case and 280mm in the second, resulting in resonators having total physical lengths of 370mm and 470mm, respectively. The average output power was measured using a calibrated calorimeter (Model 20, Laser Instrumentation, Chertsey, England) and the repetition rate measured using a Philips

PM6665 frequency monitor. Figures 3.6 (a) and (b) show the change in output energy, for a number of fixed discharge energies, with changing repetition rate.

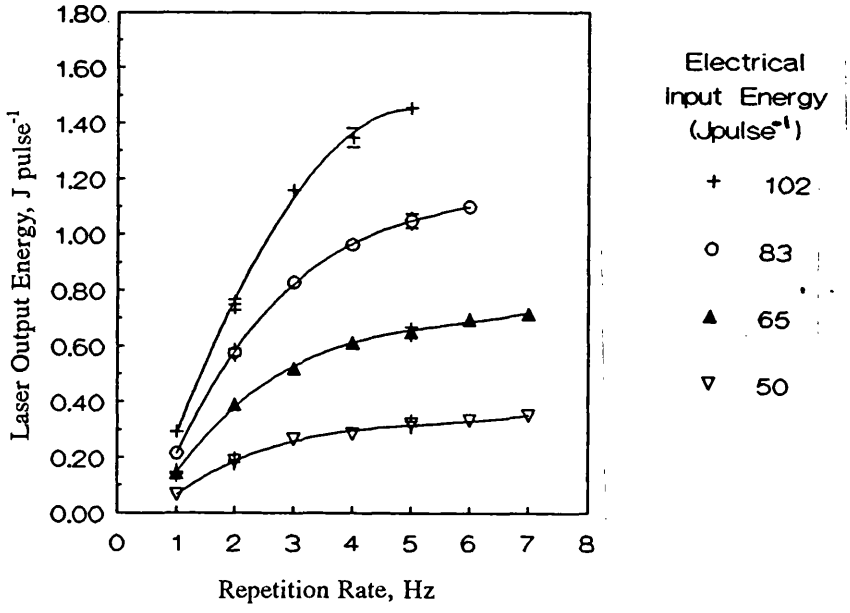

(a)

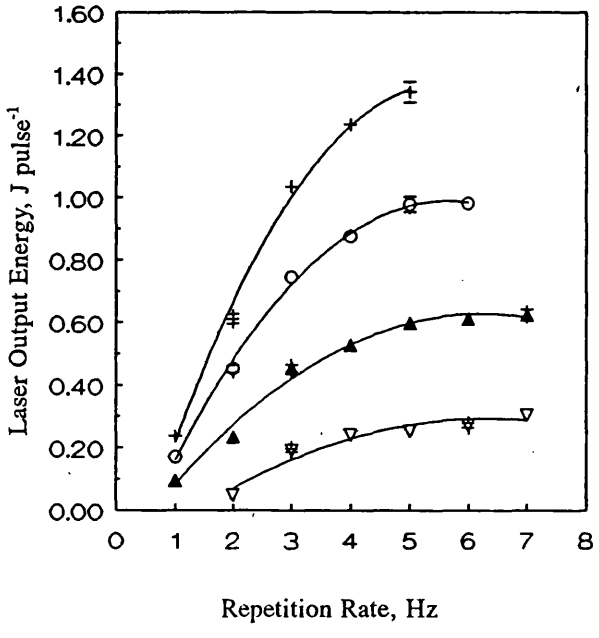

(b)

Figure 3.6 Change in laser output pulse energy with repetition rate at several pump pulse energies for laser resonators having total physical lengths of a) 370mm and b) 470mm. The other resonator parameters remaining constant.

It can be seen in both graphs that the typical pulse energy increases rapidly with increasing repetition rate from 1Hz. However, at 5-6Hz the output energy per pulse from the 470mm long resonator appears to stabilise. In contrast, the output from the 370mm long resonator increases up to 7Hz. This was the maximum allowable repetition rate due to the average power limitations of the power supply. Additionally, the maximum output energy obtained from the 370mm long resonator is consistently greater than that obtained from the 470mm version. For example, at 5Hz and for a 102J excitation discharge, the output from the shorter resonator is 8.5% greater than the output from the 470mm long resonator. This is in agreement with the expected result based on the experimental work of Frauchiger et al[50] and Charlton et al[53]. Charlton et al observed a maximum in the output energy, for a fixed energy input, at repetition rates around 15Hz for resonators 300 and 400mm long. Additionally, when a 200mm long resonator was used, repetition rates up to 35Hz could be achieved without a significant reduction in the laser output energy. However, the discharge energy was around 40 J pulse^{-1} which, when multiplied by the repetition rate, reveals that Charlton's results are comparable with those presented here.

To assess the sensitivity of the laser output to the resonator length, the rear leg of the resonator was increased in 50mm steps and the effect on the laser output energy observed, as described earlier. Figure 3.7 shows the results of the experiment for a fixed electrical discharge energy of 102 J pulse^{-1} and a fixed repetition rate of 5Hz. For resonators having rear leg lengths between about 190mm and about 300mm the output energy decreases linearly from approximately 1.4 J pulse^{-1} to about 1.0 J pulse^{-1}. However, beyond about 325mm the output drops rapidly until, at rear leg lengths of 390mm (total resonator length of 580mm) lasing is restricted to the first few lamp pulses, during which changes in the thermal lensing of the rod are causing the resonator to become unstable. Figure 3.8 shows the oscilloscope trace obtained when the output from the resonator was monitored using a InAs photodiode and integrator circuit. Each vertical line is a single laser pulse, with the height of each pulse indicating the energy contained in the pulse. It can be seen that the maximum laser output occurs for the third pulse, thereafter falling rapidly such that, for the 580mm long resonator, only seven pulses are obtained before the resonator becomes unstable and laser action ceases.

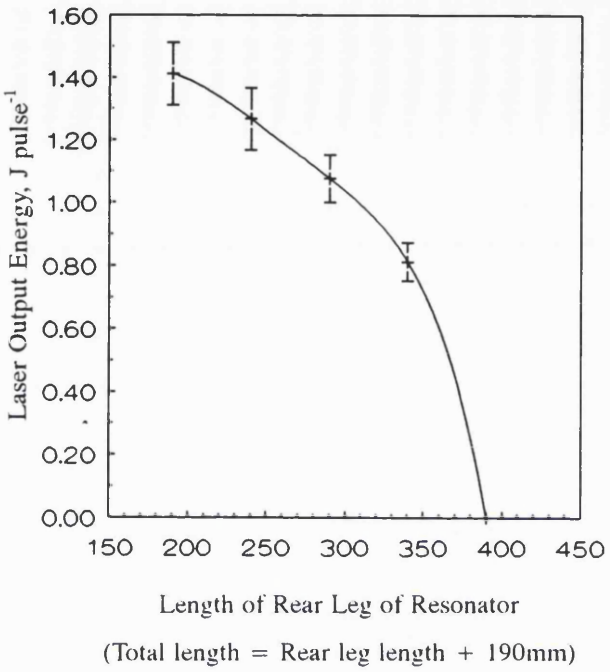

Figure 3.7 Variation in laser output energy with extension of the resonator length for a resonator containing a 3"x4mm diameter rod, the pump pulse energy and repetition rate remaining constant at 102 J pulse^{-1} and 5Hz, repectively.

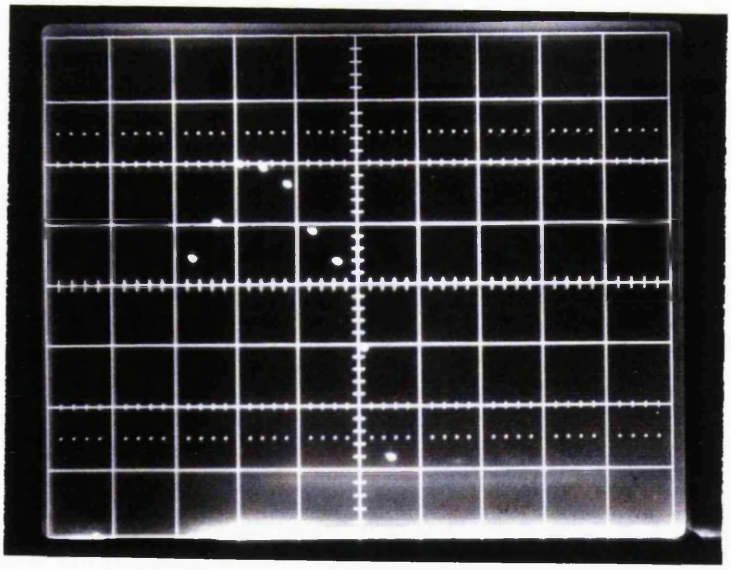

(500ms/division)

Figure 3.8 Oscilloscope trace of the first few laser pulses obtained from a 580mm long laser resonator when operated from 'cold'. The effect of changes in the thermal lensing causes the output to increase and then decrease as the resonator moves towards an instability region.

3.2.3 Sensitivity of laser output to operating temperature

Despite the four level nature of the laser action at 2.94μm, due to the terminal laser level which lies about 6500cm^{-1} above ground, temperature sensitive operation has been reported by several groups. Charlton et al[53] and Frauchiger et al[50] describe almost linear reductions in the Fixed-Q laser output energy with temperature for a given pump energy. Spring et al[131] also report a linear dependence of the threshold energy on the crystal core temperature. The authors of each attribute the effect to a number of thermally sensitive parameters. Amongst them, thermal population of the lower laser level, a decrease in the stimulated emission cross section plus line broadening and variations in the cross-relaxation coefficients. However the true cause is unknown. Also, from the available data it is not possible to determine whether the changes in the output energies, reported by Charlton et al[53] and Frauchiger et al[50], were due solely to the changes in the laser threshold energy induced by the changing temperature, or whether the laser slope efficiency was also affected. The latter effect has already been demonstrated earlier in this thesis for the CTH:YAG laser system, despite expectations that only the laser threshold would be affected.

The effect of temperature on the performance of the current laser design was investigated. The 370mm long resonator was operated at 3Hz and the output monitored as described earlier. The choice of the short resonator and the modest repetition rate was made to avoid any influence of thermal lensing which has been shown to increase when unused pump energy is lost to the crystal lattice (see section 2.3.2). The temperature was controlled by adjusting the thermostat on the circulator/chiller (RTE110-B, Neslab Ltd, Netherlands) and was measured using a Type K thermocouple and Digitron hand held display unit (R-S Supplies, Milton Keynes, England). The thermocouple sensor was located at the input manifold to the pumping chamber. Thus, the temperature is that of the coolant water at the inflow. Measurements of the temperature of the coolant water at the output manifold revealed that the temperaure of the output manifold was a constant 2$\pm$0.25°C above the input temperature. The results of measuring the output over the temperature range 21-38°C, and over a range of pump energies, are shown in Figure 3.9. It is clear from this figure that, unlike the CTH:YAG laser for which there was a significant dependence of the output energy on the operating temperature, the effect on the output energy emitted by the Er:YAG laser is comparatively small.

At the maximum pump energy of about 102 J pulse^{-1} the laser output energies at 21°C and 38°C are 0.702J and 0.685J respectively, a reduction of less than 2.5%. The changes in output energy at pump energies of 102 J pulse^{-1}, 83 J pulse^{-1} and

65 J pulse^{-1} are shown graphically in Figure 3.10.

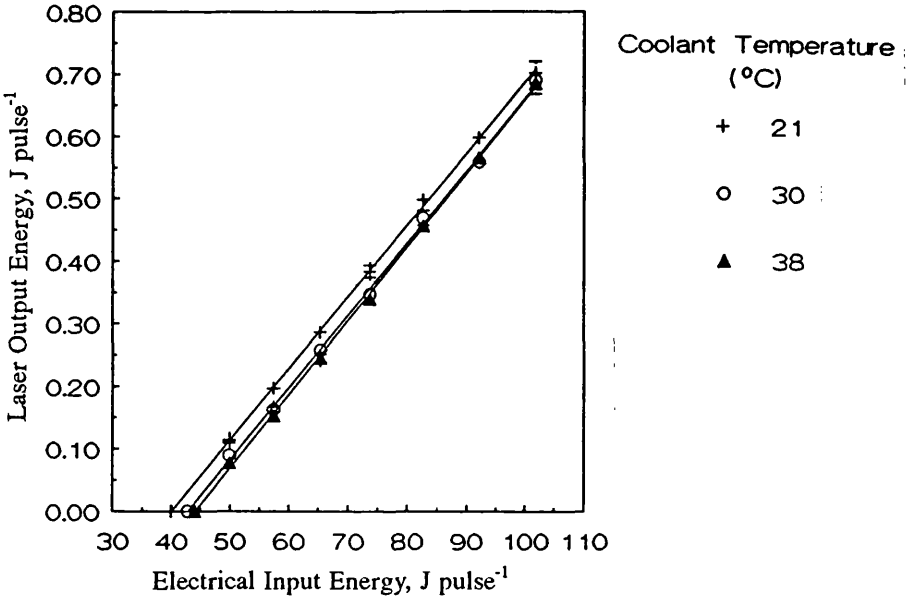

Figure 3.9 Laser output performance over a range of operating temperatures for a 370mm long resonator containing a 3"x4mm diameter Er:YAG rod pumped at 3Hz.

Compared to the results of Charlton et al[53], the laser output energy appears to be much less sensitive to temperature. However, at a similar operating level (about 120 mJ pulse^{-1} at 20°C) the reduction in laser output is much more rapid and in keeping with Charlton's experimental data.

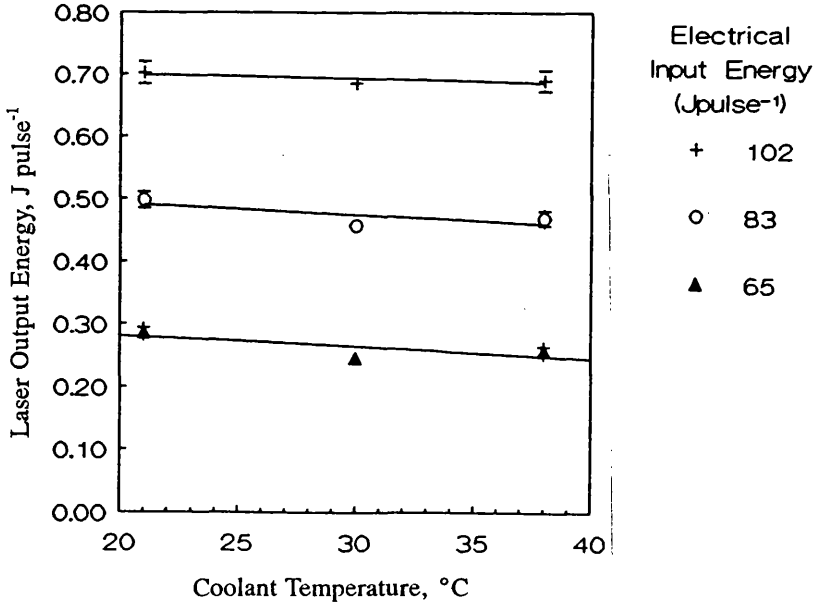

Figure 3.10 Change in laser output energy with temperature for a 370mm long resonator fixed pump pulse energies of 102J, 83J and 65J.

Analysis of the experimental data reveals that the threshold energy is increasing with temperature at a rate of approximately 0.24 J $°C^{-1}$ while the slope efficiency varies at only approximately 0.002 % $°C^{-1}$, Figure 3.11. Thus, both slope and threshold appear to be temperature sensitive, although threshold appears to be more so.

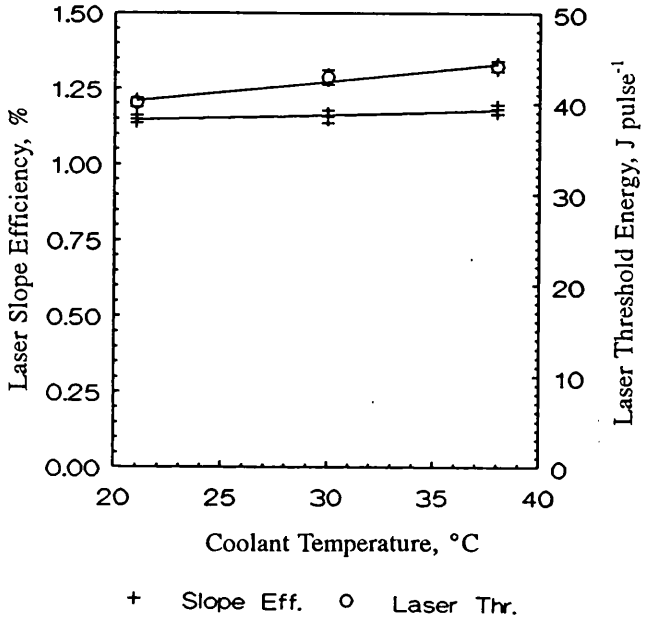

Figure 3.11 Change in laser slope efficiency and laser threshold with temperature.

Additionally, it would appear that both parameters vary linearly with temperature, although errors and the slow variation of each prevents confirmation of this. If the simple calculation of the dependence of the laser threshold on the thermal population of the lower level, according to Section 2.3.1, is applied then a linear response is again expected due to the slow variation of the thermal population in temperature range 20-40°C. However, due to the relatively high lying terminal level (compared to that of the CTH:YAG) the change in thermal population varies rapidly between 40°C and 80°C. Practical restraints prevented operation of this system at higher temperatures. The data of Spring et al[131] includes experimental points up to 55°C. However, the variation in the threshold energy obtained by them is linear with temperature throughout and, therefore, not with the thermally determined lower laser level population.

3.2.4 Discussion

Detailed investigation of some of the factors affecting the performance of the Er:YAG laser has been carried out. In agreement with the observations of other authors[48,53], the output energy is sensitive to the average pump power due to thermally induced lensing. However, the experimental results, if compared to the results obtained earlier for a

CTH:YAG rod having a similar rod diameter, indicate that the output does not reduce as rapidly as for the CTH:YAG laser. Optimisation of the laser output energy with increasing repetition rate, attributed to thermal lensing, has been observed for two experimental resonators having lengths 370mm and 470mm. The peak output occurs at 5-6Hz for the latter, while output for the former is still increasing at 7Hz, the maximum possible repetition rate due to power supply limitations.

Measurement of the influence of temperature on the laser output reveals that both threshold and slope efficiency are temperature sensitive, although the effect is weak. As a result, when operating the laser at a constant 3Hz, the output reduces by only 2.5% for a temperature increase from 21°C to 38°C when the pump energy is 102J. The relationship between threshold energy and temperature appears to be linear over this range, in agreement with Spring et al[131], although correlation to the thermal population of the lower laser level is not possible.

Investigation of the influence of other features of the laser was not possible due to the restricted availability of components. However, the choice of apparatus (pumping chamber, output coupling reflectivity etc) was based on existing data and clearly resulted in a system with excellent laser efficiency. Laser thresholds as low as 29J and slope efficiencies of 2.3% are in general agreement with the results of Charlton et al[53] although, from their work, a further reduction in the laser threshold might be expected for an increase in the reflectivity of the output coupler. Such increases would inevitably increase the risk of intracavity coating damage and would therefore be unadvisable.

Prolonged operation of the experimental Er:YAG laser system without environmental sealing of the optics resulted in damage to the optical coatings which prevented a more in-depth investigation of this laser crystal. The damage to the end faces of the rod showed two distinct features. The first were areas, approximately 250μm across, where the coating appeared roughened, and the second were sites where a collection of smaller damage sites were visible, Figure 3.12. The latter were thought to be the precursor to the larger damage sites. Dust contamination of the rod facesand ingress of moisture, which will absorbed the circulating laser power, were suspected as being the reasons for this damage.

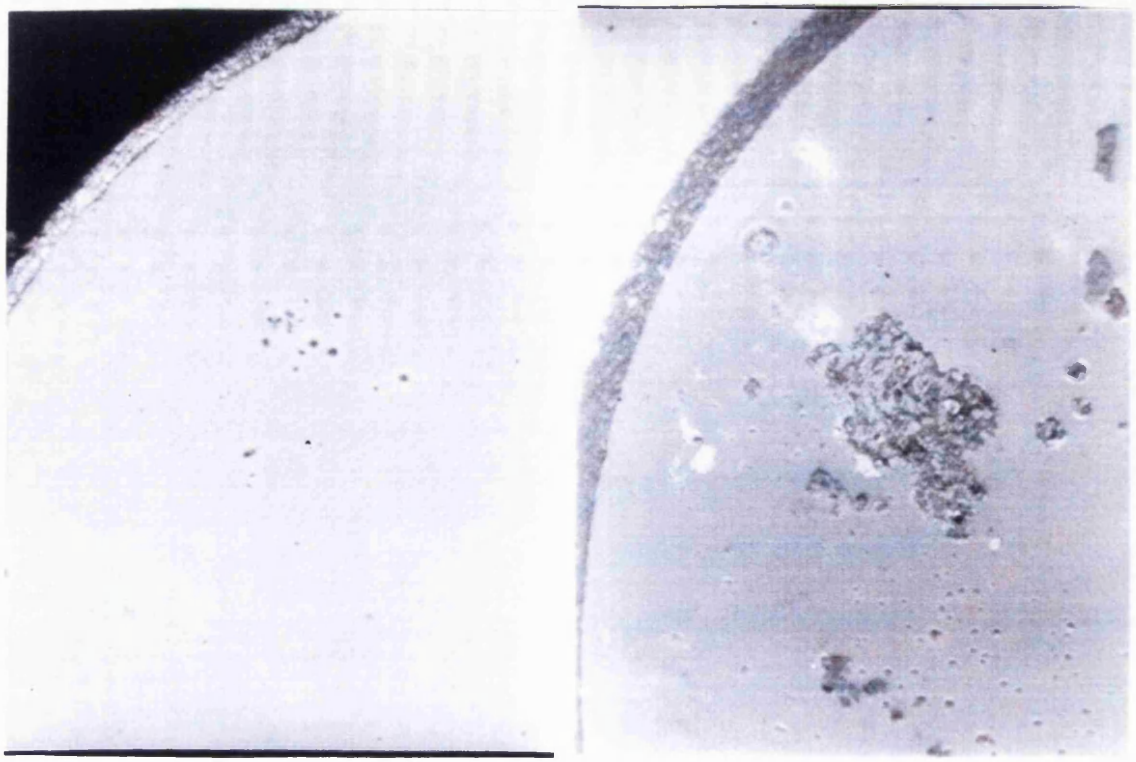

Figure 3.12 Photomicrograph of damage to the end faces of the Er:YAG rod. Damage typically appeared either as a) small point damage sites or b) larger damaged regions.

3.3 Thermomechanical Effects

Knowledge and understanding of the thermomechanical effects in laser crystals is essential if reliable operation of lasers containing these crystals is to be achieved. For steady state operation, the temperature profile which develops within a heated crystal is parabolic[92]. The temperature profile and stress effects combine to produce a radial variation in the refractive index profile. Consequently, rays of light passing through the rod are bent, the net effect being that the rod becomes an optical duct. Thermally induced lensing has been reported in almost all solid state laser crystals. For YLF crystals the variation in refractive index with temperature, dn/dT, is negative for certain polarisations and the rod can be modelled as a negative element. YAG crystals have a positive dn/dT and, therefore, the lensing effect, resulting from the development of a temperature profile, causes the rod to act as a positive lens. Changes to the induced lensing in a laser crystal can lead to a reduction in the output energy[90] and even the complete cessation of laser action from a resonator which, in its 'cold' state is otherwise capable of supporting laser action. Although the sign of dn/dT is determined by the host crystal the dopants often play an important role in

determining its magnitude as well as the magnitude of other parameters in the thermal lensing equation, and thus the total magnitude of the lensing effect.

Thermal lensing also determines the maximum output divergence angles from the resonator by changing the number of transverse modes which are free to oscillate. It is this factor which is directly responsible for the changes in the output energy since the laser depends on oscillating modes to extract the energy stored in the upper laser levels. A larger number of transverse modes will extract a greater proportion of the stored energy at the expense of increased beam divergence.

A more detailed discussion on the factors affecting thermally induced lensing in laser crystals is given in Appendix 4.

3.3.1 Thermal lensing in Er:YAG crystals

There are few reports on the amount of thermally induced lensing observed with erbium doped crystals. However, several authors acknowledge lensing of the crystal to be responsible for the reduction in the output energies from their lasers. In their early study, Bass et al[127] avoided the effects of thermal lensing by using short resonators, only 250mm long, which were insensitive to rod lensing. Later, Al'bers et al[139] reported the reduction in the output of their high repetition rate Cr:Er:YSGG laser with increasing pulse frequency. Although attributed to thermal lensing, no estimation of the degree of lensing was made. Moulton et al[140] also reported a reduction in the efficiency of a Cr:Er:YSGG laser with increasing repetition rate which was again attributed to thermally induced lensing. Although Moulton did not quantify this effect he did note that the reduction was less for the YSGG crystal than he had observed under similar operating conditions for a YAG crystal. This observation is not entirely supported by Charlton et al[144] who concluded that thermal lensing was a limiting factor in the operation of both crystals. Additionally, Charlton et al report that their YSGG crystal shattered at average input power levels below the limit expected for YAG crystals, suggesting that YSGG may not be suitable for high average power systems. In a separate publication, Charlton et al[53] demonstrate that the reduction in the laser performance at elevated repetition rates, due to thermally induced lensing, may be lessened by the addition of a transfer dye to the coolant. In the quoted example, Rhodamine 640, which absorbs wavelengths between 480nm and 630nm, allowed operation at repetition rates in excess of 35Hz where, previously, 25Hz had been the limit. Frauchiger et al[50] also report on the selective pumping of an Er:YAG crystal to reduce the thermal loading on the crystal, although no comparative data between filtered and unfiltered thermal lensing is presented. The authors do, however, calculate

the rate of induced thermal lensing for a 3"x6.35ϕmm, 40at.% doped Er:YAG crystal from HeNe measurements (see Appendix 4). Their results reveal that the Er:YAG crystal lenses four times more strongly than a Nd:YAG crystal of similar dimensions, operated under a similar set of conditions.

3.3.2 Experimental measurement of the rod lens

The causes of thermal lensing and the experimental measurement of lensing in a solid state laser crystal is discussed in Appendix 4. The lensing induced in the Er:YAG rod, over a range of pump powers was investigated using the indirect approach outlined in the Appendix. The crystal was operated in a $BaSO_4$ pumping chamber through which flowed cooling water at $25\pm0.5°C$. The crystal was pumped by the output from a single xenon flashlamp, the walls of which were cerium doped quartz to limit the amount of UV-light reaching the crystal. The average power input to the lamp was varied between 100W and 500W by changing the voltage applied to the discharge capacitors and the repetition rate. The former was measured using a high voltage probe across the capacitors while a Philips PM6665 frequency monitor was used to verify the pulse frequency. A symmetric resonator 370mm long was formed around the crystal using the available optics. To determine the laser beam divergence the spotsize in the focal plane of a 98mm focal length CaF_2 lens was measured using the technique described in Appendix 3. The beam diameter at the output of the resonator was measured using the same technique. The beam diameter was defined as the diameter containing 86.5% of the beam energy as described in Appendix 2.

The resonator was subsequently modelled on a personal computer using LaserTrace (see section 2.4.3). In the software, the rod is treated as an optical duct with a refractive index profile which varies quadratically across the diameter. The amount of variation across the profile is determined as shown in equation (A4.4), by the pump power and percentage absorption of the pump power. The former was set the same as the actual operating power, while the latter was varied to obtain a theoretical divergence which matched, to within $\pm2.5\%$, the experimentally obtained divergence. From the modelling of the CTH:YAG laser, it was expected that the output beam diameter predicted by the model would be greater than the experimentally determined value. This has been attributed to the difference in definition of the spotsize between practise (86.5% contained energy) and the model (100% contained rays). Thus, to make the model more accurately depict the practical results, the diameter of the rod in the model was reduced until the predicted output beam diameter and measured output beam diameter were within 2.5% of one another. Because of the raytracing algorithms used, it was necessary to 'unfold' the

resonator into a series of optical elements in the sequence that they would appear to a ray travelling along the mechanical axis. Examples of the input and output forms and a typical raytrace screen from the programme are shown in Figure 2.20.

The effective focal length (EFL) of the rod lens was then determined, using the software, by passing a parallel beam through the optical duct, at a given pump power and absorption, and determining the distance of the focus from the end of the rod, the back focal length (BFL). The EFL was then obtained from the sum of the BFL and half the rod length divided by the crystal refractive index (BFL+l/2n).

3.3.3 Results

The increase in full angle beam divergence with average pump power, measured for the resonator described earlier, is shown in Figure 3.13. In keeping with the results for the CTH:YAG laser reported in section 2.4.4, it is apparent that lower divergence angles are recorded for lower repetition rates, the average pump power being kept the same.

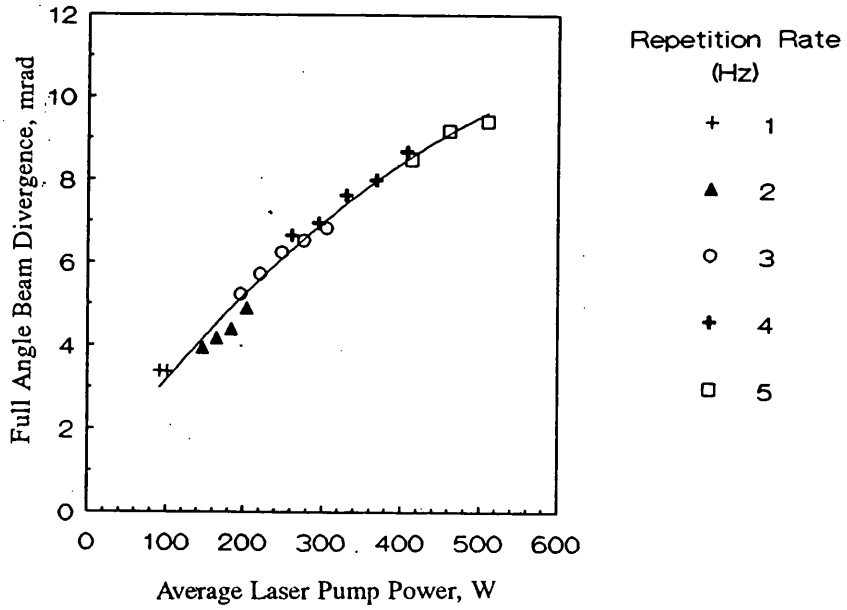

Figure 3.13 Change in output beam divergence from a 370mm long, plane symmetric resonator with average lamp power.

This is attributed to higher pulse discharge energies expended at lower repetition frequencies, which result in higher output energies and a reduction in the amount of heat left in the crystal compared to the case of lower discharge energies and higher repetition rates. The measured beam diameter at the output of the resonator was 2.75±0.1mm over the complete range of pump powers which is larger than that

measured for an equivalent sized CTH:YAG rod in a similar resonator. The reason for this may be due to either the difference in the number of transverse modes oscillating in each of the lasers or a difference in the distribution of gain throughout the crystal caused by a difference in the absorption properties of the crystal. Currently, it is not possible to compare the distribution of absorbed energy across the diameters of each of the rods and it is not possible to determine the relative contributions of either.

Over the range of measurement, the divergence of the beam from the Er:YAG laser is lower than that of the CTH:YAG laser, although differences in the resonator geometry prevent any conclusions at this stage regarding the relative amounts of thermal lensing in each crystal. As expected, the beam quality, the product of full angle beam divergence and beam diameter, increases in the same way as the increase in divergence, due to the constancy of the output beam diameter, Figure 3.14.

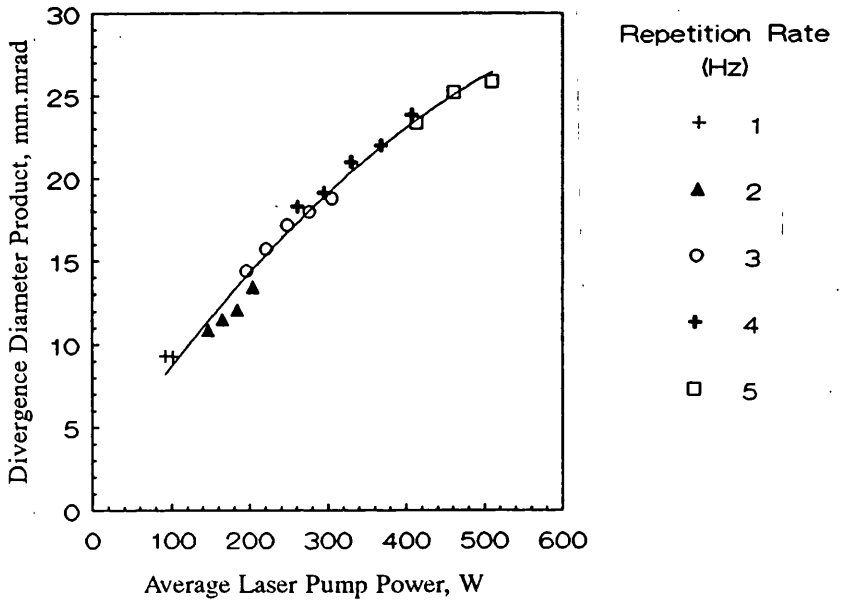

Figure 3.14 Change in output beam quality from a 370mm long, plane symmetric resonator with average lamp power.

From the divergence data displayed in Figure 3.13, the thermally induced lensing in the laser crystal was determined using LaserTrace. Figure 3.15 shows the result of the analysis (symbols) for each of the experimental points in the previous Figure.

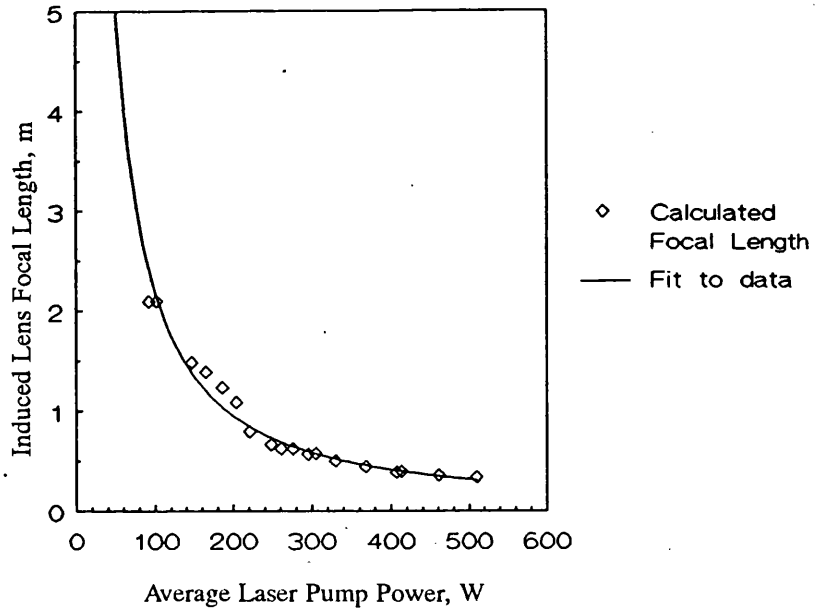

Figure 3.15 Variation in focal length induced in a 3"x4mm diameter Er:YAG rod with average pump power.

Curve fitting the data yielded an equation of the form given in equation (A4.8) reveals that the relationship between the average pump power and the thermally induced lensing can be described by

$$F = \frac{560}{P^{1.204}} \qquad (16)$$

where P here is the average pump power in watts. This equation is plotted as the solid line in Figure 3.15. This result is compared to the result obtained by Frauchiger et al[50] for a 40at.% doped crystal pumped in a twin lamp, ceramic pumping chamber, Figure 3.16. Using the relationship between the rod diameter and the amount of thermal lensing (Appendix 4, section 2), the induced focal length predicted from the results of this work for a rod of the same dimensions as that used by Frauchiger et al may be compared (solid line). The figure shows that the induced focal lengths in a 1/4" diameter rod, predicted from the experimental results obtained for the 4mm diameter rod, are noticeably shorter than those obtained experimentally by Frauchiger. There are a number of likely reasons for this. First, the rod diameter influences the efficiency with which flashlamp light is transferred to the rod, as was discussed earlier for the CTH:YAG rod (Section 2.4) which leads to stronger than predicted lensing in larger diameter rods compared to small diameter rods over the same average pump power range. Secondly, and most importantly, the pump configuration used by Frauchiger differs significantly from that used in these experiments. Whereas these experiments

were performed in a single lamp pumping chamber in which the 'reflector' was $BaSO_4$ Frauchiger used a double lamp chamber made from ceramic. Earlier experiments, detailed in Appendix 1 have shown ceramic to be inferior at transferring useful flashlamp light to the laser crystal compared to the $BaSO_4$ chamber. It is reasonable to consider that the the $BaSO_4$ chamber may also transfer a greater proportion of flashlamp light responsible for heating the crystal than the ceramic chamber. These two factors, combined with any possible effect on total flashlamp light absorption that differences in the percentage dopant level may have, explain at least some of the discrapancy between the thermal lensing predicted using the exerimental results of this work and that of Frauchiger.

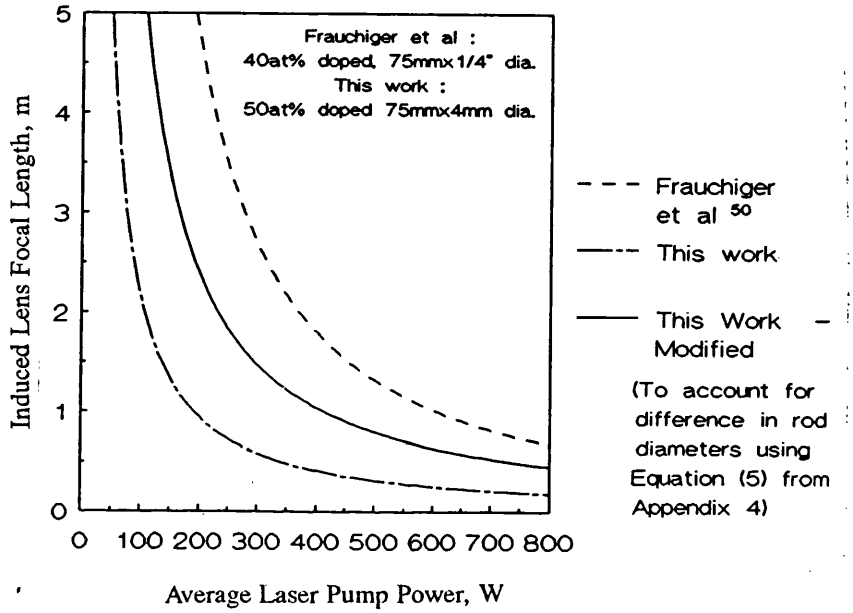

Figure 3.16 Variation in focal length induced in a 3"x4mm diameter Er:YAG rod with average pump power. A comparison between this work and the work of Frauchiger et al[50].

3.3.4 Modelling of beam divergence from a second resonator

The divergence behaviour of a second symmetric resonator was determined experimentally and compared to the behaviour predicted by modelling the resonator using LaserTrace. The results of the model and the experiment are shown in Figure 3.17. The model succeeds in predicting the divergence performance most accurately in the range 175-400W. However, beyond this region there is an obvious discrepancy between model and practise which was not observed under similar circumstances with the CTH:YAG laser. One reason for this may simply be that the

number of experimental points presented in this figure is small compared to the previous case. The collection of a large number of experimental points was hampered by damage to the end faces of the rod which occurred at elevated pump energies. Another possible reason may be variations in the spatial distribution of energy across the laser beam which may became more significant for longer resonators where the rod diameter has less influence on the output beam diameter. Due to the damage to the end faces of the rod and the absence of suitable apparatus for measuring the beam profile it was not possible to investigate this fact further.

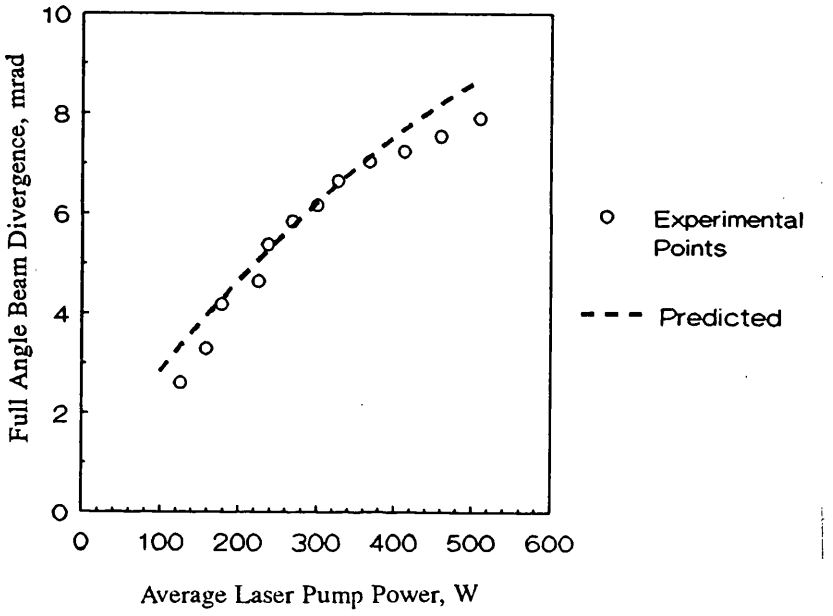

Figure 3.17 Comparison of the change in measured beam divergence with average pump power from a 470mm long resonator with the divergence predicted by the model.

3.3.5 Analysis of heating efficiency in Er:YAG crystals

The lensing effect in laser crystals is due to a combination of stress effects, thermal expansions and a thermal dependence of the refractive index. For convenience the first two effects, which contribute only a small part to the total thermal lensing, are commonly ignored[92]. If this assumption is applied to the erbium crystal then, given data for the induced focal length against average power, it is possible to calculate the fraction of the lamp power absorbed by the rod and contributing to the thermal lensing. Combining equation (16) and equation (A4.8) the fraction of the average discharge power stored in the rod, δ_p, was calculated. The results, shown in Figure 3.18, suggest that the absorbed fraction is not constant but rises rapidly from zero at low pump

powers (<50W) to around 150W after which it levels, thereafter increasing approximately linearly from a value of 0.09 to 0.12 at 600W. This non-linear behaviour is undoubtedly due to the empirical nature of the curve fit used to describe the relationship between average power and induced lensing which is different from the purely theoretical form depicted in equation (A4.5). The average level, though, reveals that typically about 10% of the pump power is absorbed into the crystal lattice. This differs from the result obtained earlier for the CTH:YAG crystal which increased more rapidly and implied that as much as 20% of the flashlamp light may be absorbed by the crystal.

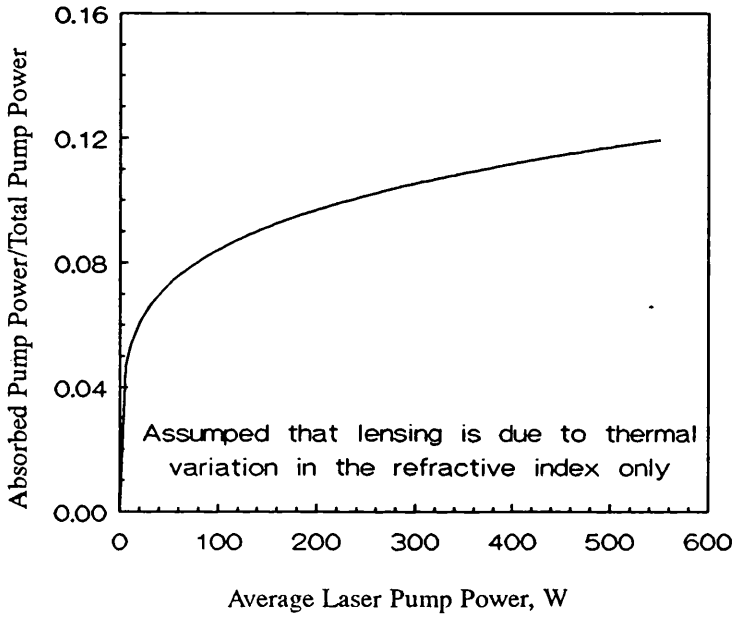

Figure 3.18 Fraction of average lamp power absorbed an Er:YAG laser crystal, calculated using the results for the variation in induced focal length with average pump power.

Although the increase in the absorbed fraction with pump power is small it may be speculated that the pump enhancement schemes described earlier may have some effect at higher pump intensities. The schemes proposed by Zhekov et al[122] involve mainly radiative transitions. However, it is feasible that non-radiative transitions, most likely those between the $^4I_{9/2}$ and $^4I_{13/2}$ levels may increase the amount of heat deposited in the crystal.

3.3.6 Discussion

A comprehensive study of the thermal lensing in an Er:YAG laser crystal has been carried out. It has been established that the focal length of the thermally induced lens,

for the crystal investigated and for the set of operating conditions used, can be described by the simple relationship

$$F = \frac{560}{P^{1.204}}$$

which is of the form described in equation (A4.8).

The thermal time constant for the Er:YAG rod is calculated in Appendix 4 and reveals that thermal equilibrium is only established at repetition rates in excess of 2.26Hz. Figure 3.19 shows the focal power of the rod calculated for the experimental data points.

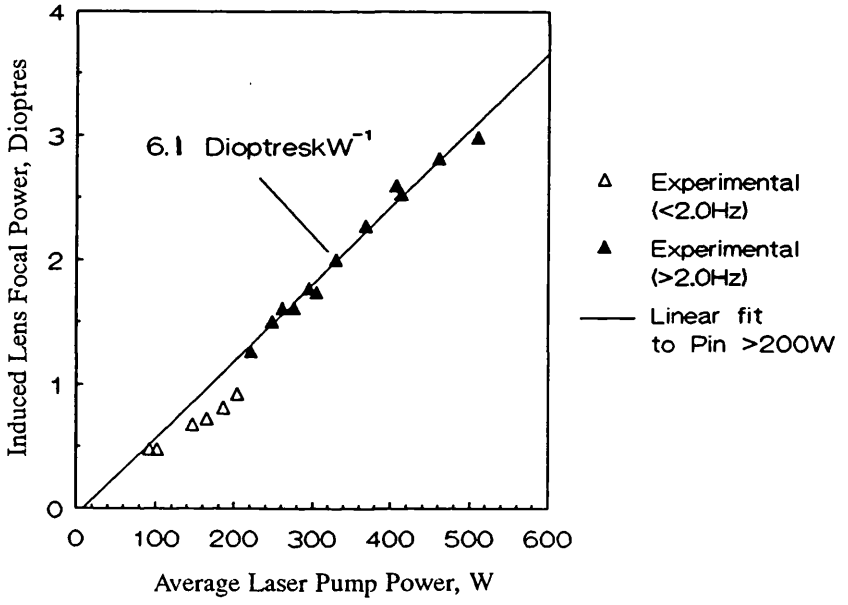

Figure 3.19 Variation in thermal lens focal power of a 3"x4mm diameter Er:YAG rod with average pump power.

The figure also shows an improved linear fit applied to the data points for average pump powers above 225W, where thermal equilibrium is assumed to have been established (maximum discharge energy approximately 100 J pulse^{-1}). The regression analysis reveals that the induced focal power increases at a rate of 6.1$\pm$0.3 Dioptres kW^{-1} and passes through the origin, in agreement with equation (7) in Appendix 4. Where the crystal is pumped at pulse repetition rates less than 2.26Hz (226W) the lens power appears to fall more rapidly with decreasing pump power. This is attributed to the heating profile established in the rod under such conditions and was observed for the CTH:YAG crystal also.

The thermal lensing, calculated by analysing the divergence performance of a simple laser resonator was then used to model a second resonator of differing dimensions. Experimental measurement of the divergence was used to verify the model. There was reasonable agreement between the two although damage to the coated end faces of the rod prevented a full evaluation being made. Attention was drawn to the coating damage by the reduction in the laser output energy over a short period of time. Although a detailed study of the damage sites was not performed, the differences in the appearance of different damage sites suggest more than one cause of damage. It was surmised that damage had been caused by the accumulation of moisture within the coatings. Additionally, dust collecting on the coated faces, initiating burning in the surface, may also have lead to damage. The former effect is particularly important for solid state lasers operating in the 2-3μm spectral region where the absorption of laser light by moisture is high and anti-reflection coatings are known to be susceptible to damage[85].

Using equation (16), the amount of pump power absorbed by the laser crystal and producing the thermal lensing was assessed. For average pump powers between 150W and 600W, the percentage of the pump light absorbed by the rod varies only between 9% and 12% respectively. Although the increase in absorption is small and may be a result of errors in the method of calculation, some increase in the heating may be expected due to the pump enhancement process which occurs at higher pump intensities. However, from the results presented here it is not possible to confirm this hypothesis and, clearly, further work would be required to confirm this.

3.4 Transient Laser Performance

The influence of the upper state lifetime on the performance of Fixed-Q lasers is discussed at the beginning of section 2.5. In summary; the excitation pulse is required to produce a population inversion which is a prerequisite to laser action. Prior to obtaining the threshold for laser action, energy stored in the upper laser level is lost at a rate determined by the upper state lifetime. To maximise the possibility of lasing, excitation pulses must be less than the lifetime otherwise useful pump energy is lost via spontaneous decay. Thus, flashlamp pulses are typically of the order of the upper state lifetime or less. Longer lifetimes allow longer pump pulses to be used which can reduce the required intensity of the pump pulse thereby increasing lamp life[80]. Once laser action has been initiated the dynamics of the laser process mean that stimulated emission occurs before spontaneous emission and the upper state lifetime becomes less important. The necessary matching between lifetime and pump duration was reported

by Zverev et al[116] for transitions from the $^4S_{3/2}$ and $^4I_{13/2}$ levels at 1.6 and 1.7μm.

Bagdasarov et al[151] also reported briefly on the effect on the output energy at a constant discharge energy when the pump pulse duration was varied between 33 and 400μs. This revealed that, for their experimental configuration, a pump pulse of 200μs produced the most efficient laser operation. Although the experimental details are insufficient to confirm that matching to the upper state lifetime is solely responsible for the optimisation (no consideration of the lamp matching parameters are mentioned) the result does agree, in principle, with the expected optimum, being close to the upper state lifetime of 320μs.

The envelope of the temporal profile of the output from Fixed-Q lasers in which the pump pulse duration and upper state lifetime are well matched is typically Gaussian which reflects the shape of the pump pulse. Contained within this envelope are a number of relaxation oscillations, with the depth of modulation between each depending on the gain of the system. The time from the start of the excitation pulse to the start of laser action is termed the 'delay-to-lasing'. It is the sum of the time taken for the population inversion to reach a level where the round trip gain exceeds the loss, plus the time taken for laser oscillation to build up from noise. The delay-to-lasing theory for three and four level lasers is developed in Appendix 5, based on the work of Siegman[105] and Zverev[106], respectively.

The theory predicts the delay-to-lasing based on the pump rate, normalised to the threshold pump rate i.e. where laser threshold is only just reached at the end of the pump pulse. It is assumed that the pump rate, W_p sec^{-1}, varies linearly with the energy discharged by the flashlamps, according to equation (4) in Appendix 5. However, the effective pump rate of the erbium scheme is increased by the additional excitation and de-excitation processes which occur at elevated pump rates[122]. The following section investigates the delay-to-lasing behaviour of the erbium laser system and compares that to the performance predicted by theory.

3.4.1 Differences between theory and practise

The theory, developed by Siegman and Zverev for three and four level laser schemes, is appropriate to excitation by a rectangular pump pulse. Although some improvement in the Gaussian shaped electrical discharge from capacitative flashlamp circuits may be obtained by building pulse forming networks (PFNs), the result is most often a bell shaped pulse, rather than a rectangular one. Power supplies capable of producing rectangular pulses of the form required to fit theory and practise are available.

However, such systems are generally limited to rectangular pulses having minimum durations of 2ms which is inappropriate for the erbium system (upper state lifetime = 320μs).

Attempts to derive equations appropriate to the experimental situation result in transcendental equations which can only be solved by numerical methods. Such work is not appropriate to the scope of this work. Thus, the rectangular pulse theory represents an approximation to the real situation. The duration of the rectangular pulse, T_p, to be used in the theory is not the same as the excitation pulse duration, T_f, which is the FWHM duration and must be determined from the experimental results. From rectangular pulse theory, the delay to the start of the laser action, t_d, is maximum where the laser threshold is reached only at the end of the pump pulse. That is, where all of the pump energy is consumed in reaching the threshold without any remaining to contribute to useful laser output, at this point $T_p = t_d$. T_p can, therefore, be obtained easily from the experimental data.

3.4.2 Measurement of the delay-to-lasing

The change in the delay between the start of the excitation pulse and the start of laser action was measured over a range of pump energies and operating conditions. The laser crystal was housed in the $BaSO_4$ pumping chamber through which flowed cooling water at 25°C. The theory developed in Appendix 5 shows that the delay depends on the pump level relative to the threshold pump level. Figure 3.6 shows that the output of the erbium laser depended strongly on the repetition rate. Thus, to introduce changes in the threshold energy, the xenon flashlamp was pulsed at either 5Hz or 3Hz. Figure 3.7 shows that the laser output also depends on the length of the resonator. Thus, to introduce further changes to the operating conditions, specifically the laser threshold, the length of the resonator was also varied. The output from the laser was monitored using an InAs photodetector (Laser Monitoring Systems, Newland Business Park, Hull) while the temporal profile of the flashlamp emission was monitored using a fast silicon photodiode. Both detectors were connected to the 50Ω input of a Tektronix 2445B, 200MHz oscilloscope which was triggered by the flashlamp circuit. The time between the start of the flashlamp envelope and the laser emission was measured using a 'time elapse' feature on the oscilloscope. Figure 3.20 shows a typical trace obtained. The upper trace is the flashlamp envelope and is the same as that shown in Figure 2.30. The duration of the excitation pulse was constant at 350μs (FWHM).

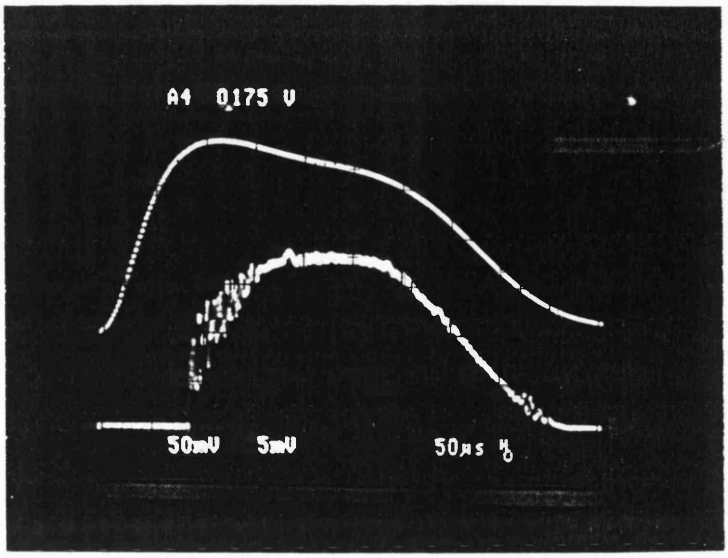

(50μs/division)

Figure 3.20 Typical oscilloscope trace obtained during measurement of the delay between the start of the excitation pulse (left hand trace) and the laser pulse (right hand pulse).

The results of the measurements are shown in Figure 3.21, plotted against the discharge energy.

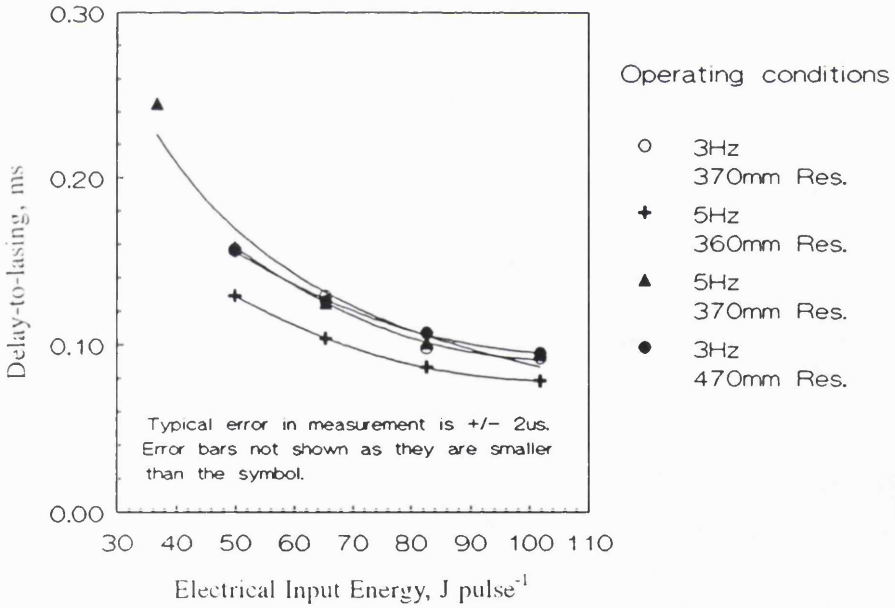

Figure 3.21 Change in the measured delay between the start of the flashlamp excitation pulse and the start of laser action with lamp discharge energy. The repetition rate and resonator length being varied in order to change the laser threshold.

The results do not show the spread between data from different operating conditions as expected. The reason for this lies in the restricted range of operating conditions

brought about largely by a lack of different reflectivity output couplers and mirror curvatures.

The data is replotted against the normalised pump energy in Figure 3.22. Shown also are the theoretical predictions of the delay-to-lasing for three and four level lasers (dashed and solid lines respectively) based on the rectangular pump pulse theory developed in Appendix 5. The effective pulse duration of the rectangular pulse used in the theory was 245μs and was obtained by applying a third order polynomial fit to the experimental data for values of the normalised energy less than r=2. To allow calculation of the atomic pump rates, which are required in the three level theory, rather than the discharge energy, the pump rate at the threshold, $W_{p,thr}$, was obtained by solving equation (A5.12a).

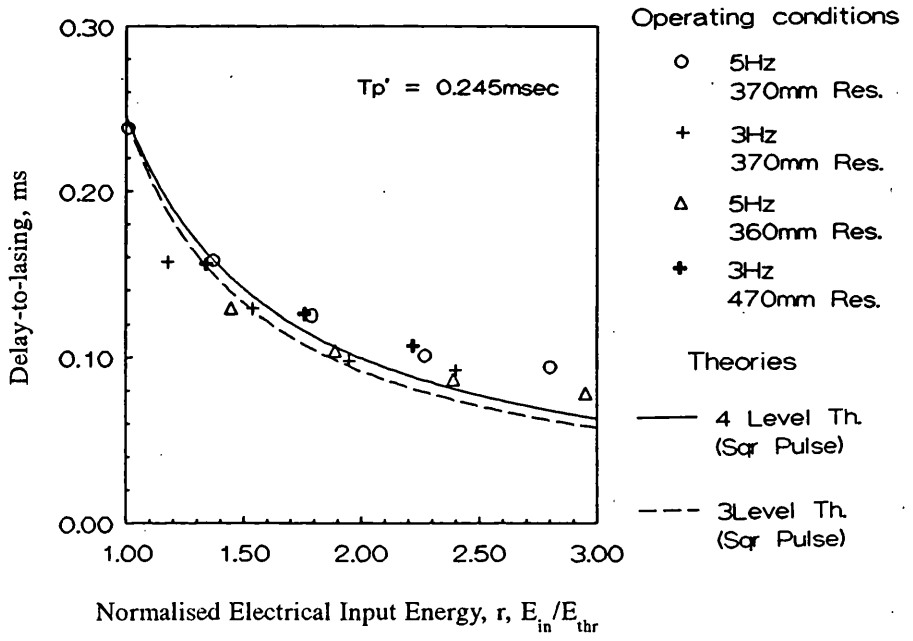

Figure 3.22 Change in the measured delay between the start of the flashlamp excitation pulse and the start of laser action with normalised discharge parameter, r. The repetition rate and resonator length being varied in order to change the laser threshold.

This was achieved by numerical methods based on a standard software package (MathCad, Version 2.5, Mathsoft Inc., Mass.) for the condition where the threshold was achieved at the end of the rectangular pump pulse, ie t_d = 245μs. As with previous data presented for the CTH:YAG laser, the x axis is the normalised pump *energy*. A linear relationship is assumed to exist between pump rate and pump energy as described by equation (A5.4). Thus, it is possible to compare both experimental data and the predicted delay for the three level system on the same axis.

3.4.3 Laser pulse duration

The output from a laser pumped with a temporally rectangular excitation pulse is expected to begin after a characteristic delay, t_d, and terminate at the end of the excitation pulse, Figure 2.34. The duration of the output pulse can then easily be calculated from the difference of the two, equation (12).

The duration of the output pulse from the laser, operated under the experimental conditions described earlier, was investigated to assess the differences between theory and practise. The output from the laser was detected using the InAs photovoltaic detector and monitored using either a Tektronix 2445B, 200MHz or a Gould 465, 100MHz, 200 Megasample/second oscilloscope. The pulse duration was defined experimentally, as always, as the full width half maximum (FWHM). Figure 3.20 shows that the temporal profile of the laser pulse follows closely that of the flashlamp, but that neither are rectangular, due to the nature of the capacitative discharge. The results of the measurements and the theory are shown in Figure 3.23 and show a clear discrepancy. The experimental data shows that the pulse duration rises rapidly from zero to approximately 0.17ms as the normalised pump energy, r, increases from 1 to 1.25. Thereafter the rate of increase is reduced and the duration increases, almost linearly, reaching a value of 0.24ms at r=3. In contrast, both three and four level theories predict a gentle, sub-linear increase in the pulse duration, only reaching 0.18ms at r=3.

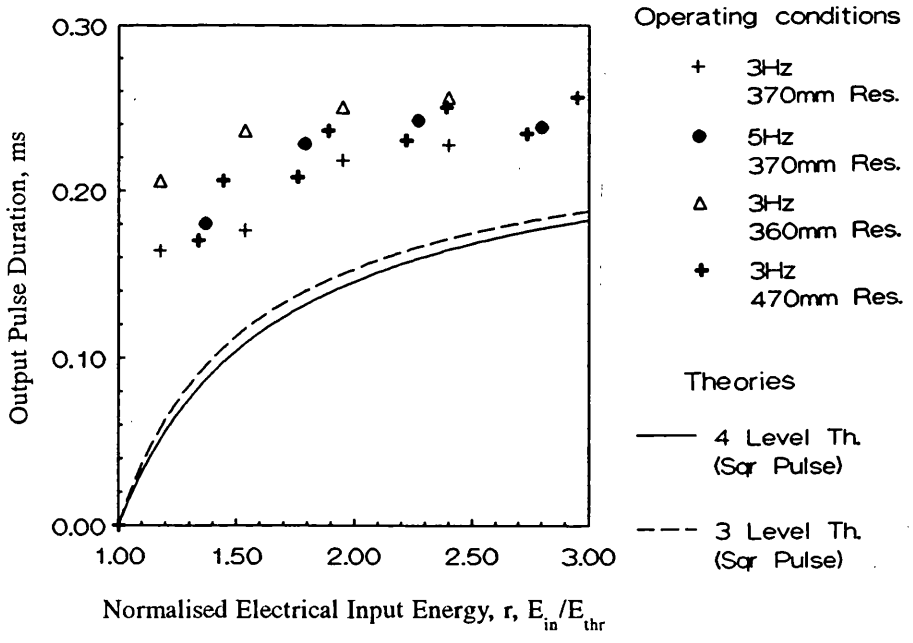

Figure 3.23 Comparison between the measured output pulse duration and that predicted from the rectangular pulse delay-to-lasing theory.

In Figure 3.24, the experimentally determined pulse durations are plotted against the output pulse energy obtained from the laser. The energy was determined by measuring the power output with a calibrated calorimeter (Model 20, Laser Instrumentation Ltd, Chertsey, England) and dividing by the pulse repetition frequency, determined using a Philips PM6665 frequency monitor. Despite the different operating conditions, it can be seen that the pulse duration remains approximately constant at a given output energy. This is a result of the insensitivity of the laser slope efficiency to the changes in the operating circumstances.

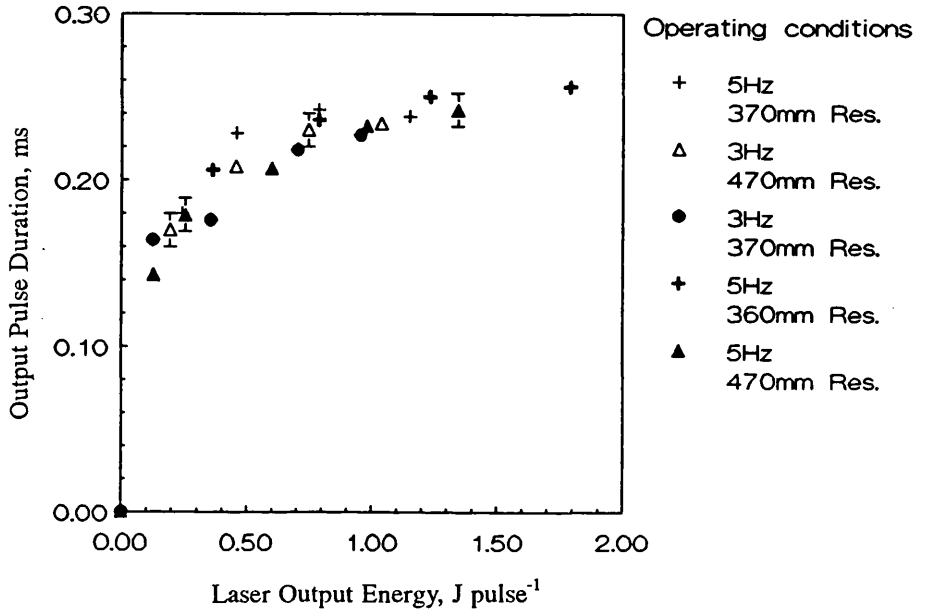

Figure 3.24 Change in output pulse duration with output pulse energy for a number of different operating conditions, each producing different laser threshold energies.

3.4.4 Discussion

The results of the delay-to-lasing measurements, plotted against the normalised pump energy, show a convergence of the experimental data points, as expected. Both theories appear to adequately describe the delay-to-lasing performance although some divergence between theory and practise is apparent for $r > 2.5$. The reason for this is unclear. Based on the anticipated enhancement of the pumping by cross-relaxation processes, a reduction in the delay-to-lasing time with increasing pump level, compared to theory, would be expected. The nature of the results suggest that the opposite is occurring, i.e. that losses from the upper laser level are increasing with pump level. However, the range of measurement is inadequate to confirm this trend and so the suggestion of an additional loss route which increases with pump rate is purely

speculative. Unfortunately, operation at higher normalised pump levels (r=3-5) was not possible due to power supply limitations. Bowman et al[34] report that for the CTH:YAG laser, the lifetime is dependent on the pump energy. In their work, a weakly pumped crystal was found to have an upper state lifetime of 9ms, compared to 3ms when 100 J cm^{-3} was delivered by a flashlamp. It is speculated that a similar process may also be occurring for the Er:YAG crystal used in these experiments. In this case the effect is more noticeable due to the lifetime of 320μs being comparable to the duration of the flashlamp (350μs).

It is noticeable also that, in contrast to the theoretical curves for the CTH:YAG laser, there is a difference between three and four level predictions. The reason for this is undoubtedly due to the upper state lifetime of the $^4I_{13/2}$ level which, being close to that of the flashlamp pulse, results in a more significant loss by spontaneous emission, rather than by stimulated emission.

The large discrepancy in the predicted laser pulse duration compared to the theories is not unexpected and was observed also for the CTH:YAG laser (see Sections 2.5.3 and 2.5.4). The reasons given previously apply equally here. To summarise, the fast rising edges of the pump and output pulses provide an adequate approximation to the leading edges of rectangular pulses for the delay-to-lasing predictions, where the leading edge is the point of measurement. However, where the trailing edge is also used (as it is in the pulse duration measurements) the slowly decaying pump pulse introduces differences to the model which affect the correlation between theory and practise.

The range of output pulse durations can be usefully compared to the pump pulse to assess the likely changes in the output pulse duration at even higher pump levels. From basic laser theory, it is known that the output commences when the round trip gain exceeds the loss. Once threshold occurs, the output follows the envelope of the excitation pulse. The maximum pulse duration is then the flashlamp duration minus the time taken to deliver the threshold energy. From the experimental results it is clear that the duration of the output pulse from the Er:YAG laser is 240-250μs, Figure 3.23. Thus, for a pump pulse duration of 350μs, it can be concluded that 100-110μs are required to deliver the 30J to 40J required to reach the laser threshold. Clearly, where the pump intensity is increased, the same energy will be delivered more quickly and the pulse duration will increase as a result of a reduction in the time taken to reach threshold. However, the rate of increase in the time taken to deliver the threshold energy will not be great. This explains the slow increase in the pulse duration for $r > 1.5$ observed in the figure.

Thus, it can be concluded that the rectangular pump pulse theory can be used to describe adequately the delay-to-lasing behaviour of the laser where the effective rectangular pump pulse, T_p, can be derived from a few simple experiments close to the laser threshold. The pulse duration, though, cannot be predicted using the same theory, due to the critical effect that the pulse shape has on the outcome of the prediction. However, it is possible to make some general statements about the changes in the output pulse duration, based both on the results of the experiments and on knowledge of the duration of the pump pulse.

3.5 Summary and Conclusions

The laser operation of erbium doped crystals operating principally at 2.94μm, where the water absorption curve exhibits a strong peak, has been reviewed. Laser operation at this wavelength was first reported by Zharikov[48] in 1975, despite reports of laser operation at wavelengths in the region 1.6μm to 1.7μm[114-117] as early as 1962. Subsequently, much attention has been directed towards the 2.94μm emission, formerly by Soviet researchers and more recently by western research groups who are interested in the nature of the interaction between the output and biological tissue.

Despite a longer lived lower laser level (around 2ms) compared to the upper state lifetime (320μs), efficient room temperature operation of crystals doped with up to 50at.% doped erbium has been reported both in pulsed[50,53] and CW[141,142] systems. This is achievable due to a number of cross-relaxation processes which assist in the depopulation of the $^4I_{13/2}$ terminal laser level and in the enhancement of pumping the $^4I_{11/2}$ upper laser level[122].

Demonstrations of the practical aspects of operating erbium lasers have been presented by Frauchiger et al[50] and Charlton et al[53,144]. Frauchiger et al demonstrated that the output from an Er:YAG resonator was adversely affected by increasing temperature and by increasing repetition rate. The former effect was investigated by Spring et al[131] but failed to provide an adequate explanation of the temperature dependence. Frauchiger's analysis of the latter indicated that thermal lensing was responsible for most of the reduction of output with lensing four times stronger in the Er:YAG crystal than in a Nd:YAG crystal operated under similar conditions.

Charlton's work revealed some important practical aspects in the design of Er:YAG lasers. In a comparison between pumping chambers made from ceramic, a silvered ellipse and packed $BaSO_4$ powder, the last mentioned outperformed the

others, producing a higher laser efficiency under a given set of operating conditions. Charlton also observed that, to obtain the maximum laser efficiency from his system, it was necessary to use an output coupling mirror with a reflectivity of 95%, indicating the low gain of the system, he also raised the possibility of intra-cavity optical damage due to high circulating intensities.

The performance of a single 3"x4mmϕ Er:YAG crystal, doped to 50at.% substitution, has been assessed and the results reported in this Chapter. The aim of the assessment was to evaluate the performance of an Er:YAG system in a way that would add to the limited amount of information currently available on the practical aspects of Er:YAG laser operation. Of key interest to the study were the laser parameters energy, beam quality (divergence) and pulse duration. These, together with some of the influences on them, make up the body of this Chapter. The work was also directed towards assisting in the development of future systems, particularly those for medical applications. Consequently, operation of the Q-Switched performance of Er:YAG lasers has not been considered. Unlike the CTH:YAG laser, for which some improvement in the precision of the interaction with biological tissue may be expected for shorter pulses[56], the strong absorption by tissue at 2.94μm results in rapid thermal relexation, in the order of 1μs. Thus, ideally, energy should be delivered in pulses shorter than 1μs and should be interspersed by gaps greater then 1μs if accumulative thermal damage is to be avoided[18]. However, published work indicates[151] that only a small amount of the Fixed-Q output energy may be obtained in the form of a Q-Switched pulse. Also, high quality electro-optic crystals, suitable for use at this wavelength, were not available. Consequently, it was decided not to investigate Q-Switching the Er:YAG laser.

Various laser resonators were formed around a 50at.% doped Er:YAG crystal. The discharge from a single xenon flashlamp was used to excite the crystal at various repetition rates. Only one set of optics was available for the experiments, and so, it was impossible to make an assessment of the optimum output coupling reflectivity for the system. However, with a short resonator formed between plane optics and an output coupling reflectivity of 82.5% laser thresholds as low as 29J and slope efficiencies of 2.2% resulted in output energies approaching 1.6 J pulse^{-1} at input energies of 100J. Measurement of the laser output energy at increasing temperatures revealed that, for a 10°C rise in the coolant temperature, the output energy decreased by an amount small compared to the errors in the measurement when the laser was operated well above threshold. This is in contrast to the results of Charlton[53] and reflects the fact that the previous data was presented for pump levels close to the threshold. Analysis of the laser performance over a range of pump

energies revealed that the threshold increased with temperature at a rate of 0.24 J $°C^{-1}$, while the slope efficiency varied by 0.002 % $°C^{-1}$. Thus, a comparatively larger difference in the output energy for operation close to threshold is to be expected.

The effect of increasing the pulse repetition rate was investigated for resonators having different lengths. For 370mm and 470mm long resonators, the output energy was observed to increase as the pulse frequency increased from 1Hz to 7Hz. A reduction in the output pulse energy occured in the longer resonator at lower repetition rates than in the shorter version, despite having the same mirror radii. Investigation of the amount of thermally induced lensing in the crystal revealed that the induced focal power of the 3"x4mmϕ rod varied at a rate of 6.1 ± 0.3 Dioptres kW^{-1} of average pump power (for data points unaffected by thermal relaxation between the pulses). This is in agreement with the results of Frauchiger et al[50] and is significantly greater than that which would be expected from a similar sized Nd:YAG crystal. Thermal lensing is, therefore, considered to be the reason for both the increase in the laser output energy with increasing pulse repetition rate and the earlier onset of the reduction in the laser output energy of the longer resonator.

From the experimental measurements of the induced thermal lensing in the crystal, an empirical equation was derived which adequately described the change in lens focal length over the available operating range, including regions where the thermal relaxation of the crystal caused a departure from the linear relationship between focal power and average pump power, given above. This equation was

$$F = \frac{560}{P^{1.204}}$$

The results used to generate this equation were used in a computer model to predict the divergence performance of a 470mm long symmetric laser resonator. The results show a good agreement between theory and practise. Some deviation between theory and practise was observed at elevated pump powers although the deviation was less than the combined error of the practical divergence measurement and the model accuracy. The collection of a larger number of data points to confirm the deviation was not possible due to damage to the end face coatings of the crystal which adversely affected the laser performance.

The amount of heat deposited in the rod by the flashlamp was assessed using

the available theory and the empirical equation describing the thermal lensing. The results suggest that between 9% and 12% of the flashlamp light is absorbed into the crystal lattice. Pump enhancement by cross-relaxation processes, which allows the otherwise self-terminating laser scheme to operate, is expected to increase the amount of heat deposited into the lattice at higher pump levels. Although some increase was observed at elevated pump *powers* the experiments cannot confirm or contradict this effect. Further work would be required to elucidate this effect.

The temporal behaviour of the laser output was investigated experimentally and compared to the predictions of a simple theory, based on a temporally rectangular excitation pulse. The results show that, using the theory for four level laser operation, the delay to the onset of lasing can be predicted to an accuracy typically better than 0.01ms. For the three level theory the prediction is different from four level theory but both theories match the experimental results quite well.

The same theories were used to predict the duration of the output pulses. However, due to significant differences between the theoretically treated rectangular pulse and the measured shapes of the pump and output pulses, neither theory was able to predict the pulse durations accurately. The FWHM pulse duration of the output pulse was found to increase rapidly with the pump level above threshold up to 0.17ms at r=1.25. Thereafter, the pulse duration increased only slowly, in keeping with expectations based on the time taken to deliver the threshold energy, reaching a value of 0.24ms at r=3. The predicted pulse duration from rectangular pulse theories was only 0.18ms at this drive level, indicating that accurate predictions of pulse duration cannot be made with this theory.

The output pulses, at the pump levels required to produce significant amounts of laser output energy, consisted of an envelope of relaxation oscillations. With the exception of the first few pulses, it did not appear that there was greater than 50% modulation between successive oscillations. Thus, although the stored energy was extracted efficiently, the temporal profile of the pulse was not exactly suited to minimising the extent of thermal damage in the tissue, based on the predicted thermal relaxation time of 1μs. Unfortunately, significant modulation, of the type required, is a typical characteristic of laser operation close to threshold and, therefore, not concomitant with high laser efficiency.

CHAPTER 4

Laser Ablation of Soft Tissue

4.1 Introduction

Laser light can be delivered directly to the tissue site using mirrors and lenses. Increasingly, endoscopic and other surgical procedures require that the light is delivered via flexible optical fibres to lesions not directly visible to the naked eye. Nd:YAG laser light at 1.06μm can easily be transmitted via conventional, all silica fibres at average powers capable of affecting large volumes of tissue. However, the nature of the interaction between 1.06μm light and tissue results in tissue coagulation, rather than ablation. This is acceptable where haemostasis and/or large volume tissue destruction is the main objective. However, where tissue ablation with a minimal amount of residual thermal damage is desired, a different interaction is required. The change from coagulation to ablation arises largely by the change to wavelengths which do not penetrate the tissue deeply. Thus, the delivered energy is deposited in a smaller volume, thereby raising the local temperature rapidly to the ablation temperature. For wavelengths shorter than the Nd:YAG laser output, but longer than 400nm, the attenuation of light is dominated by haemoglobin and other pigments. Thus, there is much variability in the effect of the laser treatment between different tissue types, according to the relative concentrations of the absorbing chromophores. For wavelengths below 400nm the individual photon energy is high enough to break the molecular bonds within the tissue. Tissue removal at short wavelengths may thus occur without residual heating and can be precise due to the high absorption. However, excimer lasers which produce wavelengths in this region of the optical spectrum make use of hazardous gases and are not well suited to use in a medical environment. Additionally, concern has been expressed[10] about potential changes in the DNA caused by the UV wavelengths possibly leading to mutagenesis. For wavelengths above 1.06μm, the attenuation of light in tissue is dominated by the water content. Typically, water constitutes about 70% of the mass of soft tissues and

thus the penetration depth of light in tissue resembles that of water above 1.5μm[10,152] and is largely independent of the tissue colouring. This means that laser lesions produced with longer wavelength light are more reproducible between different tissue types.

Currently, the CO_2 laser, which produces an output wavelength of 10.6μm, is commonly used in laser procedures where tissue ablation is required. However, the cut-off wavelength of conventional, silica based, optical fibres is around 2.5μm, Figure 2.40. Thus, CO_2 laser surgery is currently restricted to direct line-of-sight applications. Alternative materials are being developed to allow endoscopic delivery of CO_2 laser light[107] but, currently, infrared optical 'fibres' are limited to flexible waveguides. These are only capable of modest power transmission (about 25W) and also cannot be bent to small radii comparable to those achieved with conventional fibres without significant loss of transmission.

There is increasing interest in the ablative capabilities of solid state lasers which may be used alongside the Nd:YAG to provide an all solid state laser which can both cut and coagulate tissue. Due to the favourable tissue interaction properties beyond 1.5μm, attention is focused on lasers capable of producing relatively long wavelength light. The efficiency of these lasers is being improved by persistent research into the lasing characteristics. Chapters 2 and 3 of this thesis consider the practical aspects in the design of efficient laser systems based on the CTH:YAG and Er:YAG lasers, two of the most promising laser sources operating in this spectral region.

The CTH:YAG laser, operating at 2.1μm, and the Er:YAG laser, operating at 2.94μm, have become the focus of some attention by laser physicians who seek a solid state alternative to the CO_2 laser. However, there are recent reports of laser operation from transitions in the thulium ion, particularly of crystals sensitised by chromium[153]. Laser output at wavelengths between 1.945μm and 2.014μm from lasers based on Cr:Tm:YAG (CT:YAG) crystals has been reported by Pinto et al[37] although reasonable laser efficiencies, comparable to those obtained for the CTH:YAG laser, have only been reported for operation at the longer wavelengths[38]. The general desire for a change is driven by the reliability and compact size achievable with solid state devices and, in the case of the CTH:YAG laser, the availability of convenient fibre optic beam delivery which currently cannot be achieved for the CO_2 laser. While the Er:YAG laser light cannot be delivered via fibres suitable for clinical use, recent reports suggest that the development of fibres suitable for use in laser surgery will soon be available[150].

The ablation of soft and hard tissue by pulses of light from CT:YAG, CTH:YAG, and Er:YAG lasers has been assessed by a number of authors. Ablation can be assessed in a number of ways, each of which can yield useful information about the ablation efficiency. However, it is seldom possible to compare measurements made using different techniques, which means that it is not possible to review the literature and make reliable statements on the ablative performance of different laser types.

Several authors have reported the results of ablation measurements using a variety of tissue removal rate measurements. These include recording the time taken to drill through a known thickness of tissue and calculating the advancement rate per pulse[46]. Recently, many researchers have begun to adopt the measurement technique described originally by Walsh and Deutsch[45] for assessing the ablation efficiency of the pulsed CO_2 laser. The result of this analysis is a numerical value for the ablation rate which has been obtained without recourse to subjective judgment or operator influence, as can be the case in histological assessment. The rate is quoted in different ways by different researchers, although the results are usually comparable if the published work is presented adequately. Specifically, the mass loss rate has been quoted in units of mass per pulse by some and by others in mass per unit delivered energy. The set of experiments performed to obtain the results usually consider a fixed spotsize with the fluence varied by changing the individual pulse energy delivered. An exception to this are the measurements of Dickinson et al[154] who used spotsizes between 150μm and 600μm. However, their data is presented in the form of the latent heat required to ablate a unit volume of tissue or, from their additional histological analysis, the depth of tissue removal. Thus, it does not provide easy access to figures describing the mass loss efficiency.

It has been the object of many researchers to assess the ablative performance of infrared lasers by comparing them to the ablation performance obtained with other strongly absorbed laser wavelengths[155]. Others[45] choose a single laser source and a single tissue type attempting to provide quantitative assessment of the ablation performance by comparison against work by others at different wavelengths. Additionally, some researchers[156] compare the ablation efficiency obtained with a single laser type and a number of different tissue types. This reveals a second benefit to the quantitative analysis of the mass loss technique. Namely, that it allows information to be gathered on the factors affecting the process of ablation other than the wavelength and intensity of the light delivered.

It is the object of this Chapter to quantify the ablation efficiency of laser light

at 2.1μm and 2.94μm. Whereas previous reports have considered only sub-millimetre spotsizes, the development of relatively high pulse energy lasers, detailed in Chapter 2 and Chapter 3, allows larger spotsizes to be assessed. This more closely reflects the expected use of these lasers in laser surgery, in tumour excision for example. Additionally, the larger pulse energies available from the lasers allows a variety of spotsizes to be compared at similar fluences, again previously restricted to small, sub-millimetre spotsizes. Furthermore, larger spotsizes allow instant assessment based on the gross changes to the tissue observed macroscopically. These are usually difficult to identify, due, again, to small spots. To maintain a constant set of operating conditions, only one tissue type, liver, is considered. Quantification of the mass loss efficiency will allow comparisons to be drawn against existing published data with the reasons for any differences explored briefly in the discussion. Further discussion on the macroscopic observations and the changes in mass loss efficiency with laser parameters will be discussed at the end of this Chapter and in Chapter 5.

4.1.1 The propagation of light in tissue

Light incident on any boundary will undergo transmission and reflection, the relative degrees of each being dependent on the material optical properties and the wavelength of the incident light. In a much simplified model, light which is transmitted across the boundary propagates into the material and is gradually attenuated as the photons are absorbed or scattered. The penetration depth of a particular wavelength is defined as the distance that light travels in a medium before its intensity is reduced to 1/e of its original value. In materials where the reduction in intensity on axis is caused by absorption, rather than scattering, the intensity, I(z), within the tissue is described by the Lambert-Bouguer Law:

$$I(z) = I_0 \exp[-\alpha z] \qquad (17)$$

where I_0 is the intensity at the surface of the tissue, z is the distance from the tissue surface and α is the attenuation coefficient. The reciprocal of the attenuation coefficient is known as the penetration depth.

At most laser wavelengths, the propagation of the light into tissue is characterised by a series of scattering and absorption events. The probabilities per unit path length that a photon will be absorbed or elastically scattered are the absorption and scattering coefficients, μ_a and μ_s, respectively. Additionally, the scattering phase function describes the probability per unit solid angle that a photon will be scattered into an angle Θ, where $\Theta=0$ and 180° correspond to forward and

backward scattering, respectively[157]. The reduced scattering coefficient, $\mu_s(1-g)$ takes into account the possible anisotropy of scattering, where g is the mean cosine of the scatter angle, Θ. The distribution of light in tissue depends on the relative strengths of μ_a, μ_s and g. As these are functions of wavelength, the distribution of light in tissue also varies with wavelength[158]. The total attenuation coefficient of light is simply the sum of the coefficients, $\mu_a+\mu_s$. The albedo of tissue is the ratio $\mu_s/(\mu_a+\mu_s)$. Equation (17) holds only where the albedo is small (<0.1) and the total attenuation coefficient approximates to the absorption coefficient.

The principal optical coefficients, μ_a, μ_s and g can be used in a variety of theories to model the behaviour of light in tissue. These models are summarised by Welch et al in reference [159]. Essentially there are four basic models and each model is shown to be appropriate for a different set of conditions. For strongly absorbed light, the beam profile is unchanged as the beam propagates into the tissue and the intensity reduces according to the Lambert-Bouguer Law, equation (17) above. In contrast, when the albedo is higher, as is the case in turbid media such as tissue, at visible and near-infrared wavelengths, it is necessary to make use of either approximations in the equation of radiative transfer[160,161] or piece-wise modelling of single photon interactions, using Monte Carlo techniques.

Essenpreis et al[5] have also shown that, besides differences in optical properties for different wavelengths and tissue types, the thermal history of the tissue is important in modelling the propagation of light in tissue. Measurement of the absorption and reduced scattering coefficients for fresh and coagulated tissue at 1.064μm and 1.32μm revealed that, while there was little change in the absorption coefficients, the reduced scattering coefficient increased by a factor of three. Subsequent work by the same authors[162] identified that the change in this parameter was principally due to a significant change in the scattering coefficient. Theoretical models must take account of these changes if they are to predict accurately what is seen in practise. To date, all models rely on fixed values for the optical coefficients taking no account of the significant changes in optical properties reported by Essenpreis nor in changes in the tissue geometry resulting from tissue shrinkage or tissue ablation. A comprehensive review of the techniques for modelling the propagation of light in tissue, as well as an exhaustive survey of the measured optical coefficients of fresh tissue, has been published by Cheong et al[163].

The accuracy of predictions for non-ablating, non-coagulating irradiation can be verified to some extent by the use of tissue phantoms which, by careful choice of

absorbing and scattering components, can be made to resemble tissue in its most homogeneous form. Gelatin, combined with chromophores and scatterers, such as dyes and polystyrene microspheres may be used as tissue phantoms.

Using an array of fibre-optic sensors, Grossweiner et al[164] have measured the changes in distribution of a Gaussian beam incident on a gelatin phantom. Immediately beneath the surface, the profile was found to be significantly modified as a result of scattering. Additionally, as a result of back scatter, the intensity just below the surface was found to be almost one third greater than the incident intensity. This is in keeping with the results of Monte Carlo based models but not with most other models and highlights the compromise often made between accuracy and simplicity. Grossweiner also determined that, although scattering changed the light distribution pattern from a Gaussian within the first few millimetres of the tissue, continued scattering restored the distribution deeper in the tissue (12-18mm for 633nm light) to a near Gaussian.

The absorption and scattering coefficients and the angular dependance of scattering are fundamental properties of tissue determining its interaction with light and cannot be derived from simple measurements of the attenuation characteristics[157]. However, the attenuation curves for tissue and its constituent particles can provide a useful indication as to the probable relative strengths of scattering and absorption and the depth to which light might be expected to penetrate. The attenuation characteristics of the main absorbing chromophores in soft tissue were shown by Boulnois[10] in his general review of the interaction of laser light with tissue. Below 1.5μm, and above 300nm, the attenuation of light is dominated by the tissue components melanin, haemoglobin and other pigments. These can be found in varying amounts in different types of tissue and, consequently, the interaction of laser light in this spectral region can vary according to the tissue type. Above 1.5μm the absorption of light by water dominates the attenuation spectrum and scattering is relatively small. Typically, water constitutes between 60% and 80% of the mass of soft tissues. Therefore, the interaction between light above 1.5μm and soft tissue is relatively independent of tissue type and associated pigmentation[152]. Consequently, light in this spectral region is strongly absorbed in tissue and can be described reliably and accurately by equation (17).

Some of the delivered light may be lost as a result of reflection or back scatter from within the tissue itself. The fraction of light reflected from the tissue surface may be calculated using the Fresnel equations and is the same as for any other dielectric interface. Thus, the angle of incidence can play a critical role in

determining the relative amount of light coupled into the tissue. Nishioka et al investigated the rejection of 633nm light from the oesophagus[165] finding that in excess of 40% of incident light may be lost as a result of reflection and backscatter from within the tissue, depending on the angle of incidence. The result suggest that there is a marked increase in the amount of light rejected from tissue at incident angles greater than about 50°, as may be expected from Fresnel equations. The transient changes in the reflectance of tissue during exposure to pulsed 2.1μm light are reported in a later publication by Nishioka et al[166]. In this paper it is reported that the amount of light rejected from tissue also depends on the amount of energy delivered. This suggests changes to the optical properties as a result of coagulation, a fact confirmed subsequently by Essenpreis et al[162] using 1.06μm light.

4.1.2 Photothermal effects

Light which is neither transmitted through the tissue nor reflected from tissue will be absorbed. In photochemical laser medicine the absorption of photons can provide the necessary energy to initiate the release of cytotoxic agents which can destroy tissue. It is hoped that the use of drugs, such as HpD, which can be selectively administered to tumour tissue and which release these toxic agents when activated by laser light, can be used in the selective treatment of cancers in a process known as photodynamic therapy (PDT).

The temperature of tissue can also be raised by the absorption of laser light as photon energy is converted to thermal energy. As the photon distribution in the tissue depends on the absorption and scattering properties at the wavelength concerned, then so does the immediate heat distribution. Light which is strongly scattered produces a heated zone which expands beyond the extent of the incident beam radius while weakly scattered light produces a thermal zone which, prior to any heat transfer, resembles the spatial profile of the incident beam.

If the local temperature is greater than about 60°C the tissue will be coagulated. Carruth and McKenzie[167] describe the coagulation of tissue as centred around the denaturation of protein which occurs when the molecular chains unfold. Simultaneously, the collagen fibres of connective tissue shrink which can lead to haemostasis (with thrombosis assisting as a secondary effect). Tissue which has been coagulated is identifiable by the whitening which occurs. This arises as a result of changes to the structure and consequently to the optical properties of the tissue. Essenpreis et al[162] have shown that, for 1.06μm and 1.32μm light, the greatest changes occur in the amount of scattering rather than in the amount of absorption, as

might be guessed by observing the whitening of heated tissue. The rate of this change remains the subject of much speculation and interest. The work of Henriques[4], as long ago as 1947, established that a time-temperature integral relationship exists for coagulation. In simple terms, tissue will be coagulated in a characteristic time, t_1, for a given temperature, T_1. If the tissue is heated to a higher temperature, T_2, then the time taken is reduced such that $t_2 < t_1$. Although the degree of coagulation depends on both time and temperature, many consider coagulation to take place instantaneously at one particular temperature, e.g. 60°C. Others, however, believe that a more accurate interpretation is that, for every 1°C increase in the temperature, the time taken to coagulation is halved. This does not, however, mean that the thermal damage temperature is well defined. Measurement of the rate is complicated by the need for controlled temperature environments, uniform, rapid heating and optically thin samples (in order to detect coagulation by optical methods). Authors who attempt to model thermal coagulation use values for the onset of coagulation ranging between 55°C and 77°C[168, 169].

If the tissue is heated rapidly to 100°C, boiling of the intracellular water may occur[167]. The rapid, x1000, volume expansion as steam is formed leads to the rupturing of the cell wall. Some tissue is carried away in this explosive process. If the heating is slow then explosive evaporation of the cell water does not occur and water loss can proceed without significant material removal. Remaining tissue, now dehydrated, continues to absorb the incoming radiation and the temperature continues to rise. Due to the evaporation of the tissue water, absorption is no longer affected by water absorption characteristics and depends more on the remaining tissue constituents. As the temperature reaches 300-400°C, the tissue becomes carbonised and blackened. This increases the absorption and leads to a greater increase in the temperature of the tissue surface. The presence of this high temperature carbonised layer leads to extension of the thermally altered zone by heat conduction, rather than optical penetration. Above 500°C the tissue proceeds to burn and will be evaporated. Smoke may also be evident as a result of the burning process. Coagulated tissue will, with time, be replaced by scar tissue while tissue char will eventually slough off or be absorbed.

The volume of tissue affected by a single pulse (ignoring possible diffusion of heat away from the absorption zone and possible non-linear effects) is dependent on the wavelength of the incident beam. The changes in affected volume with wavelength can vary over several orders of magnitude for an otherwise constant set of pulse parameters. Also, for heavily vascularised tissue, the local blood flow can act as a heat sink and, consequently, for multiple pulses, the damage zone can be less

than expected[170], further complicating any attempts at accurate modelling. However, in most cases, the time taken to deliver the laser light is extremely short compared to the time required for heat removal by blood flow which is typically of the order of a few seconds.

Modelling of the thermodynamics of the ablation process has been attempted by McKenzie who developed a `Three Zone Model' to explain the behaviour of the carbonised, vacuolated and sub-boiling coagulated zones in tissue exposed to strongly absorbed radiation, firstly considering CO_2 laser radiation[171] and later light from erbium and holmium lasers[41]. McKenzie has also produced a very good review of the physics of the thermal process in laser-tissue interaction which covers some specific applications as well as the theoretical approaches used to analyse them[172]. Attempts to model the thermal behaviour of tissue exposed to strongly scattered radiation are limited by the inhomegeneity of the tissue and changes to the tissue optical properties and tissue volume during heating. Recently, however, Cross and Van Gemert[169] have attempted to model the case of 1.06μm ablation of aortic tissue. Using the diffusion approximation, light penetration was modelled to establish the light and, consequently, the energy profile, before applying simple energy balance equations to determine the subsequent heat rise in the tissue (neglecting heat loss by diffusion). The result is a theoretical ablation rate which is surprisingly similar to that measured experimentally, hiding the very complicated nature of the process.

Most models of ablation apply to the case where the laser energy is delivered in a time shorter than the characteristic time for heat to diffuse away from the exposed volume, such that thermal diffusion can be ignored[41,169,171]. Wherever heat is deposited in tissue, the local temperature rise causes a temperature gradient and a thermal front which, over a characteristic period of time, extends beyond its original boundary as heat is conducted away. Heat can escape by conduction in all directions, by convection and by radiation from the tissue surface. However, within the tissue it may be acceptable simply to resolve the thermal gradients, and hence the direction of heat flow, into two perpendicular directions. As most incident beams are circularly symmetric and a similar degree of symmetry exists (or is assumed to exist) in tissue, the principal directions are axial and radial. If the heat flow in each of these directions is assumed to be independent of the other then the paths of heat loss constitute a parallel circuit[174].

In the one dimensional case, the time taken for the local temperature to fall to 1/e of its original value as a result of heat diffusion, known as the thermal relaxation time, τ_{th}, is given by[12]

$$\tau_{th} = \frac{L^2}{4K} \qquad (18)$$

where K is the thermal diffusivity and L is the characteristic length of the heated volume. The characteristic length for radial heat conduction is the laser spotsize, which is clearly independent of wavelength while the characteristic length in the axial direction is the optical penetration depth, $1/\alpha$, and is clearly a wavelength dependent parameter. Using available data, many authors have attempted to estimate the thermal relaxation times in the axial direction based on absorption coefficients[39,173]. Many authors use the thermal relaxation time to estimate the time required between laser pulses for heat to dissipate, thereby avoiding accumulation of heat in the tissue and extension of the thermal damage zone. Michaels[173] attempted to do this for his calculated thermal relaxation times based on the premise that 95% of the heat should be conducted away between successive pulses, and only 5% of the heat should be lost by conduction during the pulse itself.

Numerical analysis[174] has shown that when the laser beam spotsize is much greater than the optical penetration depth, the heat loss is dominated by heat flow in the axial direction where the thermal gradient is higher. As the laser spotsize, W(z), gets smaller (therefore a smaller heated zone in the tissue) heat flow in the radial direction is increased, eventually accounting for the majority of the conducted heat loss. In the extremes, where $W(z) \gg 1/\alpha$, or $1/\alpha \gg W(z)$ it is sufficient to model heat flow in only one direction.

However, to more fully describe the situation, and to allow improved accuracy in situations where $W(z) \approx 1/\alpha$, it is more appropriate to consider the loss of heat by conduction as a parallel system, using two dimensions.

Assuming that the heat loss in the axial and radial directions are independent, Van Gemert and Welch[174] created two independent equations for thermal time constants. For a laser beam with a Gaussian intensity distribution, the axial and radial thermal relaxation times are

$$\tau_{th,z} = \frac{4\rho c}{k(\pi\alpha)^2} \qquad (19a)$$

and

$$\tau_{th,r} = \frac{\rho c W(z)^2}{2.4^2 k} \qquad (19b)$$

respectively. Due to the parallel heat flow the absolute thermal time constant $\tau_{th,T}$ is then given by

$$\frac{1}{\tau_{th,T}} = \frac{1}{\tau_{th,z}} + \frac{1}{\tau_{th,r}} \qquad (20)$$

If the laser energy is delivered in pulses which are shorter than the thermal relaxation time then there will be negligible heat flow away from the irradiated zone during the pulse. The maximum heating is, therefore, achieved in the desired zone. In such instances it is possible to achieve coagulation and, if individual pulses contain enough energy[175], ablation during a single pulse. This fact is exploited by the so-called 'superpulsed' CO_2 lasers[11] which aim to ablate tissue with minimal carbonisation and coagulation damage[14], thereby avoiding prolonged healing and increased risk of infection.

4.1.3 Other effects of light on tissue

The role of pulse length has been investigated by Cross et al[56] using Q-Switched, Fixed-Q and CW Nd:YAG lasers, such that the measurements covered laser peak powers over seven orders of magnitude. When post-mortem aortic tissue was exposed to an average power of 2W from each laser, Cross found, in cross-section, that the total area of tissue affected (coagulated + ablated) remained constant but that the area ablated increased significantly as the pulse length shortened. Although the rate of light delivery has been shown to be significant when considering thermal relaxation of the tissue, Cross considers in his introductory comments that multiphoton effects may occur when pulses of light are delivered in nanosecond time scales, resulting in ablation of tissue comparable to that observed for excimer laser ablation[42]. The rapid removal of tissue by short pulses also produces acoustic transients which propagate through the tissue, in some instances leading to additional tissue disruption.

Isner et al[176] reported on the ablative effects of the CO_2 laser in both water and blood observing the formation of optical cavities which allowed the laser light to penetrate to the tissue. Using high speed photography, the evolution of the cavities were recorded and later assessed. Isner suggests that the cavities are formed by vapours escaping from the tissue and that each laser pulse must regenerate the cavity

which dies away at the end of each pulse. In Isner's limited trials, ablation of tissue was achieved through blood layers 5mm thick where indications from the measured absorption coefficients suggest that the delivered light would normally be fully absorbed within a depth of only 0.3mm. The same effect has also been reported on by van Leeuwen et al[177] for the 2.1μm emission from the CTH:YAG laser. Here, ablation of tissue was achieved in a water field 2.5mm thick, despite a penetration depth in water at that wavelength of only about 0.4mm.

Non-linear effects can also lead to a reduction in the efficiency of tissue ablation, as demonstrated by several authors. Motamedi et al[178] have reported that thermal gradients produced in tissue change the refractive index across the profile of the beam causing the tissue to act like a lens. Defocusing of a 1mm diameter beam was observed within the first 100ms of irradiation when albumin was exposed to a continuous beam of 514nm light at 2.25W from an Ar^+ laser. Although the same effects have not been reported in studies involving soft opaque tissue, the authors suggest that such effects may explain some of the discrepancies between expected and measured tissue temperatures, particularly for small spotsizes. Undoubtedly, this effect could also reduce the efficiency with which tissue is ablated.

Another, better understood, and more commonly observed effect is plasma formation[6]. This occurs typically when intense laser beams interact with the ejected material as well as when electrons are released from the surface of superheated tissue. Plasmas are used in lithotripsy to initiate the fragmentation of kidney and gall stones. However, in tissue ablation, plasmas can reduce the effectiveness of the interaction by blocking incoming light.

Plasma blocking has been observed for pulsed laser-tissue interaction at 10.6μm by Walsh and Deutsch[45]. Measuring the loss of bone mass during exposure to 2μs pulses from a TEA CO_2 laser, the mass loss per pulse was found to be linear with increasing fluence. However, for fluences above 14 J cm^{-2}, plasmas were observed above the tissue and the mass loss per pulse remained approximately constant in spite of further increases in the fluence.

4.1.4 Holmium laser ablation of tissue

Laser radiation in the 2μm spectral region is principally provided by lasers based on crystals doped with holmium and codoped with thulium and chromium to enhance the pump efficiency. The performance of Cr:Tm:Ho:YAG (CTH:YAG) lasers operating at 2.1μm is discussed in Chapter 2 where the factors affecting the performance of

these devices are assessed experimentally. Recently, laser performance comparable to that obtained with the CTH:YAG laser has been obtained from crystals doped with chromium and thulium only[153] (CT:YAG) at 2.0μm which is closer to a local peak in the water absorption curve. However, to take full advantage of the local peak, operation at wavelengths closer to 1.92μm is required[179]. Although tunable operation of the CT:YAG laser between 1.945μm and 2.014μm has been reported[37], the efficiency at shorter wavelengths is reduced significantly. Until improvements in the laser efficiency are obtained, probably using diode pumping techniques, it is unlikely that these lasers will be widely available for medical use.

The absorption of 2.1μm light in tissue is partly dependent on the type of tissue. Published attenuation coefficients vary between 35 cm^{-1} [9] and 51.2 cm^{-1} [180] depending on the tissue selected and the measurement technique. In comparison to other key wavelengths, light at 2.1μm is 3 to 4 times more strongly attenuated than 1.06μm and 1.32μm[180] and about one fifteenth as strongly as the 10.6μm emission from the CO_2 laser, in general agreement with the water absorption coefficients of 70 cm^{-1} and 700 cm^{-1} for 2.1μm and 10.6μm in water[19], respectively.

The first reports of the use of 2.1 μm laser light in medicine appeared in 1986[19] and relied on a cryogenically cooled CW Er:Tm:Ho:YLF laser to provide the source of 2μm radiation. The authors compared the incisions made with the holmium laser and a CO_2 laser for exposures of up to 10 seconds at various powers up to 2 W. Circular incisions 300μm in diameter were made with each laser type and the zone of thermal damage around the sites compared histologically. It was found that the radial thermal damage was 200μm for both lasers, leading the authors to consider that the holmium laser may be a solid state rival to the CO_2 laser, with the extra advantage of offering fibre optic beam delivery. However, the need at that time for cryogenic cooling, which adds significant complications to the laser, was not considered.

In the same year, Sinofsky[168] published his attempts to model the thermal interaction of both the holmium and CO_2 lasers as well as the 2.94μm emission from erbium lasers. Sinofsky's modelling assumed that the intensity of the laser light was reduced in the tissue according to the simple Lambert-Bouguer Law, equation (17). A computer was used to calculate the heat deposited in the tissue and provide a thermal map of the volume. Ablated volumes were those in which the local energy content was equivalent to a temperature rise to 150°C. This included consideration of the latent energy required for vaporisation, while the threshold for coagulation was set at 60°C. Heat loss from the tissue by conduction was ignored as Sinofsky chose pulse durations and pulse repetition frequencies which were less than the

characteristic thermal time constant, equation (18). The results for the case where a Gaussian beam of diameter 1mm caused ablation of a spot also 1mm diameter suggest residual axial and radial coagulation damage extending 500μm from the edge of the ablated zone. In contrast, the axial and radial damage thicknesses for a 10.6μm beam were 80μm and 200μm, respectively. Although the results for the CO_2 beam are close to the experimental results of Lane et al[19], no conclusion can be drawn as the model neglects heat loss via thermal conduction while Lane et al use CW laser sources, in direct contradiction to the requirements for avoiding significant heat loss by conduction. In general, though, the results of Sinofsky and Lane do agree to within an order of magnitude.

McKenzie applied the absorption coefficients and laser spotsizes used by Sinofsky to his `Three zone model' which he extended from being a CO_2 laser interaction model[171] to include radiation at the erbium and holmium wavelengths[41]. His model considers the one dimensional case only ($W(z) \gg 1/\alpha$) and, as a result of his analytical approach considering the heat content at different tissue depths, key parameters in determining the relative depths of carbonised, vacuolated (coagulated tissue at 100°C) and sub-boiling coagulated zones are identified. An interesting conclusion from his work is that as long as the peak irradiance of the laser pulse is sufficiently high, then, for a given absorption coefficient, the minimum damage thickness is independent of the beam intensity. This means that delivering excess energy simply advances the ablation front into the tissue, pushing a fixed-thickness coagulation zone ahead of it, which can be argued intuitively. However, at a constant irradiance, the minimum damage thickness decreases linearly with increasing tissue absorption coefficient. Thus, strongly absorbed laser wavelengths are preferable if thermal damage is to be minimised. Applying McKenzie's model to the laser parameters used by Sinofsky, this model predicted a minimum damage depth of 654μm at 2.1μm, approximately 30% greater than that predicted by Sinofsky's model and, given the approximate approach of both models, providing a reasonable degree of agreement.

Aretz et al[181] presented the preliminary results of a study of the effect of 2.1μm laser light on normal and calcified arterial tissue, including measurements of the depth of thermal damage produced for pulsed excitation. Using spotsizes similar to those reported by Lane et al[19], reproducible damage was found to extend to a depth of approximately 200μm, in keeping with the earlier experimental results of Lane. However, considering the arguments of thermal relaxation, smaller damage depths might have been expected. The reason for this may lie in the fact that, for some of the experiments, the flow of blood near to the exposure site was suspended. This

would have reduced the cooling effect that blood is believed to have[170]. In addition to the main work, the authors also consider the effect a fluid field has in reducing the ablation efficiency of 2.1μm light, concluding that the holmium laser is effective in removing atherosclerotic deposits in a fluid environment with up to 2mm between the fibre tip and the tissue. Typical threshold fluences for ablation were 6 J mm^{-2} in air and up to 3 times this in saline.

Motamedi et al also found that 2.1μm laser pulses were capable of ablating a variety of atherosclerotic plaques, including mildly calcified deposits, making the CTH laser a candidate for angioplasty procedures[182]. Unlike the 1.06μm and 1.32μm emissions from the Nd:YAG laser, Motamedi found that the ablation efficiency of the holmium laser varied linearly with the incident fluence with only small rims of coagulation around the exposure site. In contrast, the Nd:YAG laser pulses produced increased coagulation damage around the ablation craters due to strong scattering of the light in the tissue, and showed a sublinear relationship between the ablation efficiency and pulse fluence. However, the relatively strong absorption of the 2.1μm light gave rise to tissue tearing, a phenomenon commonly associated with the strongly absorbed 2.94μm erbium laser[183].

A linear relationship between ablation efficiency, calculated from the mass loss technique described by Walsh et al[45], and the pulse fluence (energy density per pulse) was also reported by Nishioka et al[184]. When energy was delivered via a 600μm fibre in gentle contact with liver a mass loss rate of 0.16 μg J^{-1} cm^{-2} was measured. Linear regression of the data revealed a threshold for the ablation process of 50 J cm^{-2} $pulse^{-1}$ below which no mass loss was observed. This is much smaller than the value measured by Aretz et al[181] who observed thresholds for mass loss of about 600 J cm^{-2}, although the tissue type in the latter was atheromatous aortic tissue which may account for the increase in threshold. Additionally, Aretz et al performed their experiments under a variety of conditions, including under saline, and do not state clearly the conditions for which they obtained their quoted ablation figures.

In a separate publication, Nishioka[155] makes one of the few available comparisons between the ablative efficiency of CTH and CT:YAG lasers. Using the mass loss technique and *in vitro* liver tissue, the mass loss efficiency was found to be 110 μg J^{-1} and 113 μg J^{-1} for the CTH and CT:YAG lasers, respectively, and was, additionally, constant over the range of pulse fluences from the threshold up to 260 J cm^{-2}. The threshold for mass loss was evaluated by linear regression of the data and found to be 36 J cm^{-2} and 29 J cm^{-2}, respectively. However, due to the spread of data, the difference between the two laser wavelengths was not statistically significant

leading the authors to conclude that the ablation efficiency of both lasers was approximately equal. However, the mean depth of thermal damage obtained with each laser was significantly different at $450\pm45\mu m$ for the CTH:YAG laser and $374\pm19\mu m$ for the CT:YAG laser indicating that lower thermal damage can be obtained from the CT:YAG laser at $2.01\mu m$. The depths of thermal damage measured for the $2.1\mu m$ laser light are larger than those reported by Lane[19] or Aretz et al[181] and are much more in keeping with the depths predicted by the models of Sinofsky[168] and McKenzie[41]. The authors of reference [155] comment that the theoretical models predict a linear increase in the depth of thermal damage with penetration depth and use the penetration depths in water as their guide. However, applying the models to the $2.01\mu m$ emission of the CT:YAG laser, a reduction by a factor three in the thermal damage compared to that obtained for the CTH:YAG laser would be expected by virtue of the reduction in the relative penetration of $2.01\mu m$ light by the same amount. The experimental results clearly do not show this, suggesting that any similarity between predicted and measured thermal damage depth is fortuitous.

Nishioka has also reported on measurements of the time-resolved reflectance of holmium laser light from tissue[166]. Having previously shown that uncoagulated tissue reflects approximately 40% of 633nm radiation when incident at 0°[165] Nishioka measured the relative changes in the amount of $2.1\mu m$ light rejected from tissue as it became coagulated. Collecting the specularly reflected and scattered light from the tissue surface using a parabolic reflector he found that the reflectance rose with a characteristic delay which varied according to the incident pulse energy. The integrated reflectance of the tissue was also shown to vary with radiant exposure, achieving a maximum of about 18% after one pulse thereafter increasing more slowly to a final maximum of about 35%. The threshold fluence for these changes, either for single or multiple pulses, was 25 J cm^{-2}

Several researchers have attempted to evaluate the CTH laser for specific applications. Besides the assessment of $2.1\mu m$ light for angioplasty procedures[181,182], Treat et al[185] have investigated its possibilities in endoscopic surgical techniques using a system capable of delivering up to 1 J $pulse^{-1}$ at 3Hz via a $200\mu m$ diameter optical fibre. Treat supports previous reports that the ablation rate is linear with energy dose the total energy delivered per unit area, giving a figure of 25 μm $pulse^{-1}$ advancement rate when the pulse fluence is 130 J cm^{-2} and a tissue removal rate of 0.08 mm^3 J^{-1} (88 μg J^{-1} if the density of liver is assumed to be 1.1 g cm^{-3} [155]). The data presented is frequently unclear. However, one useful observation made is that the CTH laser light is capable of producing haemostasis in arteries up to 1mm

diameter by using several pulses of 700mJ, indicating that the holmium laser may offer good coagulative properties as well as good ablative properties, depending on its mode of use.

The suitability of the pulsed CTH laser was considered against competing technologies for gall stone fragmentation by Johnson et al[186]. Comparing the ultrasonic lithotripter (UL) and the electrohydraulic lithotripter (EHL) against the laser on a variety of stones, each device was found to have limitations in its ease of use. Although both the UL and EHL produced rapid results, the UL required that the stones were held in place against the probe. In contrast, the EHL fragmented all stones without making contact, although heavily calcified stones still required holding in place. The laser method effectively fragmented all stones but required a large number of shots prolonging the procedure beyond the time taken for either EHL or UL procedures.

The authors go on in the same publication to consider some of the practical aspects of using the different apparatuses, as well as the damage caused due to poor alignment between the source and the target. Overall, the authors found that, considering efficacy and safety, the UL was the most appropriate technique with the laser method least favourable. The authors conclude that the only advantages offered by the laser are the low risk of causing secondary damage to adjacent tissue and the ease of accessing stones hidden behind solid structures, such as the pelvis.

From published data, it is possible to conclude that the strong absorption properties of the 2.1μm beam result in an ablation efficiency which varies linearly with the incident fluence and produce thermal necrosis damage of typically 200-500μm, in general agreement with the limits predicted by independent theories[168,41]. The absorption behaviour of the 2.1μm light in tissue is comparable to that of the CO_2 laser beam and the emission at 2.01 μm from the CT:YAG laser, despite differences in the water absorption coefficients by factors of ten and three, respectively. In comparison to the CO_2 laser, the CT and CTH:YAG lasers have the added benefit of being solid state devices and, most importantly for endoscopic surgery, the availability of convenient fibre optic beam delivery.

4.1.5 Erbium laser ablation of tissue

The first room temperature operation of a 2.94μm Er:YAG laser was reported by Zharikov et al in 1975[48] and, despite continued work by the same workers[49] which advanced the understanding of the laser properties of erbium doped crystals, it was

not until the mid-1980s that western researchers began to consider the potential of the 2.94μm emission in laser medicine.

The emergence of the erbium laser in western medicine can largely be attributed to Esterowitz and co-workers at the American Naval Research Laboratories who, in 1985 and 1986, published a collection of papers in which preliminary investigation of the interaction between tissue and laser light at 2.94μm was reported[9,18,39,43]. Esterowitz drew attention to the fact that water, which typically makes up between 60% and 80% of tissue, has an absorption peak at around 2.9μm. Inspection of the absorption spectrum of water, Figure 1.1, suggests a very short penetration depth of this wavelength in tissue and consequently only small thermal damage zones[171]. However, the same potentially useful water absorption characteristic also meant that fibre optic transmission could only be achieved in zirconium fluoride glass fibres which are not usually suitable for medical use because of their poor mechanical properties. In their first publication in this specific area, it was revealed that pulses of only 120mJ, delivered via such fibres to *in vitro* tissue and at repetition rates up to 10Hz, produced well defined lesions in which no thermal damage was recorded. This phenomenon had only been previously observed for tissue ablation with the UV laser light from excimer lasers[43]. The reason for the effect at 2.94μm was attributed to the high absorption coefficient of water, measured by Esterowitz and Hoffman[39] as $16000 \pm 3000 cm^{-1}$ and the spiky temporal pulse shape produced by their laser which consisted of a train of 0.5μs duration pulses separated by 5-6μs, probably allowing for ample cooling between successive pulses.

These early observations by Esterowitz and co-workers prompted the first comparison of the lesions created by the erbium laser to those previously only seen with excimer lasers[43]. The results of that work were presented in a largely anecdotal form but demonstrated that precise ablation could be achieved with a minimal amount of thermal damage, comparable to the photoablative effect obtained using excimer lasers. Combining this with the prospect of convenient fibre optic beam delivery lead the authors to describe the erbium laser as the 'ideal medical scalpel'.

The theoretical background to the erbium laser's ability to produce well defined incisions in tissue was considered by Sinofsky[168] who numerically modelled the interaction of 2.94μm, 2.1μm (CTH:YAG) and 10.6μm (TEA CO_2) light with tissue to produce a map of the heat distribution in tissue (where heat loss by diffusion was neglected). The results of the model show that, for his laser parameters, a 1mm diameter spot ablated by 2.94μm light will exhibit radial and thermal damage zones of only 12μm. This should be compared to predicted radial

damage for the CO_2 and holmium laser light of 200μm and 500μm, respectively.

In reference [141] McKenzie compared the axial damage depth predicted by his model (no radial damage figures are produced in his model as it considers only the one dimensional case, ie a high absorption coefficient) to that published previously by Sinofsky[168] for similar laser beam parameters. The results were surprisingly similar for the erbium beam. In general, though, for such pulses, the histological evidence published elsewhere shows that this is the minimum achievable rather than the typical result. However, considering the very approximate approach of both models, the similarity to measured values is good.

In the late 1980s, Walsh et al[45,187] had begun to investigate the parameters affecting the ablation performance of the CO_2 laser, developing simple methods to measure the ablation properties of the strongly absorbed laser radiation. Thus, it was inevitable that the same techniques should be applied to other strongly absorbed wavelengths such as the 2.94μm erbium emission. It is Walsh and co-workers who have made the greatest contributions in this area so far.

In a pair of papers which appeared simultaneously in 'Lasers in Surgery and Medicine', Walsh et al[46,188] measured the ablation rates and efficiencies via the 'time-to-drill' technique for skin and aortic tissue as well as for bone using Fixed-Q and Q-Switched pulses. A fixed spotsize of 1mm was used at a variety of pulse energies with the etch rate calculated from the number of pulses required to drill through a known thickness of tissue. The results show an approximately linear relationship between the etch depth and the fluence per pulse in all cases, although the absolute etch depths vary considerably with tissue type. During their experiments, the authors noted that, despite a circularly symmetric laser spot, the holes generated in aortic tissue were ellipsoidal in shape. Additionally, the major axis ran consistently around the circumference of the tubular vessel, a feature which they attributed to the elastic nature of the tissue fibres. When the pulses were used to ablate bone, plasmas were observed above fluences of 18 J cm^{-2}. These were produced during each pulse and effectively blocked remaining light in the pulse, thereby reducing the overall ablation efficiency. At low fluences (<14 J cm^{-2}) the surface of the bone was seen to char after about 50 pulses, and after a total of 200 pulses ablation had ceased completely, a feature attributed to dessication of the tissue. In a comparison of the ablation efficiency of *in vitro* skin, aorta and bone, the aortic samples were found to have the lowest ablation threshold, although calculation of the threshold fluence was prevented by an irregular shaped crater. Skin and bone showed thresholds of 0.6-1.5 J cm^{-2} and 2.1-3.4 J cm^{-2} respectively. The maximum ablation

efficiencies were calculated to be 540 $\mu g\ J^{-1}$ for skin and 300 $\mu g\ J^{-1}$ for bone. From the paper by the same authors[45] in which the super-pulsed CO_2 laser ablation of skin tissue is investigated the mass loss efficiency is reported to be $235 \pm 10\ \mu g\ J^{-1}$ with a threshold fluence for ablation of $1.09 \pm 0.02\ J\ cm^{-2}$, implying that superior ablation can be obtained from the erbium laser. In general, for skin, bone, aorta and corneal tissue, Fixed-Q pulses (250μs FWHM) left a residual thermal damage of 10μm to 50μm while Q-switched (90ns FWHM) pulses produced only 5μm to 10μm of residual thermal damage[188]. In some cases, tissue damaged by the Q-Switched laser pulse showed thermal damage of only 1-2μm although this could not be achieved consistently. For Fixed-Q pulses at fluences above 80 $J\ cm^{-2}$, tearing was observed in the soft tissue samples, and, at the same time, an increase in the extent of the damage zone up to 75μm was observed. When the absorption depth in tissue, predicted from the water absorption curves, was compared to the calculated etch depth per pulse it was concluded that tissue removal by thermal vaporisation could not account for the observations. The authors conclude that tissue ablation using the erbium:YAG laser proceeds by a combination of both vaporisation and tissue disruption by rapidly expanding gases, explaining the tissue tearing.

Cummings investigated the magnitude and effect of the mechanical disruption on tissue during pulsed Er:YSGG laser ablation in his Masters Thesis[183]. Using a pendulum to detect the impulse imparted to the tissue as a result of material explosively ejected from the tissue, he reported a linear increase in the induced back pressure with pulse fluence, with a threshold for the impulse of around 10 $J\ cm^{-2}$. Although, at low fluence levels, the mass loss reported in [46] appeared to vary as a parabolic function with fluence, the variation soon took on a linear form, and had the same threshold obtained by extrapolation as that derived from Cumming's data for the start of measurable backpressure impulses. Thus, it would appear that mass loss induced by pulses of light from erbium lasers is always a combination of mechanical and thermal effects and that the threshold for this in liver is approximately 10 $J\ cm^{-2}$. Cummings additionally observed some differences according to the type of tissue considered. He argued that for tissues with weakly bound connective strands (e.g. liver) the expanding gases easily tore into the surrounding tissue whereas for tissue where the connective media was strongly bonded (e.g. aorta, skin) tissue tearing could be absent. Cummings also noted that the size of the crater was not always the same as that of the incident beam and concluded that rapid expansion of the tissue, or the tissue constituents, during the pulse was responsible. Recently, Kwark et al[189] have reported changes to the crater shape, assessed post-exposure as the change in the aspect ratio of the crater, for changes in the pulse fluence. This may be an indication that the elastic deformation reported by Cummings may influence the shape

of the crater, rather than simply its size, although this has not been proven in the literature.

Recently, Hibst[190] has reported on his measurements of recoil momentum during the ablation of bone. Using the same pendulum technique as Cummings[183], the change in recoil momemtum with pulse energy was shown to be linear for a fixed spotsize. The threshold for the effect was found by extrapolation to be 37.3 J cm^{-2}. This was four times greater than that reported by Cummings for liver and supports Cummings argument that lower thresholds for tissue tearing (associating tearing with recoil) occur in tissues where the connective tissue is not strongly bound. Hibst also measured the mass loss from the tissue by a differential weighing method (before and after) observing a linear relationship between mass loss and pulse fluence. The threshold for this effect was calculated as 7.7 J cm^{-2}, slightly higher than that reported by Walsh et al[46]. Also, although the maximum ablation efficiency calculated by Hibst was 320 $\mu g\ J^{-1}$, approximately the same as that reported previously by Walsh et al[46], the range of pulse fluences over which the rate of mass loss was linear with fluence extended as high as 550 J cm^{-2}. This compares to the maximum fluence used by Walsh et al of 25 J cm^{-2}, beyond which Walsh et al observed plasmas which limited further mass loss. The formation of plasmas at high fluences is not reported by Hibst.

Using the mass loss data, Hibst also calculated the heat of ablation to be 4.2 kJ cm^{-3}. This is in agreement with the value of 4.3 kJ cm^{-3} reported by Nuss et al[191] but notably different from the results of Charlton et al[192] who reported a value for the latent heat of ablation of 8.2 ± 1.0 kJ cm^{-3}. Although not discussed by Hibst, the reason for this difference is probably a combination of the different experimental approaches and the uncertainty involved in the estimation of the density of bone. However, in a separate publication, Dickinson et al[154], from the same research group as Charlton, use the same technique as that used by Charlton to determine the latent heat of ablation of a number of tissue types, including bone. The results presented there show a slight reduction in the latent heat for bone to 6 kJ cm^{-3} as well as the range of latent heats calculated for a variety of other tissues, including liver and aorta, which range between about 2.0 kJ cm^{-2} and about 7 kJ cm^{-2}.

Kaufmann and Hibst[44] used measurements of the ablation crater depths to compare 250μs (FWHM) 2.94μm pulses to 20ns (FWHM) 308nm excimer laser pulses incident on human tissue *in vitro* and *in vivo*. While their publication concentrated more on the excimer laser due to the flexibility of its operation, their results showed small damage depths of the order of 50μm compared to damage

depths up to about 300μm for the excimer laser, in keeping with the anecdotal observations of Esterowitz[43]. Interestingly, by increasing the repetition rate of the excimer laser above 5Hz, a significant increase in the zone of thermal damage was produced. This is contrary to the theory of photoablation and indicates the presence of thermal effects. This was not observed for the erbium laser measurements due to the 1 Hz repetition rate limit on their laser. However, the authors acknowledge a similar effect may occur with the erbium laser.

The effect of repetition rate was investigated by Walsh and Cummings[47] using the Er:YSGG laser which may be operated at higher repetition rates than Er:YAG systems. Although the output wavelength is reduced to 2.79μm as a result of the change in the host crystal, the results show that repetition rate does not have a significant effect on the cutting depth (per J cm^{-2}) in bone, although a slight reduction in the thresholds for the onset of cutting was observed in soft tissues at higher pulse frequencies. An exception to these observations was the cutting performance at 2Hz which was slightly improved. The authors attribute this effect to the improved beam profile obtained from the laser at 2Hz which was more Gaussian in shape, compared to the 'top-hat' intensity profile which was produced at higher repetition rates. However, the authors also found that from 2Hz to 30Hz, at a constant fluence of 16 J cm^{-2}, the damage zones in soft tissue (rat dermis) increased from 100μm to 300μm, respectively. This is in agreement with the predictions for increases in thermal damage with repetition rate inferred by the results of Kaufmann et al[44] and supports the argument that, even with a thermal relaxation time estimated to be of the order of 1μs from equation (18), there is some residual thermal energy in the tissue from the previous pulse as the next pulse arrives. It was also reported that the depth of damage observed in soft tissue increased with increasing pulse fluence, in agreement with Walsh et al[188].

Frenz et al[193] cite the build up of pressure as the indirect cause of increased thermal damage at higher intensities with the Er:YAG laser. Using gelatin phantoms of differing water content, the dependence of viscosity was investigated for both the 2.94μm light as well as the 10.6μm CO_2 laser beam. Frenz found that as each pulse vaporises material it also liquefies a significant portion and, due to local pressure gradients, both the vaporisation particles and the liquefied material is forced upwards and out of the crater. Furthermore, in subsequent work by the same group, Zweig et al[194] reported that, where the incident energy in each relaxation oscillation of the laser pulse is sufficient to liquefy the tissue, a series of pressure induced cavities are formed which coincide with each of the pulses. As the liquefied and ablated material is forced outwards, some of the ablative components are deposited in these cavities.

Liquefied tissue is trapped in these cavities and proceeds to cool by conduction to the adjacent tissue thereby creating increased thermal damage along the crater walls. Relaxation of the tissue at the end of the laser pulse leaves a smooth sided crater covered with ablated tissue particles and increased thermal damage radially. This is in keeping with the photographic evidence of Kaufmann and Hibst[44] obtained via electron microscopy, for 2.94μm ablation of skin.

Zweig's analysis suggests that, although the threshold for the creation of the liquid layer must be a constant temperature, the temperature of the flowing liquid will vary according to the penetration depth of the wavelength used. For strongly absorbed wavelengths, the fluid temperature is lowered and the drilling velocity is increased, while thermal damage is reduced. As the viscosity of the material was increased (in the gelatin sample case, by cooling it) the effect of liquid flow became less significant and the process of material removal became almost entirely due to evaporation in keeping with some of the earlier results with real tissue published by Walsh et al[46] where thermal damage decreased with increasing tissue stiffness.

Besides the many publications which consider the physics of the interaction between laser light at 2.94μm and tissue, few workers have evaluated the Er:YAG laser for specific clinical applications. The reason for this is probably largely due to the lack of suitable fibres for endoscopic beam delivery, although it is also true that reliable Er:YAG lasers have appeared only recently. Recently, Kwark et al[189] have reported on their experiments with erbium laser light delivered via a fluoride fibre for angioplasty. Although their work reveals more interesting features about the interaction between 2.94μm light and tissue, the fibre tip melted at typical output energies of 200 mJ pulse^{-1} thus indicating its unsuitability for use in angioplasty procedures.

In the past few years, there has been much commercial interest in the potential of excimer lasers for reshaping the surface of corneas in order to correct for refractive disorders of the eye[3]. The similarity between lesions generated by excimer lasers and erbium lasers has been reported by several authors[43,44]. Laser ablation of the corneal surface has been reported on in a number of studies[183,188] using the erbium laser but, to date, only the ArF excimer laser is used clinically for this process. Peyman et al[197] have reported briefly on the effect of Fixed-Q and Q-Switched Er:YAG laser pulses on different ocular tissues. They found that the maximum extent of tissue damage adjacent to ablation sites was only 10μm to 15μm, in agreement with [188], concluding that, despite a thermal ablation process, the microscopic effects are comparable to those obtained using the UV emission from

excimer lasers as well as the long wavelength emission (2.7-3.0μm) of the HF laser. It can be expected that, as the efficiency of erbium laser systems improves, there will be an increase in the interest in erbium lasers in this field of medicine. It is worth noting that refractive errors in the eye have been corrected by selectively coagulating and hence shrinking the cornea using the holmium:YAG laser[195]

4.2 Mass Loss Measurements

4.2.1 Materials and methods

Mass loss over a range of operating parameters was measured using the technique originally devised by Walsh et al[45]. Liver tissue was obtained from the butcher where it had been kept refrigerated at between 0°C and 2°C. Prior to use it was allowed to warm up to room temperature, typically between 19°C and 26°C. Because the ablation of tissue by 2.94μm light is dominated by the interaction between the tissue water content and the laser light, rather than the tissue pigments, no attention was paid to the colour of the tissue, nor from which animal it originated. Consequently, the liver types used in experiments with radiation from the erbium laser were either ox, lamb or pig. In contrast, the interaction between laser light at 2.1μm and tissue is possibly dependent on tissue pigments and structure. Consequently, only ox liver was used for experiments involving the holmium laser. It was observed that there was some variation in the texture of tissue from any one type of animal and that, additionally, the colouring was not consistent. However, these are not necessarily indications of changes in the percentage of water contained in the tissue and no attempt was made to control the choice of tissue on the basis of texture or colouring.

Full details of the experimental apparatus and technique used in this study are described in Appendix 6. The tissue was placed on a glass slide and weighed at regular intervals before, during and after various laser exposures. The tissue sample was placed on the pan of the balance (Mettler AC100) with the laser beam directed vertically down through a port in the protective surround of the balance. A CaF_2 lens was used to bring the beam to a waist approximately at the surface. From the resulting plots of mass loss before, during and after laser exposure, it was possible to assess the mass loss during the laser exposure, and to subtract the mass loss during that period due to natural evaporation. Thus, the mass loss due solely to the laser radiation could be calculated.

Changes to the pulse energy were made, in the case of the CTH:YAG laser,

by a combination of glass microscope slides, which absorbed 2.1μm, and small changes to the lamp discharge energy. Using these techniques, it was possible to maintain relatively constant spotsizes over the range of output pulse energies for the 2.1μm beam, as shown, for example, in Figure 4.1. Changes to the energy contained in the pulses from the erbium:YAG laser were made by inserting glass slides of varying thicknesses. This technique has the advantage of reducing the energy uniformly across the beam profile without affecting the profile and has been used by others in similar circumstances[46,190]. Both lasers were operated at a constant repetition rate of 5Hz.

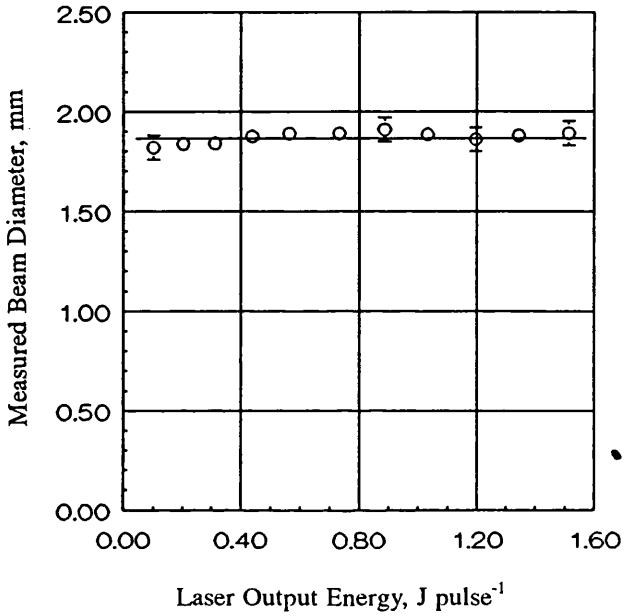

Figure 4.1 Variation in measured laser spotsize at the tissue surface with pulse energy at 2.1μm.

The amount of tissue removed with increasing dose was measured for the 2.1μm and 2.94μm laser pulses. Here dose is defined as the total amount of energy delivered per unit area of tissue due to all of the laser pulses in the exposure and is different from the pulse fluence which is defined as the energy delivered per unit of tissue area in a single pulse. The spotsize was kept constant in each case although the pulse energy was varied between experiments by the methods described earlier. The spotsizes were measured at each of the power settings using the method described in Appendix 3. The mean spotsize used in the 2.1μm measurements was 1.9$\pm$0.05mm at the tissue surface. The mean spotsize of the 2.94μm pulses was 2.9$\pm$0.05mm. The experimental error in the measurement of spotsize was $\pm$0.2mm. Pulse energies were varied in the case of the 2.1μm laser between 0.202 J pulse^{-1} and 1.514 J pulse^{-1} and for the 2.94μm laser between 0.233 J pulse^{-1} and 1.120 J pulse^{-1}. The energies were

slightly lower than those reported in the laser development chapters due to a combination of laser coating damage, which progressively reduced the output from each laser, and losses in the optics used to deliver the laser light to the specimen. The operating parameters, as well as the doses, are summarised in Table 4.1

Wavelength μm	Spot Diam. mm	Pulse Energy J	Pulse Fluence J mm^{-2}	Maximum Dose J mm^{-2}
2.1	1.9	0.202	0.072	114
"	"	0.439	0.159	127
"	"	0.732	0.261	130
"	"	0.887	0.316	111
"	"	1.197	0.441	132
"	"	1.514	0.539	121
2.94	2.9	0.233	0.035	32
"	"	0.364	0.055	25
"	"	0.437	0.065	39
"	"	0.714	0.106	31
"	"	1.120	0.167	25

Table 4.1 Summary of experimental parameters used to assess the change in mass loss with increasing dose.

Spotsizes were measured retrospectively but were found to lie in the relatively broad range in which the effect of spotsize is insignificant, as is described in Section 4.3.3. The macroscopic effect of increasing dose was also monitored and recorded in a series of photographs. In the visual 'measurements', the spotsize of the 2.1μm beam was 5.1mm while for the 2.94μm light it was 6.8mm.

The effect of pulse fluence was then assessed at both wavelengths by exposing the tissue to a fixed dose of laser light. The spotsizes were kept constant while the pulse energy was varied using the techniques described earlier. The experiments were repeated for three different spotsizes for each laser wavelength in order to determine the magnitude of any spotsize-dependent effects. The dose was determined by measuring the laser power with a calibrated calorimeter (Model 20, Laser Instrumentation Ltd., Chertsey, England) and by timing the duration of the exposure.

The spotsizes were measured initially with burnpaper and later using the method described in Appendix 3. Consequently, the dose varied from experiment to experiment, but not within any one set of experiments at a fixed spotsize. The total

dose was dictated, in part, by the available operating parameters and also by the results of the measurements of the effect of dose. These suggested that the rate of material removal for the 2.1μm pulses was independent of dose where all other parameters were constant. Thus, it was acceptable to use high doses for measurements at 2.1μm. However, the results for the 2.94μm pulses suggest that there was some reduction in the efficiency of material removal with increasing dose. Therefore, a lower total dose was selected for the measurements made at this wavelength. Table 4.2 summarises the experimental parameters used in this set of measurements.

Wavelength μm	Spot Diam. mm	Pulse Energy Range, J	Pulse Fluence Range, J mm^{-2}	Maximum Dose J mm^{-2}
2.1	1.30±0.05	0.105-1.185	0.100-0.828	41.6±5.7
"	2.80±0.05	0.112-1.573	0.018-0.261	25.1±4.8
"	4.3±0.2	0.329-1.540	0.024-0.097	24.6±1.9
2.94	2.00±0.05	0.044-1.024	0.015-0.338	16.4±0.04
"	2.90±0.05	0.076-1.040	0.011-0.155	16.9±0.02
"	5.4±0.2	0.211-1.067	0.009-0.048	12.8±0.01

Table 4.2 Summary of experimental parameters used to assess the effect of pulse fluence on mass loss for constant doses.

Photographs were again taken of the lesions created under the different operating conditions in order to allow gross observations to be recorded.

Finally, the effect of tissue thermal history was investigated by measuring the mass loss achieved at a given set of operating conditions, for 'fresh' tissue compared to coagulated tissue. Coagulation was achieved in the samples by delivering Nd:YAG laser light at 1.06μm to the tissue via an optical fibre. The output beam from the fibre was not focused and the distance between the tissue and the tip of the fibre was adjusted to achieve full thickness coagulation of the tissue samples without causing charring. Coagulation was considered to have occurred when the tissue colour changed from red to yellow and was visible on the unexposed side of the sample. Coagulation was additionally verified by slicing samples in half and visually confirming the condition. Texture also provided a good indication as to the state of coagulation, the tissue being more resilient when coagulated. The comparison between fresh and coagulated tissue was made at a fixed set of laser parameters and at only one laser spotsize, although different spotsizes were used for each laser

wavelength. Similarly, the delivered dose was kept constant for each sample, changing only with wavelength. Table 4.3 summarises the experimental parameters used in these trials.

Wavelength μm	Spot Diam. mm	Pulse Energy J	Pulse Fluence J mm^{-2}	Dose J mm^{-2}
2.1	1.70±0.05	1.202	0.523	39.3±1.05
2.94	2.90±0.05	0.631	0.094	16.4±0.04

Table 4.3 Experimental parameters used for comparison of the mass loss of fresh and laser-coagulated liver tissue.

Spotsizes were again measured retrospectively. However, initial assessment using burnpaper indicated that the selected spotsizes lay in the range in which the effect of spotsize was not important. Pulse fluences were selected, and, in the case of the 2.1μm light, chosen to maximise the ablation efficiency. In contrast, the pulse fluence for the 2.94μm light was selected to be in a region where the shape of the ablation crater would reflect the intensity profile of the laser beam. Higher fluences might be expected to yield results different to those obtained, due to the contribution mechanical effects make to the ablation efficiency and the changes in tissue stiffness following coagulation. During the experiments some measurements were carried out several times to assess repeatability.

To assist in the assessment of the lesions created during the laser exposures, a set of tissue samples were sent for histological preparation (Haematoxylin and Eosin). Although H&E staining is a commonly used histological technique, it is limited in the case of *in vitro* tissue experiments to providing no more than a cross-section of the lesion. Table 4.4 summarises the laser operating parameters used to obtain samples for histological assessment.

These laser spotsizes were chosen to provide a range of lesions which represented practical operating conditions while still providing lesions which could be assessed both macroscopically and histologically. Pulse fluences were selected to provide a range which included maximum and minimum ablation efficiency as well as conditions between the two. The dose was chosen so lesions could be produced in timescales where dehydration was not excessive during the exposure.

Wavelength μm	Spot Diam. mm	Pulse Energy Range, J	Pulse Fluence Range, J mm^{-2}	Dose J mm^{-2}
2.1	2.90±0.05	0.3,0.7,1.2	0.045,0.106,0.182	17.1±0.1
2.94	2.90±0.05	0.163,0.247, 0.391,1.020	0.024,0.037, 0.058,0.152	16.9±0.04

Table 4.4 Summary of experimental parameters used to generate laser lesions for histological examination.

4.3 Results and Preliminary Discussion

4.3.1 Effect of dose

4.3.1.1 At 2.1μm

The tissue mass removed by pulses of 2.1μm light for increasing doses is shown, for various pulse fluences, in Figure 4.2. The results show that for each pulse fluence the mass loss was linear with the dose. However, lower pulse fluences were less able to remove material. There is, therefore, a noticeable difference between the mass removed at higher doses when low pulse fluences are compared to higher fluences.

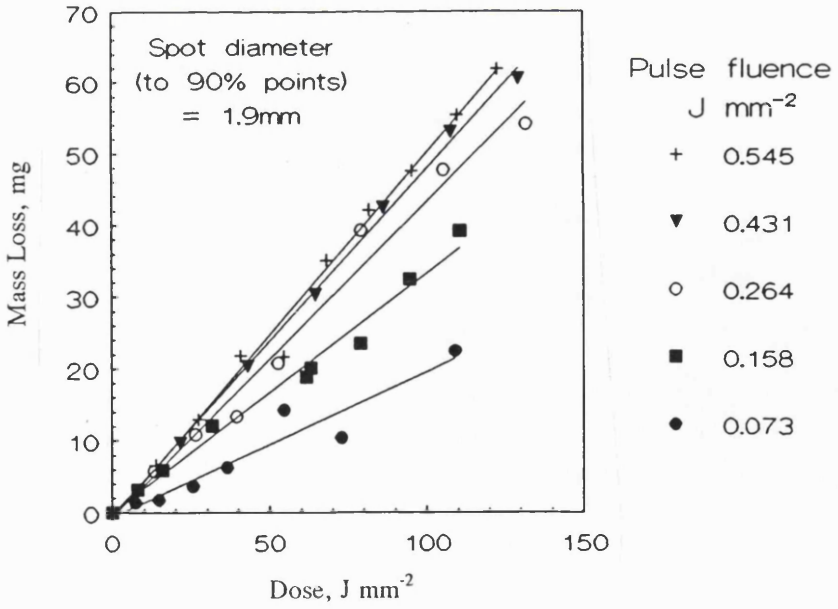

Figure 4.2 Effect of dose at 2.1μm on tissue mass loss for different pulse fluences, the spotsize remaining constant at 1.9mm.

At low pulse fluences, in the range 0.035-0.058 J mm^{-2}, the tissue was observed to undergo a series of changes which appeared to be dependent on the total dose. Figures 4.3 (a-e) are photographs taken of tissue exposed to pulse fluences at either end of this range. The full exposure details are given in the figures and reveal that coagulation of a disc, approximately the same size as the laser spotsize and which penetrates approximately 1-1.2mm axially into the tissue, was visible after delivering less than 1 J mm^{-2} to the tissue surface.

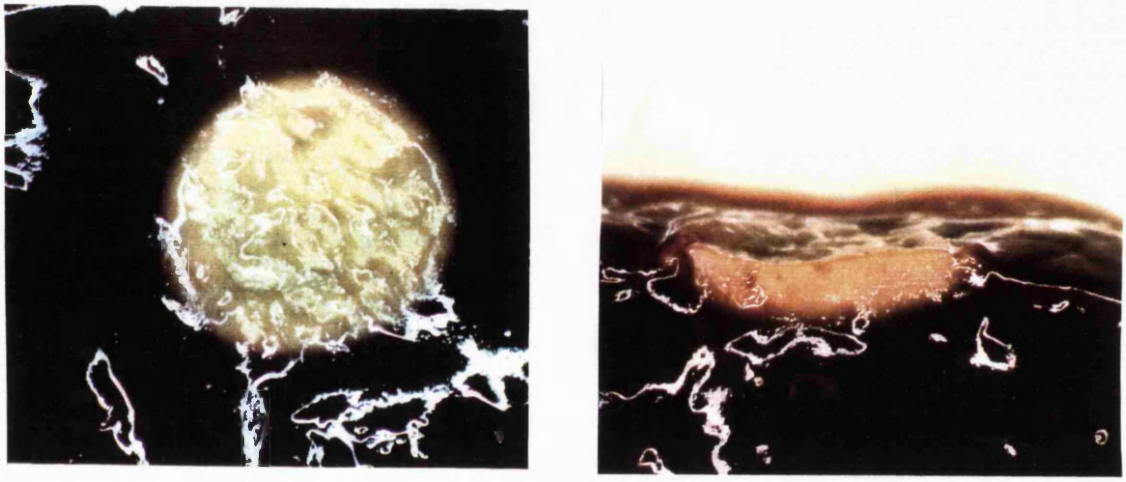

a) Dose = 0.88 J mm^{-2}

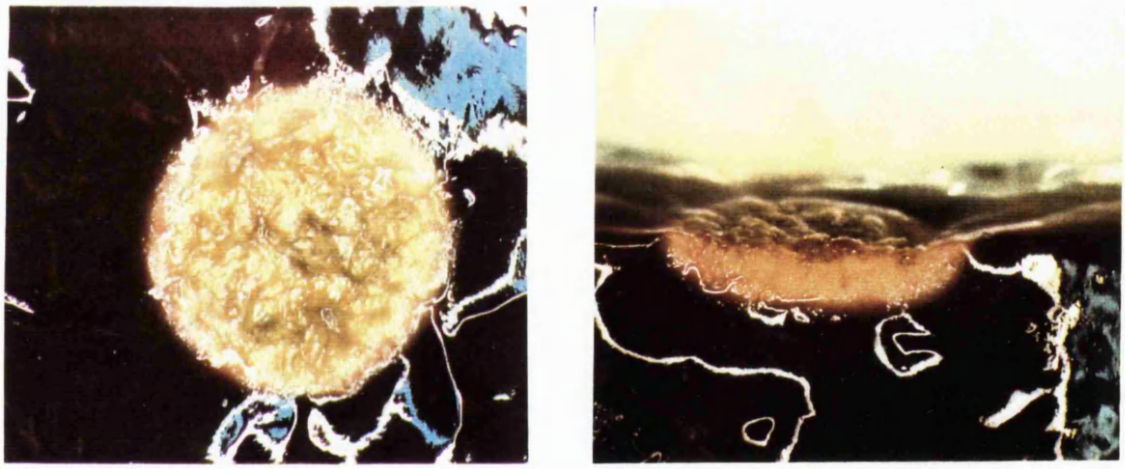

b) Dose = 1.44 J mm^{-2}

Figure 4.3 Plan and cross-sectional views of tissue irradiated by 2.1μm laser pulses at different doses, the pulse fluence and spotsize remaining constant at 0.058 J mm^{-2} and 5.1mm, respectively. (Continued overleaf).

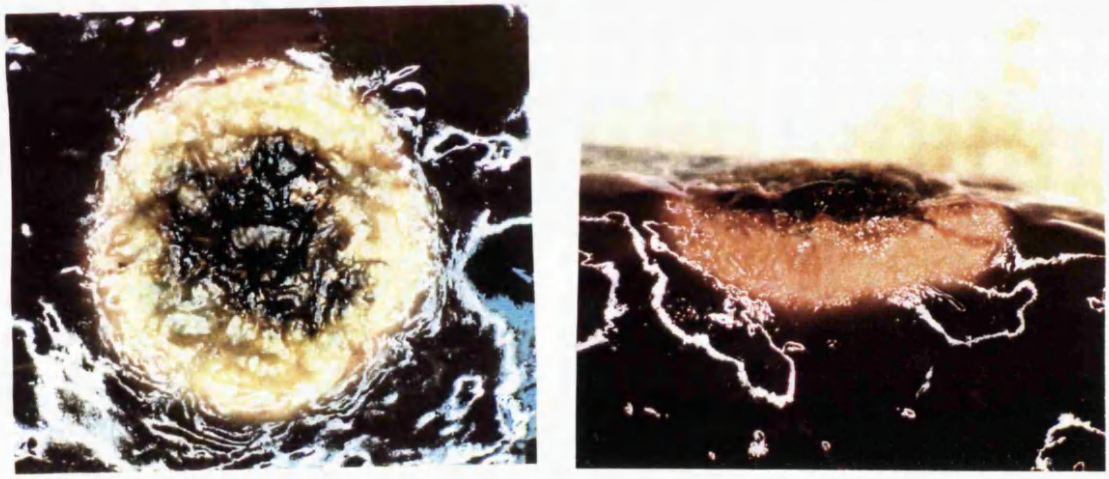

c) Dose = 2.89 J mm^{-2}

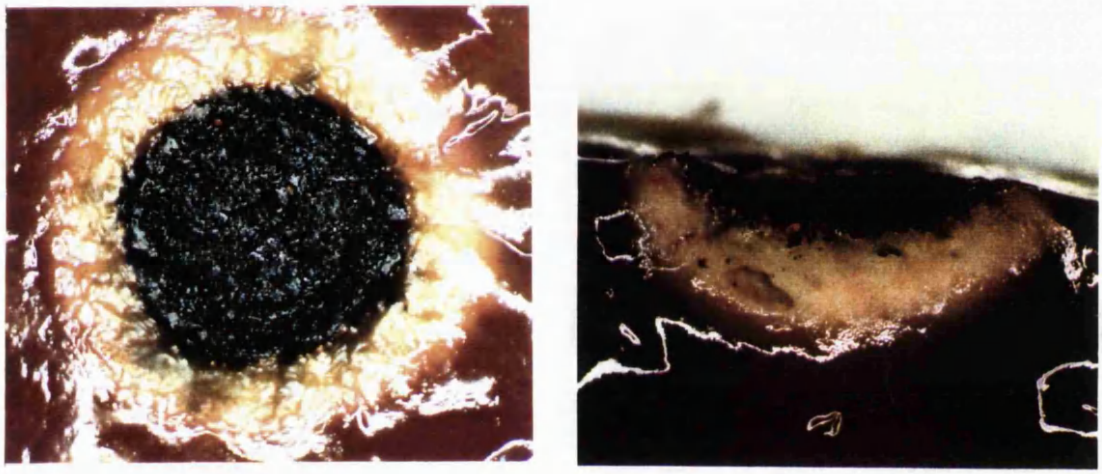

d) Dose = 8.66 J mm^{-2}

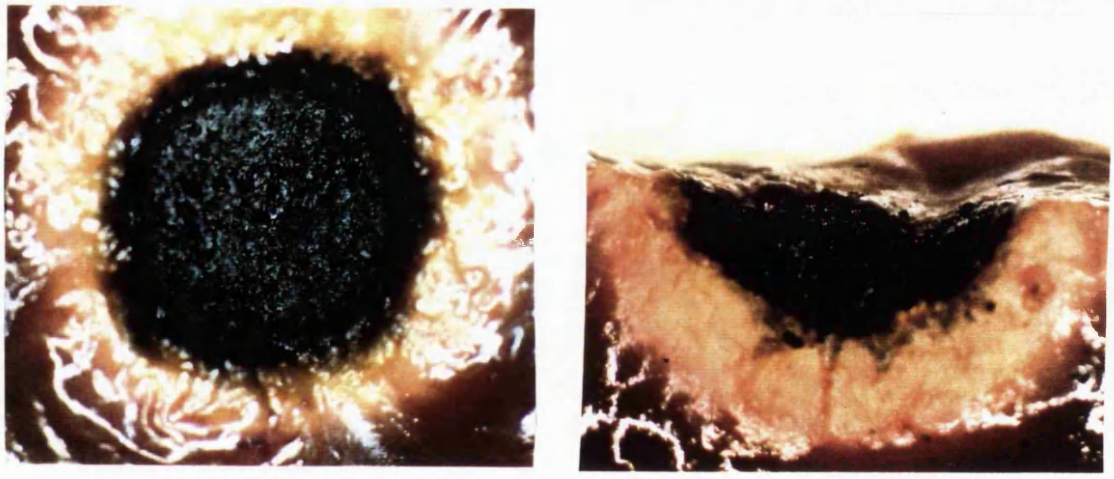

e) Dose = 17.3 J mm^{-2}

Figure 4.3 Plan and cross-sectional views of tissue irradiated by 2.1μm laser pulses at different doses, the pulse fluence and spotsize remaining constant at 0.058 J mm^{-2} and 5.1mm, respectively. (Continued from overleaf).

It can be seen in Figure 4.3 (b) that the zone of injury did not extend radially greater than the spot radius, suggesting that scattering of the laser light was insignificant. At 3-4 J mm^{-2} the surface of the disc darkened. Beyond 4 J mm^{-2} the darkened surface extended over the entire exposure site, becoming blackened due to charring. After approximately 10 J mm^{-2} had been delivered, the black surface resembled a dehydrated crust covering the tissue, with blackened, but moist, tissue underneath. Additionally, the radial extent of the tissue damage was noticeably greater, due probably to the enhancement of laser light absorption at the blackened tissue surface. This would have lead to a higher thermal gradient in all directions, thereby increasing the heat flow and its effects. However, at the same time, the cross section revealed that a crater had been formed, indicating either tissue contraction and/or tissue removal. Thus, it is reasonable to assume that mass loss in this region proceeded as a result of both dehydration and vaporisation. Above pulse fluences of 0.06 J mm^{-2} the ablation craters showed less evidence of charring and mass loss is now attributable mostly to ablation and partly to dehydration.

4.3.1.2 At 2.94μm

The results of the mass loss measurements for increasing dose are shown for the 2.94μm laser light in Figure 4.4. At low doses (< 15 J mm^{-2}), the mass removal appears to be linear with dose. However, as the dose increases, the mass loss for lower pulse fluences (< 0.054 J mm^{-2}) begins to vary sublinearly with dose.

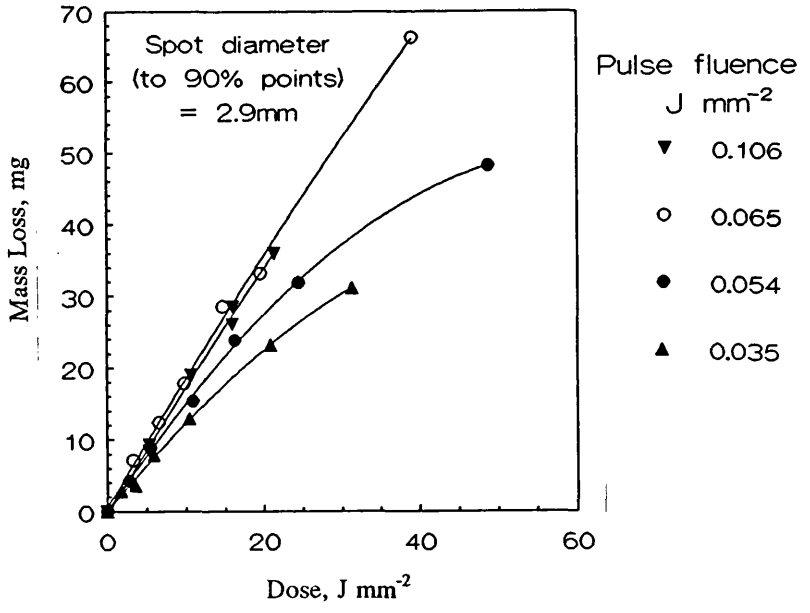

Figure 4.4 Effect of dose at 2.94μm on tissue mass loss for different pulse fluences, the spotsize remaining constant at 2.9mm.

For pulse fluences greater than 0.06 J mm^{-2}, the mass loss continues to be linear up to the maximum applied dose of about 52 J mm^{-2}.

The gross changes in the tissue during the exposure to a series of low fluence pulses (0.03 J mm^{-2}) are shown in Figure 4.5 (a-e). Delivery of a dose of less than 2 J mm^{-2} at this pulse fluence results in the ablation of a thin disc of surface tissue and the visible whitening of the exposure site, indicating coagulation. However, small pools of blood were observed on the surface of the disc, indicating that blood was still able to permeate through the coagulated layer. Around the edge of the exposure site a series of spots of coagulated blood were visible, providing a definite demarcation between the ablation crater and the surrounding tissue. Under intense white light illumination, whitening beyond the demarcation line indicated the extent of coagulation, Figure 4.5 (b). A cross-section through tissue exposed to about 5 J mm^{-2} revealed that the ablation crater consisted of smooth, but ridged, sides and a flat base. It was noticeable that the intersection between the base and sides of the crater was discontinuous. This was attributed to the very low scattering at this wavelength and the top-hat intensity profile of the laser beam at the tissue. Around the edge of the crater, a double ring of coagulated blood enclosed a band of darkened tissue which became darker as the dose increased, eventually becoming charred, Figure 4.5 (e). At doses of about 20 J mm^{-2}, the band of carbonised tissue extended fully into the crater with only the base of the ablation site remaining unaltered.

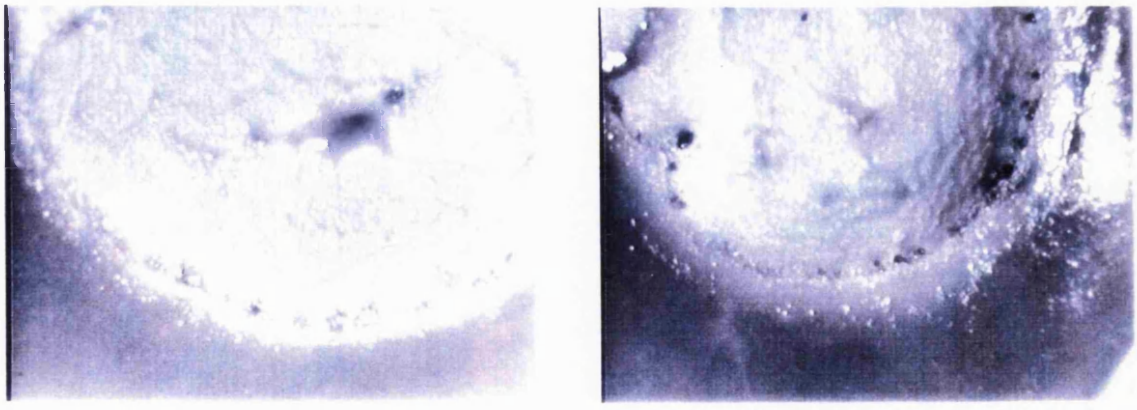

a) Dose = 1.63 J mm^{-2} b) Dose = 3.26 J mm^{-2}

Figure 4.5 Plan and cross-sectional views of tissue irradiated by 2.94μm laser pulses at different doses, the pulse fluence and spotsize remaining constant at 0.0326 J mm^{-2} and 6.77mm (by burnpaper), respectively. (Continued overleaf).

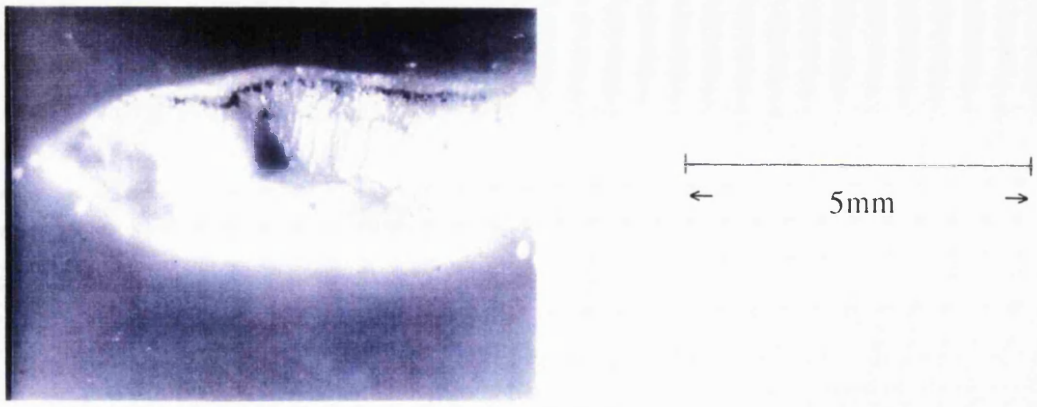

c) Dose = 4.89 J mm^{-2}

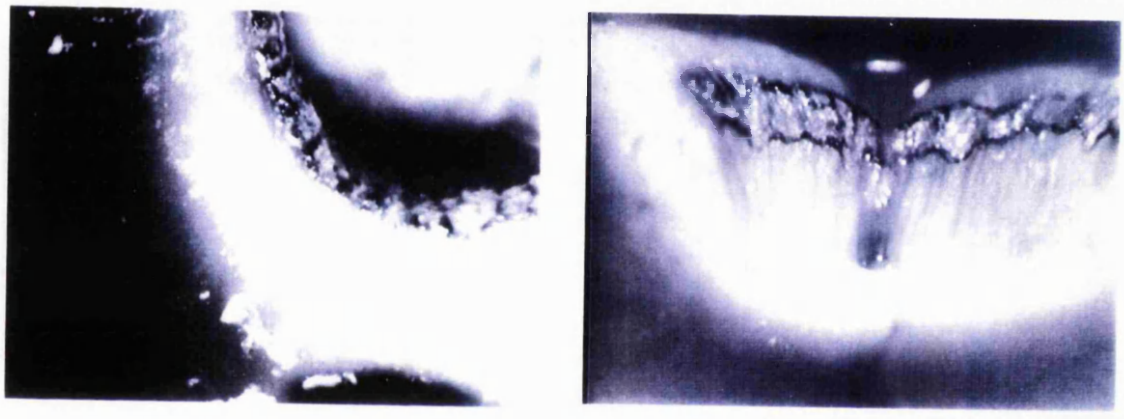

d) Dose = 9.79 J mm^{-2}

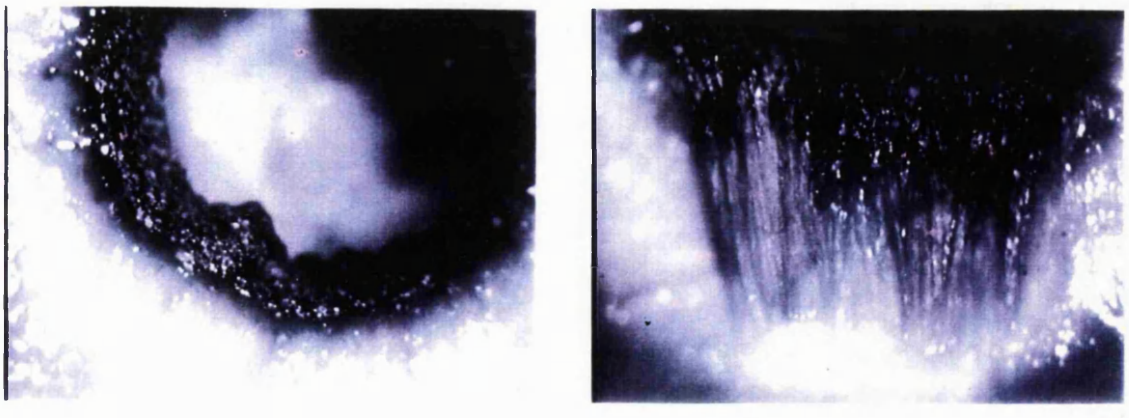

e) Dose = 19.59 J mm^{-2}

Figure 4.5 Plan and cross-sectional views of tissue irradiated by 2.94μm laser pulses at different doses, the pulse fluence and spotsize remaining constant at 0.0326 J mm^{-2} and 6.77mm (by burnpaper), respectively. (Continued from overleaf).

4.3.1.3 Comparison of 2.1μm and 2.94μm

Linear regression of the mass loss data from Figures 4.2 and 4.4 gives the amount of mass removed for each joule of laser energy incident on the tissue surface. This gradient is referred to as the mass loss efficiency (MLE) and is a useful figure against which to measure the ablation performance of different laser wavelengths. Figure 4.6 shows the result of the regression for both 2.1μm and 2.94μm laser light. The MLE increases with pulse fluence for both wavelengths but is noticeably higher for the 2.94μm light. The maximum MLE for the 2.94μm light was about 0.25mg J^{-1} and was obtained for fluences in excess of around 0.06 J mm^{-2}, while the maximum MLE for the 2.1μm light of about 0.18 mg J^{-1} was reached at 0.54 J mm^{-2}, the maximum fluence used at this wavelength. This effect is discussed further in section 4.3.2 of this Chapter.

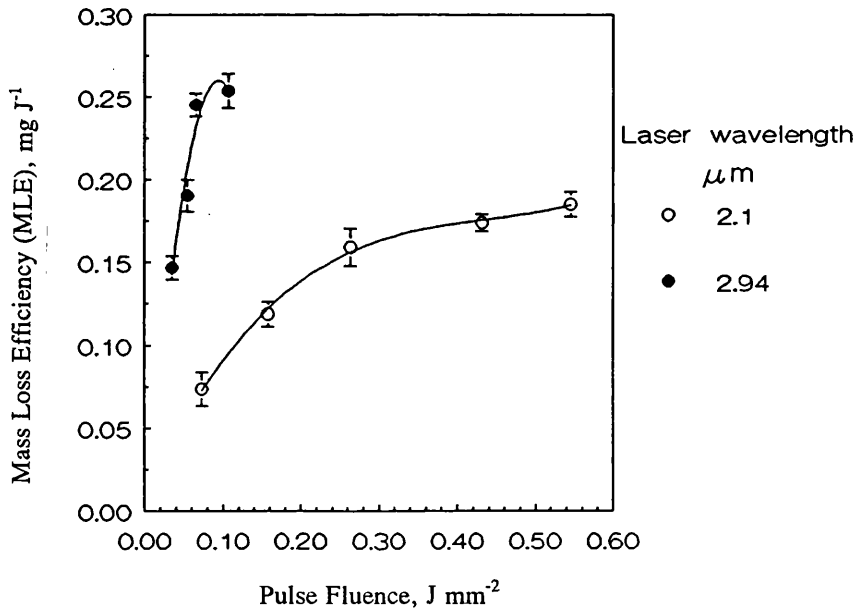

Figure 4.6 Change in mass loss efficiency with pulse fluence at 2.1μm and 2.94μm, derived from the data shown in Figures 4.2 and 4.4, respectively.

Finally, the mass loss data was used to calculate the mass loss efficiency for each experimental value (the gradient of a line through the origin and a single data point). This was expected to reveal any changes in the rate of mass removal as the dose increased which may not have been visible due to the linear regression analysis. The result of this analysis is shown in Figure 4.7 (a) and (b) for 2.1μm and 2.94μm light, respectively. The data for the 2.1μm light is scattered at the low pulse fluences, particularly at the higher doses, due to the influence of tissue charring, Figure 4.3. Overall, however, there is no major change in the rate of mass loss with dose,

indicating the constancy of the mass removal process.

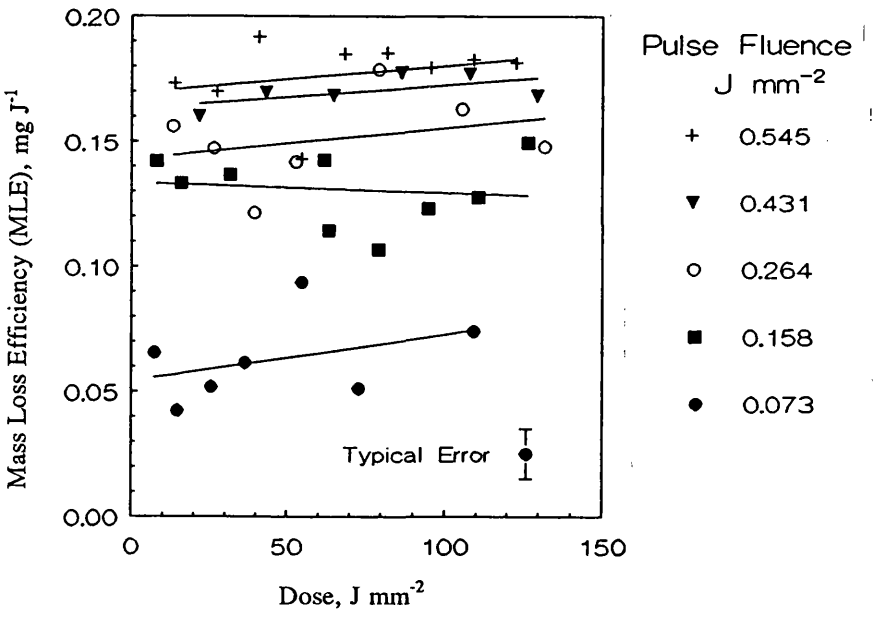

(a)

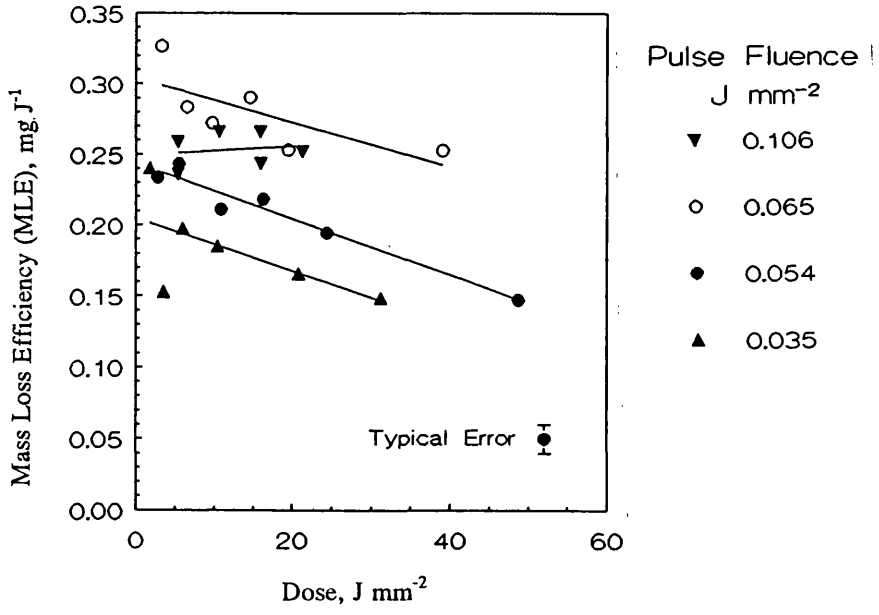

(b)

Figure 4.7 Effect of dose on mass loss efficiency at a) 2.1μm and b) 2.94μm for different pulse fluences, the spotsizes remaining the same at 1.9mm and 2.9mm, respectively (Typical error of the data $\pm$0.01 mg J^{-1}).

In contrast, the MLE results for the 2.94μm light suggest that the mass loss efficiency reduces with increasing dose for all but the highest fluence pulses. This was an unexpected observation due to the precise, highly ablative nature of the

2.94μm laser pulses. It is suggested that the rim of carbonised material which gradually extends into the crater may prevent the removal of tissue beneath it, thereby reducing the mass loss efficiency. Energy which falls onto the carbonised layer is assumed to be absorbed by the layer, thereby increasing its temperature and extending the adjacent coagulation damage and increasing the surface area over which the carbon extends. It is surmised, though not proven, that eventually the mass loss efficiency may be reduced as a result of the charring of the exposed tissue. It may also be that the final mass loss efficiency will depend on the on-axis laser intensity where high fluences may be able to ablate whole or partly charred material, thereby stemming the further extension of the charred zone.

4.3.2 Effect of pulse fluence

4.3.2.1 At 2.1μm

The results of experiments to determine the effect of pulse fluence on the MLE are shown for the 2.1μm laser pulses in Figure 4.8. The results are in agreement with the earlier observations based on the measurements of the effect of increasing dose. The MLE increases rapidly from an intercept at or near to zero, reaching a value of about 0.1 mg J^{-1} for pulse fluences of 0.04-0.10 J mm^{-2}. Above about 0.15 J mm^{-2} the MLE increases slowly with pulse fluence, increasing to 0.18 mg J^{-1} at fluences in the region of 0.5 J mm^{-2}.

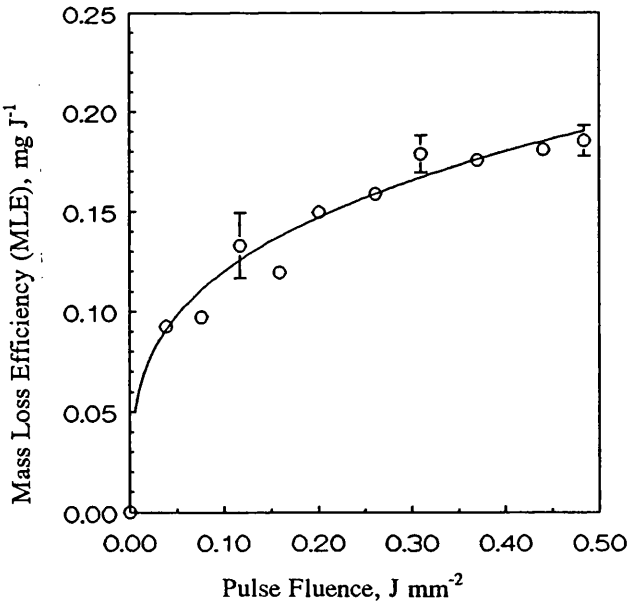

Figure 4.8 Effect of pulse fluence at 2.1μm on mass loss efficiency for a constant dose of 31.3$\pm$5.1 J mm^{-2}, the spotsize remaining constant at 1.9mm.

Figure 4.9 (a-c) shows the results of histological preparation of tissue exposed to a total dose of 17 J mm^{-2} at the pulse parameters given in Table 4.4. At the highest pulse fluence of 0.18 J mm^{-2} the cross-section through the crater reveals that the lesion is essentially circular, the edges being lined with a carbonised layer approximately 100μm thick. Beyond the charred layer there exists a zone of vacuolated tissue (tissue in which 'bubbles' are visible, caused by the sub-ablation threshold boiling of tissue water[171]). The vacuolated zone appears to extend 400-700μm from the edge of the crater, although verification of this fact is not possible due to the damage induced previously to the tissue by the freezing process and the poor demarcation provided by the H&E staining process. Around the circumference of the crater there are regions where there appears to be no thermal damage. The radius of these edges is noticeably larger than that of the charred edge.

(a) 45 mJ mm^{-2} (b) 106 mJ mm^{-2} (c) 182 mJ mm^{-2}

Figure 4.9 Histological section showing plan views of cross-sections through craters formed in tissue by 2.1μm laser pulses at different pulse fluences, the spotsize and dose remaining constant at 2.9mm and 17 J mm^{-2}, respectively.

It is suspected that, originally, the charred and vacuolated zones extended unbroken around the crater edge, but that during the histological preparation this region of tissue became separated, an effect made easier by the weakening of the tissue structure due to vacuolisation. At the lower pulse fluence of 0.106 J mm^{-2}, for the same dose, the crater is noticeably less circular. This is presumed to be due to the more pronounced effects of tissue contraction. Further evidence of increased thermal effects on the tissue are provided by the enlargement of the vacuolated tissue zone and an extension of the apparent thermally altered zone to distances up to 700μm from the crater edge. However, in this example, the carbonised zone remains approximately 100μm thick. At the lowest pulse fluence examined there are again signs that the zone of thermal damage is increased compared to the higher pulse

fluences. The carbonised zone is now observed to be 300-400μm thick, with the heavily vacuolated zone extending as far as 1300μm from the crater edge. Additionally, there is evidence that tissue contraction is beginning to cause separation of the vacuolated and carbonised zones from the remaining tissue. It is possible that if this effect was achieved completely around the crater then the healing time may be reduced due to the rapid loss of the carbonised zone, rather than by the 'normal' sloughing process.

4.3.2.2 At 2.94μm

In contrast to the slowly varying change in MLE with pulse fluence observed for the 2.1μm light, the MLE of 2.94μm laser pulses rose rapidly from an ablation threshold at somewhere between 0.005 J mm^{-2} and 0.020 J mm^{-2} reaching a peak value of 0.229$\pm$0.012 mg J^{-1} for pulse fluences greater than about 0.05 J mm^{-2}, Figure 4.10.

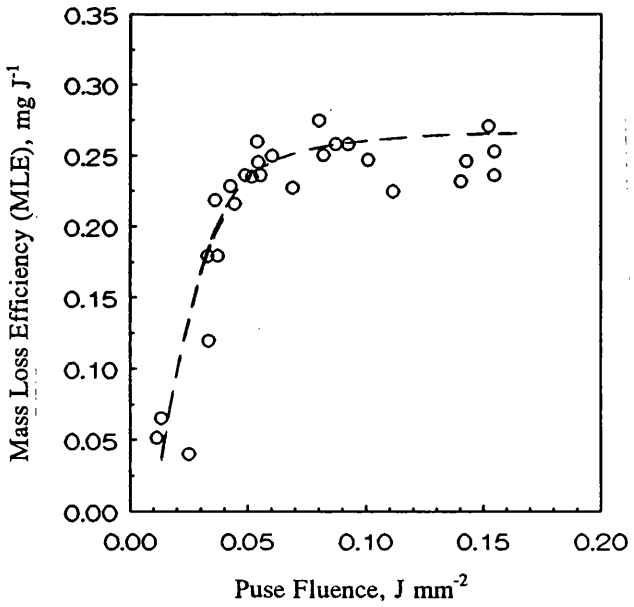

Figure 4.10 Effects of pulse fluence at 2.94μm on mass loss efficiency for a constant spotsize and dose of 2.9mm and 17 J mm^{-2}, respectively.

This plateau region was a strong indication that the maximum ablation efficiency had been achieved. Grossly, the tissue appeared quite different depending on the pulse fluence, despite the constant total dose. Significant differences were particularly noticeable between craters made at pulse energies for which the MLE was constant, i.e. in the plateau region of Figure 4.10. Several sample lesions were made at the four pulse fluences detailed in Table 4.4, photographed and then sent for histological preparation. The results are shown in Figure 4.11 (a-d).

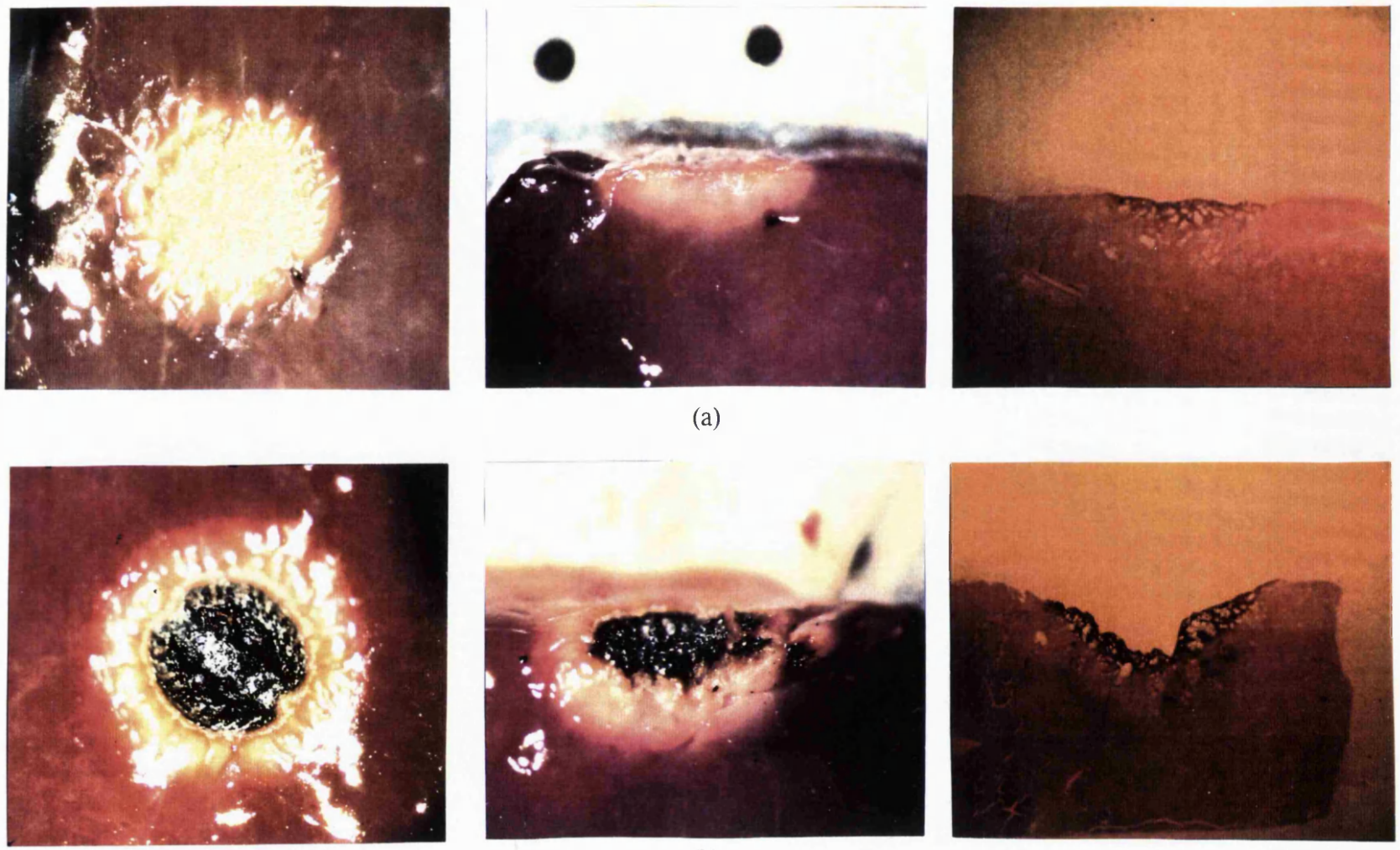

(a)

(b)

Figure 4.11 Photographic plan and cross-sectional views and histological cross-sections of tissue irradiated by 2.94μm laser pulses of fluences a) 0.0247 J mm^{-2} and b) 0.0374 J mm^{-2}, the dose and spotsize remaining constant at 25 J mm^{-2} and 2.9mm, respectively.

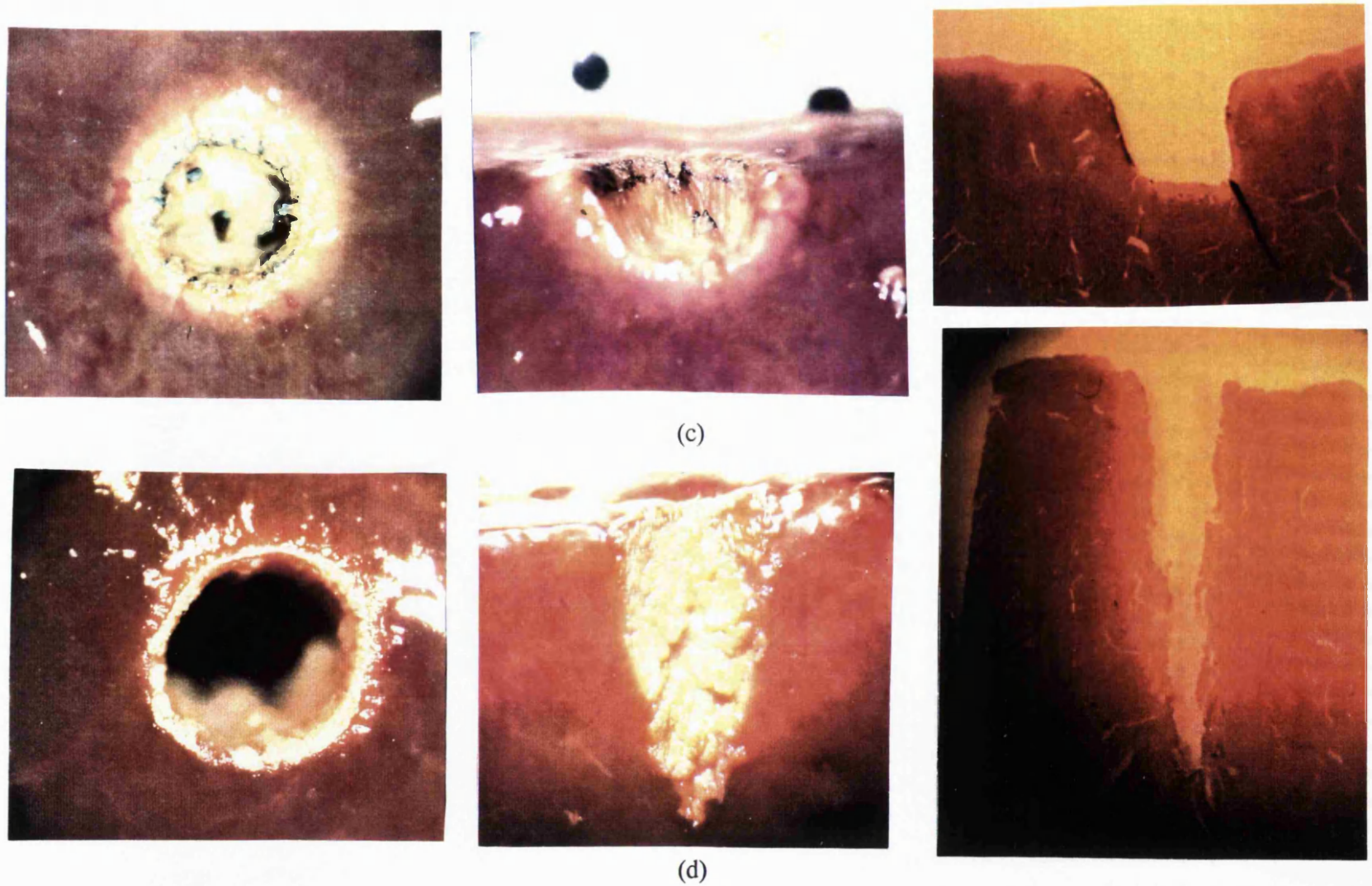

(c)

(d)

Figure 4.11 Photographic plan and cross-sectional views and histological cross-sections of tissue irradiated by 2.94μm laser pulses of fluences c) 0.0592 J mm^{-2} and d) 0.154 J mm^{-2}, the dose and spotsize remaining constant at 25 J mm^{-2} and 2.9mm, respectively.

At pulse fluences of about 0.025 J mm^{-2} there was evidence of surface coagulation over the site of the exposure and signs of tissue contraction around the periphery of the site. However, there was no evidence of tissue ablation, as witnessed by the continuous tissue surface in cross section, Figure 4.11. On macroscopic observation the thermal damage appeared to extend axially into the tissue approximately 0.5mm. This is noticeably greater than that reported by other workers in this field[188]. Histological analysis revealed that below the exposed surface large voids had been created in the tissue, presumably by tissue contraction as there had been no observation of steam escaping during exposure at these low pulse fluences.

At pulse fluences between 0.035 J mm^{-2} and 0.04 J mm^{-2} there was evidence of greater tissue contraction around the edge of the exposure site and an increased amount of thermal damage extending radially around the lesion in a rim approximately 1mm wide. The tissue was heavily charred over the exposed area with a shape resembling a cross-section through the core of an apple. Inspection of the burn produced by the laser on exposed photographic film revealed the same shape, indicating that the laser output was asymmetric (a feature not investigated during this study) and showed that the lesion accurately followed the spatial profile of the incident light. This confirmed, as expected, the absence of significant scattering effects. In cross-section the effect of tissue charring on the axial depth of thermal coagulation was obvious. The whitened tissue, which was used as an indication of the depth of coagulation extended more than 1mm beyond the bottom of the charred crater. It was concluded that temperatures higher than those normally obtained in tissue heated by 2.94μm had been generated by the presence of the carbonised layer and that heat flow from this 'superheated' zone had resulted in the increased thermal damage. Although there was evidence of a crater it was not possible to conclude what amount of mass loss had been caused by tissue vaporisation rather than dehydration. Histology confirmed these observations showing the same tissue disruption as observed in the previous lesion. Measurement of the MLE for each of these two lesions revealed a sub-maximum ablation efficiency.

At higher pulse fluences there was clear evidence of crater formation and a reduction in the visible signs of thermal damage. Figure 4.11 (c) shows the lesion created for a pulse fluence of 0.059 J mm^{-2}. The radial damage was seen to be approximately 0.5mm wide, a reduction compared to lower fluences, and there were no signs of carbonisation. In keeping with the observations made for lower pulse fluences, the surface shape of the lesion reflected the spatial profile of the laser light. The walls of the crater were free from any debris and were clearly ridged. Unlike the craters observed previously, Figure 4.5, the junction between the floor and sides of

the crater were continuous. However, the base of the crater was again flat and was in keeping with the flat-top spatial intensity profile expected of the laser beam. Around the edge of the crater was a double rimmed band of darkened tissue as had been observed previously, Figure 4.5 (c). Comparison of the pulse fluence with the results of the MLE measurements revealed that the crater was formed at the lowest fluence for which the maximum MLE was also measured. The histology of this lesion emphasised the precision of the ablation process, additionally showing that the tissue disruption observed in other lesions was absent.

When the pulse fluence was adjusted to the same level as the maximum available for the MLE measurements the crater shape changed noticeably. In contrast to the 'U' shaped crater obtained at a pulse fluence of 0.059 J mm^{-2}, the crater developed during exposure to pulses at a fluence of about 0.15 J mm^{-2}, formed a pronounced 'V', Figure 4.11 (d). Around the entrance to the crater there was no evidence that the thermal damage extended beyond the crater itself and this observation was confirmed in cross-section. Histological examination provides the best view of this lesion which tended to 'unfold' when bisected with a scalpel blade. The histology shows a marked contrast to the precise 'U'-shaped ablation crater. The lesion is clearly a 'V' shape and, although there is no evidence of extended thermal damage, either in the photographic or histological evidence, there is evidence of tissue tearing, i.e. extended non-thermal tissue damage.

Interestingly, the change in appearance of the lesions, between 'U' and 'V' shapes, at different pulse fluences coincided with changes in the results obtained for the mass loss measurements. Figure 4.12 shows the graph of mass loss before, during and after the laser exposure at the maximum pulse fluence of 0.154 J mm^{-2}.

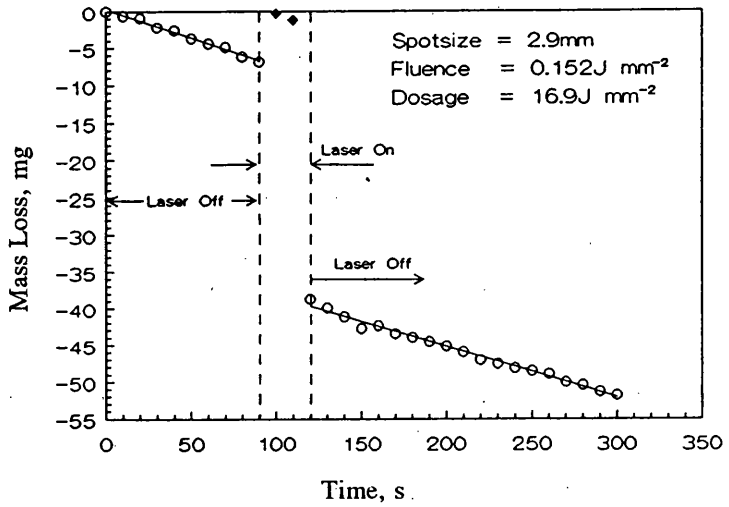

Figure 4.12 Experimental mass loss results showing instability of the displayed weight resulting from the impulse imparted to the tissue at high pulse fluences.

A significant impulse was noticeably delivered to the tissue which caused the pan balance to recoil, resulting in mass measurements which clearly were inconsistent with the mass loss at that point, as indicated in the figure. This recoil has formed the basis of impulse measurements using a pendulum reported by other authors[183,192].

4.3.3 Effect of spotsize at 2.1μm and 2.94μm

The mass loss results of the previous measurements, which showed the effect of pulse fluence on the MLE, were extended to include the mass loss measured for different spotsizes exposed to a similar range of pulse fluences, Table 4.2. The results for the 2.1μm and 2.94μm laser pulses are shown in Figures 4.13 and 4.14, respectively.

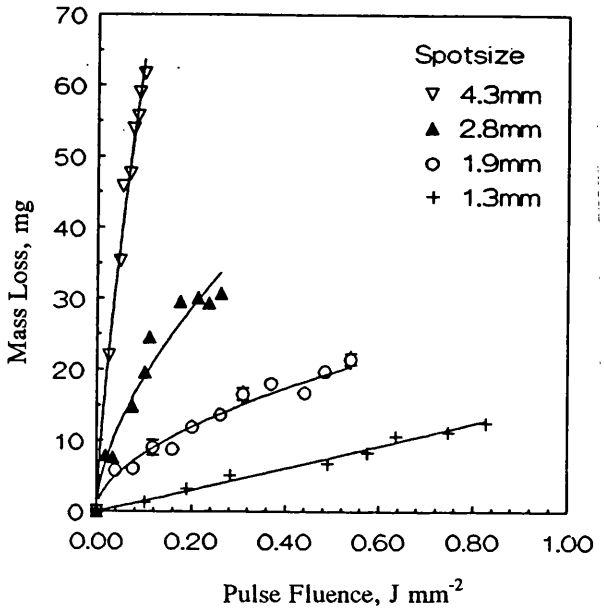

Figure 4.13 Effect of pulse fluence at 2.1μm on mass loss for different laser spotsizes, the total dose remaining constant for each spotsize.

The graphs, which present the mass loss data, show that more mass is lost for larger spotsizes. This is not surprising as, in order to maintain the fluence at a constant level between spotsizes, it is necessary to increase the pulse energy to compensate for the increase in area. It is for this reason that it is appropriate to measure the mass loss efficiency in units of mass per unit energy for a given pulse fluence. The mass loss data shows the same trends at each spotsize and was the same as that reported in the previous section. Specifically, the mass loss obtained at 2.1μm increased slowly with fluence in contrast to the 2.94μm light and did not reach a plateau level.

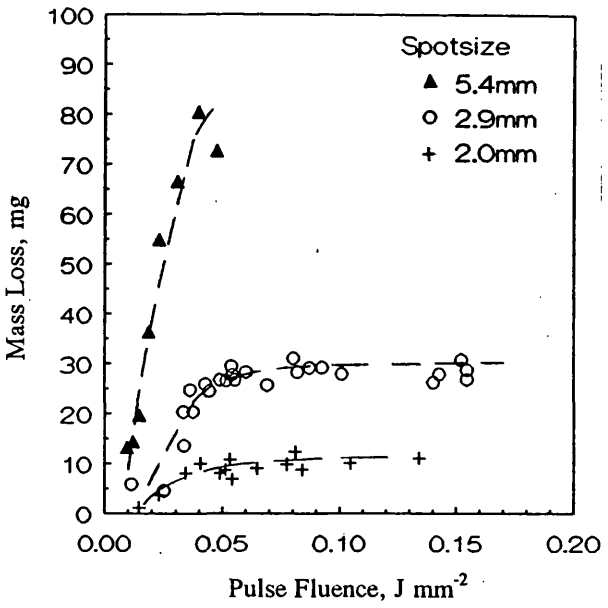

Figure 4.14 Effect of pulse fluence at 2.94μm on mass loss for different laser spotsizes, the total dose remaining constant for each spotsize.

The mass loss for the 2.94μm pulses increased rapidly with fluence from a threshold between 0.005 J mm^{-2} and 0.025 J mm^{-2}, as highlighted by the results for the 2.9mm and 5.4 mm diameter beams, before reaching a maximum value for pulse energies in excess of 0.05J mm^{-2}, as highlighted by the results for the 2.0mm and 2.9mm diameter beams. Dividing the mass loss data by the total delivered energy, to cancel the disproportionate amounts of energy delivered by the different spotsizes, reveals the extent of spotsize effects on the mass loss efficiency. The results for the 2.1μm and 2.94μm laser pulses are shown in Figures 4.15 and 4.16, respectively.

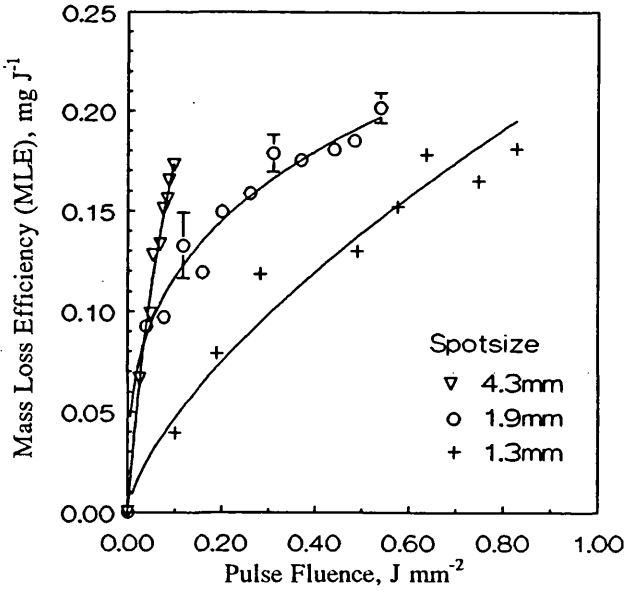

Figure 4.15 Effect of pulse fluence at 2.1μm on mass loss efficiency for different laser spotsizes, the total dose remaining constant for each spotsize.

It is clear that the results for the different laser spotsizes are compared best by normalising the data. This is done by calculating the mass loss efficiency in terms of the mass loss per unit of delivered energy. The results also show that, for both wavelengths, there is evidence of influence of the spot diameter on the MLE. This, however, is difficult to confirm in practise due to the fact that the intensity across the laser spot is averaged by the analysis whereas local hotspots may cause some variations in the rate of mass removal across the profile. However, based on the 90% contained energy spotsizes, and the error determined experimentally for this measurement, a variation in MLE with spotsize is observed. This variation suggests that, at a constant pulse fluence, larger laser spots are more efficient at removing tissue. Unfortunately, due to limitations on the available pulse energies it was not possible to extend the range of measurements of MLE for larger spotsizes over the full range of pulse fluences used for the smaller spots. Thus, it cannot be confirmed that the changes in the rate of mass removal behave in a similar fashion to the smaller spotsizes i.e that the 2.1μm pulses slowly approach a maximum or that the 2.94μm pulses rapidly attain a maximum MLE at pulse fluences of 0.05 J mm^{-2}.

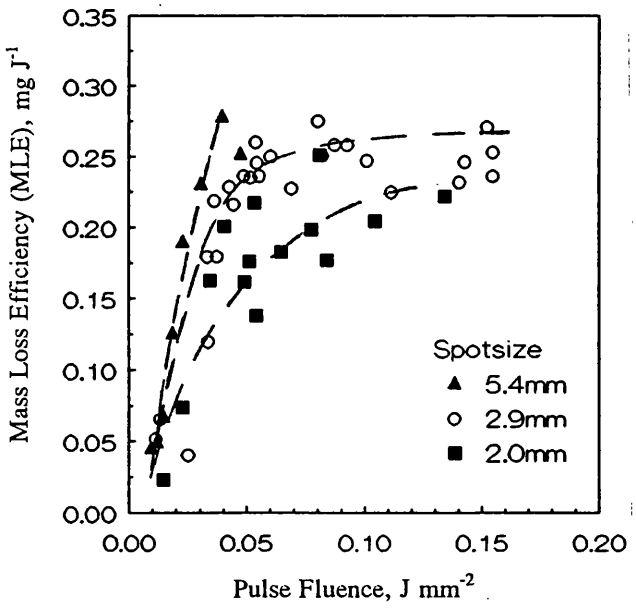

Figure 4.16 Effect of pulse fluence at 2.94μm on mass loss efficiency for different laser spotsizes, the total dose remaining constant for each spotsize.

4.3.4 Effect of tissue coagulation on mass removal at 2.1μm and 2.94μm

The results of the comparison between the rate of mass removal by 2.1μm and 2.94μm laser pulses for fresh and laser coagulated tissue are shown in Figures 4.17

and 4.18, respectively. Both figures show the surprising result that the mass loss efficiency was not affected by coagulation. This appears to be in conflict with the observations by Essenpreis et al[5] who showed a definite change in the optical properties following coagulation leading to the expectation that the mass loss efficiency would also be affected.

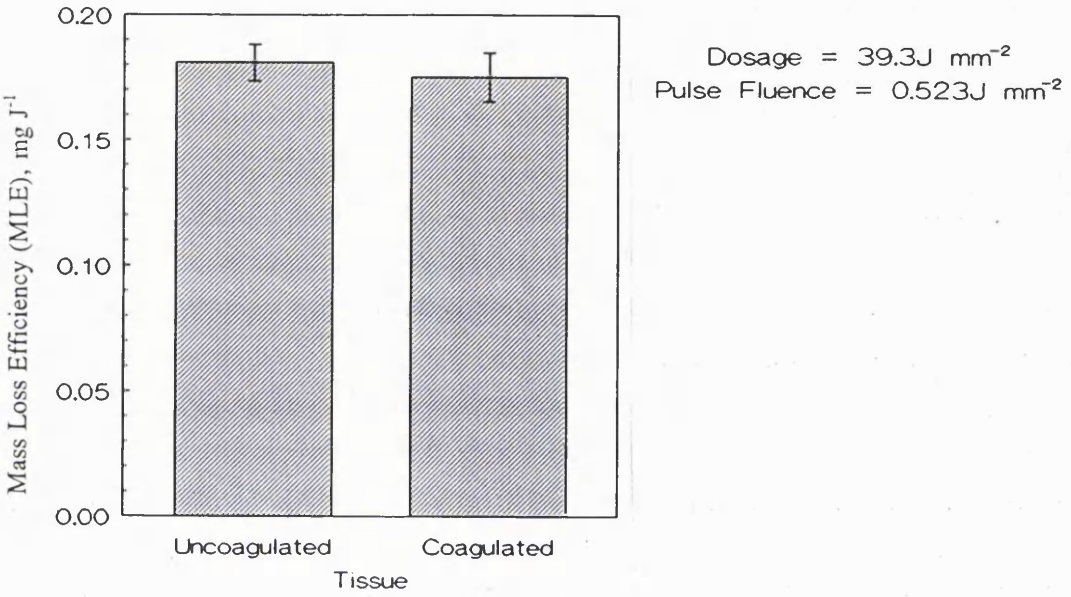

Figure 4.17 Effect of tissue thermal history on mass loss efficiency at 2.1μm, irradiation parameters remaining unchanged.

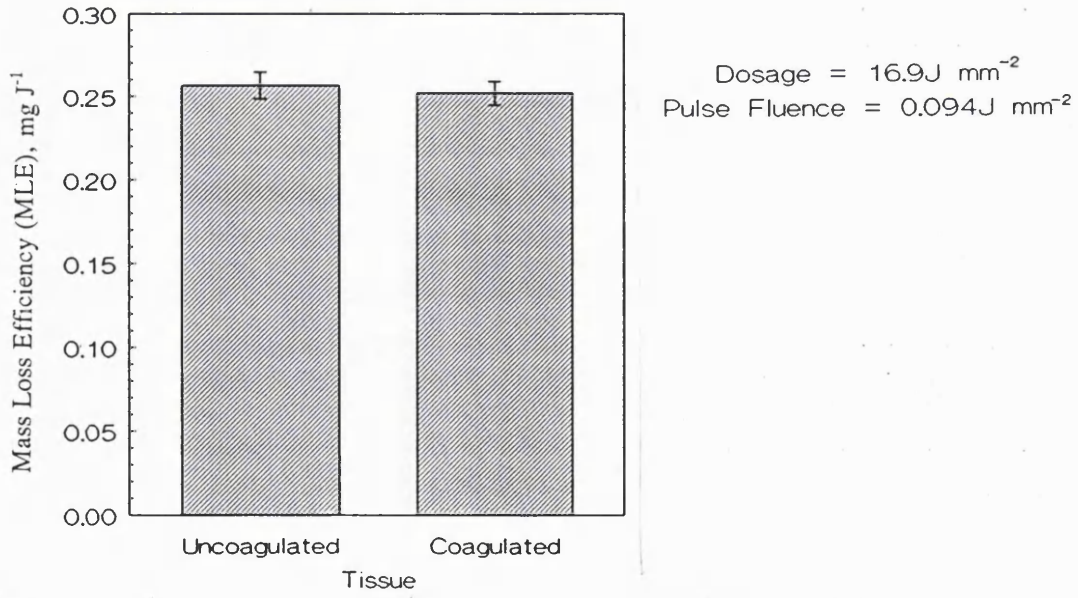

Figure 4.18 Effect of tissue thermal history on mass loss efficiency at 2.94μm, irradiation parameters remaining unchanged.

When the ablation craters were inspected visually there were clear differences between the lesions created. Figure 4.19 shows the results for the 2.94μm laser pulses. Although the entry to both craters is circular, and the zone of thermal damage in the 'fresh' tissue is small, the cross-sectional slice through the tissue reveals noticeably different crater shapes. Presentation of an accurate image showing the cross-section through the fresh tissue is limited by the collapsible nature of the tissue. However, it can be seen that the crater in the fresh tissue has a smooth transition between walls and base while the transition between walls and base for the coagulated tissue is marked by a definite discontinuity. It is noticeable also that, for the coagulated sample, the crater base seems to have a lump in its centre.

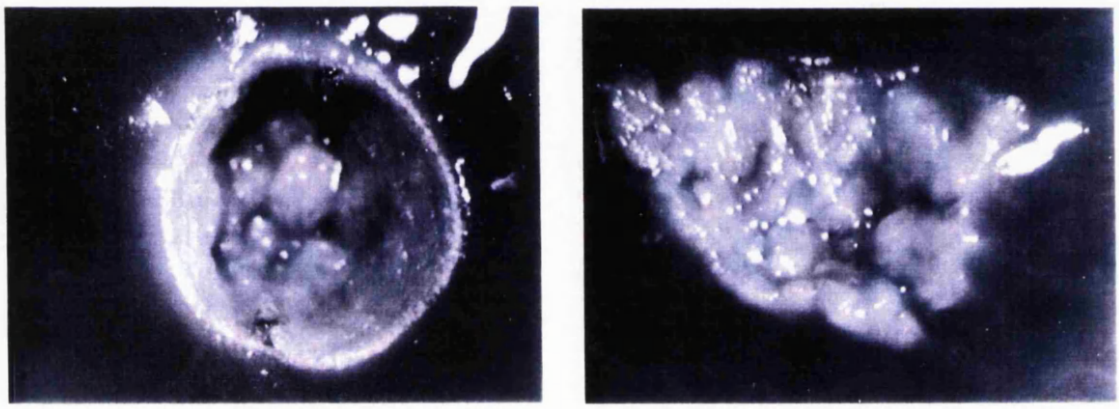

(a)

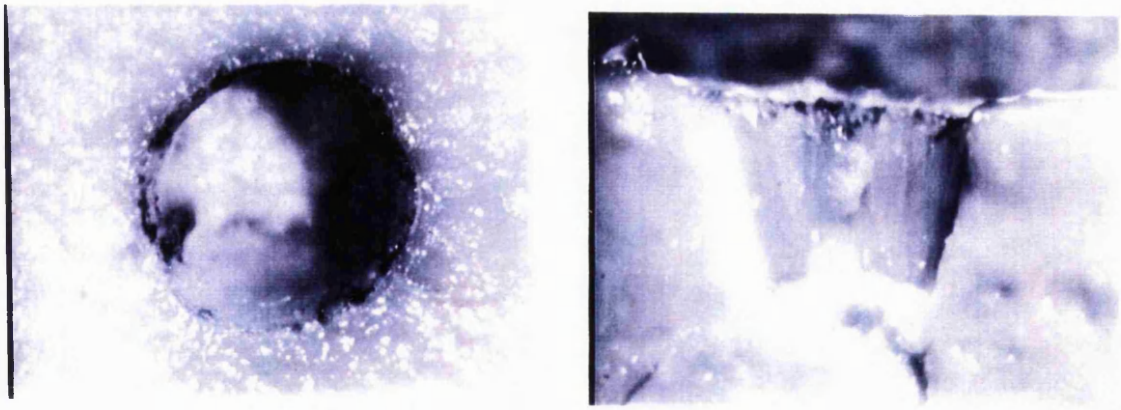

(b)

Figure 4.19 Plan and cross-sectional views of 2.94μm ablation craters in a) uncoagulated and b) coagulated ox liver tissue.

The reason for this is unclear. It is unlikely that the laser beam's spatial profile contained such an unusual energy distribution and, if it did, this would have been observed in the earlier experiments. What is more likely is that either shockwaves from the impulse imparted to the tissue lifted and separated the tissue at the base, or

that the lower layers were parted during expansion of the tissue gases. Another possibility is that the lump is not a result of tissue underneath the base lifting but rather the same tissue being forced downward by the gases expanding in the crater. Yet another possibility is that the tissue may simply have been 'protected' from the ablative action of the pulse by the blocking effect of the ablation products caught within the crater during each pulse of energy.

4.4 Discussion

The results of the mass loss measurements reveal that, for the 2.1μm laser light, the rate of mass removal was linear with increasing dose over the range of pulse fluences from 0.072 J mm^{-2} to 0.539 J mm^{-2}. Below these pulse fluences the tissue was observed to undergo a series of visible changes. As the dose increased the tissue became coagulated, dehydrated and eventually charred. At such low fluences, mass loss was still recorded, but this was attributed to dehydration rather than ablation of the tissue. The MLE increased with pulse fluence, reaching a value of 0.185 ± 0.008 mg J^{-1} at pulse fluences of around 0.5 J mm^{-2}. From the experimental data it was not possible to establish a clear threshold for the onset of mass loss, nor to differentiate between the mass loss due to dehydration and ablation at elevated pulse energies. However, it was clear that the threshold lay below 0.07 J mm^{-2}. This observation and that of the maximum MLE are in general agreement with the results reported by Nishioka et al[155,184] and Treat et al[185], although the absolute MLE measured in this work is greater than both. A comparison between the experimental results obtained in this work and that of the aforementioned authors is given in Table 4.5.

Authors	Wavelength μm	Tissue Type	Ablation Thr. J mm^{-2}	Mass Loss Eff. mg J^{-1}	Method	Ref.
This work	2.1	liver	<0.07	0.185 ± 0.008	Mass loss	
Nishioka et al	2.12	liver	0.36	0.11	Mass loss	[155]
	2.01	"	0.29	0.113	"	
Nishioka et al	2.1	liver	0.5	0.157	Mass loss	[184]
Treat et al	2.15	gastric mucosa	N/A	0.09	Histology	[185]

Table 4.5 Comparison of this work with published results from mass loss and etch-rate measurements for CTH:YAG and CT:YAG lasers.

The reason for the lower ablation threshold recorded in this work probably lies in the greater accuracy afforded by the larger spotsizes used in this work. For comparison, Nishioka used a single spotsize of 360μm to obtain the results in reference [184], measuring the diameter of the beam by translating a knife edge across the beam. While this can produce accurate details of the spot profile, particularly if the beam has a near-Gaussian intensity distribution, the authors do not reveal whether they took account of the effect that a non uniform intensity distribution would have on the measurements. In the experiments carried out for this work the laser beam was unfocused and, being made up of numerous high order transverse modes, had a top-hat profile, and, therefore, a more uniform distribution, removing the need for such analysis. Another reason for the lower threshold reported here may be the increased resolution provided again by the use of larger diameter beams. In Nishioka's work the range of pulse fluences was around 1 J mm^{-2} to 5 J mm^{-2}, compared to the 0.07 J mm^{-2} to 0.54 J mm^{-2} used here. Thus, the degree of accuracy close to the threshold is improved in this work accordingly. The reason for the relatively small discrepancy in the MLE figures between this work and that of Nishioka probably arises from the fact that MLE is determined only from the mass loss and the total delivered energy small, not the energy density. Thus, differences in the fluence due to measurement errors of the spotsize will not affect the MLE. Thus, there is good agreement between the results of this work and that reported in reference [184], the most appropriate publication against which to make the comparison.

Another possible reason for the differences between previously published figures for the MLE and the results reported in this work may be a real spotsize effect i.e. an effect which depends on the spot diameter, rather than an apparent effect which arises as a result of measurement inaccuracies. Measurement of the mass loss rate during exposure to different spotsizes over a constant range of pulse fluences shows evidence that the mass removal rate is more efficient for larger diameter beams by an amount greater than that accountable for by measurement inaccuracies. The reason for this is unclear. One explanation may be that the rate of heat loss by conduction for larger spotsizes is reduced, equation (20). Thus, for a fixed repetition rate, the heat accumulated in the zone exposed to the laser pulse will be retained between pulses to a greater degree in the larger lesions. This lowers the amount of heat required to be delivered by the next pulse in order to achieve ablation and thereby increases the ablation efficiency. Figure 4.20 shows the change in the τ_{th} with laser spotsize, calculated using equation (20) and values for the constants; α=35 cm^{-1} [39], ρ=1 g cm^{-3}, k=0.62 W m^{-1} $°C^{-1}$ and c=3.5 J g^{-1} $°C^{-1}$ [174]. The figure shows that the time constant varies considerably for increases in the beam

diameter from about 1.3mm to around 4.3mm, the range of the experimental results. Although it is often argued that the interpulse period should be greater than the thermal time constant in order to avoid the build-up of thermal damage[173], accumulation of heat in these experiments may have assisted in the ablation process, either by reducing the amount of heat required, as described above, or by increasing the extent of thermal damage. In the latter case the increase in the MLE arises as a result of increased dehydration and coagulation due to extension of the heated zone by conduction. It was not possible from the experimental results to determine the influence of either of these processes on the MLE. Therefore, the arguments presented are, currently, only speculative.

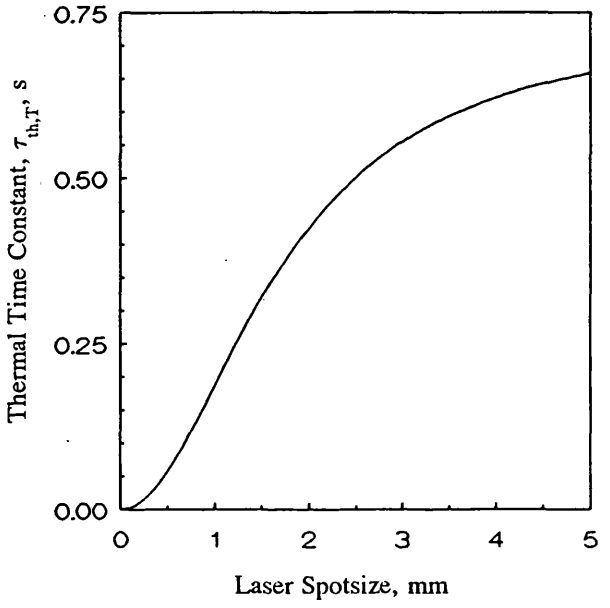

Figure 4.20 The dependence of the thermal time constant, τ_{th}, of the irradiated volume on the laser spotsize at a laser wavelength of 2.1 μm.

The mass loss removal rates for the 2.94μm pulses show the same linear response with dose as observed for the 2.1μm laser pulses. However, thermal damage was observed around the crater edge which increased with dose, eventually obscuring the soft tissue from the incoming beam over all but the central portion of the lesion. This onset of charring is signalled by the formation of a band of darkened tissue around the circumference of the crater. The formation of this band is believed to be due to the lower intensity of light which falls in that region due to the unavoidable wings on the edge of the otherwise top-hat intensity profile. This light is not intense enough to cause ablation during a single pulse and, although heat dissipation away from the exposed zone is predicted to be rapid (of the order of

$1\mu s$[18]) the repeated momentary rise of the tissue temperature to near ablation temperatures will be enough to initiate firstly coagulation and later carbonisation. This effect is most obvious at the lower pulse fluences (<0.06 J mm^{-2}) due to the increased proportion of the beam being at, or below, the ablation threshold fluence. The effect of this accumulation of heat and the subsequent damage is to slowly reduce the efficiency with which the mass is removed. At higher pulse fluences the MLE increases rapidly reaching a maximum MLE of approximately 0.24 mg J^{-1} for pulse fluences in excess of 0.06 J mm^{-2}. Table 4.6 compares the experimental results obtained in this study against the experimental results of others. Additionally, the published values of the MLE for bone are included in the table for completeness. While these results do not make any significant contribution to understanding or verifying the results obtained for soft tissue, they do highlight the large differences between results.

Authors	Wavelength μm	Tissue Type	Ablation Thr. J mm^{-2}	Mass Loss Eff. mg J^{-1}	Method	Ref.
This work	2.94	liver	0.05-0.25	0.229 ± 0.012	Mass loss	
Dickinson et al	2.94	heart	N/A	0.13	Mass loss	[154]
Hibst et al	2.94	pig skin	0.094	Linear	Etch rate	[196]
Kwark et al	2.94	aorta	0.006	Linear	Inspection	[189]
Walsh et al	2.94	skin	0.006-0.015	0.54	Mass loss	[46]
Walsh et al	2.78	liver	≈ 0.12	0.7-0.75	Mass loss	[47]
"	"	aorta/skin	0.045-0.05	0.34-0.35	" "	"
Hibst	2.94	bone	0.077	0.32	Mass loss	[190]
Kwark et al	2.94	bone	0.01	Linear	Inspection	[189]
Vari et al	2.94	bone	N/A	Linear	Etch rate	[156]
Walsh et al	2.94	bone	0.021-0.034	0.3	Mass loss	[46]

Table 4.6 Comparison of this work with published results from mass loss or etch-rate measurements for Er:YAG and Er:YSGG lasers.

This is particularly obvious in the comparison between the results of Hibst[190] and Walsh et al[46] who, despite almost identical values for the MLE, report threshold fluences for ablation which differ by a factor three. This is almost certainly due to inaccurate measurement or different assessment of the laser spotsize and emphasises the effect that this measurement can have on the results.

Other reasons for the differences between the quoted MLE measured under apparently identical experimental conditions have been discussed earlier. Several factors may affect the result including thermal history of the tissue, spatial intensity profile of the laser beam[47], tissue type and laser wavelength (some of the results are quoted for the shorter, 2.78μm, wavelength obtained from YSGG doped erbium lasers). Considering these factors, the MLE measured in this work compares favourably to previously reported values, being somewhat greater than that measured by Dickinson et al[154] for heart tissue and less than that measured by Walsh et al[46] for skin. The results also confirm the linear relationship between mass loss and dose reported previously.

Additionally, several other features of the ablation process not previously reported at the laser wavelength 2.94μm have been observed. Most significant of these is the change in crater shape which is evident after prolonged exposure to elevated pulse fluences. The change from crater shapes which mimic the intensity profile of the laser beam to ones which are a pronounced 'V' shape appears to coincide with the onset of an impulse imparted to the tissue by the ejected material. This impulse has been reported before by Cummings[183] for soft tissue and by Hibst[190] for hard tissue. The threshold for the onset, determined by scrutinising the mass loss data for each experiment to determine the offset of the mass measurements during laser exposure (see, for example Figure 4.12), was 0.085 ± 0.005 J mm^{-2} for a laser spot diameter of 2.90 ± 0.05mm. This compares favourably with the threshold of ≤ 0.1 J mm^{-2} for liver exposed to pulses of 2.78μm light in a spot of 0.5mm diameter, determined from Cummings' results. The fact that the threshold for the impulse effect reported by Hibst for bone is around 0.37 J mm^{-2} is also in keeping with these results if the predictions of the effect of tissue strength, made by Cummings, are considered.

Neither author reports the associated effect on the tissue crater shape observed during these trials. This is probably due to the fact that both Hibst and Cummings rely on a single pulse generating the impulse on a fresh, previously unexposed, piece of tissue. Thus, cumulative effects are never encountered. From the results of this work it is not possible to explain the cause of the change of crater shape. However, Cummings reports on increased tissue tearing with laser fluence, arguing, quite reasonably, that it is an effect induced by the rapid expansion of gases within the ablation crater. The same effect may also be the cause of the changes to the crater shape. Under such circumstances an increase in the level of adjacent tissue damage would be expected and this has been reported in the published literature[47].

An increase in the relative efficiency of the mass removal rate with the laser spotsize at the tissue, similar to that reported earlier for the 2.1μm light, was also observed for the 2.94μm pulses. While heat retention was provided as the argument for the increased efficiency at the shorter wavelength, the characteristic time constant at 2.94μm is dominated by axial heat flow due to the shallow penetration depth. In the range of spotsizes used the thermal time constant is about 9μs and, therefore, does not support the heat retention theory. The interaction between soft tissue and 2.94μm radiation is summarised in Figure 4.21.

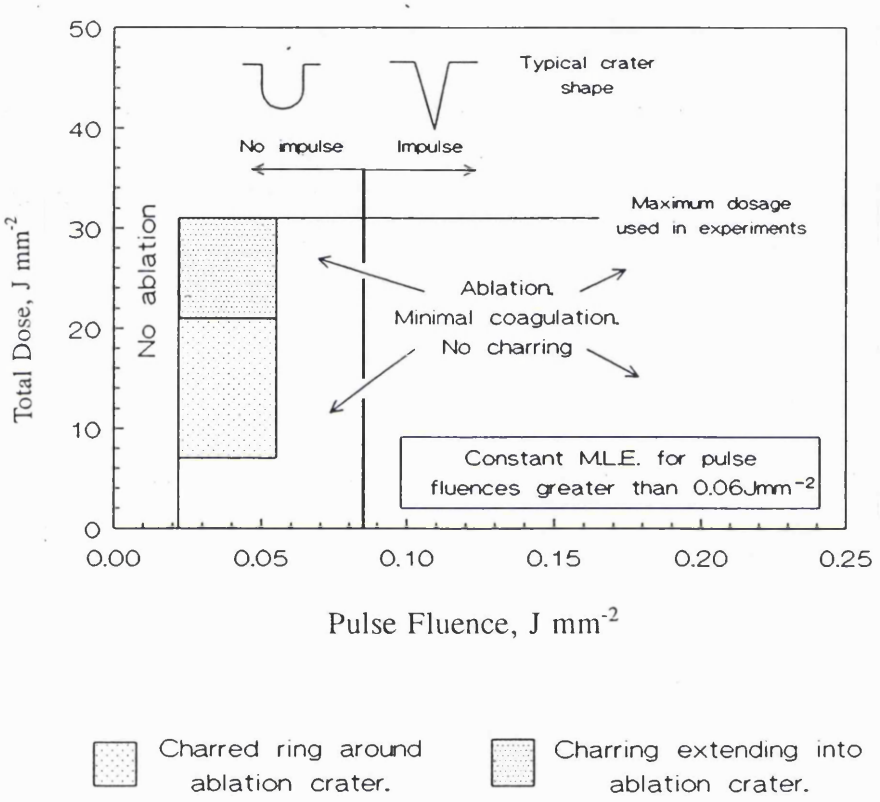

Figure 4.21 Interaction map for 2.94 μm laser pulses and *in vitro* liver tissue.

4.5 Models of Tissue Ablation

The attenuation by tissue of laser light at both 2.1μm and 2.94μm is frequently modelled using the Lambert-Bouguer Law, equation (17). This predicts an exponential reduction in the laser fluence due to absorption of the laser light by the tissue. Walsh et al describe the theoretical model for the ablation of tissue based on the exponential reduction in the light intensity in reference [45]. If the ablation process has a threshold fluence, F_{thr}, then Walsh et al predict that ablation will occur to a depth, D, per pulse at a given pulse fluence, F_0, where

$$D = 1/\alpha \ln(F_0/F_{th}) \quad (21)$$

Assuming that all of the material for which the threshold fluence is exceeded is removed without interfering with the incoming light and that excess fluence does not ablate to a deeper depth but merely increases the energy of the ejected particles (the so-called 'blow-off' theory), then the mass, M, of the tissue removed per pulse is given by

$$M = \int (\rho D)\, dA \quad (22)$$

where ρ is the tissue density and A is the area irradiated by the beam. For the case when the beam intensity is uniform across its profile, for example where the spatial intensity distribution resembles a top-hat shape, equation (22) becomes

$$M = \rho AD \quad (23)$$

Combining equations (21) and (23) result in the equation

$$M = [\rho A/\alpha]\ln(F_0/F_{th}) \quad (24)$$

which indicates that the relationship between the mass loss per pulse and the pulse fluence is logarithmic. This model is summarised in Figure 4.22 (a).

Walsh et al[45] also report on the model previously proposed by Ready[198] in which a simple relationship between mass loss and fluence is developed. This model is based on a thermodynamic assessment of ablation. Figure 4.22 (b) summarises the model graphically. Delivered energy, E, raises the local temperature of a disk of tissue uniformly by ΔT, thereafter providing the energy required to vaporise the disk.

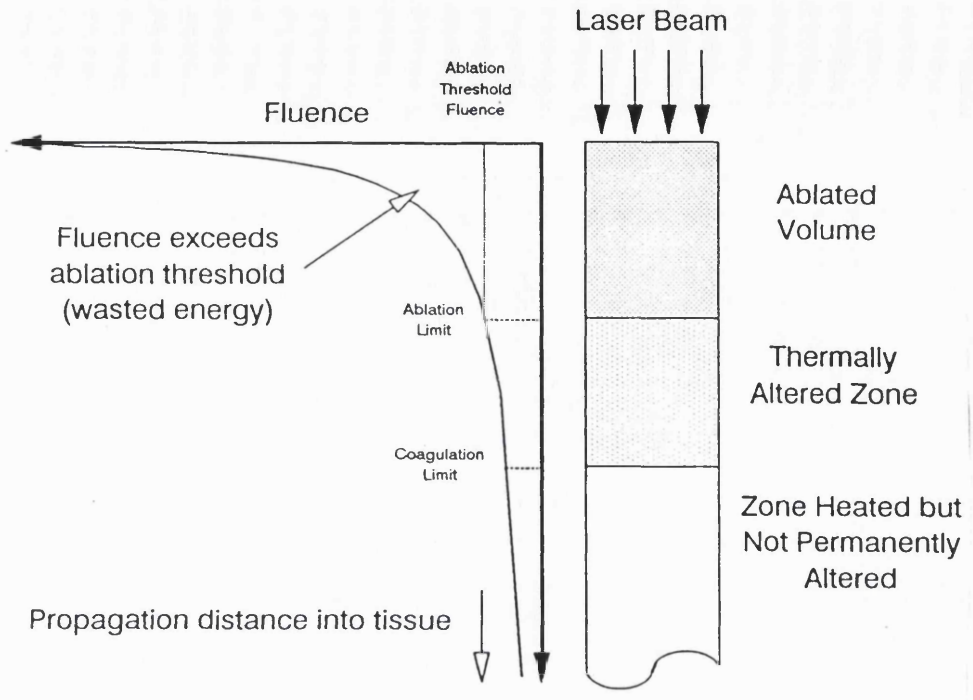

(a)

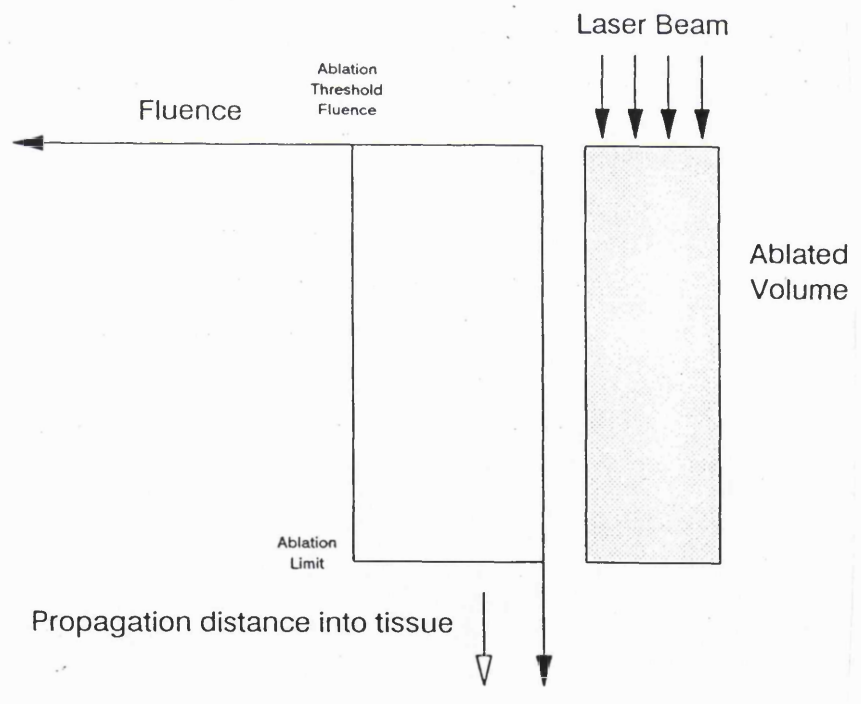

(b)

Figure 4.22 Laser ablation of tissue based on a) a non-linear model (making use of the Lambert-Bouguer Law of optical attenuation) and b) a linear model.

This is described in the familiar equation

$$E = \rho AD(C\Delta T+L) \quad (25)$$

where C is the specific heat capacity, L is the latent heat of vaporisation and D is the depth of tissue heated by each pulse. Rearranging equation (25) to obtain D gives

$$D = E/AH \quad (26)$$

where H=C T+L and is called the heat of ablation. Equation (26) is linear and has its intercept at the origin. However, this neglects the real case of finite attenuation coefficients which means that the disk has a minimum thickness, typically being related to the penetration depth of the laser wavelength. Thus, there exists a threshold fluence below which ablation does not occur. Considering tissue mass per pulse and pulse fluence, equation (26) can be rearranged as

$$M = \rho A(F_0-F_{th})/H \quad (27)$$

which is the same as that described by Walsh et al in [45]. A key feature of this theory is that all of the incident energy contributes to ablating the cylinder. Thus, it is assumed that, for pulse fluences above the threshold, all of the available energy is consumed by the ablation process, leaving none to contribute to sub-ablation heating of the tissue, unlike the logarithmic model.

Each of the theories may be compared against the experimental data by appropriate choice of the graph axes. Plotting mass loss per pulse against the logarithm of pulse fluence should produce a straight line graph according to equation (24), while equation (27), the linear model, is verified by a straight line fit when mass loss per pulse is simply plotted against the pulse fluence. Figure 4.23 shows the results of this process for the 2.1μm light from the CTH:YAG laser.

Clearly, there is a large discrepancy between the expected and actual result when the exponential model is applied. However, there is good agreement between theory and practise for the linear model. In contrast, both linear and exponential models appear to fit well to the experimental results obtained for the 2.94μm light, Figure 4.24.

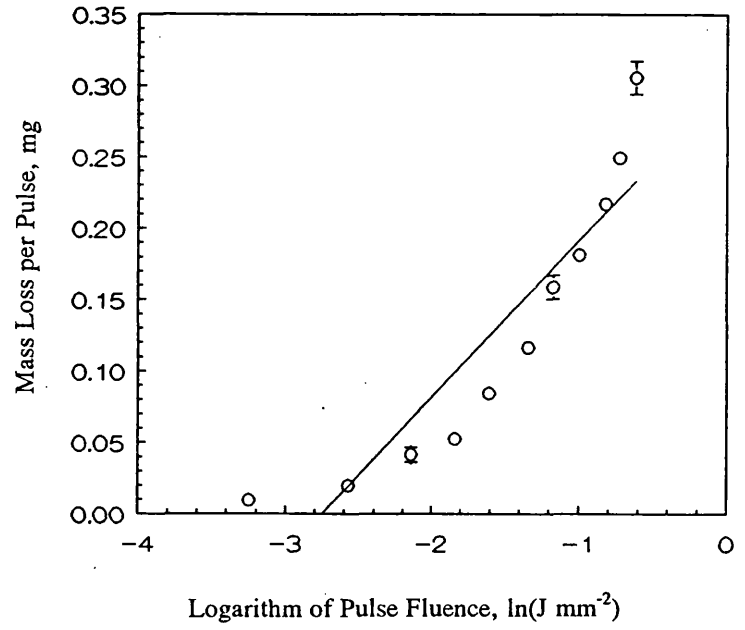

(a)

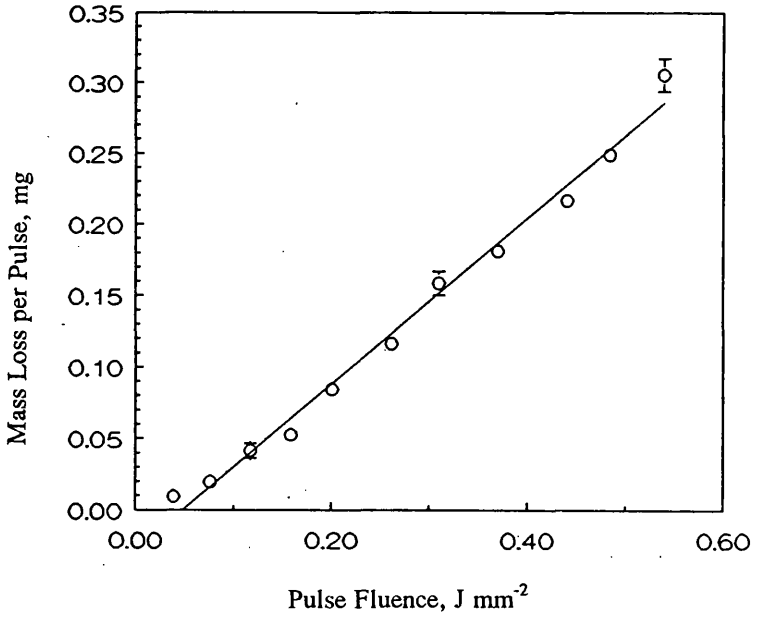

(b)

Figure 4.23 Comparison of experimental data at 2.1μm with a) the non-linear and b) the linear theory of ablation.

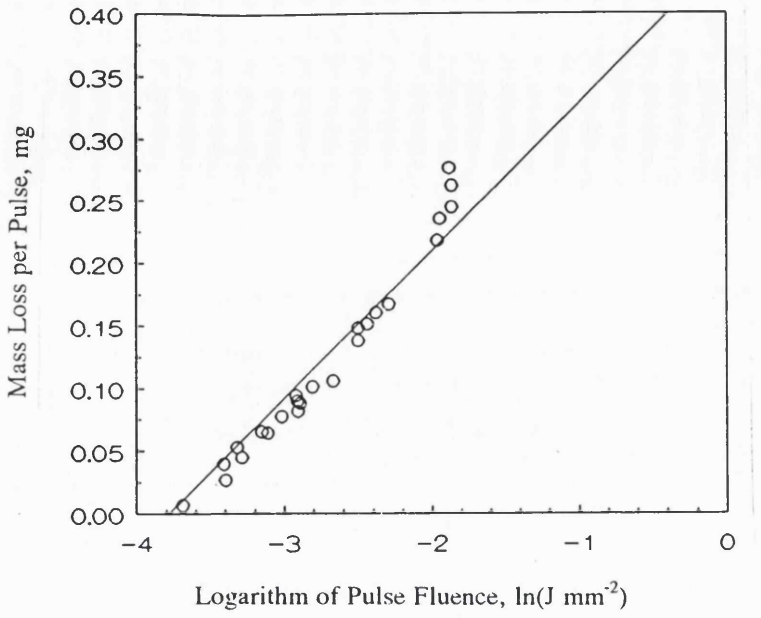

(a)

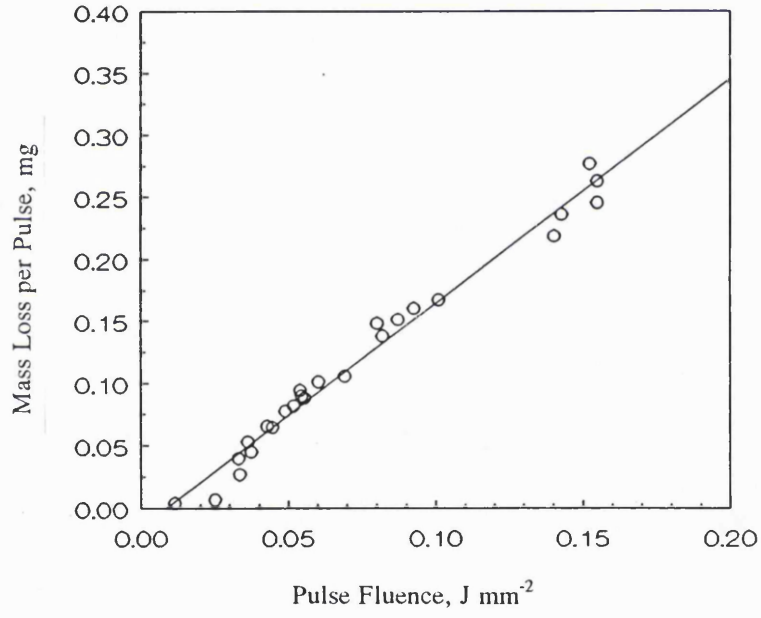

(b)

Figure 4.24 Comparison of experimental data at 2.94μm with a) the non-linear and b) the linear theory of ablation.

The conditions under which the two theories are expected to be in agreement are, firstly, where the exponential attenuation of laser energy is so rapid that almost all of the absorbed energy is converted to ablation energy leaving only a negligible amount of energy deposited in the tissue and contributing little to heating of the remaining tissue. This is, in fact, the expected case based on the known absorption properties of the 2.94μm light[39]. A second reason would be that the exponential model is linear

over the experimental range. This is investigated in Figure 4.25 in which the mass loss per pulse is compared for the two theories, calculated using the parameters obtained from analysing the straight line fit data from Figure 4.24. The result shows that, despite indications at the highest fluences that the linear model may provide the closest fit to the data, it is not possible to conclude that either model is solely appropriate. To verify that one model more accurately describes the ablation performance would require data extending to fluences beyond those used in these experiments. This, in turn, would require either higher pulse energies, which could not be achieved by the laser used, or smaller spotsizes, for which the errors in determining the beam diameter, as well as keeping it constant in the zone of ablation, may reduce the accuracy. It may even be necessary to describe the ablation process as a combination of the two theories. The exponential theory may be appropriate for the low fluence cases where the region of tissue ablated by the pulse is small compared to the total volume of heated tissue, and the linear theory for the higher pulse fluences where ejected material may not absorb incoming radiation, thereby allowing all of the incident energy to contribute to the ablation process.

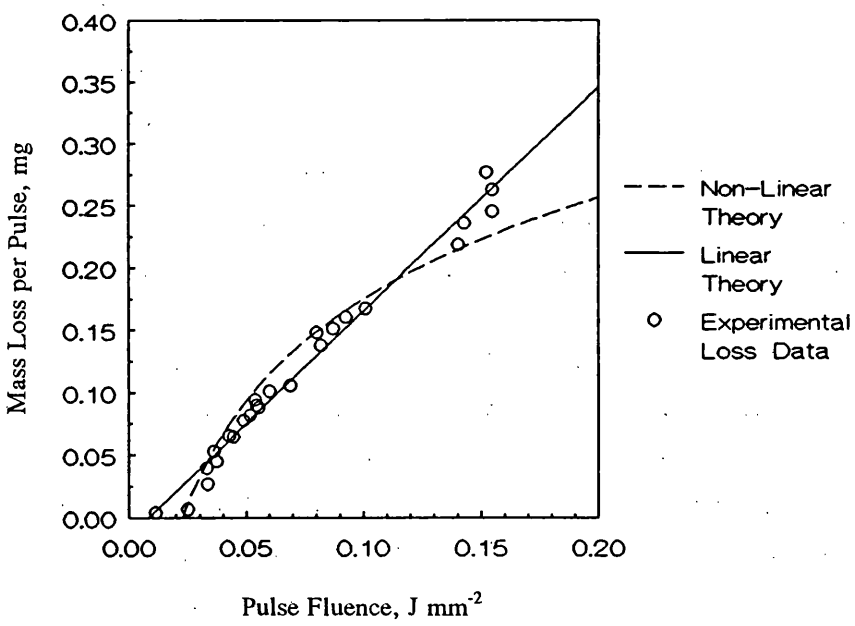

Figure 4.25 A comparison of the experimental results of tissue ablation at 2.94μm with the non-linear and linear models, showing little difference between the two models over the available experimental range.

Applying the mass loss theories to the experimental data allows calculation of other key laser parameters. From the linear model, the heat of ablation, H, is calculated for 2.1μm and 2.94μm light to be 5.213 kJ g^{-1} and 4.09 kJ g^{-1}, respectively. Assuming the density of tissue to be 1.1 g cm^{-3} [155] these figures

convert into 5.73 kJ cm^{-3} and 4.51 kJ cm^{-3}, respectively, which have the units most commonly quoted by other authors. The latter figure is similar to the figures quoted by Dickinson et al[154] for a range of tissues although is approximately twice that quoted by these authors for the specific case of liver tissue. The discrepancy is possibly due to the factors discussed earlier. Using the same technique as Dickinson to determine the heat of ablation, Charlton[85] has reported latent heats for soft tissue exposed to 2.1μm radiation in the 20-50 kJ cm^{-3}. These are significantly greater than the results presented here and are easily explained, firstly by the difference in actual and assumed crater geometry used in Charlton's analysis and secondly by the assumption of tissue density.

It is not appropriate to apply linear regression of the data for the 2.1μm radiation when plotted against the logarithm of the pulse fluence as this model clearly does not hold for that wavelength. However, it is possible to calculate from the results for the 2.94 μm light and the exponential model that the attenuation coefficient of 2.94μm light is 625 cm^{-1}, predicting a penetration depth in the region of 16μm. This is not in keeping with the expected penetration depth for 2.94μm light based on the attenuation characteristics of water[39] from which a penetration depth of about 1μm is expected. The result of this work suggests that the penetration depth is closer to that predicted for 10.6 μm radiation. Several phenomena may account for this larger than expected depth of which two may play key roles. Firstly, water constitutes only 60-80% of tissue mass. Thus, the attenuation coefficient is expected to be modified accordingly. Ignoring the attenuation characteristic of the non-water tissue constituents, the attenuation coefficient is expected to be in the range 600-800cm^{-1}, predicting penetration depths of between 12.5μm and 16.7μm in keeping with the result reported above. The second reason presented here as a possible explanation of the larger than expected penetration depth is the real increase in penetration depth which occurs as a result of mass removal during the pulse. The exponential model assumes that only the tissue in which the local fluence exceeds the threshold fluence for ablation will be removed. If tissue is removed during the pulse then some of the excess energy, the highlighted region in Figure 4.22 (a), may contribute to increasing the temperature of tissue which would otherwise be below the threshold fluence. Thus, the *effective* penetration depth is deeper than that anticipated.

From linear regression it is also possible to determine the threshold fluence for ablation. For 2.1μm radiation, using the linear model, this is 0.0475 J mm^{-2} while for the 2.94μm radiation the threshold is lower, being 0.00837 J mm^{-2} or 0.0227 J mm^{-2} for the linear and exponential models, respectively.

4.6 Conclusions

The attenuation of 2.1μm and 2.94μm radiation by biological tissue can be described by the Lambert-Bouguer Law due to the insignificance of scattering at these wavelengths. Under such conditions the residual thermal damage in tissue is expected to be minimal with most of the incident energy contributing to heating the tissue to its vaporisation temperature. A differential measurement method, known as the mass loss technique[45], was used to measure the amount of tissue removed by pulses of Fixed-Q laser radiation at 2.1μm and 2.94μm under a variety of operating conditions. The effect of increasing dose, pulse fluence and spotsize on the mass loss efficiency, MLE, (mass removed per unit of delivered energy) was investigated. Additionally, the MLE for fresh and coagulated tissue was investigated.

At 2.1μm the mass loss from tissue varied linearly with dose down to pulse fluences of about 0.075 J mm^{-2}. Below this level, mass removal proceeded mainly via dehydration rather than vaporisation leaving the tissue firstly coagulated and later charred. At these low fluence levels it was possible to obtain coagulation to a depth of 0.5-1.0mm at a delivered dose of 1.75 J mm^{-2}. This is an indication of the maximum vessel size for which haemostasis is likely to be achieved although platelet aggregation and the formation of embolisms at the elevated temperatures may increase this vessel size. These observations are in keeping with the practical observations of Treat et al[185]. The MLE was found to increase sublinearly with pulse fluence up to the maximum available fluences (0.5-0.8 J mm^{-2}).

In contrast, the rate of mass removed by pulses of 2.94μm was linear with dose only for fluences greater than 0.054 J mm^{-2}. Below this level the mass removed is only linear with dose over a small region at the start of the exposure (total dose less than about 7 J mm^{-2}). As the dose increases a rim of charred material is observed around the crater edge which extends as the dose increases until it eventually obscures most of the ablation site (for total doses greater than about 20 J mm^{-2}). Carbonised material prevents tissue from leaving the crater and, thereby, reduces the ablation efficiency at high doses. Thus, to achieve significant mass loss without charring it is necessary to operate at pulse fluences greater than 0.054 J mm^{-2}. The rapid attenuation of the low fluence light creates a disc of coagulation which appears to be less than 500μm thick, in keeping with the observations of previous workers[155,181] and indicating that haemostasis of all but the smallest capillary vessels is not achievable. Although deeper thermal penetration can be achieved by increasing the dose, it is at the expense of the surface tissue, which becomes charred. Thus, delayed healing and an increased risk of infection would be likely.

For exposure to 2.94μm pulse fluences less than 0.085 J mm^{-2}, the shape of the ablation crater is a 'U' shape, reflecting the spatial distribution of energy across the beam. However, above these fluence levels, the crater shape in cross-section changed, resembling a 'V' shape. This occurs even though the intensity profile remained unchanged. The efficiency with which the mass is removed does not appear to have been affected. However, the depth of the crater was noticeably increased while the diameter appeared reduced. This latter fact suggests that the tissue expands during the pulse which is in keeping with the observations of Cummings[183] who recorded expansion of the tissue to twice the diameter of the laser spot for fluences above 0.1 J mm^{-2}. Histological examination also reveals that tearing of the tissue occurs at these fluences, in keeping with other observations of Cummings. An increase in the extent of thermal tissue damage with fluence has also been reported in [47] and [188]. Although it was not possible to identify such effects in these experiments due to the *in vitro* nature of the experiments, it is accepted that hot debris ejected from the ablation site may become lodged into crevices in the side wall of the crater by expanding gases[193]. Thus, heat is deposited in the side walls and the extent of coagulation damage is increased.

To maintain efficient, controlled ablation using 2.94μm pulses, it is necessary, therefore, to operate in the narrow range of pulse fluences from 0.054 J mm^{-2} to 0.08 J mm^{-2}. These are typical results for a 2.9mm diameter beam and may vary slightly with spotsize. For larger spotsizes it was found that more efficient ablation may be achieved and that the threshold for this may also decrease with increasing spotsize. However, larger pulse energies, currently not easily achievable from Er:YAG lasers, would be required. For example, a 5mm diameter beam would require between 1.4 J pulse^{-1} and 1.8 J pulse^{-1} at the tissue surface in order to obtain optimal ablation conditions. Assuming a fibre optic beam delivery system with losses of 4% at each surface, zero absorption losses in the optics and without reconditioning optics at the fibre output, approximately 1.7 J pulse^{-1} to 2.2 J pulse^{-1} would be required.

A similar dependence of the ablation efficiency on the laser spotsize was observed for 2.1μm laser pulses. Because of the deeper penetration which promotes deeper thermal damage compared to the 2.94μm radiation, the MLE increases with fluence while the extent of the thermal damage zone would be expected to decrease. There is no evidence that changes in the ablation crater occur at elevated pulse fluences and, thus, there are no restrictions on the maximum recommended pulse fluence. Thus, as a general rule, to obtain the maximum ablation efficiency, high fluences ($>$0.4 J mm^{-2}) and large spotsizes are required. From the experimental data,

typical fluences of 0.3 J mm^{-2} to 0.5 J mm^{-2} are estimated to be the required fluence level for spotsizes of the order of 5mm. This necessitates individual pulse energies in excess of 20J. Although pulse energies near to these have been reported previously[32], such levels are not practicable due to the implied need for large power supplies and associated cooling apparatus. Additionally, optical damage would be more likely at such high fluences. Thus, efficient ablation of tissue by pulses of 2.1μm radiation, with minimal coagulation, will be restricted to small diameter beams.

For either 2.1μm or 2.94μm, the removal of tissue mass is not affected by the thermal history of the tissue for a given set of operating conditions (although this does not mean that the volume is the same). This suggests that tissue may be coagulated in advance of ablation. This would have the advantage of allowing operation in a relatively bloodless field, potentially decreasing the time of the procedure. While the 2.94μm light is approximately 25% more efficient at removing tissue, its high attenuation and increased precision means that it is not a suitable laser source for coagulating tissue. Thus, it would be necessary to combine the 2.94μm laser with another laser emitting light which penetrates deeply into tissue. This would most likely be a Nd:YAG laser operating at 1.06μm. The 2.1μm, CTH:YAG laser, however, may provide a compromise solution, although the maximum subsurface vessel diameter for which haemostasis could be reliably obtained would still be restricted to being less than 1mm in diameter.

Models of the ablation process have been described previously by Walsh et al[45] and have been applied by them to various tissue types using the 10.6μm emission of a TEA CO_2 laser. Using these models the experimental ablation results have been analysed. The results show that a simple linear model can be used to describe both 2.1μm and 2.94μm laser ablation, yielding values for the heat of ablation of 5.213 kJ g^{-1} and 4.09 kJ g^{-1}, respectively. A logarithmic relationship, based on the Lambert-Bouguer Law was also shown to fit the 2.94μm data. However, the fitting parameters suggested that the penetration depth of 2.94μm light in this tissue was approximately 16μm, significantly greater than that predicted by others[39]. The reasons for this were discussed. To determine beyond reasonable doubt whether the linear or logarithmic model of ablation best fits the results it would be necessary to take measurements over a greater than one order of magnitude range of pulse fluences which was not possible with the available apparatus.

CHAPTER 5

Ablation Efficiency and Energy Balance

5.1 Introduction

The physical process of tissue ablation is complex and not yet fully understood. Several factors have been shown to affect the ablation process both by previous authors[46,188] and in the preceding chapter of this thesis. Also, there are many other effects in tissue which consume energy but which do not lead to mass removal. However, it has not yet been possible to quantify the energy consumed in each of the processes. Consequently, the amount of energy converted to do useful work, i.e. tissue ablation, cannot be quantified. Quantification of the energy consumed in ablation would allow the calculation of an overall ablation efficiency against which all systems could be referenced. This factor is described here as the energy consumed solely in ablating tissue compared to the delivered energy. In agreement with convention, the efficiency is described in percentage terms. An ablation efficiency of 100% would indicate that all of the delivered energy was consumed in the ablation process and that, consequently, the maximum amount of tissue had been removed. Decreasing ablation efficiency would indicate that an increasing proportion of the delivered energy was being consumed in other processes. This efficiency differs from the mass loss efficiency, MLE, described in the preceding chapter of this thesis in that it is a dimensionless value and is a comparison between real and theoretical performance.

Energy delivered to tissue can be consumed in a number of processes. These processes are summarised in the following equality.

Energy Delivered = Ablation Energy (28)
+
Coagulation Damage Energy
+
Energy Consumed in Heating to Sub-Coagulation Temperatures
+
Other Energy 'Losses'

Specifically these losses are as follows;

Tissue Ablation Energy. Energy consumed in raising the local temperature of tissue to its vaporisation temperature, thereafter providing sufficient latent energy to cause tissue vaporisation. This is described in the equation

$$\text{Tissue Ablation Energy} = M[C(T_{vap}-T_{init})+L] \quad (29)$$

where M is the mass of tissue ablated, C is the specific heat capacity, T_{vap} is the threshold temperature for vaporisation, T_{init} is the starting temperature of the tissue and L is the latent heat of vaporisation. This is essentially the same as equation (25). Although T_{init} is easily determined T_{vap} is not known. As an approximation some authors have assumed T_{vap} to be the same as for water ($T_{vap}=100°C$)[171] while others have suggested that the tissue has to be heated to significantly higher temperatures[168] before vaporisation occurs. However, it is accepted that water in tissue will, ignoring colligative effects and any effect that pressure may have on the system, boil at 100°C. As tissue consists of between 60% and 80% water $T_{vap}=100°C$ is a reasonable figure to use. Additionally, some material may be removed at sub-ablation threshold temperatures by the explosive vaporisation of tissue water. The removal of tissue by this process depends on the tissue structure and the pulse fluence and cannot be described by thermal considerations alone.

Several researchers[154,155,184] have attempted to quantify the amount of energy required to raise a unit mass of tissue from its start temperature to the point where it vaporises. This quantity is known as the heat of ablation, H, and is described by the equation

$$H = C(T_{vap}-T_{init})+L \quad (30)$$

If the loss of laser energy to 'non-ablation causing' mechanisms is assumed to be negligible then H can be determined from mass loss measurements via equation (26).

Essentially, this assumption is valid for relatively weakly scattered, strongly absorbed laser beams and, additionally, assumes that all of the mass has been removed by the thermal process rather than by the explosive tissue vaporisation. This assumption was made in section 4.5 to analyse the dependence of mass loss on pulse fluence at 2.1μm and 2.94μm and was shown to be valid over the experimental ranges used in those experiments. Here pulse fluence has the same meaning as that defined in Chapter 4 and is the energy delivered per unit area of tissue in a single pulse. Table 5.1 summarises the published values of the heat of ablation for various tissues, including the values determined from the experimental work described in Chapter 4 using equation (27).

Authors	Wavelength μm	Tissue Type	Heat of Ablation kJ/g	Method	Ref.
This work	2.10	liver	5.21	Mass loss	
Nishioka et al	2.1	liver	9.09*	Mass loss	[155]
"	2.01	liver	8.82*	" "	"
Nishioka et al	2.1	liver	6.36*	Mass loss	[184]
This work	2.94	liver	4.09	Mass loss	
Walsh et al	2.94	skin	4.19	Mass loss	[46]
Dickinson et al	2.94	heart	7.0*	Mass loss	[154]
Hibst et al	2.94	pig skin	1.36*	Linear	[196]
Hibst	2.94	bone	3.23+	Mass loss	[190]
Nuss et al	2.94	bone	3.31+	Mass loss	[191]
Walsh et al	10.6	skin	3.87*	Mass loss	[45]

* Calculated from heat per unit volume and assuming tissue density is 1.1gcm^{-3}[155]
\+ Calculated from heat per unit volume and assuming bone density is 1.3gcm^{-3}[190]

Table 5.1 Published values of heat of ablation for various tissues

Coagulation Damage Energy. This is the energy which is consumed in raising the local temperature of tissue from its initial temperature, T_{init}, to the coagulation temperature and higher, but not to the point at which ablation occurs. This damage initially takes the form of tissue coagulation although with extended exposure this can turn to carbonisation. The work of Henriques[4] established that there is not a single temperature at which coagulation occurs but that there exists a time-temperature relationship, similar to the Arrhenius equation describing the rate of change in a chemical process. Additionally, the amount of energy consumed in the change to coagulation is not known but may also depend on the time-temperature conditions.

There are two main causes of temperature rise in tissue exposed to laser light. The first is direct heating as a result of absorption of the incident beam. The temperature profile resulting from this process is dependent on the spatial profile of the incident laser beam as well as the absorption and scattering properties of the tissue. For wavelengths where tissue absorption dominates over scattering, for example, in the mid-infrared region of the optical spectrum (1.5-20μm), the instantaneous temperature profile at the moment the laser light is absorbed is almost identical to the spatial profile of the incident beam. The attenuation of strongly absorbed light is described by the Lambert-Bouguer Law, equation (17). Figure 4.22 (a) shows the relative change in beam intensity with propagation for a beam obeying this relationship. The region below the ablated volume is the region of thermally altered tissue. The size of this zone will depend on the fluence of the pulse, the penetration depth of the laser wavelength and the duration of the exposure.

Laser energy converted to heat by the process of absorption creates a thermal gradient with the adjacent tissue and heat therefore flows away until the temperature of the two regions is equilibrated. This flow of heat to regions of tissue not affected by direct laser light absorption is the second cause of thermal tissue damage. Furzikov[12] describes the heat flow in a one dimensional case (an infinite spotsize) to produce equation (18). Here the characteristic time over which heat is dissipated depends on the square of the optical penetration depth. This implies that tissue heating caused by mid-infrared wavelengths, which have relatively short penetration depths in tissue due to water absorption, will be dissipated rapidly. In contrast, deeply penetrating wavelengths, such as the near-infrared 1.06μm emission from the Nd:YAG laser, yield long thermal relaxation times. Thus, heat resulting from absorption of these wavelengths must be given longer to diffuse away from the tissue immediately adjacent to exposed tissue otherwise cumulative heating effects can occur. The effect of thermal time constants is often cited as affecting the choice of laser repetition rate if cumulative thermal effects in tissue are to be avoided. Van Gemert and Welch[174] have considered the two dimensional case, assuming heat flow in radial and axial directions to be independent. The results of that work show that spotsize is also an important factor although the direction of heat flow must then be considered to assess the likely extent of thermal damage in each direction.

Energy Consumed in Heating to Sub-Damage Threshold Temperatures. The volume of tissue which is raised above its start temperature will be greater than the total volume visibly altered. Some tissue will be heated but not to high enough temperatures, or for long enough, to coagulate, char or ablate the tissue. The causes of temperature rise which lead to this effect are the same as those discussed above for

coagulation. Figure 4.22 (a) shows the zone of tissue for which the temperature has not reached the critical level for coagulation. Additionally, some of the laser energy will be absorbed by blood passing through the heated volume. If the energy deposited per unit volume is sufficient, then coagulation may occur according to the same principles described above. However, blood perfusion may also provide a route for the dissipation of heat. Matthewson et al[170], for example, noticed reduced thermal damage close to the hepatic artery during interstitial laser photocoagulation of the rat.

Other Energy 'Losses'. Energy is not strictly lost but may be dissipated in processes which do not contribute to the ablation process directly. An example of this is the energy consumed in deforming tissue. A reason for this effect has been suggested by Cummings[183] who explained observations of up to 100% crater expansion during laser ablation by proposing that the rapid expansion of vaporising tissue water forces the walls of the crater outwards. Thus, the expanding gases, fuelled by absorption of incident laser light, consumes laser energy to do work elastically deforming the tissue. The release of this potential energy is through the relaxation of the expanded tissue or, if the force is high enough, the rupture of tissue.

Energy will also be lost as a result of reflection from the tissue surface and backscatter from within the tissue. Fresnel's laws predict the amount of energy lost by reflection at the boundary between two dielectric media. Considering the interface between air and tissue (assuming $n_{tissue}=1.4$) yields an expected loss of less than 3% for a normally incident beam. However, Nishioka[165] has reported that reflection losses may be even greater than those predicted by the Fresnel equations. Measurement of the total amount of 633nm laser light rejected from the surface of tissue revealed that incident radiation may be lost by a combination of reflection from the tissue surface and light scattered from the bulk of the tissue. Nishioka et al[166] also investigated the transient changes in the total amount of 2.1μm light rejected from tissue during exposure to pulse fluences capable of causing coagulation. Although the amount of light rejected from the tissue at the start of a pulse was only about 8%, the amount rejected rose to as much as 18% by the end of the pulse, depending on the pulse fluence. Nishioka notes that this increase coincides with the change from fresh to coagulated tissue, indicating changes in the optical properties of the tissue. Although Nishioka does not identify the relative changes between the Fresnel reflection and the scattered component, the results of Essenpreis[5,162] suggest that increased scattering is responsible for this increase. With continued exposure, Nishioka observed that the rejection increased to a maximum of around 35%. Rejection of light via reflection and backscatter may, therefore, account for about one

third of the total delivered energy and, consequently, may account for the majority of any losses which are encountered.

Cummings[183] reports that ablation of tissue by high pulse fluences from the erbium laser can result in pieces of uncoagulated tissue being ejected in the plume. It is possible that reflection and scattering from these and the rest of the plume may also lead to loss of laser energy. Absorption by the plume is also a possibility. However, for 2.94μm, Walsh suggests that absorption by water vapour as opposed to bulk water is greatly reduced and the penetration depth in water vapour is increased to approximately 3.7mm. Thus, the loss due to absorption by water vapour is not considered to be significant. Golding[199] notes that, as a result of the formation of a heated gaseous plume above the tissue, refraction occurs which, under some instances, defocuses the incoming radiation. Such an effect would enlarge the spotsize and cause a corresponding decrease in the fluence at the tissue surface. A reduction in the fluence is likely to lead to increased thermal damage and reduced ablation.

If the laser pulse intensity is high, plasmas may be initiated which will shield the tissue surface from the remainder of the incident pulse. Walsh and Deutsch[46] report observing plasmas during the ablation of bone when exposed to pulse fluences above 25 J cm^{-2}. This coincided with a reduction in the mass loss efficiency and clearly indicated the effect of plasma blocking. This process is desirable during laser lithotripsy, during which an inverse Bremsstrahlung process results in absorption of the laser radiation causing rapid expansion of the plasma and the generation of a shockwave which can fragment the stone. However, this process represents a non-linear loss mechanism which will reduce the ablation efficiency.

Finally, some energy is provided to the ablated particles in the form of kinetic energy as they are driven away from the ablation zone. Hibst[190] has recently calculated the velocities of particles ejected from the surface of bone as it is ablated by pulses of 2.94μm radiation. Using the impulse delivered to a pendulum, he calculated that the average initial velocity of the particles was between 230 m s^{-1} and 280 m s^{-1}. Using mass loss data he concluded that less than 1% of the laser energy could be accounted for by the kinetic energy of the ablation products. No such assessments have yet been made for the ablation of soft biological tissue.

5.1.1 Ablation efficiency

The ablation efficiency, Σ_{tissue}, defined earlier, can be described in terms of the quantities discussed above as

$$\Sigma_{tissue} = \frac{\text{Tissue Ablation Energy}}{\text{Energy Delivered}} \quad (31)$$

Substituting equation (29) into equation (31) yields

$$\Sigma_{tissue} = \frac{M[C_{tissue}(T_{vap}-T_{init})+L_{tissue}]}{\text{Energy Delivered}} \quad (32)$$

However, many of the thermal coefficients are unknown, thereby making the efficiency impossible to calculate. If, however, tissue is assumed to have the thermal properties of water, and if it is assumed that, for a purely water target, all of the laser energy is consumed in the ablation process (as in the linear model shown to be appropriate earlier), then it is possible to write the denominator in equation (32) in terms of the mass of water that would be vaporised by the delivery of a unit of laser energy. Choosing for water, $C=4.18$ kJ $kg^{-1}°C^{-1}$, $L=2.26\times10^6$ J kg^{-1}[200] and assuming $T_{init}=20°C$ the expected mass of water vaporised per unit of delivered laser energy is 0.386mg. Thus, the ablation efficiency can be calculated by comparing the actual mass removed and the expected mass loss for a 100% efficient process. This is summarised in equation (33)

$$\Sigma_{tissue} = \frac{(MLE)}{0.386} \quad (33)$$

where MLE is the mass loss efficiency (in mg J^{-1}) derived from the results of the experiments detailed in the previous chapter and is equal to the mass of tissue removed, by all processes, per unit of incident laser energy.

5.2 Experimentally Determined Ablation Efficiency

The ablation efficiency was calculated for the 2.1μm and 2.94μm laser pulses using the data shown graphically in Figures 4.8 and 4.10. The results of this analysis are shown in Figure 5.1. The figure shows the mass loss efficiency data for each

wavelength and also compares the average MLE against the maximum expected for a pure water target. The change in MLE with laser spotsize and pulse fluence has been discussed earlier and would obviously be applicable to this data. For simplicity, though, only one set of data at each wavelength is presented, the previous chapter providing fuller details for each laser spot size. The analysis carried out on the data in the figure reveals that the ablation efficiency attains an average maximum value of 47.9±2.1% and 59.3±3.2% for the 2.1μm and 2.94μm pulses, repectively.

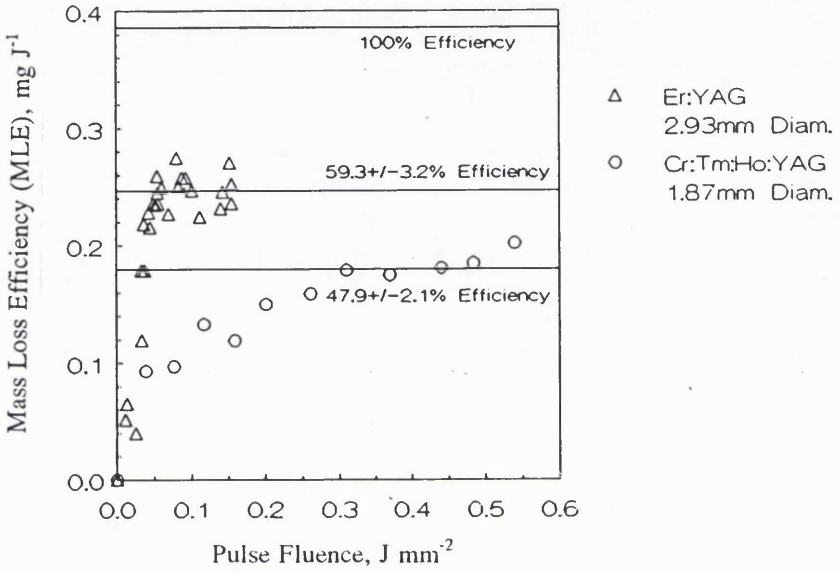

Figure 5.1 Change in mass loss efficiency with pulse fluence at 2.1μm and 2.94μm, the maximum average MLE attained at each wavelength also being expressed as a percentage of the maximum MLE expected for a water based target.

The efficiency of the 2.94μm pulses is approximately one third greater than that obtained at 2.1μm. From simple considerations of the ablation process, the speed of the ablation front, u, is, as shown by McKenzie[171]

$$u = \frac{P}{A\rho(C\ T+L)} \qquad (34)$$

Here, P is the laser power, A is the cross-sectional area of the laser spot (assumed to be irradiated uniformly), ρ is the tissue density and the other symbols have the meanings described earlier. Therefore, the mass loss for a pulse incident on the tissue for a fixed length of time will be

$$\text{Mass Loss} = \rho u A t_p = \frac{P t_p}{(C\Delta T + L)} \qquad (35)$$

where t_p is the laser pulse duration. Thus, the attenuation coefficient, α, plays no role in determining the mass of tissue removed. The results of the ablation efficiency calculations show that this is clearly not the case. The reason for this difference must lie partly in the inadequacies of the general assumptions made, but mainly to the fact that the model applies to a state of equilibrium. When equilibrium is achieved during the exposure the mass removed per unit energy remains constant. Thus, the MLE remains constant with increasing fluence. This is seen experimentally for the 2.94μm light. Here, sub-maximum ablation efficiencies are measured for pulses where non-equilibrium conditions exist for all or a significant portion of the pulse. In contrast, the mass loss efficiency for the 2.1μm light does not reach a clear maximum over the range of available fluences. Thus, it can be concluded that equilibrium conditions are not achieved for these pulses. As all tissue must first be heated to the ablation temperature before being vaporised (assuming all tissue mass is removed by purely thermal processes) then the time taken to reach the vacuolated state (tissue at the ablation temperature) is an indication of the time taken for the tissue to be vaporised. McKenzie derives, t_{vac}, the time taken to reach equilibrium in the vacuolated zone to be

$$t_{vac} = \frac{3L\rho}{\alpha P} \qquad (36)$$

which is dependent on the optical penetration depth in the tissue. The experimental results support the argument that only ablation with pulses of 2.94μm at fluences above 0.05 J mm^{-2} reach equilibrium during the pulse and that, for conditions where equilibrium is not achieved during each pulse, penetration depth determines the relative ablation efficiency of different wavelengths. Comparing the results for the two wavelengths, the energy delivered at 2.1μm but which does not lead to tissue ablation must contribute to heating the tissue to sub-ablation threshold temperatures. A simple comparison of the data suggests that, assuming no other loss mechanisms occur which are specific to either wavelength, at least 17% of the delivered laser energy is consumed in this process

If the pulse energy at 2.1μm were to be increased further, then the time to reach equilibrium would decrease and, as a result, the ablation efficiency would be expected to increase. Thus, the percentage of the delivered energy 'wasted' would be reduced. Increasing the power density has the same effect as reducing the

absorption depth. This may be achieved by switching the wavelength to one which is more strongly absorbed. 2.94μm is the solid state laser wavelength most strongly absorbed by water, and hence tissue. The ablation efficiency at this wavelength rapidly reaches its maximum. As the depth of thermal tissue damage is small, the energy consumed in thermally damaging the tissue is small compared to the ablation energy. Thus, ablation using 2.94μm laser light represents a maximum efficiency which 2.1μm laser pulses can only obtain at very high fluences. The energy consumed by thermally damaging tissue using 2.94μm light is so small that any reduction in the thermal damage at this wavelength would probably not lead to a significant increase in ablation efficiency.

5.3 Laser Energy Converted to Kinetic Energy

5.3.1 Introduction

Energy is transferred to the material ejected from the ablation crater via a number of routes. It is feasible that the ejected particles may absorb the incoming laser radiation, causing them to be ignited. Alternatively, the particles may scatter incident radiation onto areas where the local fluence lies below the ablation threshold, possibly extending the damage zones. Also, the gaseous plume may refract the incident light, leading to the same effect[199]. Recently, Hibst[190] has measured the average velocity of the ejecta from the surface of bone during ablation by 2.94μm radiation. He concluded that the velocities lay in the range 230 m s^{-1} to 280 m s^{-1} yielding a value for the total kinetic energy of the particles of less than 1% of the delivered energy. It is possible that some particles within the plume are supersonic. Zweig[194] and Cummings[183] note that the material properties play an important role in determining the ablation rate and recoil. Thus, it is possible that supersonic velocities may be obtained for other tissue types.

The velocity of the fastest particles leaving the surface of the soft tissue during ablation by 2.1μm and 2.94μm laser pulses was measured over a range of fluences. The results allowed calculation of the maximum amount of energy 'lost' in the form of kinetic energy. Additionally, they allowed speculation on the likelihood of supersonic particle velocities from the collected data.

5.3.2 Experimental technique

Fresh tissue samples were placed on a stack of microscope slides, the cumulative thickness of which had been determined using a set of calibrated vernier calipers. The laser output was directed vertically downwards onto the tissue at a spotsize of between approximately 2mm and 4mm. The laser was operated at a fixed repetition rate of 5Hz. Although repetition rate was unlikely to influence the result, the maximum pulse frequency allowed by the average power handling ability of the power supply was selected in order to maintain laser stabilty as well as to maximise the pulse energy (see Chapter 2 and Chapter 3). The pulse energy was varied, in the case of the 2.94μm laser beam by the addition of glass slides which absorbed energy according to the thickness of the stack of slides. This technique, as used by others[46], had the advantage of reducing the energy without changing its distribution. The 2.1μm radiation could not be so easily attenuated due to its higher transmission by the microscope slides. Thus, changes to the pulse fluence were made by a combination of small alterations in the flashlamp discharge energy and the addition of glass slides. Inspection of the burns obtained on burnpaper suggested that, by this technique, changes in the fluence could be obtained without noticeable changes in the laser beam diameter or top-hat intensity profile.

The spotsize was initially assessed over a 10mm depth of field using burnpaper. While this was accurate enough to determine the constancy of the spotsize it was necessary to measure the spotsizes again later to determine the 90% beam diameter and, hence, allow calculation of the pulse fluence. This was done using the variable aperture method described in Appendix 3. A 633nm HeNe beam was directed horizontally above the surface of the tissue sample and towards a silicon photodiode. This probe beam was aligned to pass across the centre of the exposure site. The use of the larger diameter 2.1μm and 2.94μm beams, made possible by the improved pulse energies available from the lasers, meant that the diameter of the probe beam was small compared to the diameter of the ablated area, thus making positioning of the probe beam easier. In front of the photodiode, the beam passed through two slits apertures separated by about 75mm to minimise scattered and reflected light reaching the detector. The photodetector was connected directly to the 50Ω input of a Gould 465, 100MHz, 200 MS s^{-1} oscilloscope. The oscilloscope was triggered by the laser power supply. A second photodiode monitored either the flashlamp emission in the case of the erbium laser or the laser output, via a beam splitter, in the case of the holmium laser (see, for example, Figure A2.7a). A schematic of the experimental setup is shown in Figure 5.2.

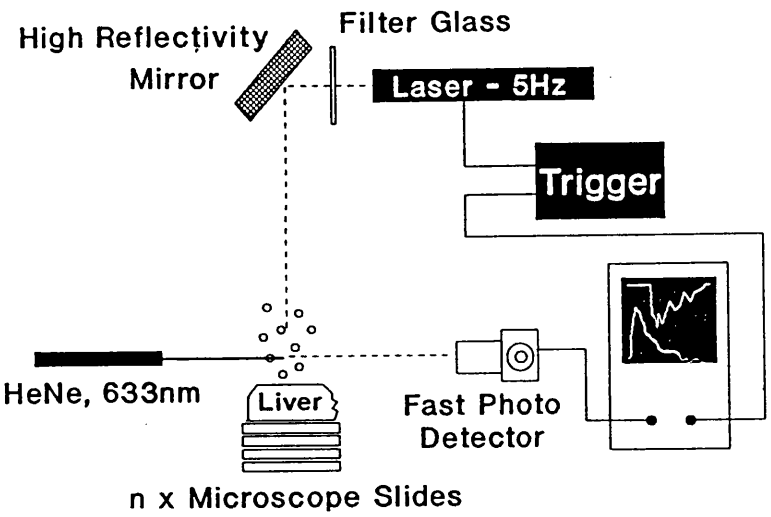

Figure 5.2 Experimental configuration for measuring the velocity of the laser plume.

Exposure of the target tissue to the laser pulses caused ablation. The passage of the ejected material through the HeNe beam could be detected by the disruption of an otherwise constant output from the fast photodetector. The delay between the start of optical emission from the laser, which coincided with the triggering of the oscilloscope to within $\pm 1\mu s$, and the first signs of interference of the HeNe beam indicated the arrival of the first particles of the plume. Figure 5.3 shows a typical trace obtained during exposure to the laser pulses. To ensure that only the time taken for particles leaving the plane of the tissue surface were recorded, the measurements were always carried out on a previously unexposed area of tissue and were always recorded within the first 1-2 seconds of the exposure. To ensure that the laser was stable during this period, the laser was operated for at least 10 seconds prior to the exposure. An extra-cavity mechanical shutter was inserted in the beam path for this purpose.

The oscilloscope trace of the photodiode output shows that the first feature occurs some time after the start of the laser pulse. Also, this feature possesses two distinct frequencies, the first being at a higher frequency. The first, 'high frequency' part of this feature was attributed to particulate material passing through the beam while the low frequency part was attributed to the effect of smoke. No attempt was made to determine the size of the particles from the frequency of the modulation although, with the velocity measurements and knowledge of the probe beam size, such a calculation would be possible.

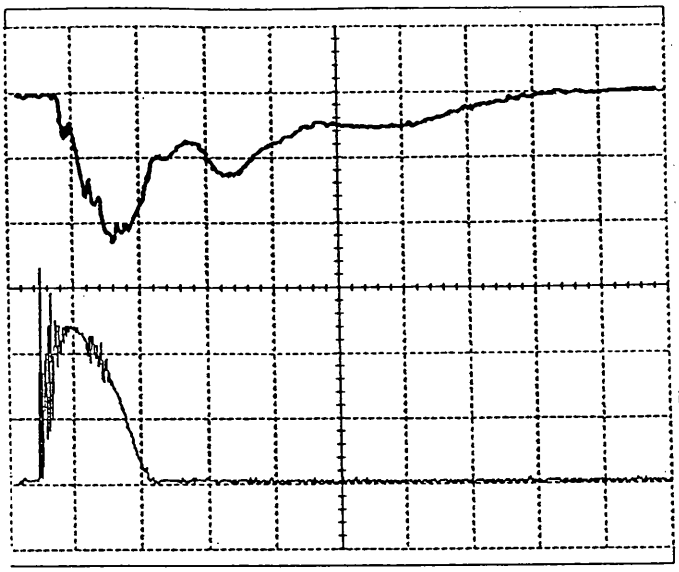

a) 200μs/division

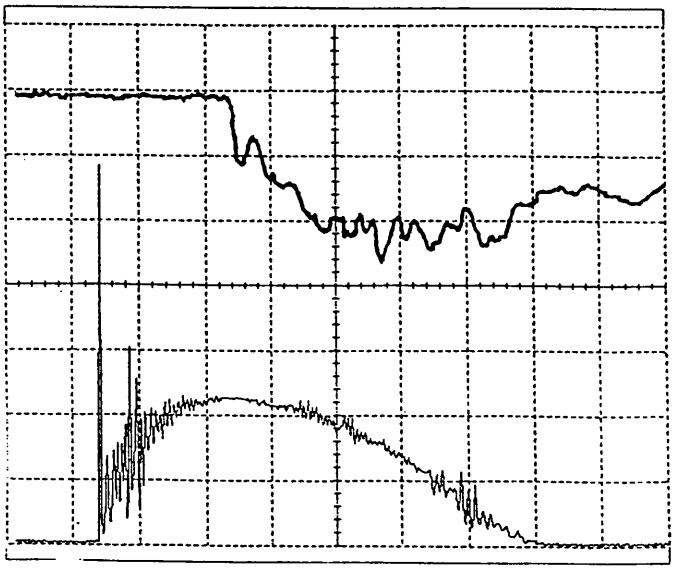

b) 50μs/division

Figure 5.3 Typical oscilloscope traces obtained during measurement of the ablation plume velocity. The lower line of each trace is the temporal profile of the Fixed-Q laser pulse while the upper line shows the changes in intensity of the 633nm probe beam due to the passage of ejected particles through it.

The experiment was repeated a number of times using a single piece of tissue to maintain a constant surface height above the glass supporting slide. However, prior to each measurement, successive slides were removed. Thus, the distance travelled by the ejected particles increased by a known distance for each

measurement. The data was then plotted as characteristic delay against slide thickness. A typical set of results for the 2.94μm laser pulses is shown in Figure 5.4.

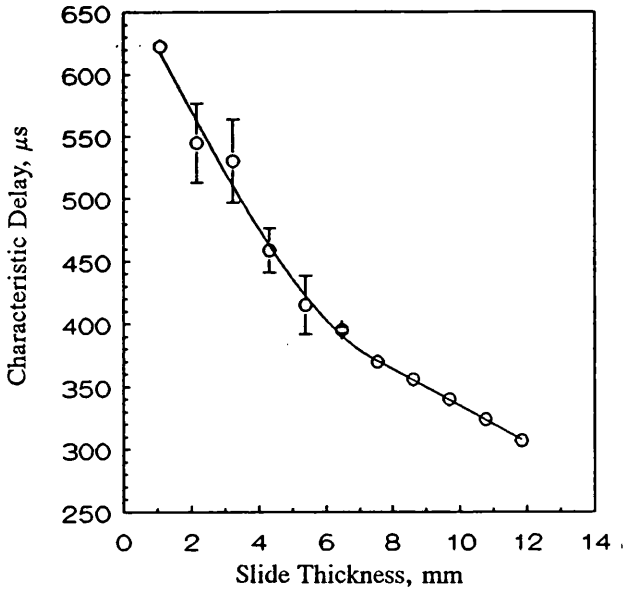

Figure 5.4 Typical result of measuring the delay between the start of the laser pulse and the first indication that ejected particles had passed through the probe beam, the number of microscope slides being changed to vary the vertical distance between the tissue surface and the probe beam. The results shown are for 2.1μm light and a pulse fluence of 0.57 J mm^{-2}.

The figure shows that for slide thicknesses greater than 7mm, the characteristic delay decreased with increasing thickness. These data points represent the region where the tissue surface is closest to the probe beam (less than 1mm away for a slide thickness of about 12mm) and the increment in delay time is simply the extra time taken to traverse the extra distance introduced by the removal of a supporting slide. Thus, the velocity of the particles may be obtained by taking the inverse of the gradient of the straight line fit for data points in this region. It was noticeable that the characteristic delay increased as the distance between the probe beam and the tissue surface increased. Also, the uncertainty in the measurement increased, as determined by repeating the measurement several times. The increase in delay time with increasing separation was attributed to either the particles slowing down under the influence of gravity, or the passage of smoke through the probe beam, the particles failing to reach this height.

The experiment was repeated at different pulse energies to determine the effect of fluence on the velocity of the particles. Several measurements were made at each set of laser parameters in order to determine the repeatability.

5.3.3 Results

Figures 5.5 (a) and 5.5 (b) show sample sets of results for exposure to 2.1μm and 2.94μm laser pulses, respectively. In contrast to Figure 5.4, the data is plotted as slide thickness against characteristic delay, so that the velocity is the gradient of the straight line fit, rather than the inverse gradient.

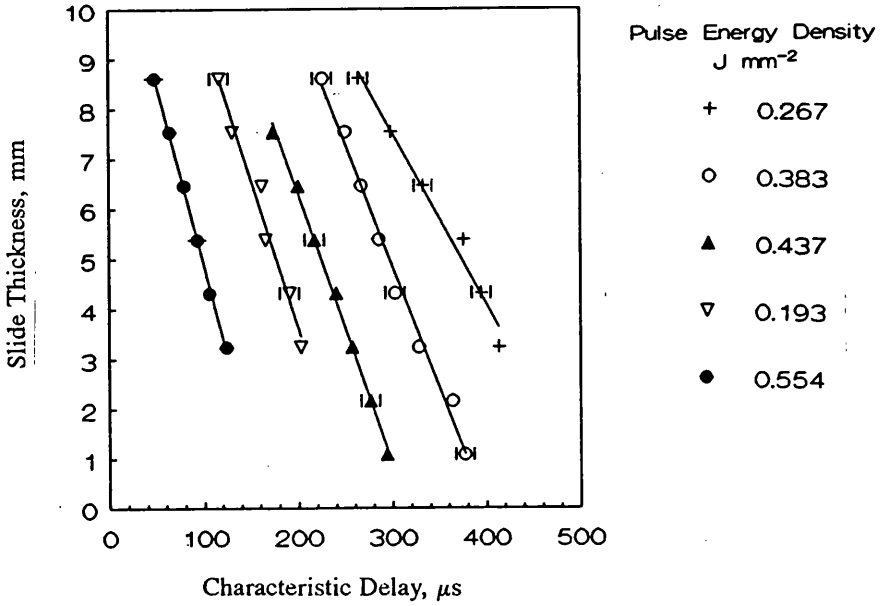

(a) CTH:YAG - 2.1μm

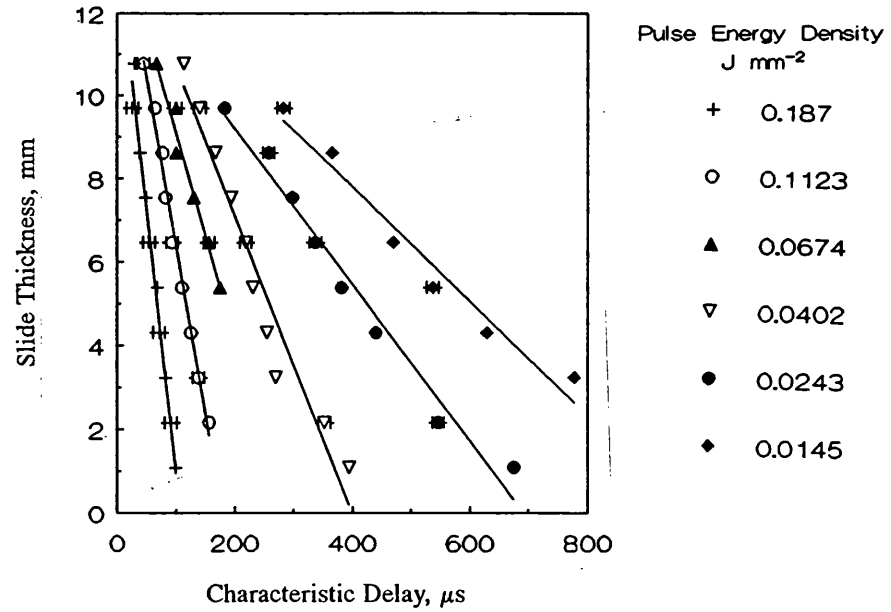

(b) Er:YAG - 2.94μm

Figure 5.5 Typical data obtained in the measurement of characteristic delay at various cumulative slide thicknesses.

The velocities calculated from data obtained over a range of pulse fluences is plotted for both laser wavelengths in Figure 5.6. A straight line fit has been applied to the data to obtain the change in particle velocity with pulse fluence. For ablation by 2.94μm radiation, the velocity of particles appears to increase linearly with the pulse fluence at a rate of 536.7$\pm$41.2 (m sec^{-1})(J mm^{-2})$^{-1}$. The velocity attained by the ejecta during ablation at 2.1μm also appears to increase linearly with pulse fluence, although at a lower rate of 101.4$\pm$22.2 (m sec^{-1})(J mm^{-2})$^{-1}$.

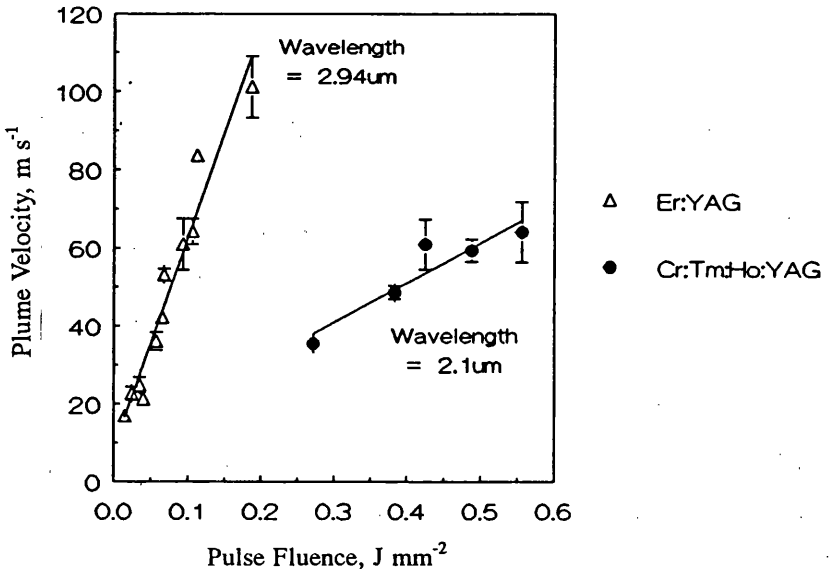

Figure 5.6 Results of calculating the change in maximum ejected particle velocity from the time-of-flight measurements made for 2.1μm and 2.94μm laser pulses.

5.3.4 Discussion

The variation in ablation velocity with pulse fluence appears to follow a linear relationship over the experimental ranges. Although there is no supporting theory to explain this observation, this relationship is, perhaps, intuitively understandable. The particles whose velocities have been determined are those leaving the tissue at the start of the ablation process. Thus, they originate from a location where the pulse fluence has not been reduced, either by attenuation as the beam propagates into the tissue, nor by the attenuation by previously ejected material. However, there is clearly a difference between the results of measurements for 2.1μm and 2.94μm light, indicating that optical penetration depth plays a role in determining the ablation velocity. This suggests that the effect is dependent on the energy deposited per unit volume of tissue. Thus, it is proposed that the relationship between ablation velocity, v_{abl}, and pulse fluence, E_A, has the form

$$v_{abl} = GE_A\alpha \quad (37)$$

where G is a constant of proportionality. Here, α is the attenuation coefficient of the laser wavelength in tissue.

If one considers that the percentage of the pulse energy converted to kinetic energy is constant, and if it also assumed that ablation efficiency is constant with increasing fluence, then the velocity must vary as the square root of fluence. Over the experimental range there is no evidence of this. It may be inferred from equation (37) that the kinetic energy of the particles in the plume will increase with the square of the pulse fluence. This would infer that an increasing proportion of the delivered energy is converted to kinetic energy with increasing fluence. In the limit all the laser energy would be converted to kinetic energy. Clearly this cannot happen in practice because some energy has to be expended on producing the plume.

The possibility of ejected particles travelling at sonic velocities has been considered. If it is assumed that the linear relationship between velocity and fluence holds for all pulse fluences, then the particles would attain sonic velocities at fluences of about 3 J mm^{-2} and about 0.6 J mm^{-2}, for 2.1μm and 2.94μm light, respectively. For a 1mm diameter beam of uniform intensity distribution, the pulse energy required to produce sonic particles velocities would thus be about 2.5J and about 0.5J, respectively. While the former figure, for the 2.1μm radiation, is somewhat higher than the typical pulse energies attained by a practical system, the figure for the 2.94μm radiation is well within the range achievable in practice. Thus, it is reasonable to suggest that sonic velocities may be attained by the ablation products produced by the more highly absorbed laser wavelengths.

The maximum fraction of incident laser energy converted to kinetic energy, assuming that all of the ablated mass is ejected at the same velocity as that measured, can be easily calculated using the results of the velocity measurements and the mass loss experiments using the equation

$$\frac{\text{Kinetic Energy}}{\text{Delivered Energy}} = \tfrac{1}{2}(MLE)v_{abl}^2 \quad (38)$$

Figure 5.7 shows the results of this calculation using the results for MLE reported in the previous chapter ($MLE_{2.1\mu m}$=0.185 mg J^{-1}, $MLE_{2.94\mu m}$=0.229 mg J^{-1}). The fraction of delivered energy converted to kinetic energy has then been converted to a percentage, in keeping with the results of the analysis presented in Figure 5.1. The

resulting curves show that the amount of energy converted to kinetic energy is extremely small, less than 0.05% for the 2.1μm pulses and less than 0.2% for the 2.94μm pulses. The curve for the 2.94μm radiation is extended to include pulse fluences beyond the experimental range where the assumption is made that the linear relationship between fluence and particle velocity continues. This demonstrates the changes to in the conversion of delivered laser energy to kinetic energy with increasing fluence. The values for 2.94μm light are approximately 20% of those measured by Hibst[190] for particles ejected from bone tissue during laser ablation. The differences being due to both larger velocities and more efficient mass removal. The difference in tissue type is also expected to have a significant influence because of large differences in their mechanical properties[183]. While the technique employed for the work described in this thesis is likely to give inherently more accurate results, the conclusions drawn from both works is the same. That is, the pulse energy converted to kinetic energy represents only a small fraction of the total delivered energy and is, therefore, not a major cause of energy loss.

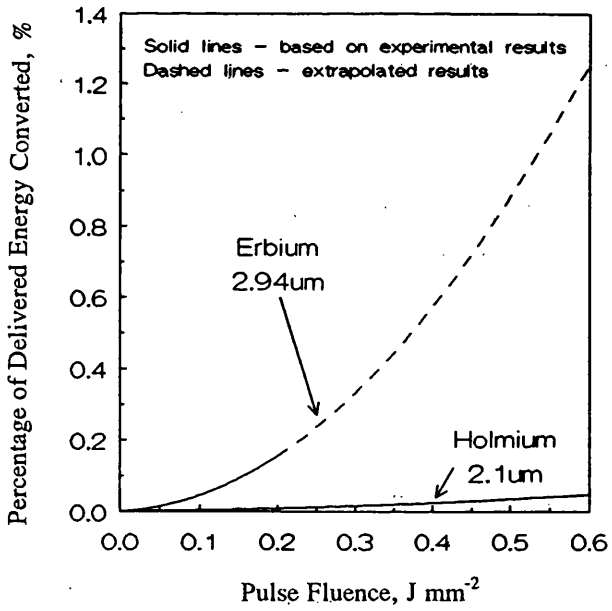

Figure 5.7 Calculated change in percentage of laser pulse energy converted to kinetic energy with pulse fluence at 2.1μm and 2.94μm.

5.4 Scattering/Reflection Losses from the Ablation Plume

5.4.1 Introduction

Essenpreis[5] has reported that the optical properties of tissue change as the tissue is coagulated. The increase in scattering is responsible for a greater rejection of light from the tissue and the whitening of tissue observed during coagulation. There is no evidence that coagulation changes the refractive index of the tissue and hence the Fresnel reflection at the tissue surface, although such an effect is likely since the tissue dehydrates as it is heated. Nishioka has measured the amount of light rejected from tissue at 633nm[165] and 2.1μm[166]. At 633nm approximately 42% of the incident light was reflected or scattered from non-coagulated oesophageal tissue for a normally incident beam. At 2.1μm the total rejection of pulsed 2.1μm laser light was found to vary according to the state of the tissue. Only 8% was rejected from the tissue prior to coagulation although this rose to about 35% as the tissue coagulated. When Nishioka attempted to identify changes in the rejection of light occuring during a pulse he found that at high energy pulses the amount rejected was 5% greater than the amount measured using low intensity pulses. Nishioka suggests that the increased 'reflectivity' at high fluences was due to either transient thermal effects on the optical properties of the tissue or scattering from the ablation products.

The source of the transient reflection observed by Nishioka was investigated in the work reported here by monitoring the temporal profile of the light reflected from the ablation site and comparing it to the temporal profile of the delivered laser pulse.

5.4.2 Experimental technique

Tissue samples were placed on a platform and irradiated by laser pulses directed vertically downwards at normal incidence. The laser was initially operated at 2.1μm using the CTH:YAG rod and later at 2.94μm using the Er:YAG rod. The pulse repetition frequency was 5Hz at all times and to ensure a measurable signal the pulse energy was the maximum available. The spotsize was approximately 2.5mm in diameter. No attempts were made to accurately determine the pulse fluence as the intended measurement was qualitative rather than quantitative. The InAs photodetector was positioned approximately 50cm from the tissue surface, oriented to face the area of the tissue exposed to the laser radiation. The position of the detector was such that an angle of about 10° was subtended between the normally incident beam and the direction of any reflected rays incident on the detector. Fresh areas of tissue were then exposed to pulses of laser light at fluences expected to cause

ablation (>0.3 J mm^{-2} and >0.1 J mm^{-2} for 2.1μm light and 2.94μm light, respectively). The temporal profile of light reflected or scattered from the tissue was then displayed on a Gould 465 digital storage oscilloscope and compared with the temporal profile of the laser pulse, obtained using a beam splitter and photodiode. The angular separation between the normally incident beam and the detector was then increased to approximately 50° and the measurements repeated. Figure 5.8 shows the experimental configuration.

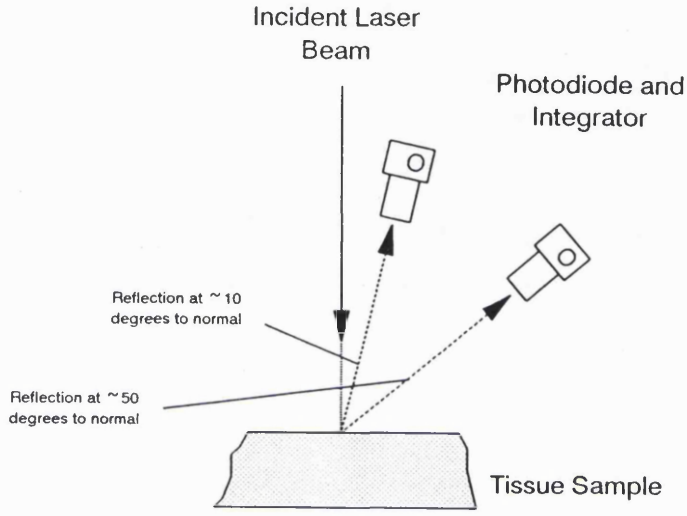

Figure 5.8 Experimental configuration for monitoring the laser light reflected from the ablation plume into different angles.

The detector was then relocated to a position below the tissue surface such that any light reflected from the tissue surface would have been unable to enter the detector, being blocked by the tissue. In contrast, light reflected or scattered from the plume above the tissue surface would still be detected. At least 10mm of tissue separated the direct line of site between the exposed surface and the detector to ensure that light scattered through the tissue and reaching the detector was minimal. To further confirm that the light monitored by the detector originated above the tissue without passing through the tissue at any stage, an opaque screen was placed between the laser beam and the detector which, when lowered to be in contact with the tissue, would block only light originating above the tissue, causing the signal to disappear. The experimental setup is shown schematically in Figure 5.9.

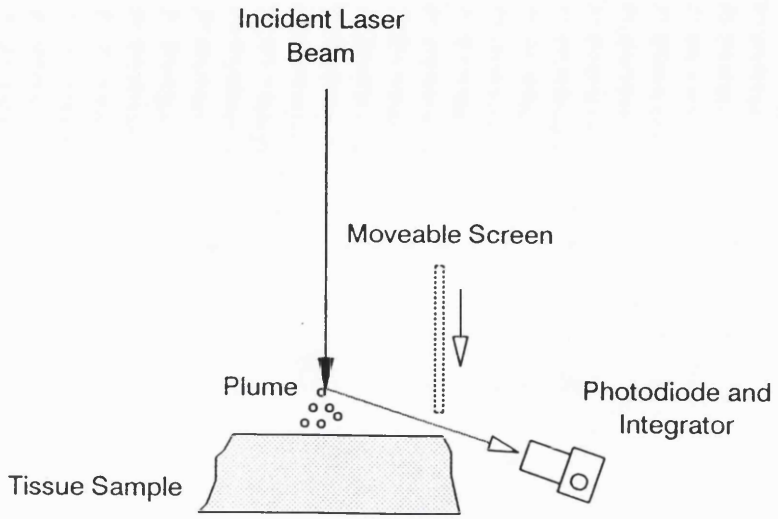

Figure 5.9 Experimental configuration for monitoring the laser light reflected from the ablation plume into angles greater than 90° and therefore originating above the tissue surface.

5.4.3 Results and discussion

The temporal profiles of the 2.1μm and 2.94μm laser pulses are shown in Figure 2.36 and Figure 5.10, respectively.

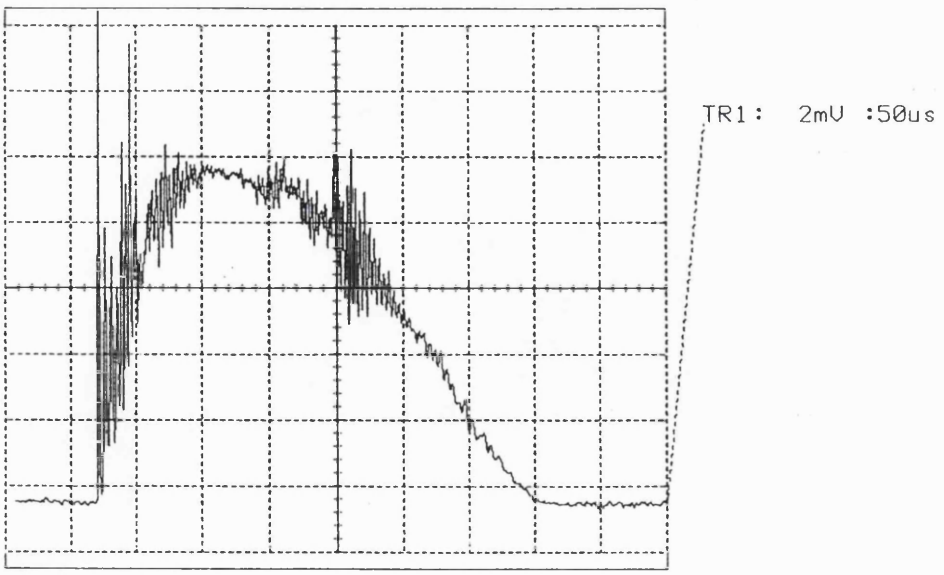

Figure 5.10 Typical temporal profile of the output laser pulse at 2.94μm.

Both pulses displayed similar temporal profiles, although the 2.1μm pulse showed slightly more modulation. This was probably due to the relatively lower pump level (for a pump pulse of about 100J, r=2 for the CTH:YAG laser compared to r=3 for the Er:YAG laser). Figure 5.11 shows the temporal traces of the reflected/scattered signals for the case of the 2.94μm laser pulses incident on tissue at a fluence of approximately 0.12 J mm^{-2}. The detector in this instance was about 10° to the normal. The first trace is the signal obtained during the first few seconds of the laser exposure while the second trace was obtained after an exposure of 20-30 seconds.

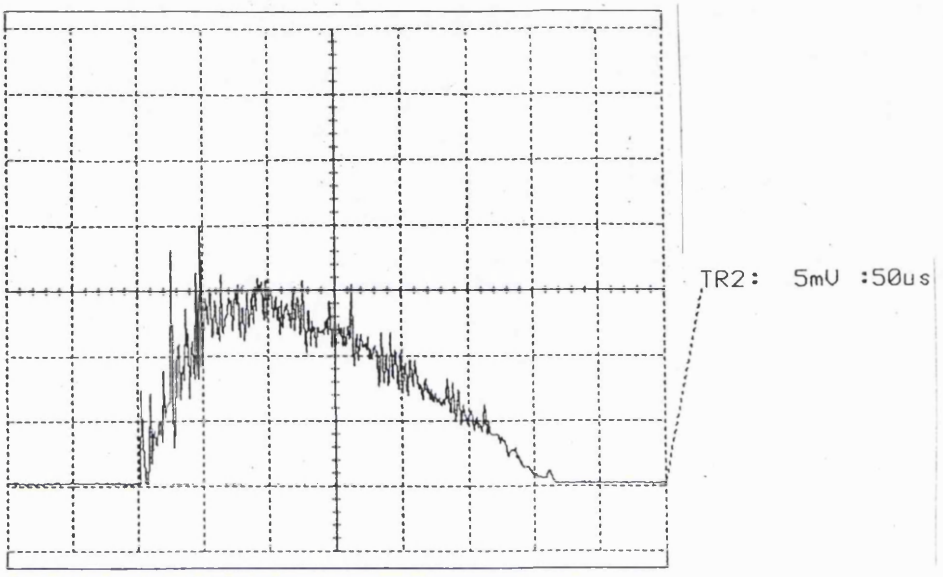

a) After about 3 seconds exposure.

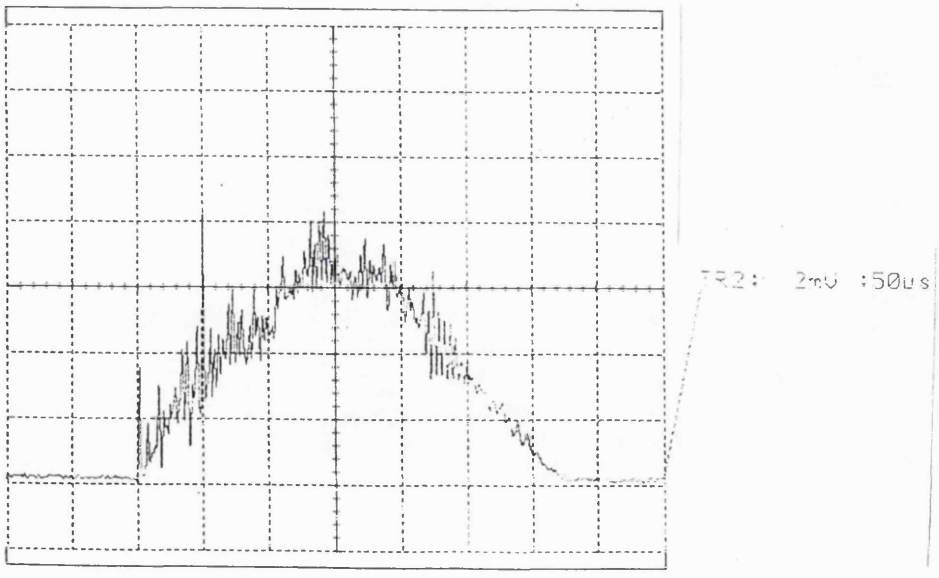

b) After about 20-30 seconds exposure.

Figure 5.11 Temporal profile of laser light reflected and scattered from or near the tissue surface into an angle of about 10° to the normal during pulsed laser ablation of tissue at 2.94μm. The pulse fluence was about 0.11 J mm^{-2}.

It appears that, in both cases, the intensity of the leading edge of the laser pulse had been reduced, suggesting that, until some of the laser energy had been delivered, the source of reflection or scatter did not exist, or was not suitably directed. Figure 5.12 shows the signals monitored by the detector at approximately 50° to the normally incident beam, but in all other respects under the same operating conditions.

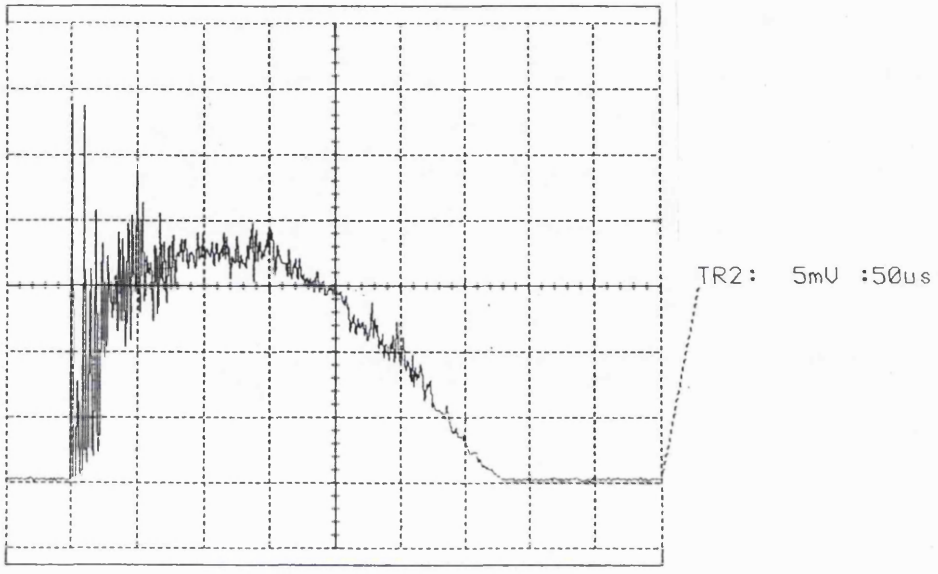

a) After about 3 seconds exposure.

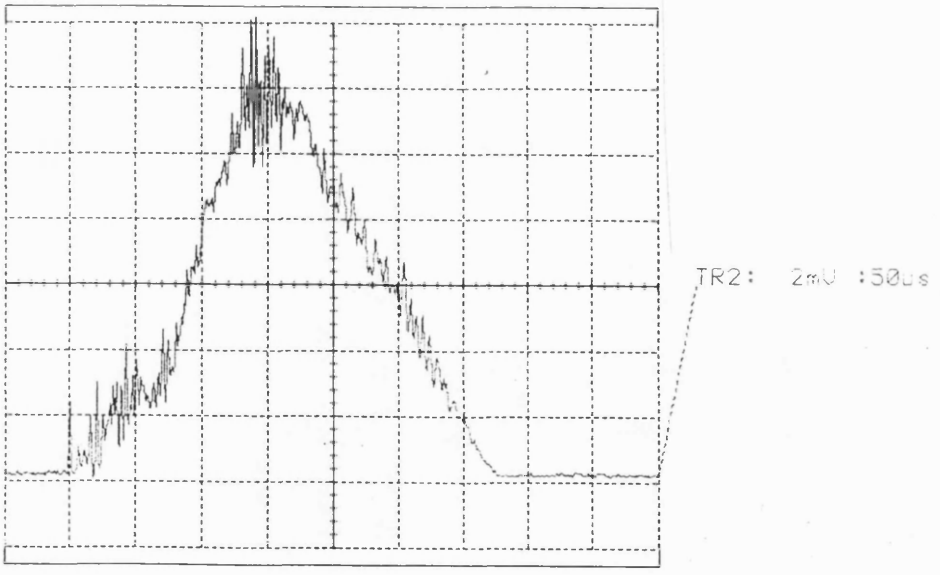

b) After about 20-30 seconds exposure.

Figure 5.12 Temporal profile of laser light reflected and scattered from or near the tissue surface into an angle of about 50° to the normal during pulsed laser ablation of tissue at 2.94μm. The pulse fluence was about 0.11 J mm^{-2}.

In this instance, it is noticeable that, for the light detected during the first few seconds of the exposure, the temporal profile of the Fixed-Q pulse is faithfully reproduced by the detector. However, the signal obtained 20-30 seconds after the beginning of the exposure displays the same loss of the leading edge of the pulse. The implication of this and the preceding figure are that a transient amount of reflection or scatter was occurring, in keeping with the results of Nishioka[166]. Initially, light was reflected and scattered from the uncoagulated surface of the tissue. However, during each pulse a transient source of reflections and scatter is generated which directs some of the pulse away from the tissue. If tissue heating is assumed to be responsible for the change in optical properties, then it is reasonable to assume that these changes would happen only once. That is, after the first few pulses have been delivered, the ablation front would move into the tissue simultaneously moving a fixed thickness coagulation front ahead of it[171]. Although each ablating pulse must remove part of the coagulated zone, it is not expected that all of the coagulated zone is removed to expose fresh underlying tissue. However, such behaviour is possible and cannot be ignored.

Figure 5.13 shows the temporal profiles recorded under the same conditions as those in Figure 5.12, with the exception that the pulse fluence was reduced to approximately $0.05 J mm^{-2}$. Under these conditions, only tissue coagulation was observed. The traces do not display the same attenuation of the leading edge of the laser pulse, despite the change in optical properties of the tissue. Thus, it can be concluded that some of the laser pulse energy is lost via normal reflection and/or scattering processes, but that there is also a second effect which is responsible for the change in temporal profile during ablative pulses. This second effect may be caused by either the plume or the exposure of underlying uncoagulated tissue, or the effect of laser plume.

The trace obtained from the detector under the experimental conditions shown in Figure 5.9 reveals the true source of the modifications to the temporal profile of the reflected/scattered pulse, Figure 5.14. The trace was obtained at the start of the exposure and at a fluence at the tissue surface of about $0.185 J mm^{-2}$, a level at which tissue ablation was certain to occur. The loss of the leading edge of the pulse profile is consistent with the earlier observations. Later traces displayed the same temporal profile but at reduced intensities. To check that the signal did not arise from light propagating through the tissue, the opaque card was introduced (see Figure 5.9) to ensure the signal disappeared completely.

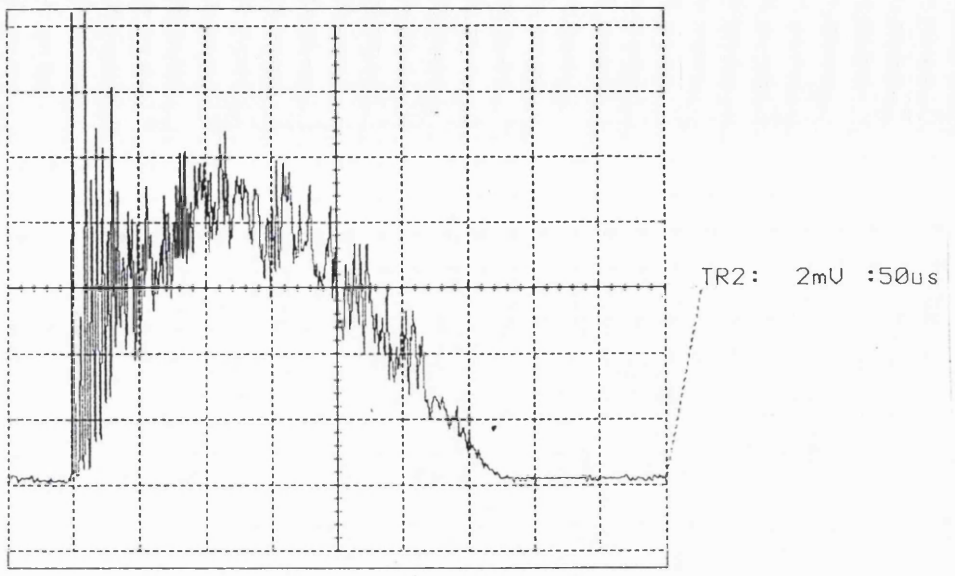

a) After about 3 seconds exposure.

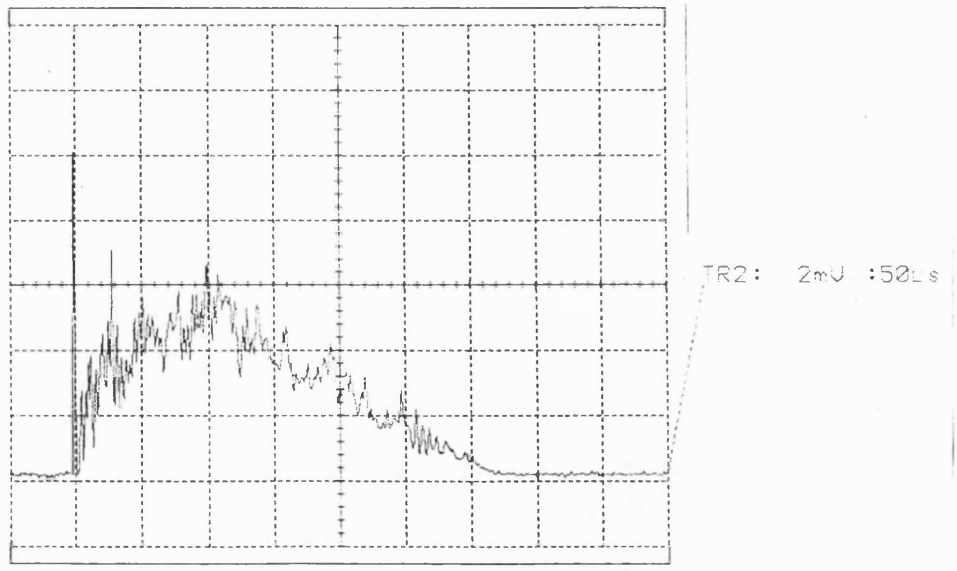

b) After about 20-30 seconds exposure.

Figure 5.13 Temporal profile of laser light reflected and scattered from or near the tissue surface into an angle of about 50° to the normal during pulsed laser ablation of tissue at 2.94μm. The pulse fluence was about 0.046 J mm^{-2}.

Thus, although changes in the optical properties undoubtedly modify the rejection of incident light at all intensities, the temporary formation of a plume of debris above the tissue increases this energy loss mechanism.

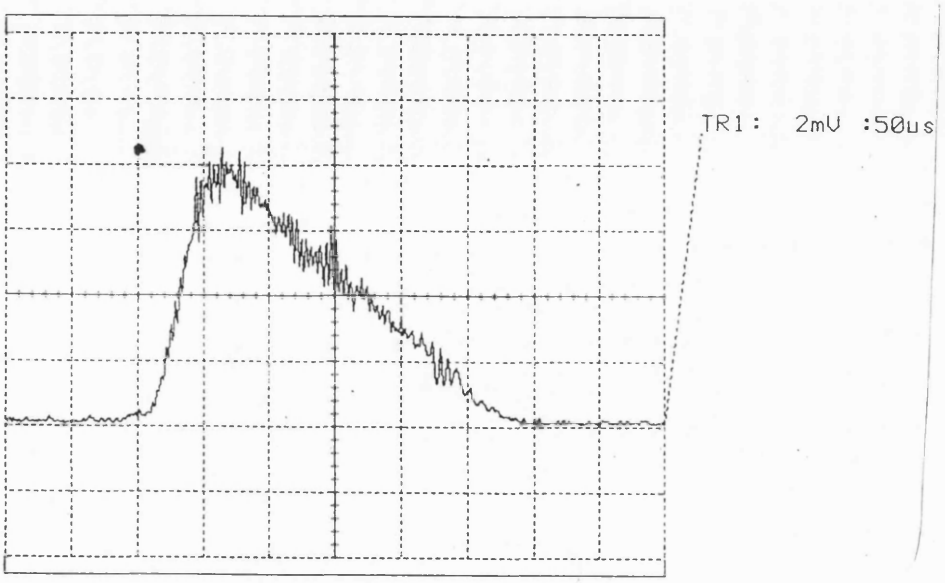

Figure 5.14 Temporal profile of laser light reflected and/or scattered from above the tissue into an angle of at $>90°$ during pulsed laser ablation of tissue at 2.94μm. The pulse fluence was 0.11 J mm^{-2}.

5.5 Discussion and Conclusions

The various routes by which pulsed laser energy is consumed during thermal ablation of tissue have been discussed. Most often, the desired route is for energy to be consumed in ablating the tissue with a minimal amount of energy expended in causing coagulation damage. Several other factors introduce losses which can reduce the efficiency with which ablation proceeds. Amongst these are reflection from the tissue surface as well as absorption and scatter by the laser plume or plasmas formed during exposure to intense pulses of radiation. Additionally, a number of mechanical process occur which may be responsible for significant portions of the 'lost' energy. Some of these loss mechanisms have been investigated.

An ablation efficiency has been defined as the amount of tissue mass removed by all mechanisms during the exposure, expressed as a percentage of the expected mass reduction if the target had been purely water and all of the laser energy had been consumed in vaporising that water. The data presented in the previous chapter have been recalculated in terms of this efficiency. The changes in the ablation efficiency with laser parameters were the same as those reported earlier. The maximum average ablation efficiency obtained was 47.9$\pm$2.1% and 59.3$\pm$3.2% for the 2.1μm and 2.94μm pulses, respectively. Thus, compared with a water target, it

would appear that losses significantly reduce the amount of material removed. Thermal damage during pulsed ablation at 2.94μm is minimal, and energy consumed in raising the temperature of the tissue water is typically small when compared to the energy consumed in the vaporisation process. Thus, it may be concluded that only a small amount of energy is consumed in coagulating the tissue during exposure to 2.94μm radiation. In contrast, there is a significant volume of thermal damage and hence a large energy loss associated with pulsed laser ablation of tissue at 2.1μm.

Material ejected from the ablation crater leaves the exposed zone at speed. Thus, some of the laser energy is converted to kinetic energy. The maximum percentage of laser energy converted to kinetic energy has been determined by measuring the velocity of the fastest particles ejected from the tissue surface and by using the mass loss data obtained in the previous chapter. The results of this analysis reveal that only a small fraction of the laser energy ends up as kinetic energy, even when the *maximum* possible kinetic energy is considered. The velocities of particles increases linearly with the pulse fluence at both 2.1μm and 2.94μm. The rate of change of particle velocity with fluence was 101.4 ± 22.2 (m sec^{-1})(J mm^{-2})$^{-1}$ and 536.7 ± 41.2 (m sec^{-1})(J mm^{-2})$^{-1}$ for 2.1μm and 2.94μm light, respectively. As a consequence of this linear dependence of the particle velocity on pulse fluence, the kinetic energy of the particles increased with the square of the fluence. Typically, at the pulse fluences investigated, less than 0.05% of the delivered energy was converted to kinetic energy at 2.1μm. The figure for the 2.94μm pulses was less than 0.2% of the delivered energy, at otherwise identical operating conditions. This increase is attributed to the increase in local energy density as a result of the smaller penetration depth at the longer wavelength. The percentage of energy converted to kinetic energy at 2.94μm also shows a more rapid increase with the pulse fluence. The implication of the linear relationship between fluence and particle velocity is that, in the limit, all of the pulse energy is converted to kinetic energy. Further studies in this area are required. The low percentage of total delivered energy converted to kinetic energy is consistent with the experimental findings of Hibst[190]. However, these results show that kinetic energy is not a major loss mechanism and recovery of this energy would not contribute greatly to the ablation process.

Nishioka et al[166] have indicated that rejection of as much as 35% of the incident light may occur from soft tissue during exposure to pulses of 2.1μm light. Such energy losses would explain the deficiencies in the calculated ablation efficiencies. Nishioka also reports transient increases in the rejection which he suggests may be either surface reflections or reflection/scatter from the ablation plume. Experiments have been performed to determine the location of the source of

these transient losses. These experiments revealed that light is scattered from above the tissue surface, implying that the plume material is responsible for the transient behaviour. Light was found to be reflected into all of the angles considered (10°, 50° and >90° to the normally incident beam). A step change in the rejected energy was also noted, the result of plume formation. It is concluded that the laser pulse is initially subjected to only the normal Fresnel reflections arising from the step change in refractive index at the air-tissue boundary, and backscatter from within the tissue. However, as ablation commences, the resulting plume begins to scatter some of the energy in the remainder of the pulse.

Tissue ablation using pulses of 2.94μm radiation demonstrated that at high fluences (>0.1 J mm^{-2}) the shape of the crater changed dramatically from a 'U' shape, which reflected the 'U' shaped intensity distribution across the beam profile, to a 'V' shape. This 'V' shaped crater exhibited a significant amount of mechanical damage. This effect is attributed here and by other authors[183] to rapid expansion of the tissue due to the expansion of vapours. Whatever the mechanism, it is clear that tissue tearing during pulsed laser ablation of tissue at 2.94μm is another way in which laser pulse energy may be consumed. No figures are presented in this study to indicate the amount of energy involved in this process. This is because the real source of the tearing has not been identified and because the complexity of any suitable or relevant calculations are considered to beyond the scope of this thesis.

The work in this chapter shows that increases in the ablation efficiency resulting from judicious choice of operating parameter other than the laser wavelength may be difficult to obtain. In the previous chapter it was shown that ablation efficiency rises with pulse fluence, increasing no further above a certain fluence. However, work in this chapter has shown that, at the same time, the ablated material can begin to block part of the incoming laser radiation. Also, the laser energy lost as kinetic energy of the plume increases rapidly with fluence, again suggesting the need for lower fluences. To effectively increase the ablation efficiency, it would be necessary to maintain the peak power of the laser pulse while reducing the duration of the laser pulse to a time less than the time taken for the formation of a plume. From the experimental observations this would suggest laser pulse durations less than 150μs as being optimal.

CHAPTER 6

Conclusions

6.1 Introduction

The recipe of an ideal laser system for ablating tissue would include the beneficial features of the CO_2 and Nd:YAG lasers. Specifically it would be based on solid state laser technology to provide reliability. It should operate at a wavelength capable of being delivered via biocompatible optical fibres without significant losses, but should be strongly absorbed by water to obtain the precision in removing tissue similar to that of the CO_2 laser with a small depth of thermal damage necessary for coagulation of the operating field. Additionally it should be capable of producing sufficient average power to rapidly ablate tissue volumes (i.e. tens of watts) and should be able to do so efficiently so as to allow a compact power supply, running from a single phase electrical supply, to be used. Over the desired operating range the laser should be stable and should not require elaborate resonator designs which complicate alignment and maintenance. It should also be able to operate at room temperature to avoid the need for expensive chillers or cryogenic cooling apparatus and, if possible, should not require an external water cooling circuit.

The work reported in this thesis shows that solid state laser systems, operating at room temperature and above, can be operated in a pulsed mode at energies capable of efficiently ablating soft biological tissue. In order to obtain the desired performance from the laser it is necessary to take account of the different thermal effects in the laser rods and the most appropriate wavelength to obtain the tissue effect. Also, it is necessary to operate the laser in a regime where the most efficient ablation can be obtained. This work also identifies the likely outcome of laser exposure under conditions where tissue ablation is not at its maximum efficiency.

This work shows that the 2.94μm erbium:YAG laser is well suited to precise

tissue ablation under controlled operating conditions. Although the precision afforded by this wavelength may be superior to that of the CO_2 lasers, higher powers are available from CO_2 systems and, because neither laser wavelength can be transmitted endoscopically, it is unlikely that lasers based solely on erbium crystals will become widely used in clinical procedures in the near future. Where modest powers are acceptable and it is possible to gain direct access to the exposure site, tissue ablation using the Er:YAG laser offers positive advantages over the CO_2 systems. These advantages stem from the inherently longer operating lifetime of solid state devices and the relatively compact design possible. Specialities to which the Er:YAG laser may be well suited include procedures in dentistry and refractive surgery.

CTH:YAG laser light can easily be transmitted through available optical fibres and, thus, these systems are well suited to endoscopic procedures. However, high fluences are required to achieve maximum ablation efficiency. This means either high pulse energies are required or only small areas of tissue may be treated at any one time. Failure to operate under these conditions will result in an extension of the zone of thermal injury and, consequently, an increase in the healing time. Alternatively, the CTH:YAG laser should be applied to areas where there is minimal risk of causing serious damage to soft tissue, for example in arthroscopy. However, the depth of thermal damage caused by the CTH:YAG laser is still significantly less than that caused by the Nd:YAG laser operating at 1.06μm and where a single laser source is required to both ablate and coagulate tissue the holmium laser represents a good compromise.

An appropriate extension to the tissue interaction experiments reported in this thesis would be an investigation of the ablative properties of CO_2 and excimer lasers, using the same measurement techniques, over a similar range of fluences and doses. Of particular interest would be the precision available by each of these laser types in regions of high fluence where permanent tissue deformation was observed when using 2.94μm light.

6.2 Overall Conclusions

6.2.1 Laser performance

1 Efficient operation at room temperature of both CTH:YAG and Er:YAG lasers at 2.1μm and 2.94μm, respectively, was demonstrated, allowing pulsed output energies in excess of 1.5J. The holmium laser is more sensitive to

changes in the coolant temperature than the erbium laser. Between coolant temperatures of 20°C and 35°C the threshold pump energy of the holmium laser varied linearly at a rate of 1.16 ± 0.06 J $°C^{-1}$. The laser slope efficiency was also adversely affected by increases in the coolant temperature. The rate of this change also depended on the resonator configuration as a result of the changes in resonator stability which resulted from changes in the residual heat loading of the crystal. In contrast both the laser threshold and laser slope efficiency of the erbium laser remained relatively constant with temperature.

2 The thermally induced lens power in 4mm diameter CTH:YAG and Er:YAG rods due to absorbed pump power varies at a rate of 8.0 Dioptres kW^{-1} and 6.1 Dioptres kW^{-1}, respectively. Both crystals, therefore, lens more strongly than Nd:YAG rods of similar dimensions. Empirical equations describing the change in induced thermal lensing with average pump power for 4mm diameter crystals in the pump range 0-500W are

$$F = \frac{3024}{P_{in}^{1.527}} \quad \text{for the CTH:YAG crystal}$$

and

$$F = \frac{560}{P_{in}^{1.204}} \quad \text{for the Er:YAG crystal}$$

3 The CTH:YAG crystal dissipates about 20% of the available pump energy as heat in the crystal lattice, almost twice the amount dissipated in the Er:YAG crystal. However, the thermal lensing measured in each crystal does not vary by a similar factor due to the inferior heat conduction properties of the Er:YAG crystal.

4 Thermally induced lensing changes the resonator stability conditions resulting in changes to the output energy extraction and the output beam divergence. Because of the greater amount of thermal lensing in CTH:YAG rods these changes will be more significant for CTH:YAG laser system compared to systems containing either Er:YAG or Nd:YAG rods. Using simple ray tracing computer programmes it is possible to model the behaviour of resonators containing these crystals over a range of average pump powers, thereby allowing the influence of thermally induced lensing to be assessed prior to operating the laser.

5 A reduction in the energy extraction efficiency of CTH:YAG laser crystals due to thermal lensing can lead to an increase in the amount of heat dissipated

in the crystal lattice, thereby increasing the thermal lensing without an increase in the average pump power. This may affect the efficiency with which energy is extracted by changing the transverse mode structure of the oscillating beam. Reductions in the average extracted power due to this effect will again increase the amount of thermal lensing, leading to premature rollover of the resonator.

6 Thermal lensing in the Er:YAG laser is not sensitive to the energy extraction efficiency and, as such, represents a more practical laser system for tissue ablation.

7 For both CTH:YAG and Er:YAG lasers the delay between the start of the excitation pump pulse and the laser emission can be predicted using simple theories based on a rectangular pump pulse profile. The duration of the rectangular pulse used in the model needs to be determined through a few simple experiments. Both laser systems may be modelled using either three or four level theories. For pump pulses in excess of 9ms there may be some divergence between three and four level theories. However, for most practical systems such pump pulses are not used.

8 Rectangular pump pulse theories based on three and four level laser theory cannot be used to predict the laser pulse duration or to identify the type of pump scheme operating.

9 At 2.1μm, transmission percentages through 320μm and 200μm optical fibre of 90% are possible, despite the relatively high divergence of these lasers which limits the achievable focused spotsize. These figures are approximately 20% greater than those reported previously in the literature[108]. The improvement in transmission appears to be due mainly to improvements in the surface quality of the input and output fibre faces. Up to 1.15J per pulse has been delivered from the end of low OH content fibres. These pulse energies are typical of those required for laser surgery.

6.2.2 Laser ablation of tissue

10 The Er:YAG laser ablates tissue more efficiently than the CTH:YAG laser due to the stronger attenuation of the 2.94μm laser wavelength by tissue water.

11 The difference in ablation efficiency between the CTH:YAG and Er:YAG lasers is less than that expected from simply considering the attenuation coefficients of each wavelength.

12 A linear relationship between pulse fluence and mass removed per pulse most

accurately models the experimental results for both 2.1μm and 2.94μm laser wavelengths. This is in contrast to the exponential model most commonly applied which assumes energy is deposited according to the Lambert-Bouguer Law. This result implies that ablation commences during the laser pulse, a fact verified during the experiments.

13 The amount of tissue removed per unit of delivered laser pulse energy increases linearly with fluence for pulses of 2.1μm. However, the ablation efficiency of 2.94μm is constant for pulses above 55 mJ mm^{-2}. This is because, at the lower fluences, a carbonised layer extends from the edges of the exposed zone, eventually obscuring most of the ablation site and preventing further tissue ablation. Absorption of incident 2.94μm light by the carbonised layer is responsible for an increase in the thermally damaged zone compared to the thermal damage observed with higher, purely ablative, pulse fluences.

14 The efficiency of mass removal is unaffected if the tissue is coagulated using the unfocussed output from a Nd:YAG laser at 1.06μm prior to exposure at either 2.1μm or 2.94μm. Thus, tissue ablation in a bloodless field may be achieved using a dual laser wavelength system where one beam is weakly attenuated by tissue and the other is strongly absorbed by tissue water.

15 There is some evidence that, at equivalent pulse fluences, more tissue is removed per unit of delivered energy for larger laser spotsizes than for small ones.

16 During ablation at 2.94μm the shape of the ablation crater changes dramatically as the pulse fluence is increased. Below 85 mJ mm^{-2}, but above 55 mJ mm^{-2}, the shape of the crater reflects the spatial distribution of energy in the beam having a 'U' shaped cross-section. At increased fluences the cross-section of the crater resembles a 'V' shape. The appearance of these craters coincides with the onset of a significant impulse which is delivered to the tissue, presumably the recoil effect following the explosive ablation of tissue.

17 At elevated fluences, where the ablation crater cross-section is 'V' shaped, there is increased tearing of the tissue. There is no evidence from *in vitro* experiments that ablated particles are trapped in the tears in the tissue which some have suggested will lead to an increase in the extent of thermal damage. Consequently, ablation with pulses of 2.94μm light at fluences above 85 mJ mm^{-2} is not recommended if precise incisions with minimal tissue damage are required.

18 The velocities of tissue particles ejected from the surface of tissue during pulsed laser ablation at 2.94μm and 2.1μm vary linearly with fluence. The

velocities measured for the 2.94μm wavelength are considerably greater than those measured for the 2.1μm light. At the available fluences velocities of approximately 100 m s^{-1} and 60 m s^{-1} have been measured during pulsed ablation at 2.94μm and 2.1μm, respectively. The maximum kinetic energy of the ablation plume represents less than 0.05% of the total pulse energy at 2.1μm and less than 0.2% of the total pulse energy at 2.94μm. Thus, kinetic energy does not represent a major loss factor in the tissue ablation process.

19 Some laser energy is lost by reflection and scattering from the particles within the ablation plume. Laser light from particles may be scattered in all directions.

20 The most efficient tissue removal is achieved using the 2.94μm light from the Er:YAG laser. Pulse fluences must be in the region 55-85 mJ mm^{-2} in order to avoid increased damage to adjacent tissue. Thermal damage will increase with lower fluences while tissue tearing will occur at higher fluences. There may be some variation in the recommended operating range of fluences depending on the tissue type.

21 Further improvements in the efficiency of mass removal may arise from continued investigations into the effects of pulse duration and repetition rate.

22 Laser ablation by pulses of 2.94μm light from the Er:YAG laser is more efficient and leads to reduced thermal damage compared to the performance of the CTH:YAG laser.

References

[1] Porphyrin-Sensitised Photodynamic Inactivation of Cells: a Review
J. Moan
Lasers in Med. Science, Vol. 1, No. 1, pp. 5-12, 1986

[2] Short-Pulsed Nd:YAG Laser Microsurgery of the Eye: Biophysical Considerations
C. A. Pulifiato, R. F. Steinert
IEEE J. Quant. Electron., Vol. QE-20, No. 12, pp. 1442-48, December 1984

[3] Excimer Lasers in Opthalmology
J. Marshall
Optician, pp. 15-24, 13 November 1987

[4] Studies of Thermal Injury (The Predictability and the Significance of Thermally Induced Rate Processes Leading to Irreversible Epidermal Injury)
F. C. Henriques
Archives of Pathology, Vol. 43, pp. 489-502, 1947.

[5] Changes in Optical Coefficients of Rat Liver *in vitro* during Pulsed Nd:YAG Laser Irradiation.
M. Essenpreis, P. Van der Zee, S. M. L. Andrew, P. Gewehr, T. N. Mills
Proc. Conference on Optics in the Life Sciences, Garmisch, 1990

[6] Laser-Produced Plasmas in Medicine
S. J. Gitomer, R. D. Jones
Laser-Tissue Interaction, SPIE Vol. 1202, pp. 118-32, 1990

[7] Basic Mechanisms in Laser Lithotripsy. 1: Opto-Acoustic-Mechanical Analysis
Z. X. Jiang, C. Whitehurst, T. A. King
Lasers in Med. Science, Vol. 6, No. 4, pp. 443-50, December 1991

[8] Laser Lithotripsy with a 504nm Pulsed Dye Laser: *In Vitro* Fragmentation Related to Stone Weight and Pulse Energy
D. J. C. M. Sterenborg, C. R. Erkens, T. M. De Reijke, F. W. Van Der Meulen, H. H. P. Van Akker, M. J. C. Van Gemert
Lasers in Med. Science, Vol. 5, No. 1, pp. 65-69, 1990

[9] Angioplasty with a Laser and Fiber Optics at 2.94μm
L. Esterowitz, C. A. Hoffman, D. C. Tran, K. Levin, M. Storm, R. F. Bonner, P. Smith, M. Leon
Optical and Laser Technology in Medicine, SPIE Vol. 605, pp. 32-36, 1986

[10] Photophysical Processes in Recent Medical Laser Developments : A Review
J-L. Boulnois,
Lasers in Medical Science, Vol. 1, No. 1, pp. 47-66, 1986.

[11] For Example;Product Literature - 150 GOLD CO_2 Laser
Surgilase Inc., I-95 Corporate Park
33 Plan Way, Warwick
Rhode Island, 02886,
U.S.A.

[12] Different Lasers for Angioplasty : Thermooptical Comparison.
N. P. Furzikov
IEEE J. of Quantum Electon., Vol. QE-23, No. 10, pp. 1751-55, 1987

[13] Use of Pulsed Energy Delivery to Minimise Tissue Injury Resulting from Carbon Dioxide Laser Irradiation of Cardiovascular Tissues.
L I. Deckelbaum, J. M. Isner, R. F. Donaldson, S. M. Laliberte, R. H. Clarke, D. N. Salem
J. Am. Coll. Cardiol., Vol. 7, pp. 898-908, 1986

[14] Superpulsed Lasers : Minimising Thermal Damage with Short Duration, High Irradiance Pulses.
E. R. Hobbs, P. L. Bailin, R. G. Wheeland, J. L. Ratz
J. Dermatol. Surg. Oncol., Vol. 13, No. 9, pp. 955-64, September 1987

[15] Comparative Study of Continuous and Pulsed CO_2 Laser on Tissue Healing and Fertility Outcome in Tubal Anastmosis
S. Z. A. Badawy, M. M. El Bakry, M. S. Baggish
Fertility and Sterility, Vol. 47, No. 5, pp. 843-47, May 1987

[16] Argon Versus Neodymium YAG Laser Photocoagulation of Experimental Canine Gastric Ulcers
F. E. Silverstein, R. L. Protell, D. A. Gilbert, C. Gulacsik, D. C. Auth, M. B. Dennis, C. E. Rubin
Gastroenterology, Vol. 77, pp. 491-96, 1979

[17] Eyesafe Coherent Laser Radar Systems at 2.1μm using Tm,Ho:YAG Lasers
S. W. Henderson, C. P. Hale, J. R. Magee, M. J. Kavaya, A. V. Huffaker
Opt. Lett., Vol. 16, No. 10, pp. 773-75, 15 May 1991

[18] Mid-IR Solid State Laser with Fiber Optics as an Ideal Medical Scalpel
L. Esterowitz, C. A. Hoffman, Levin K., M. Storm
Proc. of the International Conference on Lasers (Las Vegas), pp. 68-71, 1985

[19] Comparative Study of the Surgical Application of Holmium and CO_2 Lasers
R. J. Lane, C. A. Pulifiato, M. G. Knights
Proc., Conference on Lasers and Electro-Optics (CLEO), paper TUL4, 1985

[20] Optical Laser Characteristics of Ho^{+3} in $CaWO_4$
L. F. Johnson, G. D. Boyd, K. Nassau
Proc. IRE Correspond, Vol. 50, pp. 87-88, January 1962

[21] Efficient, High Power Coherent Emission from Ho^{3+} Ions in Yttrium Aluminium Garnet, Assisited by Energy Transfer
L. F. Johnson, J. E. Geusic, L. G. van Uitert
Appl. Phys. Lett., Vol. 8, No. 8, pp. 200-202, 15 April 1966

[22] 2.1μm Laser of 20W Output Power and 4 Percent Efficiency from Ho^{3+} in Sensitised YAG
D. P. Devor, B. H. Soffer
IEEE J. Quant. Electron., Vol. 8, No. 2, pp. 231-234, 1 February 1972

[23] Ho Laser with 50W Output and 6.5% Slope Efficiency
R. Beck, K Gürs
J. Applied Physics, Vol. 46, No. 12, pp. 5224-25, December 1975

[24] 2.12 Micron Ho:YAG Laser
B. M. Antipenko, A. S. Glebov, T. I. Kiseleva, V. A. Pis'mennyi
Sov. Tech. Phys. Lett., Vol. 11, No. 6, pp. 284-85, June 1985

[25] 2μm Room Temperature Laser Operation of Cr:Tm:Ho:YAG
M. Storm, L Esterowitz, M. Kokta
Proc., Conference on Lasers and Electro-Optics (CLEO), paper FP5, 1987

[26] Energy Transfer Processes Among Cr, Tm and Ho Ions in Yttrium Aluminium Garnet Crystals
G. Armagan, A. M. Buoncristiani, B. Di Bartolo, A. T. Inge
Proc. Tunable Solid State Lasers, paper WE4, 1989

[27] Efficient Room-Temperature Operation of Cr^{3+} Sensitised, Flashlamp-Pumped 2μm Lasers
G. J. Quarles, A. Rosenbaum, I. D. Abella, C. L. Marquardt, L. Esterowitz
Optical and Quant. Electron., Vol. 22, pp. S141-S152, 1990

[28] CW Double Cross Pumping of the $^5I_7$-$^5I_8$ Laser Transition in Ho^{3+} Doped Garnets
E. W. Duczynski, G. Huber, V. G. Ostroumov, I. A. Shcherbakov
Appl. Phys. Lett., Vol. 48, No. 23, pp. 1562-63, 9 June 1986

[29] Two for One Photon Conversion Observed in Alexandrite Pumped Tm, Ho:YAG at Room Temperature
G. J. Kintz, R. Allen, L. Esterowitz
Proceedings, Conference on Lasers and Electro-Optics (CLEO), post deadline paper, 1987

[30] Private Communication, N. Hodgson, Festkörper Institüt, Berlin, Germany

[31] High Efficiency 2.09μm Flashlamp-Pumped Laser
G. J. Quarles, A. Rosenbaum, C. L. Marquardt, L. Esterowitz
Appl. Phys. Lett., Vol. 55, No. 11, pp. 1062-64, 11 September 1989

[32] 17J Ho-Laser at 2 Microns
H. -O. Teichmann, E. W. Duczynski, G. Huber
High Power Solid State Lasers, SPIE Vol. 1201, pp. 74-81, 1988

[33] Erbium and Holmium Lasers: A Comparative Study
A. Charlton, M. R. Dickinson, P. F. Hicks, T. A. King
Private Communication of Unpublished Paper, 1990

[34] Laser and Spectral Properties of Cr,Tm,Ho:YAG at 2.1μm
S. R. Bowman, M. J. Winings, R. C. Y. Auyeung, J. E. Tucker, S. K. Searles, B. J. Feldman
IEEE J. Quant. Electron., Vol. 27, No. 9, pp. 2142-49, September 1991

[35] Thermomechanical Properties of Cr:Tm:Ho:$Y_3Al_5O_{12}$
J. E. Marion
GRA, Vol. 91, No. 6, 15 March 1991

[36] High Efficiency Flashlamp Pumped CTH:YAG Lasers Operated Above Room Temperature
S. J. Hamlin, J. D. Myers, T. R. Rexrode
Technical Digest, Advanced Solid State Lasers, Paper ME1, 17 February 1992

[37] Tunable, Flashpumped Operation of a Cr:Tm:YAG Laser Between 1.945 - 2.014μm
J. F. Pinto, L. Esterowitz
Topical Meeting on Advanced Solid State Lasers, Paper WC3, 7 March 1990

[38] Flashpumped, Room-Temperature 2μm Laser with a 5% Slope Efficiency
G. J. Quarles, A. Rosenbaum, C. L. Marquardt, L. Esterowitz
Solid State Lasers, SPIE Vol. 1223, pp. 221-30, 1990

[39] Laser-Tissue/Water Interaction of the Erbium 2.9μm Laser
L. Esterowitz, C. Hoffman
Lasers in Medicine, SPIE Vol. 712, pp. 196-97, 1986

[40] Infrared Optical Fibres for Surgical Applications
R. W. Waynant, M. N. Ediger, M. Fink
J. of Laser Applications, pp. 45-49, Spring 1990

[41] An Extension of the Three-Zone Model to Predict the Depth of Tissue Damage Beneath Er:YAG and Ho:YAG Laser Excisions
A. L.. McKenzie
Phys. Med. Biol., Vol. 34, No. 1, pp. 107-114, 1989

[42] Far-Ultraviolet Ablation of Atherosclerotic Lesions
R. Linsker, R. Srinivasan, J. J. Wynne, D. R. Alonso
Lasers in Surg. Med., Vol. 4, pp. 201-206, 1984

[43] A Comparison of the Erbium Mid-IR Laser and the Short Wavelength UV Excimer Lasers for Medical Applications
L. Esterowitz, C. A. Hoffman, M. Storm
Lasers in Medicine, SPIE Vol. 712, pp. 536-39, 1986

[44] Pulsed Er:YAG and 308nm UV-Excimer Laser: An *In Vitro* and *In Vivo* Study of Skin-Ablative Effects
R. Kaufmann, R. Hibst
Lasers in Surg. Med., Vol. 9, pp. 132-40, 1989

[45] Pulsed CO_2 Laser Tissue Ablation: Measurement of the Ablation Rate
J. T. Walsh Jr., T. F. Deutsch
Lasers in Surg. Med., Vol. 8, pp. 264-75, 1988

[46] Er:YAG Laser Ablation of Tissue: Measurement of Ablation Rates
J. T. Walsh, T. F. Deutsch
Lasers in Surg. Med., Vol. 9, pp. 327-37, 1989

[47] Effect of Pulse Repetition Rate on Erbium Laser Ablation of Soft and Hard Tissue
J. T. Walsh, J. P. Cummings
Preprint Copy by Private Request, Laser Tissue Interaction, SPIE Vol. 712, 1990

[48] Stimulated Emission from Er^{3+} Ions in Yttrium Aluminium Garnet Crystals at 2.94μm
E. V. Zharikov, V. I. Zhekov, L. A. kulevskii, T. M. Murina, V. V. Osiko, A. M. Prokhorov, A. D. Savel'ev, V. V. Smirnov, B. P. Starikov, M. I. Timoshechkin
Sov. J. Quant. Electron., Vol. 4, No. 8, pp. 1039-40, February 1975

[49] Radiative and Nonradiative Transitions Exhibited by Er^{3+} Ions in Mixed Yttrium-Erbium Aluminium Garnets
T. T. Basiev, E. V. Kharikov, V. I. Zhekov, T. M. Murina, V. V. Osiko, A. M. Prokhorov, B. P. Starikov, M. I. Timoshechkin, I. A. Shcherbakov
Sov. J. Quant. Electron., Vol. 6, No. 7, pp. 796-99, July 1976

[50] Power Limits of a YAG:Er Laser
J. Frauchiger, W. Lüthy
Optics and Laser Tech., Vol. 19, no. 6, pp. 312-15, December 1987

[51] New Data on Stimulated Emission of Crystals Containing Er^{3+} and Ho^{3+} Ions
A. A. Kaminskii, T. I. Butaeva, A. O. Ivanov, I. V. Mochalov, A. G. Petrosyan, G. I. Rogov, V. A. Fedorov
Sov. Tech. Phys. Lett., Vol. 2, No. 9, pp. 308-310, 1976

[52] Absorption, Luminescence, and Stimulated Emission Investigations in $Lu_3Al_5O_{12}$-Er^{3+} Crystals
A. A. Kaminskii, T. I. Butaeva, V. A. Fedorov, Kh. S. Bagadasacov, A. G. Petrosyan
Phys. Stat. Sol., Vol. 39, pp. 541-48, 1977

[53] High Repetition Rate, High Average Power Er:YAG Laser at 2.94μm
A. Charlton, M. R. Dickinson, T. A. King
J. Modern Optics, Vol. 36, No. 10, pp. 1393-1400, 1989

[54] Spectroscopic Properties, Energy Transfer, and Laser Operation of Pulsed Holmium Lasers
Y. Kalisky, J. Kagan, D. Sagie, A. Brenier, C. Pedrini, G. Boulon
J. Appl. Phys., Vol. 70, No. 8, pp. 4095-100, 15 October 1991

[55] Transmission of 2.94μm Laser Radiation by Zirconium Fluoride Optical Fibres
C. Whitehurst, M. R. Dickinson, A. Charlton, T. A. King
Infrared Fiber Optics, SPIE Vol. 1048, pp. 141-44, 1989

[56] The Role of Pulse Length in Limiting Distant Damage to Vascular Tissue Caused by the Laser
F. W. Cross, J. K. Wright, T. J. Bowker, S. G. Bown
Lasers in Med. Sci., Vol. 2, No. 3, pp. 175-81, 1987

[57] Temperature Dependence of Pulsed Laser Threshold in YAG:Er^{3+},Tm^{3+},Ho^{3+}
R. L. Remski, D. J. Smith
IEEE J. Quant. Electron., Vol. QE-6, pp. 750-751, January 1970

[58] High Efficiency Room-Temperature 2.06-μm Laser Using Sensitised Ho^{3+}:YLF
E. P. Chicklis, C. S. Naiman, R. C. Folweiler, D. R. Gabbe, H. P. Jenssen, A. Linz
Appl. Phys. Lett., Vol. 19, No. 4, pp. 119-21, 15 August 1971

[59] Stimulated Emission in Multiply Doped Ho^{3+}:YLF and YAG - A Comparison
E. P. Chicklis, C. S. Naiman, R. C. Folweiler, J. C. Doherty
IEEE J.Quant. Electron., Vol. QE-8, No. 2, pp. 225-30, February 1972

[60] Stimulated Emission from Ho^{3+} at 2μm in HoF_3
D. P. Devor, B. H. Soffer, M. Robinson
Appl. Phys. Lett., Vol. 18, No. 4, pp. 122-24, 15 February 1971

[61] Pulsed Ho:YAG Oscillator and Amplifier
N. P. Barnes, D. J. Gettemy
IEEE J.Quant. Electron., Vol. QE-17, No. 7, pp. 1303-08, 7 July 1981

[62] TEM_{00} Mode Ho:YLF Laser
N. P. Barnes, D. J. Gettemy, N. J. Levinos, J. E. Griggs
LASL Optics Conference, SPIE Vol. 190, pp. 297-304, 1979

[63] Chromium Doped Scandium Gallium Garnet Crystals as Active Media of Lasers Utilising Ho and Tm Infrared Transitions
E. V. Zharikov, S. P. Kalitin, V. V. Laptev, V. G. Ostroumov, Z. S. Saidov, V. A. Smirnov, I. A. Shcherbakov
Sov. J. Quant. Electron., Vol. 16, No. 1, pp. 145-47, January 1986

[64] Efficiency Optimisation for a Flashlamp Pumped Room Temperature 2-μm Laser
A. Rosenbaum, G. J. Quarles, C. L. Marquardt, L. Esterowitz
Proc., Conference on Lasers and Electro-Optics (CLEO), paper TUE5, 1989

[65] High Efficiency 2.09 Micron Laser
G. J. Quarles, C. L. Marquardt, L. Esterowitz, A. Rosenbaum
Proc., Tunable Solid State Lasers Conf., paper WD3, 1989

[66] Laser Studies of Cr,Tm,Ho:YAG
S. R. Bowman, M. J. Winings, R. C. Y. Aeyeung, S. K. Searles, B. J. Feldman
Opt. Soc. Amer. Annual Meeting, Presented Paper, November 1989.
Copy by Private Request

[67] 30Hz Operation of 2μm Ho and Tm Lasers
T. Becker, G. Huber, H. -J. v. d. Heide, P. Mitzscherlich, B. Struve, E. W. Duczynski
Opt. Comms., Vol. 80, No. 1, pp. 47-51, December 1990

[68] TEM_{00} Enhancement in CW Nd:YAG by Thermal Lensing Compensation
F. A. Levine
IEEE J. Quant. Electron., Vol QE-7, pp. 170-72, April 1971

[69] Spectroscopic Investigation of the Cr to Tm Energy Transfer in Yttrium Aluminium Garnet Crystals
G. Armagan, B. Di Bartolo, A. M. Buoncristiani
Journal of Luminescence, Preprint of Paper to be published October 1989

[70] Holmium GSAG:Cr^{3+}:Tm^{3+}:Ho^{3+} Crystal Laser (2.09μm) Operating at Room Temperature
A. N. Alpat'ev, E. V. Zharikov, A. I. Zagumenni, D. A. Zubenko, S. P. Kalitin, G. B. Lutts, M. A. Noginov, V. A. Smirnov, A. Umyskov
Sov. J. Quant. Electron., Vol. 19, No. 11, pp. 1400-02, November 1989

[71] Short Pulsed 2.1μm Laser Performance of Cr,Tm,Ho:YAG
S. R. Bowman, M. J. Winings, S. Searles, B. J. Feldman
IEEE J. Quant. Electron., Vol. 27, No. 5, pp. 1129-31, May 1991

[72] Conversion of Absorbed Energy in YAG:Cr+Tm+Ho Crystals
B. M. Anitpenko, A. S. Glebov, T. I. Kiseleva, V. A. Pismennyi
Opt. Spectrosc. (USSR), Vol. 64, No. 2, pp. 221-224

[73] Spectroscopic Characterisation of Dynamical Processes for Tm,Ho:YAG Lasers
G. Armagan, A. M. Buoncristiani, B. Di Bartolo, W. C. Edwards, A. T. Inge
Proc., Advanced Solid State Lasers Conf., paper WA5, March 1990

[74] Spectroscopy and Diode Laser-Pumped Operation of Tm,Ho:YAG
T. Y. Fan, G. Huber, R. L. Byer, P. Mitzscherlich
IEEE J. Quant. Electron., Vol. 24, No. 6, pp. 924-33, June 1988

[75] Energy Transfer (Tm←→Ho) and Upconversion Processes in YSGG:Cr^{3+}:Tm^{3+}:Ho^{3+} Laser Crystal
M. A. Noginov, I. A. Shcherbakov, V. A. Smirnov, D. A. Zubenko
Proc. Advanced Solid State Lasers, March 18-20, 1991
Paper TuA6, pp. 127-129

[76] Structure, Spectroscopy and Stimulated Emission of Crystals of Yttrium Holmium Aluminium Garnets
M. Kh. Ashurov, Yu. K. Voron'ko, E. V. Zharikov, A. A. Kaminski, V. V. Osiko, A. A. Sobol', M. I. Timoshechkin, V. A. Fedorov, A. A. Shabaltai
Inorg. Mater., Vol. 15, pp. 979-83, 1979

[77] Private Communication, G. J. Quarles, Naval Research Labs., Washington DC, USA

[78] A 30 year warranty is currently offered on ceramic pumping chambers in lasers built by Lumonics Ltd, Rugby, England

[79] Design of Flashlamp Driving Circuits
J. P. Markiewicz, J. L. Emmett
IEEE J. Quant. Electron., Vol. QE-2, No. 11, pp. 707- 11, November 1966

[80] Flashlamp Data, Book 3, Q-Arc, Cambridge, England

[81] Lasers, Chapter 13, pp. 486-89
A. E. Siegman
University Science Books (1986)

[82] Solid-State Laser Engineering, Chapter 3.4, pp. 84-88
W. Koechner
Springer-Verlag (1976)

[83] Solid-State Laser Engineering, Chapter 3.3, pp. 83-84
W. Koechner
Springer-Verlag (1976)

[84] Solid-State Laser Engineering, Chapter 3.6, pp. 98-102
W. Koechner
Springer-Verlag (1976)

[85] Private Communication, A. Charlton, Schuster Lab., University of Manchester, Manchester, England

[86] Imaging of Optical Modes-Resonators with Internally Variable Lenses
H. Kogelnik
Bell Syst. Tech. J., Vol. 44, p 455, 1965

[87] A 2μm Holmium Laser
H. Lotem, Y. Kalisky, J. kagan, D. Sagie
IEEE J. Quant. Electron., Vol. 24, No. 6, pp. 1193-1200, June 1988

[88] Comparison of Spectroscopic Properties of Tm and Ho in YAG and YLF Crystals
G. Armagan, A. M. Buoncristiani, A. T. Inge, B. Di Bartolo
Proc. Advanced Solid State Lasers, March 18-20, 1991
Paper TuC3, pp. 166-168

[89] Lasers, Chapter 6.1, Steady-State Laser Population and Population Inversion, pp. 245-8
A. E. Siegman
University Science Books (1986)

[90] Performance of Ho:Tm:Cr:YAG and Ho:Tm:Er:YAG as a function of temperature
N. P. Barnes, P.L. Cross, D. J. Gettemy, M. R. Kokta
Proceedings, Tunable Solid State Lasers Conf., pp. 215-21

[91] The Physics and Technology of Laser Resonators, Chapter 11, pp. 154-62
G. Burrows, (Edited by D. R. Hall and P. E. Jackson)
Adam Hilger, Institute of Physics Publishing Ltd., 1989

[92] Solid-State Laser Engineering, Chapter 7.1, pp. 344-82
W. Koechner
Springer-Verlag (1976)

[93] Investigation and Optimisation of Extraction Efficiency, Beam Quality and Misalignment Sensitivity of Optical Resonators Incorporating Non-Linear Interactions.
PhD Thesis, 1991
Norman Hodgson
Festkörper Institüt, Berlin, Germany

[94] The Physics and Technology of Laser Resonators, Chapter 7.3, pp. 115-16
P. E. Jackson, (Edited by D. R. Hall and P. E. Jackson)
Adam Hilger, Institute of Physics Publishing Ltd., 1989

[95] Average Power Performance of Chromium Sensitised Mid-IR Lasers
P. F. Moulton, D. M. Rines, J. G. Manni
Proc., Conference on Lasers and Electro-Optics (CLEO), paper WF8, 1989

[96] Pulse Periodic Holmium Laser for Medical Applications
B. M. Antipenko, Yu. D. Berezin, V. A. Buchenkov, V. M. Zhurba, T. I. Kiseleva, V. V. Lazo, A. A. Nikitichev, V. A. Pis'mennyi
Sov. J. Quantum Electron., Vol. 19, No. 11, pp. 1509-11, November 1989

[97] Private Communication - S. R. Bowman, Naval Research Laboratory, Washington D.C., USA

[98] LaserTrace™. A raytracing software package for IBM compatible PCs. Developed by Walther Goethals, Senior Optical Engineer at Lumonics Ltd., Rugby, Warwickshire.

[99] Elements of Modern Optical Design, Ch. 6, Exact RayTraces, pp. 177-229
D. O'Shea
Publ. J. Wiley and Sons

[100] Mode Coupling in Optical Fibres used for Spot Welding.
K. Schildbach
Centre for Manufacturing Technology Netherlands, Philips Bedrijven B.V. Eindhoven, Netherlands
Private communication of preprint paper

[101] Absorbed Pump Power, Thermal Profile and Stresses in a CW Pumped Nd:YAG Crystal.
W. Koechner
Appl. Optics, Vol. 9, No. 6, pp. 1429-34, June 1970

[102] Experience at Lumonics has shown that pumping a single rod with two flashlamps, in a ceramic pumping chamber designed to accommodate the two lamps results in a reduction in the overall laser efficiency to $\approx 70\%$ of the single lamp case. (Where the single lamp is the same as any one of the two and the ceramic pumping chamber is designed for single lamp operation)

[103] Solid-State Laser Engineering, Chapter 7.1, p. 355.
W. Koechner
Springer-Verlag (1976)

[104] Private Communication - Prof. Günter Huber, Institut für Angewandte Physik, Universität Hamburg, Hamburg, Germany

[105] Lasers, Chapter 6.3, Transient Laser Pumping, pp. 245-48
A. E. Siegman
University Science Books (1986)

[106] Neodymium Activated Yttrium Aluminium Garnets.
G. M. Zverev, Yu. D. Golyaev, E. A. Shalaev, A. A. Shokin
J. Soviet Laser Research, Vol. 8, No. 3, pp. 189-279, May 1987

[107] Characterisation of Single Crystal Sapphire Fibers for Optical Power Delivery Systems.
D. H. Jundt, M. M. Fejer, R. L. Byer
Appl. Phys. Lett., Vol. 55, No. 21, pp. 2170-72, 20 November 1989

[108] Transmission Properties of Optical Fibres at Two Laser Wavelengths: 660nm and 2100nm.
A. Moslem, B. Jassemnejad, R. C. Powell
Opt. Mat., Vol. 1, pp. 27-40, 1992

[109] Taking a value for the refractive index, in optical quartz, at the nominal laser wavelength of $2.1\mu m$, as $n=1.43668$ from the Spindler & Hoyer, Precision Optics Catalogue, 1989, page A63

[110] Q-Switched Laser Utilising an Yttrium Scandium Gallium Garnet Crystals Activated with Holmium Ions.
A. N. Alpat'ev, E. V. Zharikov, S. P. Kalitin, V. A. Smirnov, A. F. Umyskov, I. A. Shcherbakov
Sov. J. Quant. Electron., Vol. 18, No. 5, pp. 617-18, May 1988

[111] Generation of a Giant Pulse in the TEM_{00} Mode ($2.088\mu m$) in a Flashlamp Pumped YSGG:Cr:Tm:Ho Crystal.
A. N. Alpat'ev, E. V. Zharikov, S. P. Kalitin, V. A. Smirnov, A. F. Umyskov, I. A. Shcherbakov
Sov. J. Quant. Electron., Vol. 19, No. 4, pp. 438-39, April 1989

[112] Q-Switched resonator alignment procedure, as detailed in handbook for HyperYag Scientific Series laser, Lumonics Ltd, Rugby, England

[113] Solid-State Laser Engineering, Chapter 10.1, Table 10.1, p 511
W. Koechner
Springer-Verlag (1976)

[114] Optical Maser Action in $CaWO_4$.
Z. J. Kiss, R. C. Ducan Jr.
Proc. IRE (Correspondence), Vol. 50, p 1531, June 1962

[115] Stimulated Emission at 1.663μm from Er^{3+} Ions in $YAlO_3$.
M. J. Weber, M. Bass, G. A. De Mars, K. Andringa, R. R. Monchamp
IEEE J. Quant. Electron., p 654, October 1970

[116] Induced Emission by Trivalent Erbium Ions in Crystals of Yttrium-Aluminium Garnet.
G. M. Zverev, V. M. Garmash, A. M. Onishchenko, V. A. Pashkov, A. A. Semenov, Yu. M. Kolbatskov, A. I. Smirnov
Translation from Zhurnal Prikladnoi Spektroskopii, Vol. 21, No. 5, pp. 820-23, November 1974

[117] Stimulated Emission from Er^{3+} Ions in CaF_2.
Yu. K. Voron'ko, G. M. Zverev, A. M. Prokhorov
Soviet Physics JETP, Vol. 21, No. 6, pp. 1023-25, December 1965
Translated from J. Exptl. Theoret. Phys. (U.S.S.R.), Vol. 48, No. 6, pp. 1529-1808, June 1965

[118] Stimulated Emission at 0.85μm in Er^{3+}:YLF.
E. P. Chicklis, C. S. Naiman, A. Linz
Paper C10, Quant. Electron. Conference, Montreal, 1972

[119] Coherent Oscillations from Tm^{3+}, Ho^{3+}, Yb^{3+} and Er^{3+} Ions in Yttrium Aluminium Garnet.
L. F. Johnson, J. E. Geusic, L. G. Van Uitert
Appl. Phys. Lett., Vol. 7, No. 5, pp. 127-29, September 1965

[120] Energy Levels and Crystal-Field Calculations of Er^{3+} in Yttrium Aluminum Garnet.
J. A. Koningstein, J. E. Geusic
Phys. Rev., Vol. 136, No. 3A, pp. A726-28, 2 November 1964

[121] Spectrum of Stimulated Emission due to Self-Saturating Transitions in High-Concentration Media.
V. I. Zhekov, V. A. Lobachev, T. M. Murina, A. M. Prokhorov
Sov. J. Quant. Electron., Vol. 11, No. 2, pp. 279-81, February 1981

[122] Efficient Cross-Relaxation Laser Emitting at 2.94μm.
V. I. Zhekov, V. A. Lobachev, T. M. Murina, A. M. Prokhorov
Sov. J. Quant. Electron., Vol. 13, No. 9, pp. 1235-37, September 1983

[123] Continuous Wave and Q-Switched Infrared Erbium Laser.
S. A. Pollack, D. B. Chang, N. L. Moise
Appl. Phys. Lett., Vol. 49, No. 23, pp. 1578-80, 8 December 1986

[124] CW 2.8μm Laser Emission from Er:$LiYF_4$ at 77K.
H. Chou, Z. Zhan, H. P. Jenssen
Tunable Solid State Lasers Conference, Technical Digest Series, Vol. 20, Optical Society of America, pp. 185-86, 1987

[125] Laser Pumping of Ho, Tm, Er-Doped Garnet Lasers at Room-Temperature.
G. Huber, E. W. Duczynski, K. Petermann
Tunable Solid State Lasers Conference, Technical Digest Series, Vol. 20, Optical Society of America, paper MC1, p 18, 1987

[126] Laser Pumping of Ho-, Tm-, Er-Doped Garnet Lasers at Room-Temperature.
G. Huber, E. W. Duczynski, K. Petermann
IEEE J. Quant Electron., Vol. 24, No. 6, pp. 920-23, June 1988

[127] Operation of the High Dopant Density Er:YAG at 2.94μm.
M. Bass, W. Q. Shi, R. Kurtz, M. Kokta, H. Diegl
Tunable Solid State Lasers II, Edited by Budgor, Esterowitz and DeShazer
Springer-Verlag, N.Y., pp. 300-305, 1986

[128] Thermal Conductivity of a $Y_{1.5}Er_{1.5}Al_5O_{12}$ Crystal in the Temperature Range 5-300 K.
S. R.Arutyunyan, Kh. S. Bagdasarov, A. P. Dodokin, A. M. Kekerov
Sov. J. Quant. Electron., Vol. 14, No. 6, pp. 870-71, 1984

[129] Data sheet for Nd:YAG crystals - Litton Airtron, Charlotte, NC, USA

[130] Influence of Samarium Filter on the Performance of Nd:YAG, Cr:Nd:GSGG and Er:YAG Lasers.
P. Greve, B. Metz
SPIE ECO-2 Conference, April 1989

[131] Temperature Dependence of a 2.94μm YAG-Er Laser and Population of the Laser Levels.
R. Spring, W. Lüthy
J. Appl. Phys., Vol. 69, No. 2, pp. 581-83, 15 January 1991

[132] Laser Action and Spectroscopic Properties of Er^{3+} in $YAlO_3$.
M. J. Weber, M. Bass, G. A. DeMars
J. Appl. Phys., Vol. 42, No. 1, pp. 301-5, 1 January 1971

[133] New Data on the Three-Micron Lasing of Ho^{3+} and Er^{3+} Ions in Aluminates having the Perovskite Structure.
A. A. Kaminskii, V. A. Fedorov, I. V. Mochalov
Sov. Phys. Dokl., Vol. 25, No. 9, pp. 744-46, September 1980

[134] Three-Micron Laser based on $YAlO_3$ Crystals with a High Concentration of Ho^{3+} and Er^{3+} Ions.
A. A. Kaminskii, V. A. Fedorov, A. O. Ivanov, I. V. Mochalov, L. I. Krutova
Sov. Phys. Dokl., Vol. 27, No. 9, pp. 725-27, September 1982

[135] Cascade Laser Generation by Er^{3+} Ions in $YAlO_3$ Crystals by the Scheme $^4S_{3/2} \rightarrow {}^4I_{9/2} \rightarrow {}^4I_{11/2} \rightarrow {}^4I_{13/2}$.
A. A. Kaminski
Sov. Phys. Dokl., Vol. 27, No. 12, pp. 1039-41, December 1982

[136] Polarisation Properties and new 3μm Lines in $YAlO_3$.
S. Schnell, M. Stalder, W. Lüthy
J. de Physique, Vol. C7, No. 12, pp. 371-73, December 1987

[137] Five New 3μm Lines in $YAlO_3$.
M. Stalder, W. Lüthy, H. P. Weber
Optics Letters, Vol. 12, No. 8, pp. 602-4, August 1987

[138] Simultaneous, Multiple Wavelength Lasing of (Er, Nd):$Y_3Al_5O_{12}$.
W. Q. Shi, R. Kurtz, J. Machan, M. Bass, M. Birnbaum, M. Kokta
Appl. Phys. Lett., Vol. 51, No.16, pp. 1218-20, 19 October 1987

[139] Low Threshold YSGG:Cr:Er Laser for the 3-μm Spectral Range with a High Pulse Repetition Rate.
P. Al'bers, V. G. Ostroumov, A. F. Umyskov, S. Shnell, I. A. Shcherbakov
Sov. J. Quant. Electron., Vol. 18, No. 5, pp. 558-59, May 1988

[140] Spectroscopic and Laser Characterisation of Er,Cr:YSGG.
P. F. Moulton, J. G. Manni, G. A. Rines
IEEE J. Quant. Electron., Vol. 24, No. 6, pp. 960-73, June 1988

[141] Continuous-Wave Lasing of Erbium Ions in YSGG:Cr^{3+}:Er^{3+} Crystals in the 3μm Range at Room Temperature.
M. A. Noginov, V. A. Smirnov, A. F. Umyskov, G. Huber, H. Stange, I. A. Shcherbakov.
Sov. J. Quant. Electron., Vol. 20, No. 10, pp. 1185-89, October 1990

[142] CW Laser Operation from Er:YAG, Er:GGG and Er:YSGG.
B. J. Dinerman, P. F. Moulton
Advanced Solid State Lasers Conference, New Mexico, USA, paper Pd2, 1992

[143] CW and Pulsed 2.8μm Laser Emission from Diode-Pumped Er^{3+}:$YLiF_4$ at Room Temperature.
G. J. Kintz, R. Allen, L. Esterowitz
Appl. Phys. Lett., Vol. 50, No. 22, pp. 1553-55, 1 June 1987

[144] A Comparative Study of Er:Cr:YSGG and Er:YAG Lasers.
A. Charlton, N. M. Wannop, M. R. Dickinson, T. A. King
Advanced copy of preprint paper, by private request, June 1990

[145] Cross Section of the $^4I_{11/2}$-$^4I_{13/2}$ Laser Transition in Er^{3+} Ions in Yttrium-Erbium-Aluminum Garnet Crystals.
E. V. Zharikov, V. I. Zhekov, T. M. Murina, V. V. Osiko, M. I. Timoshechkin, I. A. Shcherbakov
Sov. J. Quant. Electron., Vol. 7, No. 1, pp. 117-19, January 1977

[146] Solid-State Laser Engineering, Chapter 2.3, Table 2.4, p. 54.
W. Koechner
Springer-Verlag (1976)

[147] Polarisation of 3μm Laser Emission in $YAlO_3$:Er.
M. Stalder, W. Lüthy
Opt. Comms., Vol. 61, No. 4, pp. 274-76, 15 February 1987

[148] Energy Transfer Characteristics of the $^4S_{3/2}$ Level of Er^{3+} in YAG.
I. Ursu, A. Lupei, S. Georgescu, V. Lupei, A. M. Prokhorov, V. I. Zhekov, T. M. Murina, M. I. Studenikin
Opt. Comms., Vol. 72, No. 34, pp. 209-13, 15 July 1989

[149] Laser Properties of Selectively Excited $YAlO_3$:Er.
J. Frauchiger, W. Lüthy, P. Albers, H. P. Weber
Optics Letters, Vol. 13, No. 11, pp. 964-66, November 1988

[150] Private Communication - Dr David Dawes, Director Engineeering, Litton Airtron Crystal Products Division, Charlotte, NC, USA

[151] Giant Laser Radiation Pulses from Erbium-Doped Yttrium Aluminium Garnet Crystals.
Kh. S. Bagdasarov, V. I. Zhekov, L. A. Kulevskii, V. A. Lobachev, T. M. Murina, A. M. Prokhorov
Sov. J. Quant. Electron., Vol. 10, No. 9, pp. 1127-31, September 1980

[152] Transmission Measurements on Various Tissue Samples Between 1064 and 2000nm.
D. Blanc, M. J. Colles
Lasers in Medical Science, Vol. 5, pp. 71-75, 26 September 1989

[153] Efficient Room-Temperature Operation of a Flashlamp pumped, Cr,Tm:YAG Laser at 2.01μm.
G. J. Quarles, A. Rosenbaum, C. L. Marquardt, L. Esterowitz
Optics Letters, Vol. 15, No. 1, pp. 42-44, 1 January 1990

[154] Studies of Er:YAG Laser Interaction with Soft Tissue.
M. R. Dickinson, A. Charlton, T. A. King, A. J. Freemont, R. Bramley
Lasers in Medical Science, Vol. 6, No. 2, pp. 125-31, June 1991

[155] Comparison of Tissue Ablation with Pulsed Holmium and Thulium Lasers.
N. S. Nishioka, Y. Domankevitz
IEEE J. of Quant. Electron., Vol. 26, No. 12, pp. 2271-75, December 1990

[156] Erbium:YAG Laser Ablation of Meniscus, Cartilage, Tendon and Bone.
S. G. Vari, W. Q. Shi, H. Loertscher, M. Fishbein, T. Papaionnou, W. S. Grundfest
Copy of preprint paper, by private request

[157] The Physics of Photodynamic Therapy, Section 5.2, Models of Light Propagation in Tissue.
B. C. Wilson, M. S. Patterson
Phys. Med. Biol., pp. 340-53, 1986

[158] Fundamentals of Laser Light Interaction with Human Tssue, Especially in the Cardiovascular System.
D. Haina, M. Landthaler
Thorac. Cardiovascular Surgeon, Vol. 36, pp. 118-25, 1988

[159] Practical Models for Light Distribution in Laser-Irradiated Tissue.
A. J. Welch, G. Yoon, M. J. C. Van Gemert
Lasers in Surg. Med., Vol. 6, pp. 488-493, 1987

[160] a) New Contributions to the Optics of iItensity Light Scattering Materials.
P. Kubelka
J. Opt. Soc. America, Vol. 38, No. 5, pp. 448-57, May 1948

b) New Contributions to the Optics of Intensity Light Scattering Materials.
P. Kubelka
J. Opt. Soc. America, Vol. 44, pp. 330-35, 1954

[161] Development and Application of Three-Dimensional Model for Laser Irradiated Tissue.
G. Yoon, A. J. Welch, M. Motamedi, M. J. C. Van Gemert
IEEE J. Quant. Elec., Vol. 23, No. 10, pp. 1721-23, 1 October 1987

[162] Changes in Scattering Phase Function of Rat Liver at 1.064μm and 1.32μm following Coagulation.
M. Essenpreis, P. Van der Zee, P. S. Jones, P. Gewehr, T. N. Mills
Lasers in Surg. Med., Suppl. 3, p5, 1991

[163] A Review of the Optical Properties of Biological Tissues.
W. F. Cheong, S. A. Prahl, A. J. Welch
IEEE J. Quant. Electron., Vol. 26, pp. 2166-85, 1990

[164] Gaussian Beam Spread in Biological Tissues.
L. I. Grossweiner, J. L. Karagiames, P. W. Johnson, Z. Zhang
Appl. Optics, Vol. 29, No. 3, pp. 379-83, 20 January 1991

[165] Reflection and Transmission of Laser Light from the Esophagus: the Influence of Incident Angle.
N. S. Nishioka, S. L. Jacques, J. M. Richter, R. R. Anderson
Gastroenterology, Vol. 94, No. 5, pp. 1180-85, 1988

[166] Reflectance during Pulsed Holmium Laser Irradiation of Tissue.
N. Nishioka, Y. Domankevitz
Lasers in Surg. Med., Vol. 9, pp. 375-81, 1989

[167] Medical Lasers - Science and Clinical Practice.
J. A. S. Carruth, A. L. McKenzie
Medical Science Series, Publ. Adam Hilger, 1986

[168] Comparative Thermal Modelling of Er:YAG, Ho:YAG and CO_2 Laser Pulses for Tissue Vaporisation.
E. Sinofsky
Lasers in Medicine, SPIE Vol 712, pp. 188-92, 1986

[169] A Thermal Appraisal of the Ablation Process in Canine Aorta *in vivo* using a 100μs Pulsed Nd:YAG Laser.
F. W. Cross, M. J. C. Van Gemert
Lasers in Medical Science, Vol. 6, No. 4, pp. 373-78, December 1991

[170] Biological Effects of Intrahepatic Neodymium:Yttrium-Aluminium-Garnet Laser Photocoagulation in Rats.
K. Matthewson, P. Coleridge-Smith, J. P. O'Sullivan, T. C. Northfield, S. G. Bown
Gastroenterology, Vol. 93, pp. 550-57, 1987

[171] A Three Zone Model of Soft Tissue Damage by a CO_2 Laser.
A. L. McKenzie
Phys. Med. Biol., Vol. 31, No. 9, pp. 967-83, 1986

[172] Physics of Thermal Processes in Laser-Tissue Interaction.
A. L. McKenzie
Phys. Med. Biol., Vol. 35, No. 9, pp. 1175-1209, March 1990

[173] Part of MS Thesis presented by Jonathon Michaels
J. Michaels
M S Thesis, 1990

[174] Time Constants in Thermal Laser Medicine.
M. J. C. Van Gemert, A. J. Welch
Lasers in Surg. Med., Vol. 9, pp. 405-21, 1989

[175] Comparison of Continuous-Wave and Pulsed Excitation for Interstitial Neodymium-YAG Laser Induced Hyperthermia.
K. Matthewson, P. Coleridge-Smith, T. C. Northfield, S. G. Bown
Lasers in Medical Science, Vol. 1, No. 3, 197-201, July-Sept 1986

[176] Mechanisms of Laser Ablation in an Absorbing Fluid Field.
J. M. Isner, S. R. DeJesus, R. H. Clarke, D. Gal, A. J. Rongione, R. F. Donaldson
Lasers in Surg. Med., Vol. 8, pp. 543-54, 1988

[177] Transmission of 2.1μm Laser Pulses Through Water.
T. G. J. M. van Leeuwen, M. J. van der Veen, R. M. Verdaasdonk, C. Borst
Conf. Abstracts, Laser and Balloon Angioplasty and Restenosis, Maastricht, Netherlands, 27-28 April 1990

[178] Thermal Lensing in Biological Medium.
M. Motamedi, A. J. Welch, W. F. Cheong, S. A. Ghaffari, O. T. Tan
IEEE J. Quant. Electron., Vol. 24, No. 4, pp. 693-96, April 1988

[179] A 1.96μm Cr:Tm:YAG Medical Laser.
J. F. Pinto, L. Esterowitz, R. F. Bonner
Private Communication, December 1990

[180] Optical Properties of Rat Liver Between 350 and 2200nm.
P. Parsa, S. L. Jacques, N. S. Nishioka
Appl. Optics, Vol. 28, pp. 2325-30, 1989

[181] Effects of Holmium-YSGG Laser Irradiation on Arterial Tissue: Preliminary Results.
H. T. Aretz, J. R. Butterly, E. J. Jewell, S. E. Setzer, S. M. Shapshay
Optical Fibers in Medicine IV, SPIE Vol. 1067, pp. 127-32, 1989

[182] Pulsed Infrared Ablation of Vascular Tissue.
M. Motamedi, P. Prcevski, S. M. Zheng
Conf. Abstracts, Laser and Balloon Angioplasty and Restenosis, Maastricht, Netherlands, 27-28 April 1990

[183] Tissue Tearing Caused by Pulsed Erbium Laser Induced Ablation Pressure.
J. Cummings
Chapter Three, M S Thesis
Biomedical Engineering Dept., Northwestern University, Evanston, IL, USA, 1990

[184] Ablation of Rabbit Liver, Stomach and Colon with a Pulsed Holmium Laser.
N. S. Nishioka, Y. Domankevitz, T. J. Flotte, R. R. Anderson
Gastroenterology, Vol. 96, pp. 831-37, 1 January 1989

[185] Preliminary Evaluation of a Pulsed 2.15μm Laser System for Fibre Optic Endoscopic Surgery.
M. R. Treat, S. L. Trokel, R. D. Reynolds, V. J. DeFilippi, J. Y. Liu, M. G. Cohen
Lasers in Surg. Med., Vol. 8, pp. 322-326, 1 January 1988

[186] Comparison of Methods for Transcatheter Fragmentation of Gallstones.
J. P. Johnson, M. C. Oz, R. S. H. Chuck, M. R. Treat
Surgical Endoscopy, Vol. 3, pp. 7-10, January 1989

[187] Pulsed CO_2 Laser Tissue Ablation: Effect of Tissue Type and Pulse Duration on Thermal Damage.
J. T. Walsh, T. J. Flotte, R. R. Anderson, T. F. Deutsch
Lasers in Surg. Med., Vol. 8, pp. 108-18, 1988

[188] Er:YAG Laser Ablation of Tissue: Effect of Pulse Duration and Tissue Type on Thermal Damage.
J. T. Walsh, T. J. Flotte, T. F. Deutsch
Lasers in Surg. Med., Vol. 9, pp. 314-26, 1989

[189] An Analysis of Er:YAG Laser for Angioplasty: Delivery System, Ablation Capability, and the Effect of Water Content.
B. Kwark, S. Rastegar, V. Vaidyanathan, H. F. Taylor
Lasers in Life Sciences, Vol. 5, pp. 113-28, 1992

[190] Mechanical Effects of Erbium:YAG Laser Bone Ablation.
R. Hibst
Lasers in Surg. Med., Vol. 12, pp. 125-30, 1992

[191] Infrared Laser Bone Ablation.
R. C. Nuss, R. L. Fabian, R. Sarkar, C. A. Pulifiato
Lasers in Surg. Med., Vol. 8, pp. 381-91, 1988

[192] Erbium-YAG and Holmium-YAG Laser Ablation of Bone.
A. Charlton, M. R. Dickinson, T. A. King, A. J. Freemont
Lasers in Medical Science, Vol. 5, No. 4, pp. 365-73, December 1990

[193] Instabilities in Laser Cutting of Soft Media.
M. Frenz, A. D. Romano, A. D. Zweig, H. P. Weber, N. I. Chapliev, A. V. Silenok
J. Appl. Phys., Vol. 66, No. 9, pp. 4496-45, 1 November 1989

[194] A Comparative Study of Laser Interaction at 2.94μm and 10.6μm.
A. D. Zweig, M. Frenz, V. Romano, H. P. Weber
J. Appl. Phys. B, Vol. 47, pp. 259-65, 1 January 1988

[195] Application of the holmium:YAG laser for refractive surgery: An update of clinical progress.
D.S. Durrie, T. Seiler, V.P. Thompson, M.C. King, A.C. Sacharoff, J.D. Hunkeler, D.F. Muller
Biomedical Optics '93, Technical Abstracts, Paper 1877-12, Los Angeles, USA
16th-22nd January, 1993

[196] Effects of Laser Parameters on Pulsed Er-YAG Laser Skin Ablation.
R. Hibst, R. Kaufmann
Lasers in Medical Science, Vol. 6, No. 4, pp. 391-97, December 1991

[197] Effects of an Erbium:YAG Laser on Ocular Structures.
G. A. Peyman, N. Katoh
International Opthalmology, Vol. 10, pp. 245-53, 1987

[198] Effects of High Power Laser Radiation.
J. Ready
New York Academic Press, 1971, pp. 103,147

[199] Private Communication - Doug Golding, Medical Laser Development Engineer, Carl Zeiss Inc., Thornwood, NY, USA

[200] Tables of Physical and Chemical Constants, 15th Edition
G. W. C. Kaye, T. H. Laby
Publ. Longman Scientific and Technical, Longman, 1986

APPENDIX 1

Pumping Chamber Materials

A1.1 Introduction

Pumping chambers can be divided into two distinct categories; focusing and diffuse. The former often consists of an elliptical cross-section cavity in which the rod and a single lamp lie at the two foci. For multi-lamp systems a complicated geometry of multiple ellipses can ensure that light emitted from each lamp is reflected towards the rod. The interior surface of the chamber is usually a polished metal coating such as gold or silver, both of which have excellent broad band reflectance properties in the visible part of the spectrum. However, although focusing chambers often provide better near term efficiency than diffuse types the metallic surfaces tarnish rapidly under the extreme conditions found inside the chamber during use. Additionally, the focusing effect of these chambers concentrates the pump light in precise locations within the rod which can reduce the laser efficiency when high energy extraction in multi-transverse beams are required. Diffuse chambers are more suitable where an homogeneous distribution of the pump light through the rod is required. Usually the rod and lamp are located as close as possible to one another to ensure the maximum direct light transfer. For this reason the chambers are also sometimes called close-coupled. Light which reaches the walls of the chamber is reflected from within the diffuse material which lines the inside of the cavity. Pumping chambers made of ceramics are often used for commercial systems offering both good diffuse reflectance properties and long term resistance to degradation. Other materials can also be used in diffuse chambers although none to-date have achieved the reliability of the ceramics[A1.1]. With the emphasis placed on the lifetime requirements of a practical laser system and the high energy extraction required, only diffuse chambers were considered during the development of the lasers.

A1.2 Diffuse Pumping Chambers Used in this Work.

Three diffuse chambers were assessed experimentally to determine the most efficient at transferring flashlamp light to the rod. Two of the chambers were based on a commercial laser manufacturers' assembly (Lumonics Part No. M6118101B) and were identical in every respect except for the diffusing material used which was either Lumonics standard ceramic or Spectralon, a proprietary material with a high reflectivity in the visible portion of the spectrum[A1.2]. The third was a proprietary pumping chamber assembly in which the diffusing material was $BaSO_4$ (I.R Sources, Brookline, NH, USA). In all cases the cross-section shape of the diffuser was a 'race-track' with the rod and lamp centres separated by a characteristic distance, s, Table A1.1. The ceramic and Spectralon chambers included an additional Pyrex tube over the laser rod which served to direct the cooling water flow as well as provide an additional UV filter.

Diffusing Material	Lamp-to-Rod Separation s, mm
Ceramic	7.5
Spectralon	7.5
$BaSO_4$	6.0

Table A1.1 Lamp-to-rod separations for tested pumping chambers.

Identical resonators were constructed with each of the three pumping chambers in turn. A 3" long by 5mm diameter Cr:Tm:Ho:YAG rod was pumped by a xenon filled flashlamp at 1Hz in a 400mm long resonator formed between a high reflectivity 5m rear mirror and an 80% reflecting plane output coupler. The output at a constant cooling temperature of 20°C was recorded using a calibrated calorimeter (Model 20, Laser Instrumentation Ltd., Chertsey, England). The results show that the best performance was obtained for the chamber using Spectralon as the diffuse reflector, producing 10% more power than the $BaSO_4$ chamber and almost three times the performance of the ceramic chamber at the maximum input energy of 100 J $pulse^{-1}$, Figure A1.1.

The chambers were then operated repeatedly over a period of weeks to monitor the long term stability. While both the ceramic and $BaSO_4$ chambers showed no sign of deterioration the output obtained from the Spectralon chamber fell by 30% within a couple of weeks. When the chamber was dismantled blackened pits were

discovered on the surfaces of the material closest to the flashlamp. The exact cause of the damage was not established although photo-dissociation of the material due to the high intensities of U.V. radiation was suspected[A1.3]. Subsequent to discovering the damage it was decided to carry out all further laser tests with the $BaSO_4$ chamber. A second version of this design was therefore obtained to operate with the 4" long Cr:Tm:Ho:YAG rods. Charlton et al report on a similar exercise comparing the performance of different pumping chambers for the erbium crystal[A1.4]. Their results confirm what might be expected from a simple comparison of the absorption bands of the Cr:Tm:Ho:YAG and the Er:YAG crystals, specifically, that, due to the strong absorption over a significant part of the visible region of the spectrum in both crystals, the $BaSO_4$ chamber is also best suited for use with the erbium laser. A chamber suitable for use with a 3"x4mmϕ erbium:YAG rod was subsequently obtained.

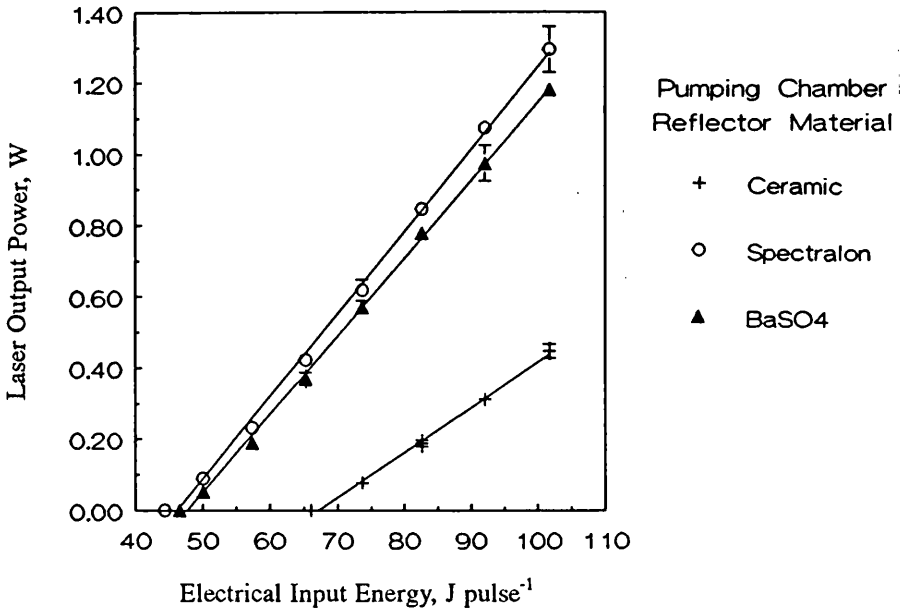

Figure A1.1 Laser output performance for a 3"x5mm diameter CTH:YAG rod operated in three different pumping chambers, all other laser parameters remaining constant.

References used in Appendix 1

[A1.1] Lumonics Ltd, Rugby, report that lasers fitted with ceramic pumping chambers are still in regular use after 20 years.

[A1.2] Data sheets for Spectralon SRM-99LG, Labsphere Inc., North Sutton, NH, USA

[A1.3] Private Communication - A. Springsteen, Reflectance Research Chemist, Labsphere Inc., North Sutton, NH, USA

[A1.4] High Repetition Rate, High Average Power Er:YAG Laser at 2.94μm
A. Charlton, M. R. Dickinson, T. A. King
J. Modern Optics, Vol. 36, No. 10, pp 1393-1400, 1989

APPENDIX 2

Flashlamp Characteristics

A2.1 Introduction

Light from the flashlamp is used to excite the active laser ions from the ground state to the upper laser level. In co-doped laser crystals the pump scheme includes the excitation of ions to an elevated state from which they decay transferring excitation energy to the active ion. The object in the design of the flashlamps and the electrical discharge circuit is to convert the electrical energy stored in the capacitor bank to the excitation wavelengths of the crystal as efficiently as possible.

Because the excited levels in the laser crystal decay with a characteristic time constant it is important to transfer the excitation energy and initiate laser action in a time less than the upper laser level lifetime to prevent unnecessary loss. For this reason pump pulses of the order of, or less than, the fluorescence lifetime of the laser level are required. Additionally, it is necessary in the discharge circuit design to consider the matching of the circuit to the lamp which is a dynamic load, varying in inductance and capacitance throughout the discharge. A poorly matched circuit will cause the discharge to oscillate resulting in inefficient conversion of the electrical energy to useful light output. Secondly, poor matching will result in a reduction in the number of pulses the lamp is able to emit before either spontaneously failing or being degraded by sputtering of the cathode material on the lamp envelope. The design theory of flashlamps is adequately covered in the texts supplied by the lamp manufacturers[A2.1] while the work of Emmett and Markiewicz remains the standard text for the design of single stage discharge circuits[A2.2].

A2.2 Flashlamp Construction

The flashlamps used were supplied by Lumonics Ltd, Rugby, Warwickshire and consisted of a quartz tube having an inside diameter of 4mm and a wall thickness of 1mm. The envelope was doped with samarium to provide filtering of the UV emission from the lamp which may cause rod solarisation. The anode was made from thoriated tungsten and the cathode from a porous tungsten which included a barium compound to reduce the work function. The gas fill was xenon, chosen because of its broad band emission in the visible part of the spectrum at typical pulse pumped current densities (> 1000 Amps cm^{-2}) which overlaps well with the absorption bands of both erbium ions and chromium ions the chief absorber in Cr:Tm:Ho:YAG crystals, Figure A2.1.

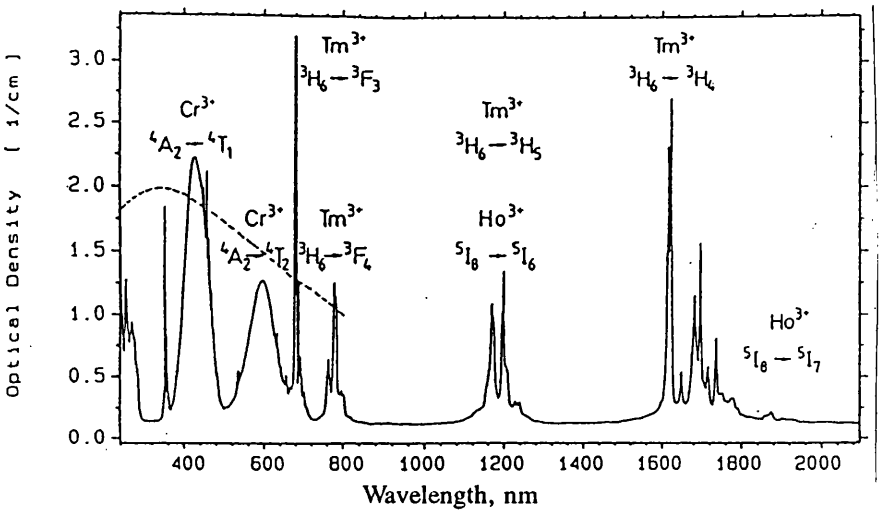

(a)

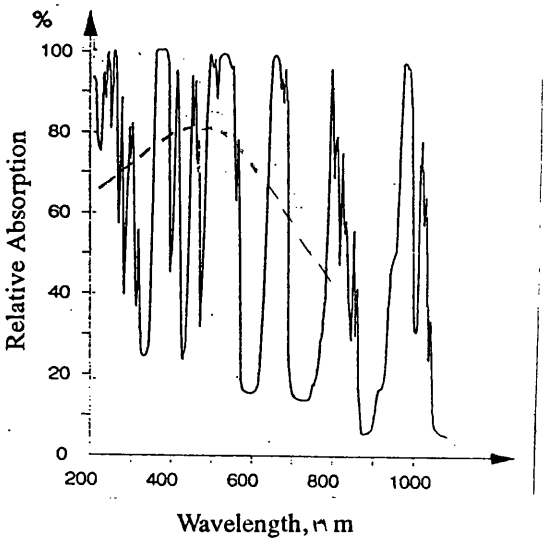

(b)

Figure A2.1 Absorption spectrum of a) the CTH:YAG crystal and b) the Er:YAG crystal overlayed with the emission envelope of the pulsed xenon flashlamp.

The arc length of the lamp was 67mm for use with 3" rods and 92mm for 4" rods, (Lumonics part numbers 12280070A and 12280020A, respectively). Consequently, the rods were pumped by light entering the crystal radially over 87.9% and 90.6% of their lengths, respectively. However, the true pumped length exceeds this value due to the diffuse nature of the pumping chamber (see Appendix 1 of this thesis). The maximum pumped length of the crystals, taking into account the diffusing effect of the pumping chamber was, therefore, estimated at approximately 95% of the rod length, this being approximately 72mm and 97mm for the 3" and 4" rods, respectively. The fill pressure was 450 Torr which was the suppliers' standard, although an experimental 760 Torr version of the 67mm arc length lamp was obtained for comparative purposes. Higher gas pressures are known to give better conversion of the electrical energy to optical energy in the visible region of the spectrum[A2.1] but result in lamps which are harder to trigger.

A2.3 Charging Circuit

The maximum average power which can be dissipated in the laser crystal is limited by the thermo-mechanical properties of the crystal and the efficiency of the system used to extract the heat. To prevent excessive thermal strain on the crystal which may have resulted in thermal fracture the maximum average discharge power was chosen to be less than 200W per inch of pumped crystal length[A2.3]. Consequently a charging circuit with a maximum power delivery of 500W was selected. Figure A2.2 shows a schematic of the charging circuit.

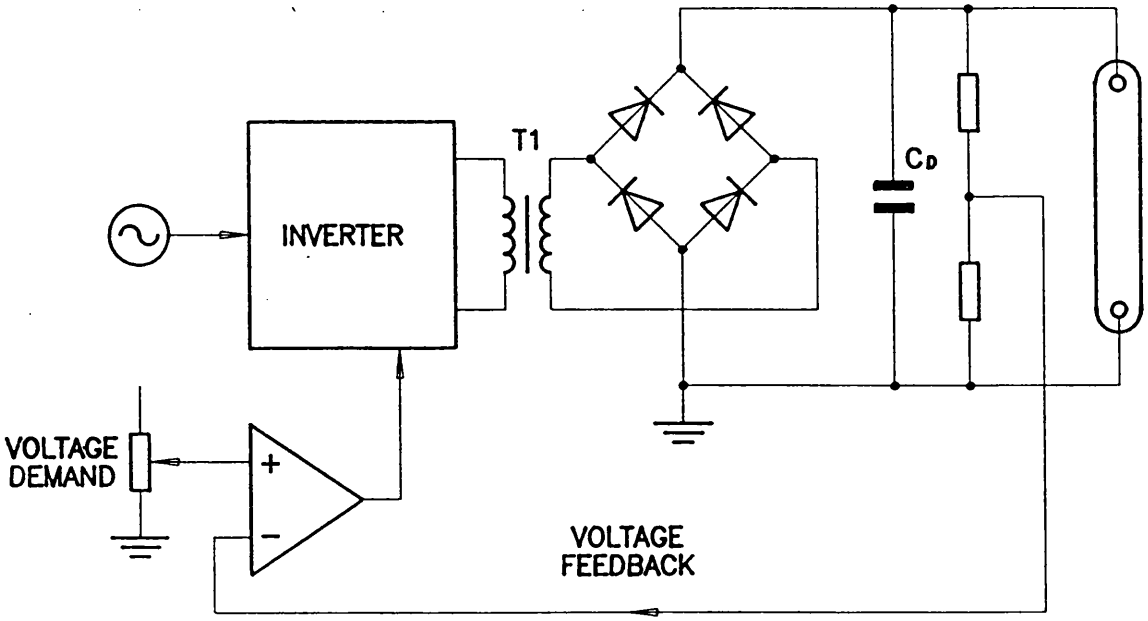

Figure A2.2 Schematic of the PSU charging circuit. (C_D = main discharge capacitor).

A2.4 Trigger and Simmer Circuit

To reduce the demands on both the electrical circuit and the flashlamp the lamp was series triggered in advance of the first pump pulse by a 6kV, 450ns pulse. A low level discharge in the lamp was then maintained by a simmer circuit operating continuously at about 80 milliamps. An SCR was subsequently used to switch between the main pulse discharge from the storage capacitors and the simmer current. Figure A2.3 shows the trigger and simmer circuits.

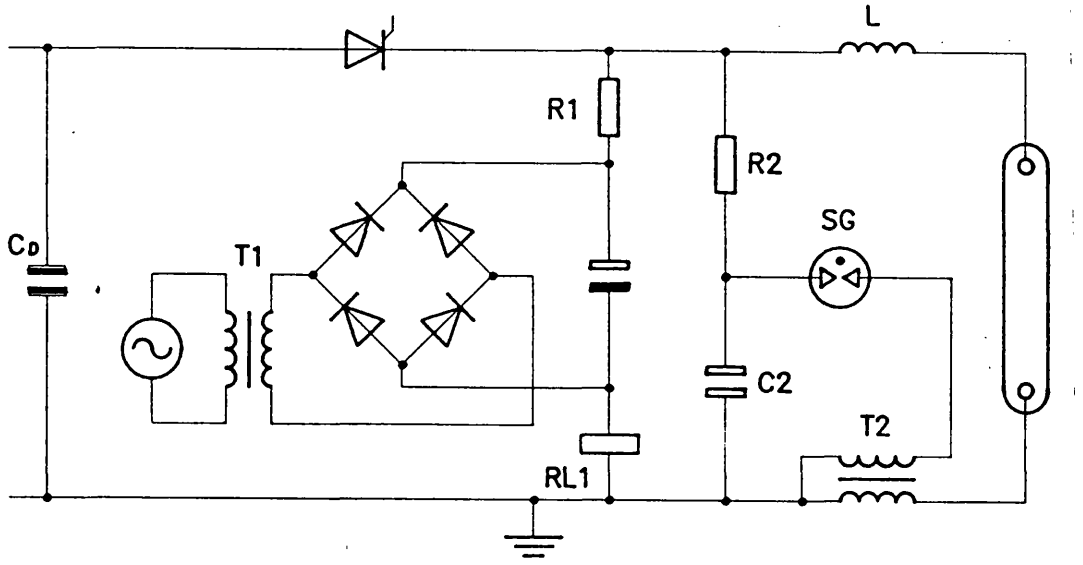

Figure A2.3 Schematic of the trigger and simmer circuits. (C_D = main discharge capacitor).

A2.5 Discharge Circuit

The maximum discharge voltage was limited by the design of the charging circuit to 999v. From reviewing the published literature it was concluded that discharge energies up to a maximum of 100 J pulse^{-1} would be required to obtain useful (in excess of 1J) laser output energies for both erbium and holmium lasers[A2.4, A2.5]. The discharge energy is related to the storage capacitance, C, and the discharge voltage, V_{in}, by the equation

$$E_{in} = \tfrac{1}{2}C(V_{in})^2 \qquad (1)$$

Consequently the total discharge capacitance was selected to be about 200μF.

The discharge inductance, L, was selected by considering the circuit damping parameter and the required pulse duration. The damping parameter, α, is given by the equation

$$\alpha = K_o/(V_o Z_o)^{1/2} \quad (2)$$

where K_o is the impedance parameter of the lamp and is given by $K_o = 1.28(\text{Pressure}/450\text{Torr})^{0.2} \times (\text{arc length/bore diameter})$ for a xenon filled lamp and Z_o is the circuit impedance calculated from the equation $Z_o = (L/C)^{1/2}$. For the discharge circuit to be adequately matched to the lamp α should be between 0.7 and 1.1[A2.2]. Figure A2.4 shows the variation of the matching parameter with discharge inductance for the 67mm arc length lamp at typical extreme discharge voltages of 700v, and 999v. It can be seen that to stay within the acceptable limits of the damping parameter the circuit inductance should be in the range $58 < L < 177\mu H$.

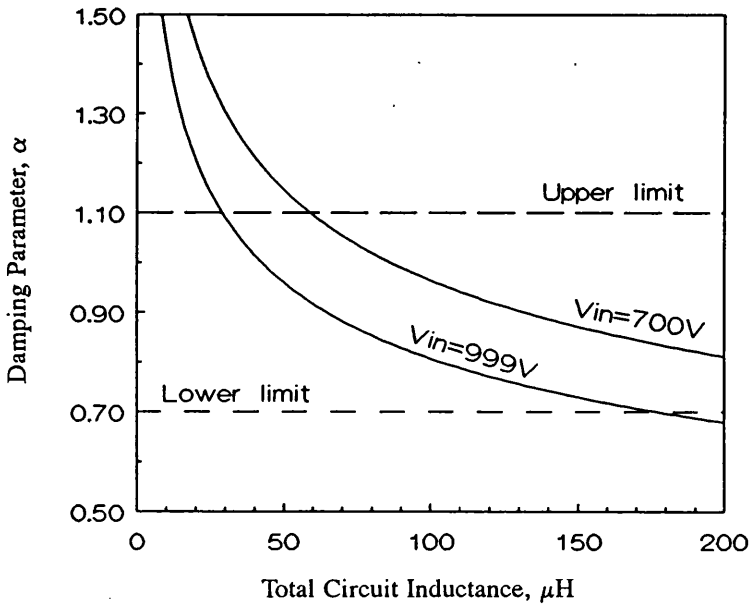

Figure A2.4 Variation in α, the discharge circuit damping parameter, with total circuit inductance for a 67mm arc length, 4mm diameter bore, xenon flashlamp filled to a gas pressure of 450 Torr.

The duration of the discharge from a single stage is given by the equation

$$T_p \approx 3(LC)^{1/2} \quad (3)$$

where T_p is the pulse width between the 10% current points. Substituting the ranges of acceptable circuit inductances yields values for T_p of between 323μs and 565μs. A

total discharge circuit inductance of 120μH was selected to fall mid-range between the limits. The expected current pulse duration, T_p, was consequently 465μs which is acceptable for pumping both erbium and holmium crystals.

Finally, the expected lifetime of the lamps was considered to ensure that the circuit represented a practical design and that there was no danger of spontaneous explosion of the lamp due to overloading. The single lamp explosion energy, E_x, is the discharge energy for which spontaneous failure of the lamp is likely to occur and is calculated from the equation

$$E_x = K_e(T_p/3)^{½} \quad (4)$$

where K_e is the lamp single explosion constant and is calculated using K_e=Qld where l and d are the lamp arc length and bore diameter in cm and Q is the quartz tubing coefficient and is approximately 24600 for bore diameters less than 8mm[A2.1]. Substituting the appropriate parameters for the flashlamps into equation (4) produces values for E_x of 821J. Therefore the maximum 100 J pulse^{-1} discharge represented 12.2% of the single pulse explosion energy. The predicted lifetime of a lamp operating under such conditions is given by the equation

$$N = (E_{in}/E_x)^{-8.5} \quad (5)$$

where N is the total number of pulses expected before failure. For the maximum discharge energy the lifetime was thus $\approx$60 million pulses, which is an acceptable level for a practical system.

For operation with the 92mm arc length the discharge was left unaltered. This resulted in a damping parameter of 1.06 for V_{in}=999V rising to 1.26 for V_{in}=700V which, although above the original limit was still considered to be acceptable. The expected lifetime for this lamp was calculated using equation (5) to be roughly 875 million pulses. For lifetimes calculated above 3 million pulses, electrode effects become more significant. Material is deposited on the inside of the quartz tube which blocks the emission from the plasma and results in an overall loss of efficiency. Consequently, it was anticipated that this would be the main limitation on the lifetime rather than spontaneous explosion.

The intensity of the broadband emission from a xenon flashlamp depends greatly on the current flowing through the arc. Thus, it is desirable that lamps switch on and reach their maximum operating current as quickly as possible. Consequently,

discharge circuits consisting of several similar stages are often used to form a pulse forming network (PFN). The result of this is that the temporal profile of the discharge current pulse resembles a number of the single stage discharges overlapped with a short delay between each. The net effect of this being that the temporal shape of the discharge pulse begins to look square. Thus the lamps are effectively switched on faster, thereby maximising the spectral output over the duration of the pulse. This also has an added advantage over the single stage discharge circuit in that the overall peak current is reduced. While this may not seem beneficial in terms of producing the maximum intensity, the lower peak current reduces the charge transfer rate and reduces the rate at which the cathode is degraded, thereby extending the flashlamp lifetime. Although these processes do have some effect on the discharge pulse duration and the matching parameter the effect is small enough to be ignored, particularly where there are a small number of stages in the PFN.

A2.6 Experimental Optimisation of a Multi-stage PFN Flashlamp Driver Circuit.

Two multi-stage PFN's were constructed and compared at a fixed drive level to determine the most efficient configuration for pumping Cr:Tm:Ho:YAG, Figure A2.5.

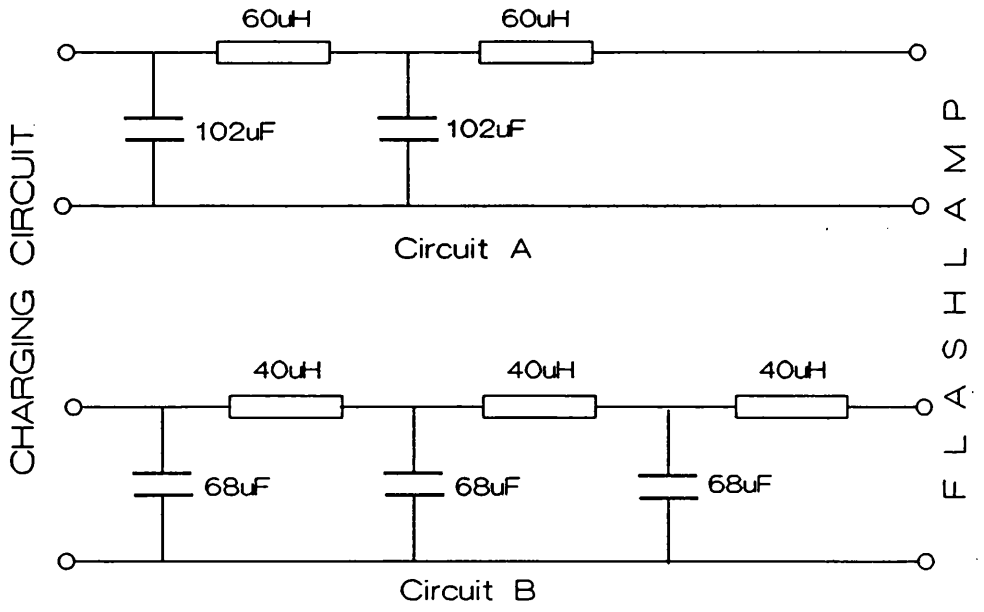

Figure A2.5 Pulse forming networks investigated for discharging pump energy through a xenon flashlamp to excite the CTH:YAG laser crystal.

The circuits were used to drive a 67mm arc length lamp the broad band light output being recorded using a fast Si photodiode linked to an oscilloscope. Figure A2.6 shows that the light from the lamp consisted of a double peaked bell-shaped pulse with a low intensity tail for both circuits. The pulse durations (FWHM) of the flashlamp pulses obtained were approximately equal at 350μs.

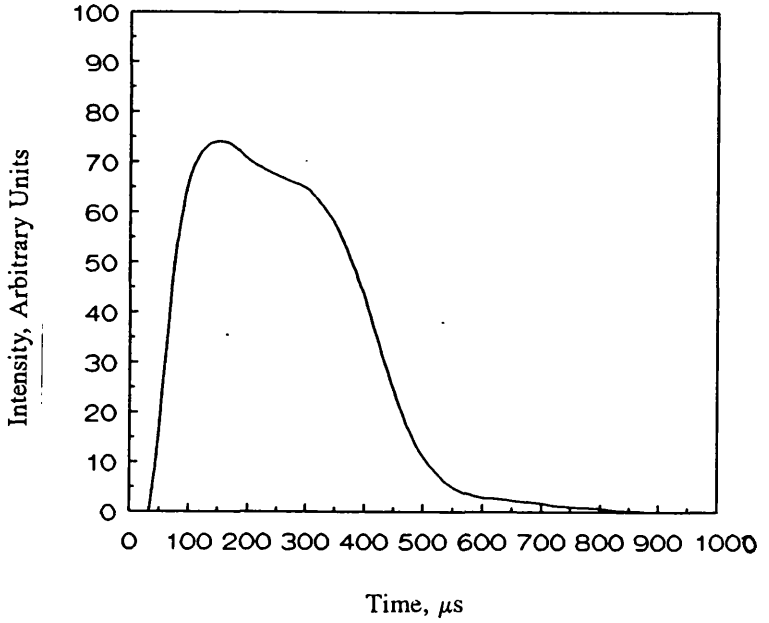

(a)

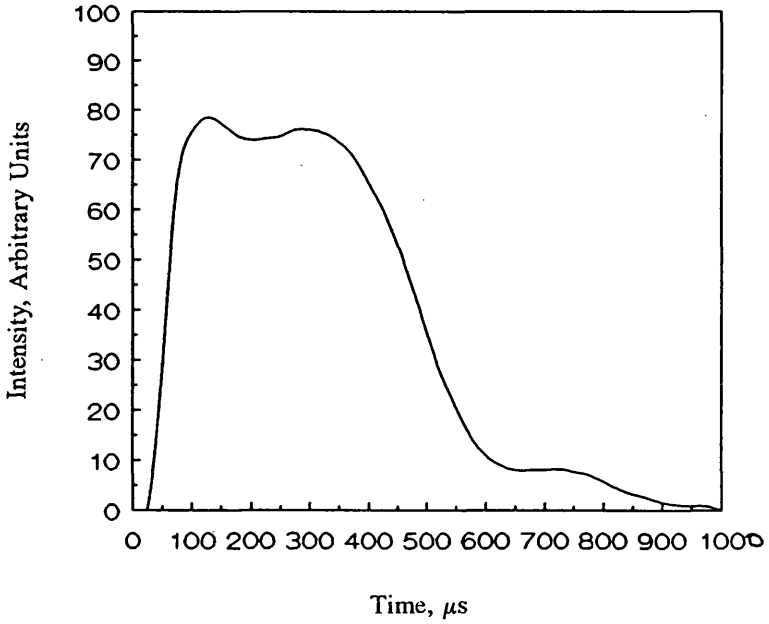

(b)

Figure A2.6 Typical excitation pulse envelope obtained from a xenon flashlamp excited by the discharge of stored energy through a pulse forming network containing a) 2x60μH inductors and b) 3x40μH inductors.

The pumping efficiency of each circuit was compared by contrasting the laser pulse energy obtained from a Cr:Tm:Ho:YAG laser under a set of constant operating conditions. A 3"x5mm diameter crystal, housed in a ceramic pumping chamber, was placed at the centre of a 400mm long resonator formed between a 5m radius of curvature rear mirror and a plane 80% reflecting output coupler. The pulse repetition rate was constant at 1Hz and the temperature of the coolant water a constant 20°C. The laser output power was determined over a range of discharge energies using a calibrated calorimeter. The results show that the two stage PFN, resulted in more efficient laser operation producing approximately 17.5% more power than the three stage circuit under identical test conditions, Figure A2.7. Subsequently the two stage PFN (circuit A in Figure A2.6) was used for all further work.

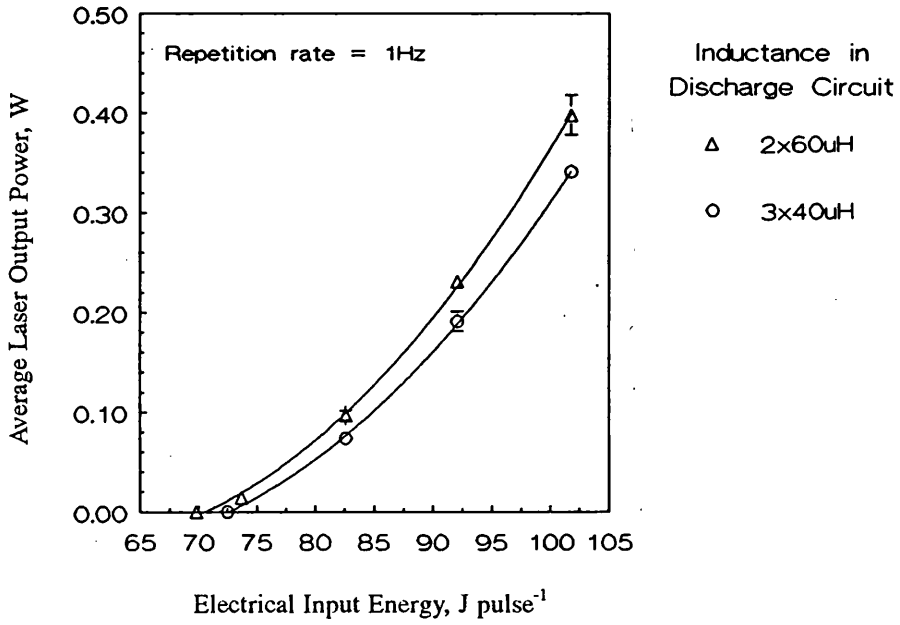

Figure A2.7 Laser performance obtained from a 3"x5mm diameter CTH:YAG crystal excited by discharging stored capacitative energy through pulse forming networks consisting of 2x60μH inductors (upper curve) and 3x40μH inductors (lower curve).

References used in Appendix 2

[A2.1] Flashlamp Data, Book 3, Q-Arc, Cambridge, England

[A2.2] Design of Flashlamp Driving Circuits
J.P. Markiewicz and J.L. Emmett
J. Quant. Electron., Vol. QE-2, No. 11, November 1966

[A2.3] Private Communication - A. Charlton describes failure of 4" crystals at average pump powers of $\approx$ 1kW

[A2.4] High Repetition Rate, High Average Power Er:YAG Laser at 2.94μm
A. Charlton, M. R. Dickinson, T. A. King
J. Modern Optics, Vol. 36, No. 10, pp 1393-1400

[A2.5] High Efficiency 2.09μm Flashlamp-Pumped Laser
G. J. Quarles, A. Rosenbaum, C. L. Marquardt, L. Esterowitz
Appl. Phys. Lett., Vol. 55, No. 11, pp 1062-64, 11 September 1989

APPENDIX 3

Measurement of Multimode Laser Beam Spotsizes

A3.1 Introduction

Unless special steps are taken to limit the operation of the laser resonator to TEM_{00} then the laser will operate in a number of transverse modes or multimode. The distribution of energy in a multimode beam depends on the geometric configuration of the resonator and the thermal effects and gain distribution in the crystal. The energy distribution across the spatial profile of a multimode beam cannot be described by a simple equation as it is the superposition of many different modes each with different peak intensities. Consequently the output profile is most commonly described qualitatively as being 'top hat'. Similarly the distribution of ray angles is not a Gaussian function (like the TEM_{00} beam). When a multimode beam propagates into the far field a non-Gaussian (and non top hat) profile is formed. Because of the non Gaussian nature of multimode laser light many of the equations describing the behaviour of the light have to be modified. Amongst these is the definition of laser beam spotsize.

A3.2 Spotsize Definition for Multimode Laser Beams

Different key researchers have chosen to define the spotsize of a multimode beam in different ways. According to Siegman, it is appropriate to define the spotsize W(z), at a distance z along the propagation axis, using the relationship:

$$W(z) = w(z)\sqrt{N} \qquad (1)$$

where N is the order of the highest Hermite (or Laplace) polynomial present as a

solution in the resonator and w(z) is the diameter of the TEM_{00} mode at the same point[A3.1]. Siegman shows that where N is large (>10) then this spotsize approximates to the distance between the outermost peaks of the N^{th} mode in the resonator, Figure A3.1. While this definition has a mathematical basis, lending itself to the modelling of resonators and beams it is not convenient in practical measurement of the spotsize as the outermost peaks cannot usually be measured due to the overlaying of many high order modes.

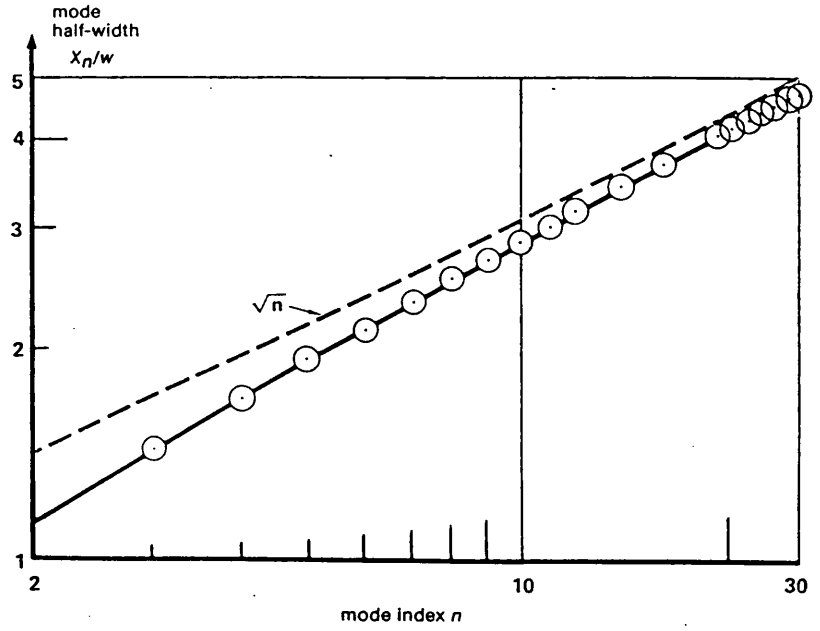

Figure A3.1 Comparison between the spotsize defined by the N^{th} hermite mode of the resonator (upper dashed curve) and the distance to the outer most peaks of the transverse laser profile (solid line). After Siegman[A3.1].

The definition of spotsize most commonly used by researchers is based on the definition for the TEM_{00} beam and is simply the diameter which contains 86.5% of the total laser energy. Although the use of this definition arises from the TEM_{00} definition of the $1/e^2$ intensity points the figure of 86.5% is arbitrary for multimode beams and is often replaced by 90%[A3.2]. For this work the standard 86.5% contained energy diameter is used throughout. The principal advantage of this definition is its identity with the TEM_{00} case which allows the same measurement technique to be applied without needing to know the degree of multimodality.

As each transverse mode in the beam will contain rays with different maximum divergence angles the profile of the beam will change along the propagation axis. The spot diameter is therefore sensitive to the distance along the axis and the mixture of transverse modes which make up the beam. Despite these

changes Koechner states that the ratios of different mode diameters remains constant at any point along the propagation axis[A3.2] leading to the relationship between the spot diameter and far field divergence of TEM_{00} and higher order modes of

$$W(z) = C_{mn}w(z) \quad (2a)$$

$$\Theta = C_{mn}\alpha \quad (2b)$$

where W(z) and w(z), and Θ and α, are the multimode and TEM_{00} spotsizes and divergences respectively and C_{mn} is a scaling factor which depends only on the number of the highest transverse (mn^{th}) order mode in the beam. Combining equations (2a) and (2b) at the waist condition yields $W_0(z)\Theta = C^2_{mn}w_0(z)\alpha$ which is a constant and relates the beam quality of the TEM_{00} and the multimode beam via the constant C^2_{mn}. (Here, the subscript 0 indicates that the spot beam is at a waist.) This is the same as the M^2 factor described by Sasnett[A3.3] and can be shown to be related to N in equation (1) via the relationship

$$C^2_{mn} = N \quad (3)$$

Thus, it is possible to link practical measurement of the beam properties to theoretical values when the fundamental properties of beam waist diameter and far field divergence are considered.

A3.3 Measuring Spotsizes

The diameter of the multimode beam was measured using the aperture method[A3.4]. The plane of the measurement was first identified. For divergence measurements this was the focal plane of a positive lens such that the spotsize was described by equation (A4.9). For general spotsize measurements used to determine the spotsize of a beam incident on tissue samples the measurement plane was identified by simple measurement of the focusing geometry. The experimental set up used is shown in Figure A3.2. A photodetector (InAs for 2.94μm and PbS or PbSe for 2.1μm) was located on the axis of the beam to monitor the amount of light transmitted through apertures of different diameters centred in the beam. To ensure linearity and reduce the risk of damage to the detector the beam was filtered after the aperture. The transmitted light was then collected and focused with a lens towards a diffuser placed over the detector. The integrated output from the detector was then displayed on an oscilloscope and compared with the signal obtained without any apertures in place.

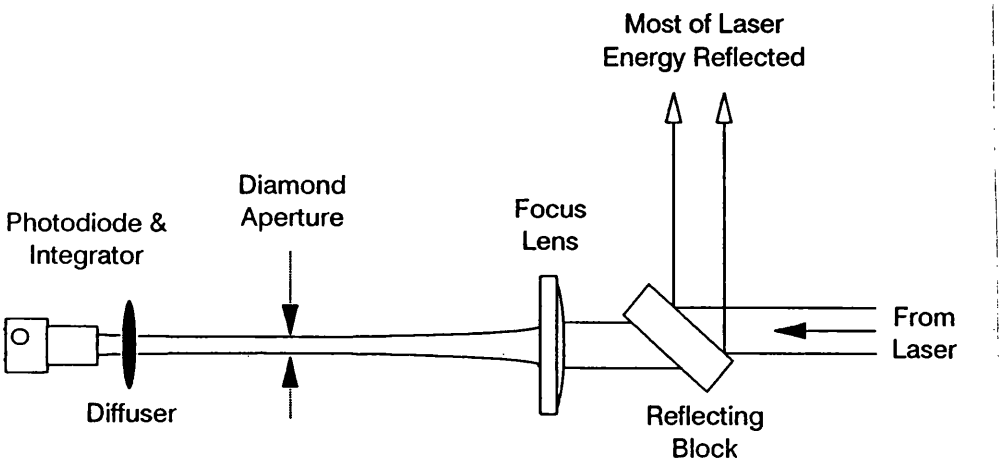

Figure A3.2 Experimental arrangement for measuring laser spotsizes.

Repeating the measurement for a variety of apertures allowed a picture of the transmission profile to be built up from which the 90% transmission diameter could be obtained, Figure A3.3.

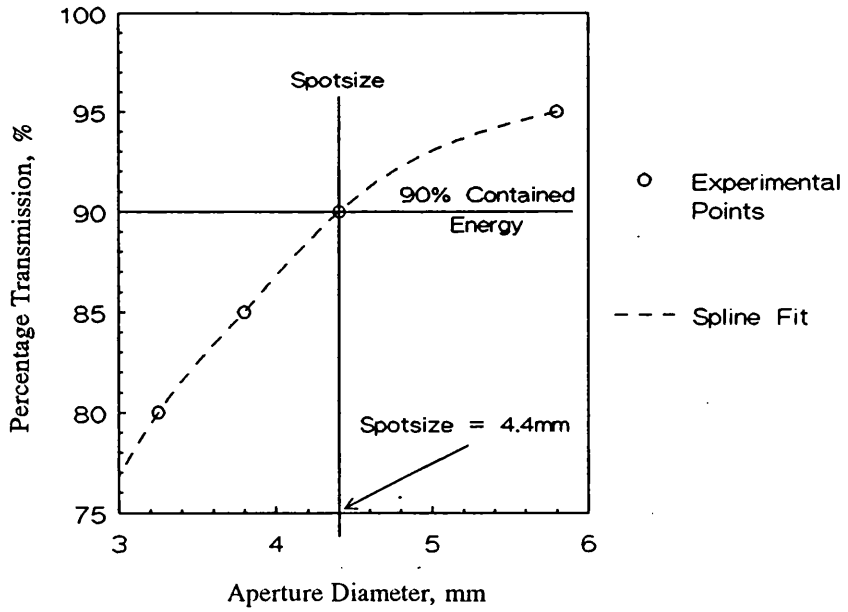

Figure A3.3 Typical plot of percentage transmission through a series of different apertures, showing simple method of determining the laser spotsize in the measurement plane.

A3.4 Errors

For divergence measurements the positioning of the aperture relative to the lens (focal plane) can be important. For this reason long focal length lenses were used of the order of 100-200mm with the measurement plane identified more accurately using an autocollimator technique. Thus the error due to the spot profile changing on either side of the focal plane could be safely ignored. Additionally, as a result of using long focal length lenses for both general spotsize and divergence measurements the resulting spotsizes were large (cf short focal lengths) and inaccuracies in the aperture diameter became less significant. The apertures used were made from stainless steel to reflect any of the incident light not transmitted thereby reducing the risk of thermal expansion during the measurement. The apertures were drilled through 2-3mm thick disks and were measured subsequent to use and found to be circular and to within the specified diameter to better than ± 0.2mm. Figure A3.4 shows that the percentage error due to aperture measurements is approximately $\pm 6.5\%$ at diameters of 3mm falling to approximately $\pm 3.5\%$ for 6mm diameter apertures.

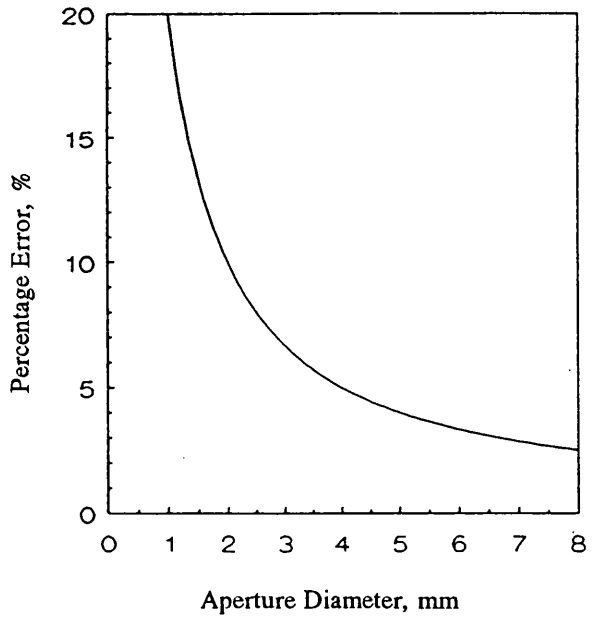

Figure A3.4 Change in the percentage error in the measured laser spotsize with aperture diameter.

Errors which may have arisen from nonlinearities in the photodetector and associated electronic integrator circuit, were made negligible, compared to the above errors, by using filters to reduce the intensity of the light signal incident on the detector, until a linear response was observed, and by virtue of the similar signal

levels for 100% and 90% energies. The linearity was confirmed by comparing the signal obtained against a calibrated calorimeter (Model 20, Laser Instrumentation Ltd, Chertsey, England). The resolution on the oscilloscope meant that the percentage transmission measurement was ±2%.

A3.5 Effect of Beam Profile on Mass Loss Measurements

The peak intensity, I_p of a TEM_{00} beam is related to the average intensity, I_{av}, measured across the beam diameter ($1/e^2$ points) via the relationship $I_p = I_{av}\sqrt{2}$. However the variable beam profile of multimode beams means that the peak intensity present in the profile cannot be related back to the defined spotsize by a mathematical formula. Thus the spotsize provides only a guide to the extent of the energy distribution and not the distribution itself. Fortunately, for near field beams the distribution is approximately described by a top hat and it is reasonable to assume the peak intensity is approximately the average intensity. Consequently, the spotsize and energy density figures quoted for mass loss measurements while based on the average energy density will closely approximate the peak energy density also.

References used in Appendix 3

[A3.1] Lasers, Chapter 17.5, pp 685-94
A. E. Siegman
University Science Books

[A3.2] Solid-State Laser Engineering, Chapter 5.1.6, p 187
W. Koechner
Springer-Verlag (1976)

[A3.3] The Physics and Technology of Laser Resonators, Chapter Nine
M Sasnett (edited by D. R. Hall and P. E. Jackson)
Adam Hilger, Institute of Physics Publishing Ltd., 1989

[A3.4] Terminology and Test Methods for Lasers
ISO/TC 172/SC 9/WG 1 - N 38 (Working Draft), 1992-05-29
Optics and Optical Instruments; Lasers and Laser Related Equipment; Test Methods for Widths, Divergence and Radiation Characteristic Factor of Laser Beam.

APPENDIX 4

Thermal Lensing

A4.1 Introduction

The laser crystal absorbs only some of the energy emitted by the flashlamp. Although the absorbed light is spread over a broad continuous band in the visible and near IR part of the spectrum, only a small proportion ends up in the upper laser levels. The rest is absorbed into levels which do not ordinarily contribute to the lasing process. Energy from these levels is either re-emitted in the form of photons, which may be re-absorbed by other ions starting the process over again, or lost to the crystal lattice as phonons. The non-radiative loss of energy results in local heating of the crystal. Assuming that there is negligible heat flow during the lamp pulse then the temperature distribution in the crystal immediately after the first lamp pulse will be the same as the light absorption distribution[A4.1]. However, where the crystal is repetitively pulsed at a rate faster than the heat can flow away then the heat accumulates and a steady state temperature is produced. The temperature variations in the crystal result in a radial variation in the refractive index which in the YAG host can make the rod act like a graded index duct, or in a more simple approximation, like a positive lens. The amount of lensing induced by heating in solid state lasers is an important consideration in the calculation of the divergence properties of resonators. Consequently it is important to establish the lensing behaviour of laser crystals to allow modelling of resonators to proceed. Some advanced computer models can deal with the duct form of the thermally induced lens[A4.2] although adequate predictions can be obtained from thin lens approximations.

A4.2 Repetitively Pulsed Crystals

The steady state temperature distribution which is established in the rod at sufficiently high repetition rates creates a radial variation in the refractive index, n, due to the temperature dependencey of n, dn/dT. Additionally, the stresses in the crystal create variations in the refractive index due to the photo-elastic effect. The combination of these refractive index perturbations acts to turn the rod into a graded index duct with a quadratic profile, n(r)[A4.3].

$$n(r) = n_o(1-2r^2/b^2) \quad (1)$$

where n_o is the index of refraction on axis, r is the radial distance and b is a constant which depends on the rod radius. Koechner derives the radial variation of n in terms of the mechanical constants of the material as

$$n(r) = n_o\left[1 - \frac{P_a}{2AKL}\left(\frac{1}{2n_o}\frac{dn}{dT} + n_o^2\alpha_t C_{r,\phi}\right)r^2\right] \quad (2)$$

where P_a is the average power dissipated in the crystal, L is the rod length, A is the end face area, K is the thermal conductivity, α_t is the thermal expansion coefficient and $C_{r,\phi}$ represents the two elasto-optical coefficients for radial and tangential components respectively.

Where the induced focal length, F_r of the rod lens is much greater than the rod length then the focal length is given by[A4.4].

$$F_r = b^2/4n_oL \quad (3).$$

Combining equations (1), (2) and (3) yields an equation for the rod focal length of

$$F_r = \frac{KA}{P_a}\left[\frac{1}{2}\frac{dn}{dT} + n_o^3\alpha_t C_{r,\phi}\right]^{-1} \quad (4)$$

Finally, a third term is required which takes account of the expansion of the rod due to heating. Koechner describes the end effects as creating spherical surfaces on the ends of the rod. The inclusion of this effect can be shown to add a third term between the brackets[A4.5] in equation (4).

$$F_r = \frac{KA}{P_a}\left[\frac{1}{2}\frac{dn}{dT} + n_o^3\alpha_t C_{r,\phi} + \frac{\alpha r_o(n_o - 1)}{L}\right]^{-1} \quad (5)$$

where r_o is the rod radius.

The most significant contribution to the induced focal length is made by the thermal dependence of the refractive index which accounts for over 75% of the induced lens for YAG crystals doped with neodymium ions[A4.3]. Consequently equation (5) is often reduced in the literature to

$$F_r = \frac{M}{P_{in}} \quad (6)$$

where

$$M = \frac{2KA}{\delta_p}\left[\frac{dn}{dT}\right]^{-1} \quad (7).$$

and P_{in}, the average pump power, is related to the absorbed power via the efficiency parameter, δ_p, where $P_a = \delta_p P_{in}$. The assumptions leading to equation (6), the non-linear thermo-mechanical behaviour of some crystals and variation in the absorption parameter, δ_p, due to heat extraction as laser power, means that the dioptric lens power induced is seldom linear with the average pump power. It is not uncommon to see equation (6) modified in published literature[A4.6] to

$$F_r = \frac{M}{(P_{in})^n} \quad (8)$$

which provides a better fit to experimental data, where n is a fitting parameter. Typically n varies around unity, being greater than one for YAG and less than for glasses[A4.7].

A4.3 Thermal Time Constant

When the first pump pulse is applied, or if sufficient time has been allowed for cooling since the last pulse, then the temperature profile is the same as the light absorption profile in the crystal[A4.1]. Thus the greatest heating is around the circumference of the crystal. The lens which is initially formed in crystals with a

positive dn/dT takes the form of a negative lens rapidly becoming an abberated positive element as heat is simultaneously conducted into the centre of the crystal and is carried away by the coolant from the barrel surface[A4.8]. The time taken for the centre of the rod to decay to 1/e of its' initial value is defined as the thermal relaxation time τ_r and is given in reference [A4.9] as

$$\tau_r = \frac{C\rho r_o^2}{4K} \qquad (9)$$

where C and ρ are the specific heat capacity and mass density respectively.

Where the time between pump pulses is less than τ_r the heat accumulates. Under these conditions individual pump pulses create only a transitory effect on the net induced focal length and the refractive index profile is described by the parabola of equation (1). Using equation (9) and the appropriate parameters (substituting those of Nd:YAG where data is not available for the crystal under consideration) the minimum repetition rates for equations (1) - (7) to hold can be calculated, Table A4.1.

Active ion	Parameter		Units	τ_r secs	Minimum Rep. Rate Hz
Erbium	C	0.536*	J (g m K)$^{-1}$		
	ρ	4.55+	g cm^{-3}		
	K	0.055#	W cm^{-1} K^{-1}		
	r_o	2.0	mm	0.443	2.26
Holmium	C	0.548*	J (g m K)$^{-1}$		
	ρ	4.68*	g cm^{-3}		
	K	0.0664*	W cm^{-1} K^{-1}		
	r_o	2.0	mm	0.386	2.6
	r_o	2.5	mm	0.604	1.7

+ Source - Data sheets for Nd:YAG, Litton

* Source - Thermomechanical properties of Cr:Tm:Ho:$Y_3Al_5O_{12}$
J. E. Marion, GRA, Vol. 91, No. 6, Mar 15, 1991

\# Source - S. R. Arutyunyan, Kh. S. Bagdasarov, A. P. Dodokin, A. M. Kekerov
Sov. J. Quant. Electron., Vol. 14, No. 6, pp 870-71, 1984

Table A4.1 Calculated thermal relaxation times for CTH:YAG and Er:YAG laser rods

The results of the calculations, shown in the table, imply that operating at repetition rates between 1 and 5 Hz a steady state thermal lens may not be established. However the experimental observation of Hotz, working with Nd:YAG and Nd:Lu:YAG[A4.8] suggest that the coolant does not remove heat as effectively as is assumed in Koechner's calculations. Hotz observed thermal relaxation times which were approximately three times greater than those calculated using equation (9). Extrapolating Hotz' observations to holmium and erbium doped YAG the critical repetition rates for thermal equilibrium to be established would be one third of those calculated.

A4.4 Effect of Thermal Lensing on Laser Performance

The stability of an empty laser resonator is described by the familiar g parameters. Most laser resonators operate in a stable geometry where $g_1 g_2 \leq 1$. The inclusion of an optical duct in the resonator whose focal length changes according to the average pump power modifies the form of the equations for g_1 and g_2 to include the effect of the lensing on resonator stability[A4.4]. As a consequence the transverse mode structure will vary as changes in the pump power create different values of g_1 and g_2. The observable effect of these changes is a change in the transverse mode structure in the near field and a change in the far field beam divergence. Additionally, changes in the transverse mode structure can result in changes to the efficiency with which stored energy is extracted from the rod.

A4.5 Experimental Determination of Thermal Lensing

The amount of thermal lensing induced in a crystal at a given input power can be determined either directly or indirectly.

1) Direct method

The amount of lensing induced in a rod can simply be found by locating the distance from the principal plane of the rod lens to the focus of a beam of parallel light focused by passing it through the rod. Where the measured focal length is long compared to the rod length the principal plane can be assumed to fall on the output rod face thereby simplifying the process. This technique has been used to determine the induced focal lengths in the Nd:YAG crystal where the 633nm beam from a helium-neon laser can be conveniently transmitted to act as the parallel light source. However, for both the Cr:Tm:Ho:YAG and Er:YAG rods the 633nm beam is

strongly attenuated and cannot provide sufficient intensity for a direct measurement of the thermal lensing to be made.

2) Indirect method

Although lensing has several effects on the laser output the most significant is usually the changes in the beam divergence which affect the size of the spot which can be achieved in the focal plane of a positive lens via the equation

$$d_s = F\alpha \qquad (9)$$

where d_s is the diameter of the spot (see Appendix 3), F is the lens focal length and α is the full angle beam divergence. Measurement of the spotsize in the focal plane of a lens of known focal length can thus provide an indication of the degree of thermal lensing. Computer software designed to model laser resonators produces predictions for the far field divergence for a given set of operating conditions. If the geometry of the resonator is known (length, mirror curvatures, refractive indices and the focal length of any intra-cavity optics) then it is possible to iteratively identify the equivalent thermal lensing which would result in the divergence value measured.

A4.6 Conclusions

Heat is deposited in a laser crystal by the non-radiative loss of pump light from excited ions. Where the heat is not conducted away from the rod rapidly a quadratic refractive index profile is established and for a positive dn/dT the rod acts like a positive lens modifying the transverse mode structure within the resonator. The far field divergence of the output beam is critical in determining the spotsize which can be achieved at the focus of a positive lens and provides a useful parameter for assessing the thermal lensing. The divergence at a given pump power can easily be determined using commercially available software. The thermal lensing arises from several effects but can be described by a simple equation, equation (8), which is based on the fact that one effect contributes over 75% of the focal power observed, equation (8). An empirical form of equation (8) which provides a better fit to experimental data is more useful if subsequent resonator modelling is to be carried out.

References used in Appendix 4

[A4.1] Power Limits of a Er:YAG Laser
J. Frauchiger, W. Lüthy
Optics and Laser Technology, Vol. 19, No. 6, pp 312-15, December 1987

[A4.2] For example LaserTrace™, a ray tracing program developed by Wather Goethals, Senior Optical Engineer at Lumonics Ltd, Rugby, to model optical resonators and beam propagation.

[A4.3] Solid State Laser Engineering 1st Ed., Chapter 7, pages 348-355
W. Koechner,
Springer-Verlag (1976)

[A4.4] Imaging of Optical Modes-Resonators with Internally Variable Lenses
H. Kogelnik
Bell Syst. Tech. J., Vol. 44, p 455, 1965

[A4.5] Solid State Laser Engineering 1st Ed., Chapter 7, page 353
W. Koechner,
Springer-Verlag (1976)

[A4.6] Pump Power Stability Range of Single-Mode Solid-State Lasers with Rod Thermal Lensing.
S. De Silvestri, P Laporta, V. Magni
IEEE Journal of Quant. Electron., Vol. 23, No. 11, Nov 1987, pp. 1999-2003

[A4.7] The Role of Rod Position in Single Mode Solid State Lasers: Optimization of a CW Mode-Locked Nd:YAG Laser.
S. De Silvestri, P Laporta, V. Magni
Opt. Comms., Vol. 57, pages 339-344, 1986

[A4.8] Thermal Transient Effects in Repetitively Pulsed Flashlamp-Pumped YAG:Nd and YAG:Nd,Lu Laser Material
R. F. Hotz
Appl. Optics, Vol. 12, no. 8, pp 1834-38, August 1973

[A4.9] Solid State Laser Engineering 1st Ed., Chapter 7, pages 374
W. Koechner, Springer-Verlag (1976)

APPENDIX 5

Delay-to-Lasing

A5.1 Introduction

Laser emission does not commence at the instant the flashlamp light is turned on. A finite time is required during which the ions, which are normally distributed amongst the energy states according to Boltzmann statistics, are elevated to excited states eventually leading to a population inversion and the gain of the system overcoming the loss. Laser emission then builds up from amplification of spontaneous emission noise from the excited levels. The sum of the time taken for the inversion to reach a level where the gain exceeds the loss and the build-up time is defined here as the delay-to-lasing.

A5.2 Population Inversion

Ions are elevated to an excited state by the pump source at a rate $W_p(t)$ which is dependent on a number of factors including the time dependent intensity of the output from the flashlamp, the efficiency of the pumping chamber reflector and the spectral overlap between the pump pulse and the absorption bands of the crystal. Ions excited to the upper laser level will re-emit their excitation energy in the form of phonons or photons which, in the absence of stimulated emission, will be at a rate $1/\tau_f$ per second, where τ_f is the flourescence lifetime of the laser level. If the pump rate is greater than the rate of loss then the population of the upper laser level will eventually exceed that of the lower level and a population inversion will have been developed.

A5.2.1 Three level laser

The rate equation for a three level laser system pumped at a constant rate, W_p, has been derived by Siegman[A5.1] as

$$\frac{\Delta N(t)}{N} = \frac{(W_p\tau_f-1)-2W_p\tau_f\exp[-(W_p\tau_f+1)t/\tau_f]}{W_p\tau_f+1} \qquad (1)$$

where $\Delta N(t)$ is the time varying difference between the population densities of the upper and lower laser levels N_2-N_1, N is the total popualtion of the combined upper and lower laser levels (all other levels are assumed to relax into either N_1 or N_2 faster than either the pump or the loss rates) and t is time. If the pump pulse duration is short compared to the fluorescent lifetime τ_f then Siegman shows that equation (1) can be reduced to the simpler form

$$\frac{\Delta N(t)}{N} \approx 1-2e^{-W_pT_p} \qquad (2)$$

which implies that the inversion at the end of the pump pulse depends only on the total energy in the pulse and not on either its duration or even its shape.

The time taken to reach a population inversion, td, is obtained by considering the time elapse before $\Delta N = 0$. Equation (1) then becomes

$$td_3 = \frac{\tau_f\ln[2W_p\tau_f/(W_p\tau_f-1)]}{W_p\tau_f+10} \qquad (3)$$

which cannot be solved without knowledge of the pump rate. However, at the threshold pump level the delay to lasing is the same as the pulse duration and a value for the threshold pump rate, $W_{p,th}$ can be obtained numerically. Knowing $W_{p,th}$ the pump rate at any level above threshold can be approximated assuming the relationship

$$W_p = (E_{in}/E_{th})W_{p,th} \qquad (4)$$

where E_{in} and E_{th} are the pump energies at a level above threshold and at threshold respectively. Implicit in this approximation is the linear relationship between discharge energy and the atomic pump rate and the absence of temporal effects (the conclusion from equation (2)).

A5.2.2 Four level laser

The population density of the upper laser level, N_3, in a four level laser system is derived by Zverev et al[A5.2] as

$$N_3(t) = Nae^{-t/\tau f}\int^{t} W_p(t)e^{t/\tau f}\,dt \qquad (5)$$

where Na represents the total population of all four levels in the system. The population difference between the upper and lower laser levels is thus

$$\Delta N(t) = N_3(t)-N_2 \qquad (6)$$

where the population density N_2 is the population deteremined by Boltzmann statistics.

Equation (5) can easily be solved for a constant pump rate W_p and yields the result

$$\Delta N(t) = NaW_p\tau_f[1-e^{-t/\tau f}] - Nae^{-E20/kT} \qquad (7)$$

where E_{20} is the energy gap between the terminal laser level and ground, k is the Boltzmann constant and T is temperature. Attempts to solve equation (5) for a time varying pump intensity profile (such as a parabola) result in a transcendental equation which can only be solved numerically and serve no use in this analysis. Equation (7) can be solved under the conditions where laser threshold is just reached. Under such conditions the threshold pump rate $W_{p,th}$ results in $\Delta N = 0$ at a time equal to the pump pulse duration, T_p, and the population of the lower laser level is

$$Nae^{-E20/kT} = NaW_p\tau_f[1-e^{-Tp/\tau f}] \qquad (8)$$

Substituting this result into equation (7) for the non laser threshold condition where the population inversion is reached yields

$$td_4 = -\tau_f \ln[1-(1/\alpha)+(1/\alpha)e^{-Tp/\tau f}] \qquad (9)$$

where α is the ratio $W_p/W_{p,th}$ and is equivalent to E_{in}/E_{th} from equation (4).

A5.3 Laser Build-up Time

The time taken for the output pulse to build up from spontaneous noise is derived by Siegman in Lasers[A5.3] as

$$T_b \approx \frac{\tau_c \ln(I_{ss}/I_0)}{(r-1)} \qquad (10)$$

where τ_c is the cavity decay time, r is the ratio of the inversion above threshold and I_{ss}/I_0 is the ratio of the steady state intensity over the initial noise level.

Although neither the system loss, which determines the cavity lifetime, nor the ratio of the steady state intensity over the noise intensity are known it is possible to approximate the typical build-up time for solid state lasers, Table A5.1.

Resonator Length	Round Trip Losses (%)	I_{ss}/I_0	r	Build-up Time (μs)
450mm	10	10^8	1.1	5.5
	10	10^{12}	1.6	1.4
	40	10^8	1.1	1.4
	40	10^{12}	1.6	.45nsec

(Parameters based on experimental set-up and data quoted by Siegman[A5.2].)

Table A5.1 Calculated build-up times

The longest build-up times are observed at pump levels close to laser threshold where the time taken for a population inversion to be created approaches the laser pump pulse duration, T_p. Consequently if the pump pulse duration is significantly longer than the build-up time, T_b, then the additional delay to the onset of lasing caused by the build-up time can be ignored. Similarly, as the pump rate is raised above the threshold pump rate the build-up time reduces to the order of less than a couple of microseconds. Again, if the time taken to develop the population inversion is significantly longer than the build-up time then the build-up time can be ignored in calculating the delay-to-lasing.

A5.4 Conclusion

The total time elapse from the start of the pump pulse to the onset of lasing is the sum of the time taken to produce a population inversion and the time taken for the laser pulse to build up from spontaneous noise within the cavity. For three and four level lasers the time taken to create the population inversion is described by different equations. The total delay-to-lasing times, T_d', for three and four level lasers are

$$T_{d,3}' = T_{d,3}+T_b \qquad (11a)$$

and

$$T_{d,4}' = T_{d,4}+T_b \qquad (11b)$$

respectively. Consequently, for the same pumping rate and the same upper state fluorescent lifetime, the total delay to the start of laser action wil be different between three and four level systems. For most conditions where the laser build-up time is short compared to the delay T_d equations (11a) and (11b) reduce to

$$t_{d,3} \approx \frac{\tau_f \ln[2W_p\tau_f/(W_p\tau_f-1)]}{W_p\tau_f+1} \qquad (12a)$$

and

$$t_{d,4} \approx -\tau_f \ln[1-(1/\alpha)+(1/\alpha)e^{-Tp/\tau f}] \qquad (12b).$$

References used in Appendix 5

[A5.1] Lasers, Chapter 6, pp 243-262
A. E. Siegman
University Science Books (1986)

[A5.2] Neodymium Activated Yttrium Aluminium Garnets
G. M. Zverev, Yu. D. Golyaev, E. A. Shalaev, A. A. Shokin
J. Soviet Laser Research, Vol. 8, No. 3, pp 189-279, May 1987

[A5.3] Lasers, Chapter 13.1, p 494
A. E. Siegman
University Science Books (1986)

APPENDIX 6

Measurement of Ablation Rate of Tissue

A6.1 Introduction

The lesions created in tissue have been assessed in a number of different ways by different authors[A6.1, A6.2, A6.3, A6.4]. The choice of technique is dependent on a number of factors amongst them available resources and tissue type. By far the greatest determining factor though is the end result that is required. For instance where the possibility of perforation is being investigated the sensible options are the time-to-drill technique for *in vitro* work or histological analysis *in vivo*.

For the investigation of tissue ablation by 2.1μm and 2.94μm laser light reported in this thesis the mass loss technique developed by Walsh for 2.94μm and 10.6μm[A6.2], and used by Nishioka[A6.5] for 2.1μm and Dickinson[A6.6] for 2.94μm has been used. Additional characteristaion of the lesions was carried out by visual inspection and histology. The choice of measurement technique was determined by a number of factors, these were;

a) acceptance of the technique as applicable to 2.1μm[A6.5] and 2.94μm[A6.6],
b) existence of published data at both 2.1μm and 2.94μm for comparison,
c) *in vitro* nature of experiments and history of samples,
d) relative freedom from operator opinion or influence,
e) availability of digital pan-balance suitable for measurement,
f) relative speed of measurement (cf histology),
g) ease of use.

A6.2 Mass Loss Measurement - Experimental Apparatus and Method

The technique of measuring mass loss is described in the original work by Walsh et al[A6.2] and subsequent work by Nishioka[A6.5] and Dickinson[A6.6]. The experimental set-up is shown in Figure A6.1. Light from the laser was directed vertically down using high reflectivity mirrors onto the surface of the tissue sample which rested in the pan of a digital pan balance (Mettler AC100). The pulse energy was varied by the addition of glass slides at normal incidence to the beam for 2.94μm light and by a combination of glass slides and varying the pump pulse energy for 2.1μm. The laser was operated at 5Hz in all cases. The beam was focused onto the surface of the tissue using a variety of CaF_2 lenses. The diameter of the spot incident on the tissue was initially assessed using burnpaper and later using apertures[A6.7]. Burnpaper was used to ensure that the variation in the spot diameter between the initial surface plane and the final surface plane did not vary by more than 0.25mm. In general it was possible to maintain the burn diameter to 0.1mm by using long focal length lenses and positioning the tissue approximately at the beam waist created by the lens.

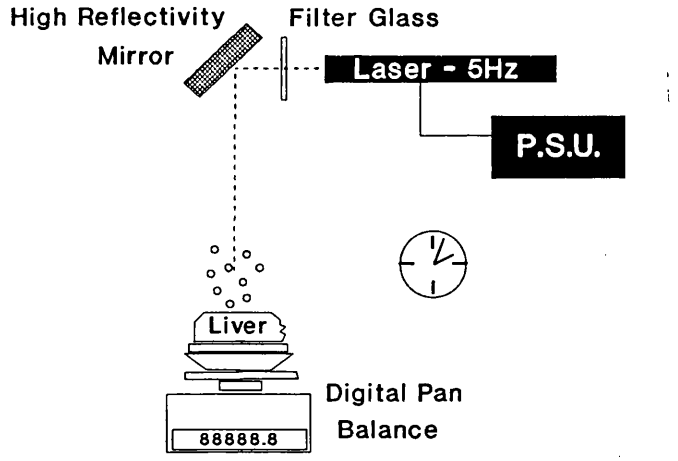

Figure A6.1 Experimental arrangement for measuring the tissue mass loss.

Samples of liver approximately 20mmx20mm were cut from approximately 10mm thick slices of liver obtained from a local butcher. The samples had all been prefrozen prior to purchase. Before use the slices were kept refrigerated but were allowed to warm up to room temperature (19-26°C) before being exposed to laser radiation. The samples were positioned on a 1mm thick glass slide which was placed on the pan of the balance. Although digital, there was no direct computer link via RS232 interface as used by others[A6.2,A6.5]. Consequently, readings were taken by an

observer who recorded the readout at 10 second intervals. The balance was reset to zero so that the indicated value was the actual mass loss and was always negative. Before and after the laser exposure the mass loss as a result of evaporation was monitored for at least 90 seconds. This allowed mass loss due to evaporation during the laser exposure to be accounted for in the calculation of mass loss due to direct laser exposure. The actual laser exposure was controlled using a mechanical shutter operated by a simple timer circuit. To eliminate thermal effects in the laser crystal which may have changed the mode structure in the crystal the laser was operated for at least 10 seconds prior to starting the exposure.

The readings were plotted on a time axis to reveal the rate of mass loss with time. Figure A6.2 shows that the rate of mass loss was different before, during and after the exposure but was constant in each case.

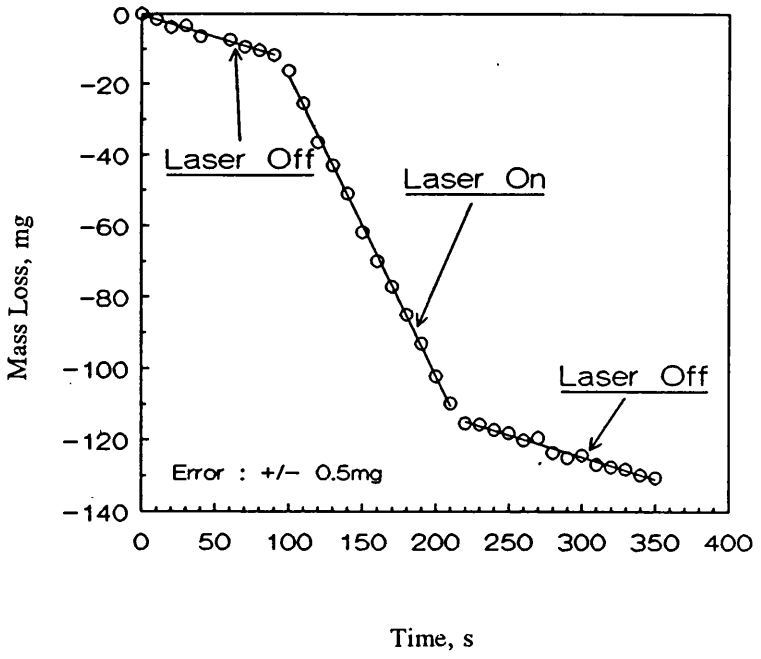

Figure A6.2 Typical plot of tissue mass loss before, during and after laser exposure.

Fitting a straight line to the sets of data for before and after the laser exposure allowed the actual mass loss due to the laser exposure to be calculated, Figure A6.3.

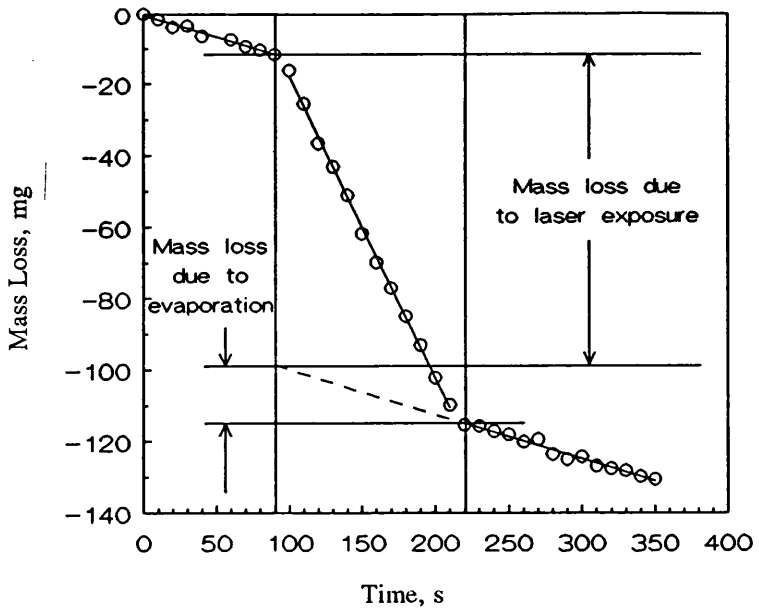

Figure A6.3 Calculation of the mass loss due to laser radiation from the experimental results.

A6.3 Errors

The mass loss is defined as the mass of tissue removed as a result of exposure to laser radiation. The mass loss efficiency (MLE) has the same definition as that used by Walsh[A6.2] and is simply the mass loss divided by the total delivered energy (mg J^{-1}). Consequently the sources of error are,
in the mass;

a) the calibration accuracy of the pan balance,
b) the accuracy with which the readout could be observed,
c) the method of extrapolation to remove the mass loss due to evaporation during the laser exposure,
d) the effect of ablation debris falling back onto the pan balance,

and in the delivered energy;

e) the calibration of the calorimeter,
f) determining the total number of delivered pulses,
g) determining the reflection/scattering losses from the surface of the tissue to establish the energy absorbed,

The pan balance was a Mettler AC100 unit with a resolution to 0.1mg and a calibration accuracy stated as $\pm$0.05mg. The method of recording the readout was subject to systematic and random errors. Taking a large number of readings (>9)

and applying linear regression to the readings helped to reduce the effects of random and some systematic errors. The total error in the regressed line fit was consequently taken from the software used to fit the data to a straight line. This allowed a maximum and minimum mass loss to be determined, Figure A6.4. The actual mass loss was taken as the intersection of the regressed lines (Figure A6.3) while the error in this value was the largest deviation from this caused by considering the regression errors. This method resulted in larger errors for longer laser exposures.

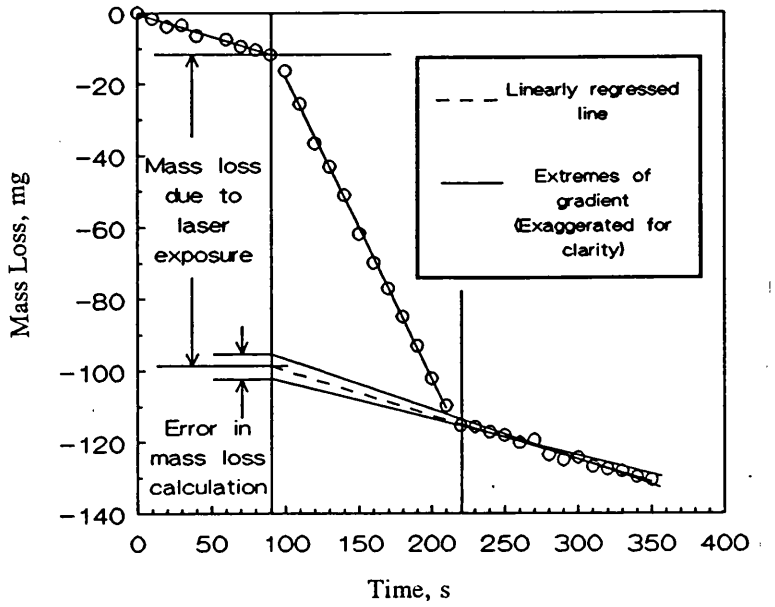

Figure A6.4 Calculation of the error in determining the mass loss due to laser exposure.

No account could be taken of the ablation debris which fell back onto the balance although there was no visible evidence that particles were falling either directly back onto the sample or onto other parts of the pan.

The average laser power was measured using a volume absorbing calorimeter (Model 20, Laser Intsrumentation Ltd, Chertsey, England) which was supported over the pan balance after the turning mirror and focusing optic. The calorimeter had recently been recalibrated and was accurate to $\pm 2\%$ (traceable to N.P.L.). The single pulse energy was calculated by dividing by the repetition rate which was measured using a Philips PM6665 frequency monitor. No attempt was made to measure or calculate the amount of laser energy lost as a result of reflection or backscatter.

The timer used to control the laser delivery had a response time significantly less than the interpulse period of the laser. The shutter was the same as the basic

shutter mechanism used on Lumonics scientific products and was able to open within 0.1ms and close within the interpulse period (<200ms). As the timer was not synchronised to open or close during the interpulse period it was reasonable to conclude that the shutter could control the number of delivered pulses to ± 1 shot.

In addition to the errors inherent in the measuring devices and techniques, a natural spread in results is anticipated due to inhomogeneities in the tissue. To assess this, selected experimental points were repeated several times in order to produce an average and standard deviation value. In the figures in the main text of this thesis the sets of data are normally presented with error bars indicating the average and standard deviation of these repeated measurements. The experimental errors are included only in the figures where separate sets of experimental data are compared.

A6.4 Summary

The method of mass loss introduced by Walsh et al was used to assess the efficiency of material removal by laser radiation of *in vitro* room temperature, prefrozen, liver tissue. The technique has been used elsewhere at both of the wavelengths used in this study[A6.5, A6.6] and was considered particularly suitable due to its freedom from influences such as operator technique. The main source of error in calculating the MLE is the measurement of light absorbed by the tissue. However in keeping with other work the MLE was calculated assuming 100% absorption of the incident energy. The errors in the measurements made are summarized in Table A6.1. The variation of the process due to tissue variability is indicated by error bars on the figures which arise from repeat experiments and are $\pm$ one standard deviation.

Parameter	Contributes to	Error	Due to:
Mass	Mass Loss	2%	Balance calibration
Mass loss	Mass loss	Not considered	Falling debris
Mass loss	Mass loss	+See below	Regression analysis
Power	Delivered energy	2%	Calorimeter calibration
Repetiton rate	Delivered energy	2%	Frequency monitor
Number of pulses	Delivered energy	1 shot	Shutter Synchronisation
Absorbed energy	Delivered energy	Not considered	Reflection/scattering

+ Calculated on an individual basis for selected sample sets.

Table 6.1 Summary of errors in determining the Mass Loss Efficiency

References used in Appendix 6

[A6.1] Private Communication - Frank Cross MS FRCS,Consultant Surgeon, Dept. of General Surgery, The Royal London Hospital, London.
A cat hair was used as a depth gauge to determine the depth of lesions created by a laser in arterial tissue

[A6.2] Pulsed CO_2 Laser Tissue Ablation: Measurement of the Ablation Rate
J. T. Walsh, T. F. Deutsch
Lasers Surg. Med., Vol. 8, pp 264-75, 1988

[A6.3] Private Communication - A. Charlton, Schuster Lab.,
University of Manchester, England

[A6.4] Er:YAG Laser Ablation of Tissue: Measurement of Ablation Rate
J. T. Walsh, T. F. Deutsch
Lasers Surg. Med., Vol. 9, pp 327-37, 1989

[A6.5] Ablation of Rabbit Liver, Stomach, and Colon with a Pulsed Holmium Laser
N. S. Nishioka, Y. Domankevitz, T. J. Flotte, R. R. Anderson
Gastroenterology, Vol. 96, pp 831-37, 1989

[A6.6] Studies of Er:YAG Laser Interactions with Soft Tissue
M. R. Dickinson, A. Charlton, T. A. King, A. J. Freemont, R. Bramley
Lasers in Med. Science, Vol. 6, No. 2, pp 125-31, June 1991

[A6.7] Terminology and Test Methods for Lasers
ISO/TC 172/SC 9/WG 1 - N 38 (Working Draft), 1992-05-29
Optics and Optical Instruments; Lasers and Laser Related Equipment; Test Methods for Widths, Divergence and Radiation Characteristic Factor of Laser Beam.